Investigation of Oscillatory Brain Networks in Essential Tremor and Parkinson's Disease: The Clinical and Behavioral Relevance of Subcortico-Cortical Coupling

Inaugural-Dissertation

zur Erlangung des Doktorgrades
der Mathematisch-Naturwissenschaftlichen Fakultät
der Heinrich-Heine-Universität Düsseldorf

vorgelegt von

Alexandra Kathrin Steina
aus Mettmann

Düsseldorf, Februar 2025

aus dem Institut für Klinische Neurowissenschaften und Medizinische Psychologie
der Heinrich-Heine-Universität Düsseldorf

Gedruckt mit der Genehmigung der
Mathematisch-Naturwissenschaftlichen Fakultät der
Heinrich-Heine-Universität Düsseldorf

Referent: Prof. Dr. Alfons Schnitzler

Korreferent: Prof. Dr. Thomas Heinzel

Tag der mündlichen Prüfung: 28.04.2025

Preface

This thesis comprises my work at the Institute for Clinical Neuroscience and Medical Psychology, Heinrich Heine University Düsseldorf, from December 2019 to February 2025. The content of the dissertation is based on the following articles:

- **Article I**
  Neuronal oscillations predict deep brain stimulation outcome in Parkinson's disease
  Jan Hirschmann*, Alexandra Steina,* Jan Vesper, Esther Florin, & Alfons Schnitzler
  Brain Stimulation **15**, 792-802 (2022)
  https://doi.org/10.1016/j.brs.2022.05.008
  *These authors contributed equally to this work.
- **Article II**
  Mapping Subcortico-Cortical Coupling—A Comparison of Thalamic and Subthalamic Oscillations
  Alexandra Steina, Sarah Sure, Markus Butz, Jan Vesper, Alfons Schnitzler, & Jan Hirschmann
  Movement Disorders **39**, 684-693 (2024)
  https://doi.org/10.1002/mds.29730
- **Article III**
  Oscillatory coupling between thalamus, cerebellum and motor cortex in essential tremor
  Alexandra Steina, Sarah Sure, Markus Butz, Jan Vesper, Alfons Schnitzler, & Jan Hirschmann
  Movement Disorders **40**, 896-905 (2025)
  https://doi.org/10.1002/mds.30165
- **Article IV**
  Modulations of thalamo-cortical coupling during voluntary movement in patients with essential tremor
  Alexandra Steina, Sarah Sure, Markus Butz, Jan Vesper, Alfons Schnitzler, & Jan Hirschmann
  Preprint on bioRxiv; https://doi.org/10.1101/2025.02.15.638416
  Currently under review in NeuroImage Clinical.

The two following manuscripts were also published during my doctorate. They are not part of this dissertation, but **Article VI** will be briefly discussed in section 1.2.3

- **Article V**
  Exploring the electrophysiology of Parkinson's disease with magnetoencephalography and deep brain recordings
  Fayed Rassoulou, Alexandra Steina, Christian Hartmann,Markus Butz, Alfons Schnitzler & Jan Hirschmann
  Scientific Data **11**, 889 (2024) https://doi.org/10.1038/s41597-024-03768-1
- **Article VI**
  Dissecting deep brain stimulation evoked neural activity in the basal ganglia
  Sohail Noor, Alexandra Steina, & Cameron McIntyre
  Neurotherapeutics **21**, e00356 (2024) https://doi.org/10.1016/j.neurot.2024.e00356

Abstract

Deep brain stimulation (DBS) is a surgical therapy that alleviates symptoms in movement disorders such as essential tremor and Parkinson's disease, by delivering electrical stimulation to disease-specific deep brain structures. In addition to therapeutic benefits, the implantation of electrodes for DBS provides a unique opportunity to record electrical activity in otherwise inaccessible regions of the brain. Studies of this activity have revealed pathological alterations of neuronal oscillatory activity. Further, it has been shown that oscillatory activity can be synchronized across spatially separated areas, potentially reflecting inter-regional communication.

The present thesis aimed to characterize oscillatory brain networks in Parkinson's disease and essential tremor. The goal was to advance our knowledge about the pathological mechanisms underlying both diseases and to clarify the significance of subcortico-cortical coupling for both behavior and therapy. For this, four studies were performed that combined magnetoencephalography, a non-invasive recording technique that measures activity from the cortex, with recordings from DBS electrodes. In Parkinson's disease, signals were recorded from the subthalamic nucleus (STN) and in essential tremor from the ventral intermediate nucleus of the thalamus (VIM).

Study 1 sought to explore whether local synchrony within the STN and STN-cortex coupling could predict the reduction of symptom severity achieved by DBS. The study showed that particularly the coupling between STN and cortex was informative about DBS outcome, implying that it may serve as a biomarker indicative of the response of patients with Parkinson's disease to DBS therapy.

In contrast, in essential tremor, oscillatory coupling between the VIM and cortex is far less characterized, and its behavioral and clinical importance remains to be determined. To close this knowledge gap, Study 2 investigated VIM-cortex coupling at rest and compared it to STN-cortex coupling. Interestingly, the cortical regions and frequency bands involved were similar to those observed for the STN, suggesting that certain aspects of subcortico-cortical coupling may reflect universal properties of oscillatory brain networks.

To further uncover the pathological mechanisms underlying essential tremor, Study 3 aimed at characterizing oscillatory activity during action tremor, the main symptom

of essential tremor. The study demonstrated that oscillatory coupling at tremor frequency between VIM, motor cortex and cerebellum increased in the presence of tremor, suggesting that pathological synchronization of oscillatory activity may contribute to disease pathology of essential tremor. Moreover, tremor amplitude correlated with the strength of synchronization between VIM and motor cortex, indicating that this oscillatory interaction may serve as a neural marker of tremor severity.

Study 4 examined whether synchronization between the VIM and cortex changes when patients engage in voluntary movements. The study revealed frequency-specific modulations of VIM-cortex coupling, including a decrease in coupling strength in the beta frequency range (13–21 Hz), a phenomenon that has been observed across other diseases and midbrain nuclei. In line with Study 2, these results suggest that movement-related modulations of oscillatory activity might reflect universal principles of motor network dynamics, rather than being specific to a disease.

The thesis advances our understanding of STN-cortex oscillatory coupling in Parkinson's disease and VIM-cortex coupling in essential tremor, emphasizing the clinical and behavioral significance of subcortico-cortical interactions. The presented studies offer new insights into general properties of oscillatory brain networks and their role in disease, while suggesting that subcortico-cortical coupling could serve as a clinical marker to enhance future therapies.

Kurzfassung

Die tiefe Hirnstimulation (THS) ist eine chirurgische Therapie, die die Symptome von Bewegungsstörungen wie essentiellem Tremor und Morbus Parkinson lindert, indem elektrische Pulse an krankheitsspezifische tiefe Hirnstrukturen abgegeben wird. Neben den therapeutischen Vorteilen bietet die Implantation von Elektroden für die THS die einzigartige Möglichkeit, elektrische Aktivität in ansonsten unzugänglichen Regionen des Gehirns aufzuzeichnen. Untersuchungen dieser Aktivität haben pathologische Veränderungen der neuronalen oszillatorischen Aktivität aufgezeigt. Außerdem hat sich gezeigt, dass die oszillatorische Aktivität über räumlich getrennte Hirnareale hinweg synchronisiert ist, was möglicherweise interregionale Kommunikation widerspiegelt.

Die vorliegende Arbeit zielte darauf ab, oszillatorische Hirnnetzwerke bei Morbus Parkinson und essentiellem Tremor zu charakterisieren. Ziel war es, unser Wissen über die pathologischen Mechanismen, die beiden Krankheiten zugrunde liegen, zu erweitern und die Bedeutung der subkortiko-kortikalen Kopplung sowohl für das Verhalten als auch für die Therapie zu klären. Zu diesem Zweck wurden vier Studien durchgeführt, in denen Magnetoenzephalographie, eine nicht-invasive Methode zur Messung kortikaler Aktivität, mit Aufzeichnungen von den THS-Elektroden kombiniert wurde. In Parkinson wurden die Signale aus dem Nucleus subthalamicus (STN) und beim essentiellen Tremor aus dem Nucleus ventralis intermedius des Thalamus (VIM) aufgezeichnet.

In Studie 1 wurde untersucht, ob die Synchronität von lokaler Aktivität innerhalb des STN und die Kopplung zwischen STN und Kortex die durch THS erzielte Verringerung der Symptomschwere vorhersagen können. Die Ergebnisse zeigten, dass insbesondere die Synchronisation zwischen STN und Kortex auf den THS-Erfolg hinweist. Diese Beobachtung deutet darauf hin, dass die interregionale oszillatorische Kopplung als Marker genutzt werden könnte, um den Therapieerfolg vorherzusagen.

Im Gegensatz dazu ist die oszillatorische Kopplung zwischen VIM und Kortex beim essentiellen Tremor weit weniger erforscht, und ihre verhaltensbezogene sowie klinische Bedeutung ist noch unklar. Um diese Wissenslücke zu schließen, untersuchte Studie 2 die VIM-Kortex Kopplung in Ruhe und verglich sie mit der STN-Kortex Kopplung. Interessanterweise waren die beteiligten kortikalen Regionen und Frequenzbänder denen des STN ähnlich, was darauf hindeutet, dass bestimmte Aspekte

der subkortiko-kortikalen Synchronität universelle Eigenschaften oszillatorischer Netzwerke des Gehirns widerspiegeln könnten.

Um die pathologischen Mechanismen des essentiellen Tremors weiter zu entschlüsseln, untersuchte Studie 3 die oszillatorische Aktivität während des Aktionstremors, dem Hauptsymptom der Erkrankung. Die Ergebnisse zeigten, dass die oszillatorische Kopplung in der Tremorfrequenz zwischen VIM, Motorkortex und Kleinhirn bei Auftreten des Tremors verstärkt wurde, was darauf hindeutet, dass eine pathologische Synchronisation oszillatorischer Aktivität zur Krankheitsentstehung beitragen könnte. Darüber hinaus korrelierte die Tremoramplitude mit der Stärke der Synchronisation zwischen VIM und motorischem Kortex, was darauf hinweist, dass diese Interaktion als neuronaler Marker für die Stärke des Tremors dienen könnte.

Studie 4 untersuchte, ob sich die Synchronisation zwischen VIM und Kortex verändert, wenn Patienten freiwillige Bewegungen ausführen. Die Studie zeigte frequenzspezifische Modulationen, darunter eine Abnahme der Kopplungsstärke im Beta-Frequenzbereich (13–21 Hz). Dieses Phänomen ist auch bei anderen Erkrankungen und in anderen Mittelhirnkernen zu beobachten. Im Einklang mit Studie 2, deuten diese Ergebnisse darauf hin, dass bewegungsbezogene Modulationen der oszillatorischen Aktivität eher universelle Prinzipien von motorischen Netzwerken widerspiegeln als krankheitsspezifische Mechanismen.

Die Dissertation erweitert unser Verständnis der oszillatorischen Kopplung zwischen STN und Kortex in Morbus Parkinson und zwischen VIM und Kortex im essentiellen Tremor und betont die klinische und verhaltensbezogene Relevanz subkortiko-kortikaler Interaktionen. Die präsentierten Studien liefern neue Erkenntnisse über allgemeine Eigenschaften oszillatorischer Netzwerke und ihre Rolle bei Krankheiten, während die Studien auch darauf hindeuten, dass subkortiko-kortikale Kopplung als klinischer Marker zur Verbesserung zukünftiger Therapien beitragen könnte.

Contents

1 Introduction

Movement disorders, such as Parkinson's disease (PD) or essential tremor (ET) are neurological conditions causing motor symptoms, such as slowed, or involuntary movements. These symptoms can severely impair patients' quality of life by limiting their ability to perform everyday tasks [1]. One major risk factor for developing a movement disorder is age [2,3]. As the number of individuals over the age of 65 is expected to double by 2030, concerns are growing about a corresponding increase of movement disorders [4]. While both PD and ET are currently not curable, various therapies can provide symptom relief [5,6]. One effective surgical intervention is deep brain stimulation (DBS), which involves the implantation of electrodes into a disorder-specific target [7,8]. However, some patients experience loss of benefit over time, and stimulation can induce adverse side effects [9]. This, combined with the expected demographic shift, highlights the urgent need to optimize therapies.

Understanding the pathophysiological mechanisms underlying diseases and to disentangle pathological and physiological activity is crucial for advancing therapies. Electrophysiological recording techniques are valuable tools for providing insights into neuronal dynamics and identifying neural correlates reflecting disease states [10]. Neuronal oscillatory activity, rhythmic fluctuations of neuronal activity, has been shown to be linked to behavior [11,12]. In the context of movement disorders oscillations can be pathologically altered [13]. Recordings from various sites of the brain reveal that oscillations between different regions are coupled and this coupling is often interpreted as communication between the regions involved [14,15]. Coordinated interactions between different parts of the brain are important for cognition and behavior and alterations in coupling might be related to different disease states [16].

In the case of PD, oscillatory coupling and its relation to PD pathology have already been described in great detail. The present thesis builds on this knowledge to determine whether oscillations are informative about DBS outcomes. In contrast, less is known about oscillatory brain networks in ET. This thesis addresses this gap by characterizing oscillatory coupling during tremor, rest, and voluntary movement in patients with ET. The following general introduction will give a brief overview about electrophysiological recording techniques and neuronal oscillations. Moreover, it will give an insight into symptoms and pathology of ET and PD and describe how neuronal oscillations are related to behavior and disease.

1.1 Electrophysiology

The human brain gives rise to behavior, processes sensory information, regulates emotions, coordinates movement, enables cognition and memory [17]. While neurons serve as the brain's fundamental processing units, it is the organization of these neurons into specialized ensembles that is believed to give rise to intelligent behavior [18, 19]. The human brain contains around 100 billion neurons, which transmit and process information [20]. A neuron consists of a soma, an axon, and dendrites. Signals travel from a neuron's axon through synapses to neighboring dendrites (see fig. 1.1). The information transfer depends on temporary ion movements across membranes, generating electrical currents. When an action potential, a rapid voltage change across the axonal membrane, reaches an axon terminal, it triggers neurotransmitter release into the synaptic cleft. This leads to excitatory or inhibitory post-synaptic potentials (EPSPs/IPSPs), with EPSPs increasing and IPSPs reducing the probability of an action potential in the next neuron [21].

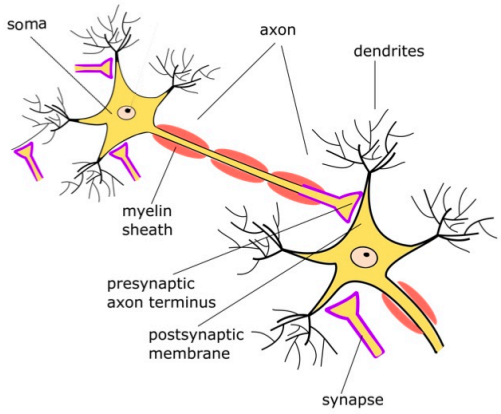

Figure 1.1: **Schematic drawing of two neurons.** When an action potential in one neuron travels towards the synpase, neurotransmitters are relased into the synaptic cleft. This can either cause the next neuron to be excited or inhibited. Image taken from my master's thesis "Movement performance and brain activity under deep brain stimulation at different frequencies".

1.1.1 Measuring Electrophysiological Activity

Neuronal activity can be measured on different scales, from microlevel recordings of single cell spiking to macroscale recordings capturing the summed activity of larger neuronal populations. Recordings can be invasive, with electrodes of various sizes measuring electric activity at a location within the brain. Non-invasive techniques, like electroencephalography (EEG) or magnetoencephalography (MEG), detect electric and magnetic fields outside the skull, that are generated by larger volumes of tissue. The cellular processes that contribute to the measured fields are briefly described in Box 1.

Box 1 Extracellular Field Potentials

All active cellular processes, such as post- and presynaptic potentials, action potentials, afterpolarizations, and neuron-glia interactions, generate transmembrane currents, that produce electric and magnetic fields, detectable in the extracellular space [22, 23]. Single neuron action potentials can be measured at the microscale, with spiking activity manifesting as high-frequency signals ($>600\,\mathrm{Hz}$) [24]. Field potentials, on the other hand, represent the summed activity of neuronal populations and include signals measurable by macroelectrodes, MEG or EEG. Here the signal with frequencies $<600\,\mathrm{Hz}$ is typically relevant [25]. When activity is measured on larger spatial scales encompassing groups of neurons, the recorded field results from the superimposition of numerous sources, making it challenging to determine individual contributions [22]. However, signals from multiple compartments must co-occur in time, to create an measurable signal. Based on this assumption postsynaptic potentials are thought to contribute most to the fields measured by MEG and LFP recordings. Although the signal of individual postsynaptic potentials is small (1-10 fAm) [26], their slow dynamics (10-100 ms) and the large number of synapses make temporal overlap likely [22]. While action potentials generate stronger signals, their brief duration ($<2\,\mathrm{ms}$) and low chance of synchronous firing suggests a smaller contribution to the field potential [22]. However, contributions may differ between recording technique (LFP vs. MEG) or recording location (cortex vs. sub-cortex). Furthermore, neuronal architecture and geometry shape the recorded fields.

Magnetoencephalography

Magnetic fields measured by MEG (see fig. 1.2A) typically range from $50-500\,\mathrm{fT}$ [27]. The basic principles of MEG are explained in Box 2. It is thought that approximately 10^5 pyramidal neurons are the primary contributors to these signals due to their long apical dendrites oriented in parallel [28]. Further, EPSPs are thought to dominate the MEG signal, as IPSPs produce only small extracellular currents and thus contribute less to the extracellular field [29]. During an EPSP, positive ions flow into the dendrite at the site of the synapse, leading to passive outward currents at other sites along the dendrite. This causes the apical dendrite to become more electropositive intracellularly (more electronegative extracellularly) compared to the basal dendrite and soma. This potential difference generates a current flow within the dendrite, called primary current, as well as a volume current in the extracellular space, referred to as secondary current [28]. At a distance from the source, such as it is the case in MEG recordings,this spatial charge separation can be approximated by a current dipole. MEG sensors primarily detect signals from pyramidal neurons that are oriented tangentially to the skull, rather than those that are radially oriented (see fig. 1.2B). The magnetic field $B(r)$ at a location r captured by MEG arises from both

primary $J^P(r')$ and secondary currents $J^V(r')$ at location r' which can be described by the law of Biot-Savart [27, 30]:

$$B(r) = \frac{\mu_0}{4\pi} \int J(r') \times \frac{r - r'}{||r - r'||} dv' \tag{1.1}$$

where μ_0 represents the permeability in free space. The pyramidal neurons' structure supports large dipoles and strong magnetic fields. Their parallel orientation minimizes field cancellation, forming what is known as an "open-field" configuration. Neurons with other structures, such as spherical dendrites, are thought to contribute less to the MEG signal due to greater field cancellation ("closed-field") [31]. Computational modeling for EEG activity has recently pointed toward a greater contribution of action potentials, presynaptic spikes, and afterpolarizations than previously assumed [22]. This might also apply for MEG recordings. Although cortical activity is believed to dominate the MEG, signals from deeper brain structures such as hippocampus [32], cerebellum [33], and thalamus [34] or brainstem [35] have also been reported.

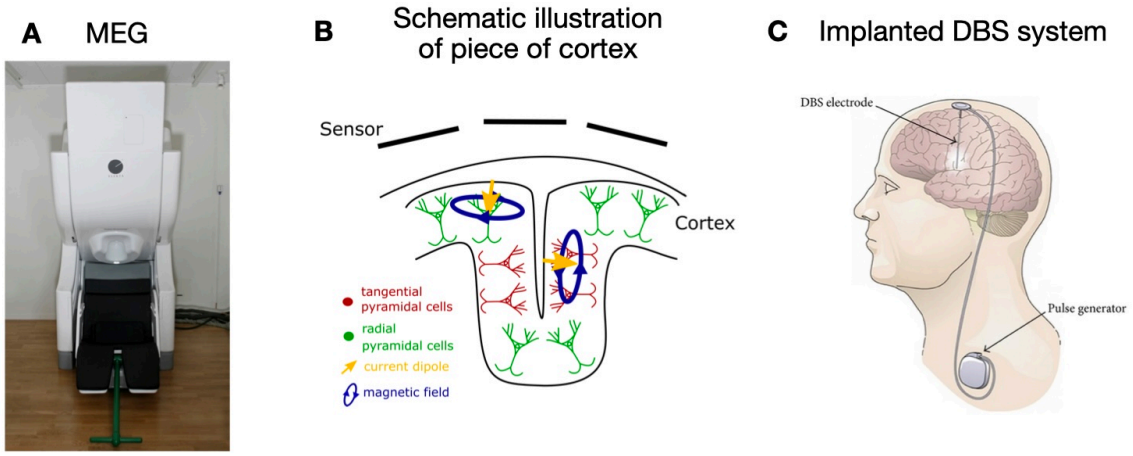

Figure 1.2: **MEG and DBS system. A** 306-channel MEG system (MEGIN) at Universitätsklinikum Düsseldorf. **B** Schematic illustration of piece of cortex. MEG sensors mainly pick up signals from pyramidal neurons that are tangentially oriented to the skull than from pyramidal neurons that are radially oriented. Image taken from my master's thesis. **C** Schematic illustration of implanted DBS system. The electrodes are connected with the implanted pulse generator via extension cables. Figure taken from [36]. CC BY 3.0.

Box 2 Principles of Magnetoencephalography

The brain's magnetic fields are several orders of magnitude smaller than the earth's magnetic field. To detect these tiny fields, highly sensitive sensors like Superconducting Quantum Interference Devices (SQUIDs) are needed. SQUIDs, cooled with liquid helium, operate in the superconducting state [27]. They consist of a superconducting loop interrupted by insulating layers called Josephson junctions. In a superconductor, electrons form Cooper pairs, which move resistance free through the loop and can tunnel through the Josephson junctions. The basic principle of measuring the magnetic flux with a SQUID involves inserting a bias current into the loop, which splits evenly and flows in the same direction through the two halves of the superconducting loop. When an external magnetic field is applied to the ring, a screening current arises and flows in the same direction as the bias current in one half and in the opposite direction in the other half of the ring. This causes a measurable voltage across the Josephson junctions. If the magnetic flux increases, the SQUID will switch to the next magnetic flux quantum, reversing the current flow in the ring [37, 38]. The SQUIDs are connected to flux transformers, such as planar gradiometers and axial magnetometers, to help capture and focus the magnetic fields. Planar gradiometers consist of two adjacent coils and measure the difference of the magnetic fields between these two points, while axial magnetometers consist of a single coil and measure the absolute magnetic field. Both magnetometers and gradiometers are arranged in the MEG helmet such that they scan the whole head [27, 37]. To prevent the brain's magnetic fields to be superimposed by stronger external magnetic fields, the MEG is installed in a shielded room. However, power line noise, electric devices in the MEG chamber or non-brain signals such as muscle contraction or heartbeats cause artefacts in the MEG. When analyzing brain signals, the data is usually cleaned from artefacts, by visual inspection and the removal of epochs or channels containing artefacts or by more advanced methods such as signals space separation [39], temporal signal space separation [40] or independent component analysis [41].

Source Reconstruction

When analyzing MEG data, it is of interest to localize the neuronal sources that generate the signal on sensor level. This process, known as source reconstruction, requires solving the "forward problem", followed by solving the "inverse problem" [28]. The forward problem estimates the signal generated by a known source. In MEG, the forward model estimates the magnetic field at sensor level based on a given source configuration, taking sensor geometry and head anatomy into account. To limit the number of potential sources, typically a finite grid is constructed, with each grid point representing a source. As described above, the neural current at a grid point location is approximated as a current dipole. Then, starting with the

quasistatic approximation of the Maxwell's equations, the magnetic flux density at a given location can be derived from the law of Biot-Savart [27]. Based on this, a projection matrix, so-called leadfield $\boldsymbol{L}$, is calculated describing how the neural sources $\vec{s}$ are projected to the sensors, resulting in the signal $\vec{b}$ at sensor-level (see fig. 1.3) [42].

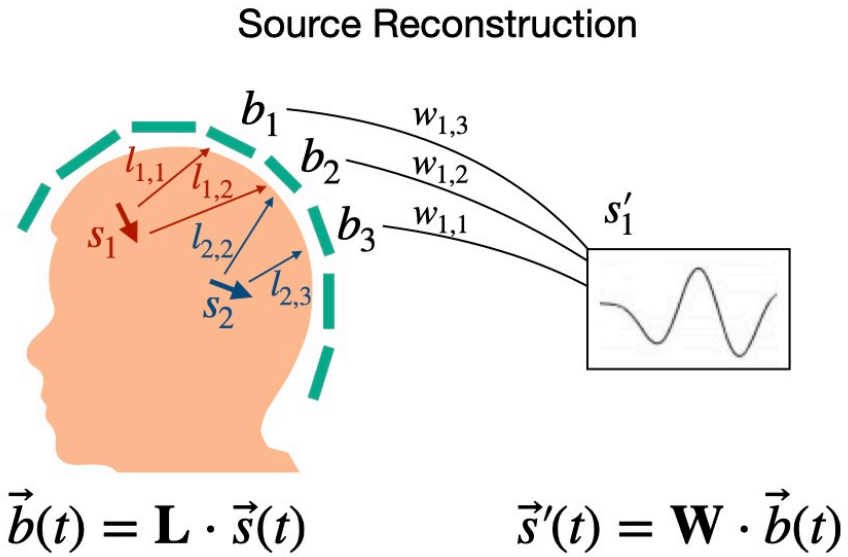

Figure 1.3: **Schematic illustration of source reconstruction.** Forward solution: The leadfield matrix $\boldsymbol{L}$ describes, how the sources $\vec{s}$ are projected to a sensor at location i, resulting in the sensor-level signal $\vec{b}$. Inverse solution: The reconstructed sources $\vec{s}'$ can be written as a linear combination of $\vec{b}$, by using a weight matrix $\boldsymbol{W}$. Based on the forward solution, the weight matrix $\boldsymbol{W}$ is optimized under constraints to find a solution for the inverse problem.

The next step in source reconstruction involves solving the inverse problem. The aim of the inverse problem is trying to find the neuronal sources $\vec{s}'$ that reflect the measured signal best, under consideration of the forward problem. However, one major challenge of the inverse problem is that it is ill-posed, as the enormous number of sources maps to a limited number of sensors [27]. This means that the solution of the inverse problem is not unique and different combinations of sources can produce similar patterns of sensor-level activity [43]. Hence, *a priori* assumptions are necessary to find a weighting matrix $\boldsymbol{W}$ that projects the sensor-data $\vec{b}$ to the reconstructed source space $\vec{s}'$ (see fig. 1.3). Numerous approaches such as minimum norm estimation or beamforming exist that put constraints on the data [44,45]. A beamformer performs spatial filtering of sensor-level data to distinguish between signals arriving from a source of interest and those originating elsewhere [43]. The main assumption of beamforming is that spatially separated sources are uncorrelated. Taking the forward solution into account, the goal of the beamformer filter is to

determine the optimal weighting for each sensor to enhance the signal from the source of interest, while minimizing contributions from all other sources. Different beamformers exist such as linearly constrained minimum variance [46] or dynamic imaging of coherent sources [47].

Intracranial Local Field Potential Recordings

Electrodes placed within the brain for surgical therapy provide the unique opportunity to capture signals that are either not measurable or only partially measurable through non-invasive methods. They offer a more precise localization than MEG recordings but are limited to the specific brain regions chosen as stereotactic targets. Intracranial signals can be measured by micro- or macroelectrodes. Microelectrodes have a small diameter and can detect single-neuron spiking [48]. Macroelectrodes, such as the ones implanted for DBS (see fig.1.2C), have a larger diameter and pick up the summed activity of neurons in the vicinity of the electrode [49]. The signal measured by these electrodes is referred to as local field potential (LFP).

Similar to MEG, it is assumed that synaptic currents dominate the signal detected by DBS-macroelectrodes. However, identifying the exact sources of LFPs in deep brain structures is more challenging, because for example basal ganglia structures and the thalamus are less organized than cortex and seem to lack the open-field arrangement described for pyramidal neurons [48,50,51].

In addition to synaptic currents, single cell spiking seems to contribute to the LFP in lower frequencies as well. In the VIM and STN, bursts of action potentials have been demonstrated to be related to LFP activity [52,53], while action potential outside of bursts do not contribute much to the LFP signal [53]. The term "burst" refers to a pattern of rapid firing of a group of neurons over a short period of time. Typically, bursts contain multiple spikes within a short time window, interleaved by longer intervals without spiking activity [54].

Alternatively, LFPs recorded from subcortical structures may originate from volume-conducted signals generated by cortical activity [55]. However, the impact of volume conduction is assumed to be influenced by the reference scheme chosen. Monopolar referencing is thought to detect volume-conducted cortical signals [48]. In monopolar referencing, all electrode contacts are referenced to a common distant contact, such as the mastoid in LFP recordings. In contrast, bipolar referencing schemes have shown to minimize the impact of volume conduction [48]. Bipolar referencing means that the signal at an electrode contact is referenced against a signal from another contact nearby instead of a distant common source. In LFP-recordings, the voltage measured across two adjacent contacts is typically subtracted.

1.1.2 Neural Oscillations

A feature of neuronal activity is its rhythmic repetition over time, known as neuronal oscillations. These oscillations are ubiquitous throughout the mammalian brain and they are associated with various behavioral and cognitive processes [11, 12]. Notably, neuronal oscillations tend to occur in distinct frequency bands, which are commonly defined as delta (2–4 Hz), theta (4–8 Hz), alpha (8–12 Hz), beta (13–35 Hz; low-beta 13–21 Hz; high-beta 21–35 Hz), gamma (35–90 Hz), and high-frequency oscillations (>200 Hz) see fig. 1.4A [56, 57]. Modulating oscillatory activity through transcranial alternating current stimulation or DBS has been shown to influence behavioral outcomes. For example, DBS in the theta range improved working memory in patients with PD [58] and transcranial current stimulation in the beta range slowed movements in healthy subjects [59]. These findings further underpin the link between the oscillations and behavior [60]. This connection seems particularly relevant in movement disorders, where pathological alterations in rhythmic activity often correspond to specific symptoms [16].

Despite the clear association, there is an ongoing debate about whether oscillations play a causal role in neural processing or are simply epiphenomenal [61]. Recently, it has been pointed out that part of this discussion has been influenced by a misunderstanding of the term oscillation, and it has been proposed to distinguish between two separate entities: 'oscillations-in-process', rhythmic repetitions of physiological events, and 'oscillations-in-measurement', rhythmic patterns in the recorded signals [62].[1] Oscillations-in-process are present on molecular, cellular, synaptic and network level [63]. Many neurons have pacemaker properties, meaning that they can fire spontaneously in an oscillatory manner [64, 65]. At network level, reciprocal interactions between inhibitory and excitatory neuronal populations can generate oscillatory activity patterns in both groups [66].

Synchronization of Local Neuronal Populations

'Oscillations-in-process' can synchronize neuronal populations at different frequencies, with the synchronized neurons undergoing more or less the same regular periodic changes in excitability [14, 15, 67]. This synchronized activity may be detectable as 'oscillations-in-measurement', rhythmic patterns in the signal measured by MEG or LFP. Techniques like Fourier and wavelet transforms, temporal filters, and linear projections are commonly used to quantify the characteristics of oscillations-in-measurement [56, 68, 69]. The basis of Fourier analysis is outlined in Box 3. Spectral power is commonly used to quantify the degree of local synchrony.

[1] It should be noted, that while it is generally assumed that 'oscillations-in-process' are measurable as 'oscillations-in-measurement', an oscillation in one entity can occur independently of an oscillation in the other entity [62].

Box 3 Spectral Analysis

Fourier transformation is a technique that transforms a time-domain signal into frequency-domain. It can be used to decompose a signal into its constituent frequencies and extracts phase and amplitude as a function of frequency [56]. Since neuronal time series are finite due to limited recording length, a discrete Fourier transform is required to map a neuronal time-series into the frequency domain. The result is the complex valued Fourier coefficient $S_X(f, n)$ for a frequency f, which can be derived by

$$S_X(f, n) = \sum_{t=0}^{T-1} X(t, n) e^{-i2\pi f \frac{t}{T}} \tag{1.2}$$

with $X(t, n)$ representing the discrete signal of a given epoch n with length T [70]. Spectral power is defined as the squared Fourier amplitude at a given frequency.

$$S_{XX}(f, n) = \langle S_X(f, n) S_X(f, n)^* \rangle \tag{1.3}$$

with * denoting the complex conjugate. Narrow-band peaks in the power spectrum are assumed to indicate the presence of oscillatory components in the signal at specific frequencies. Differences in power across experimental conditions may reflect changes in neuronal synchronization or changes in the number of neurons contributing to the signal. However, such differences can also arise from aperiodic or 1/f activity, characterized by an exponential power decay [23,71]. This component may reflect shifts in the balance of excitatory and inhibitory potentials [72] and varies across individuals and recordings, potentially confounding interpretations of oscillatory activity. Separating the spectrum into periodic and aperiodic components allows for the isolation of genuine oscillatory power (periodic component of the signal) [73].

The Fourier Transform does not caputure the temporal dynamics of a signal, as it assumes a stationary signal. To capture the temporal dynamics of a signal, wavelet transforms can be performed, which yield power or coherence as a function of both frequency and time [74].

Synchronization of Distant Neuronal Populations

Coordinated interaction between spatially distant brain regions is important for cognition and behavior [12,75]. While structural connections provide the anatomical basis for these interactions [76], cognitive processes likely require more dynamic communication mechanisms for flexible signal transmission [14]. Oscillations are proposed as one mechanism for inter-areal communication. The phase of oscillatory activity creates time windows of enhanced sensitivity to incoming signals alongside time windows of higher probability for generating outgoing signals [14]. The alignment of excitable phases between different brain regions can be quantified by coherence

(see Box 4 and fig. 1.4B). Coherence plays a key role in the communication-through-coherence (CTC) hypothesis, which posits that phase synchronization enhances effective communication between neuronal populations [14, 15, 77]. The CTC hypothesis proposes that synaptic input from a transmitting neuronal group is more likely to trigger action potentials in a receiving group if it arrives during an excitable phase, thereby facilitating communication. Conversely, arrival during a non-excitable phase hinders communication. Consequently, it is suggested that when a neuronal assembly receives inputs from multiple presynaptic neuronal populations, it will preferentially respond to the input from the group with which it is phase-coherent. However, the causal role of coherence has been debated and it has been suggested that coherence might be a result of communication rather than its cause (coherence-through-communication [78]). For example, it was shown that local rhythms in two neuronal populations do not need to be synchronized for coherence to occur [78, 79].

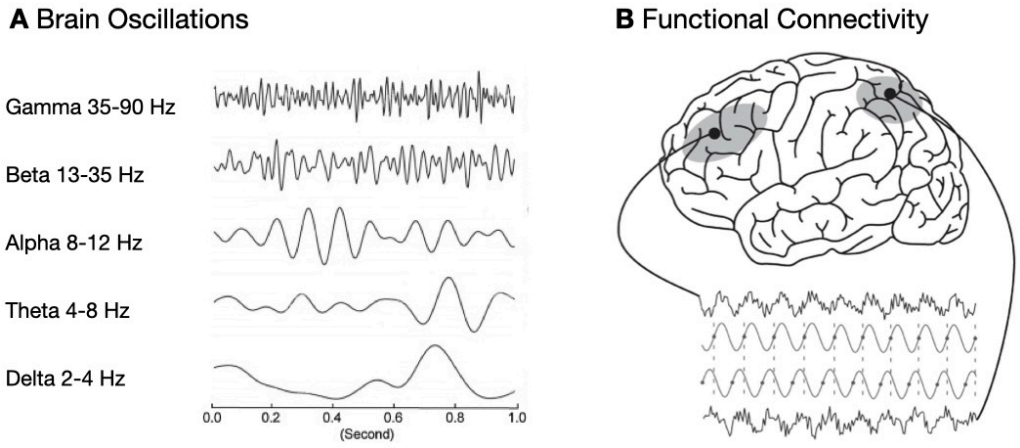

Figure 1.4: **Neuronal oscillations. A** Oscillations in different frequency ranges Figure taken from [80]. Reprinted with permission from Elsevier. **B** Schematic illustration of functional connectivity between two spatially separated cortical regions. These regions are said to be coherent (coh = 1) when they keep a constant phase and amplitude difference over time. Figure taken from [81]. Reprinted with permission from Elsevier.

Box 4 Functional Connectivity

Functional connectivity refers to the temporal correlation between neurophysiological events occurring at different locations in the brain [82]. It can be assessed by coherence for example. Coherence Coh is used to quantify phase synchronization between neuronal oscillations [83]. It describes the linear dependency between two signals, indicating whether they maintain a stable phase and amplitude relationship over time at a given frequency f.

$$Coh(f) = \frac{|\sum_{n=1}^{N} S_{xy}(f,n)|}{\sqrt{(\sum_{n=1}^{N} S_{xx}(f,n))(\sum_{n=1}^{N} S_{yy}(f,n))}} \tag{1.4}$$

with the cross-spectral density $S_{xy}(f,n) = \langle S_X(w,n)S_Y(f,n)^* \rangle$, the auto-spectral densities S_{xx} and S_{yy} and n describing the trial number $n = 1...N$ [70]. Coherence values range between zero ("not coherent") and one ("perfectly coherent).

Connectivity can also be assessed using methods like Granger causality, which statistically estimates the directionality between two signals. A common method for computing Granger causality involves fitting autoregressive models. In an autoregressive model, a time series $Y(t)$ is expressed as a weighted sum of its past values $Y(t-\tau)$ and a noise term $\epsilon(t)$:

$$Y(t) = \sum_{\tau=1}^{p} a(\tau)Y(t-\tau) + \epsilon(t) \tag{1.5}$$

with τ referring to the time lag of the preceding samples, p describing the model order and $a(\tau)$ representing the weight for each $Y(t-\tau)$ term [83]. Now, a signal X is said to Granger cause another signal Y if incorporating the past values of both X and Y improves predictions about the future of Y compared to using only the past values of Y [83]. For this, a second model, a bivariate autoregressive model is estimated, describing the time-series $Y(t)$ with both past values $Y(t)$ and past values of $X(t)$:

$$Y(t) = \sum_{\tau=1}^{p} b(\tau)Y(t-\tau) + \sum_{\tau=1}^{p} c(\tau)X(t-\tau) + \eta(t) \tag{1.6}$$

with $b(\tau)$ and $c(\tau)$ representing the respective weights of the lagged values of $Y(t)$ and $X(t)$ and $\eta(t)$ referring to the noise term. Granger causality GC is then obtained by comparing the ratio of the variances of $\epsilon(t)$ and $\eta(t)$ [83]:

$$GC_{X \to Y} = ln\left(\frac{var(\epsilon)}{var(\eta)}\right) \tag{1.7}$$

1.2 Movement Disorders

1.2.1 Parkinson's Disease

PD affects around 1 % of the population older than 60 years [84]. The main symptoms of PD are bradykinesia (slowness of movement), 4–8 Hz resting tremor, rigidity (muscle stiffness) [85]. Other motor symptoms are postural instability, gait disturbances, impaired eye movement, problems with speech and bladder control [85,86]. Non-motor symptoms such as depression, sleep disorders, and dementia are also common [87]. Both genetic and environmental factors are involved in the etiology of PD and age is the most robust risk factor [88]. To date, it is not possible to cure PD, but effective drugs such as levodopa (L-Dopa) exist for the therapy of motor systems in PD. However, some motor symptoms such as freezing of gait, are not always responsive to L-Dopa and after several years of therapy, medication-induced side-effects, such as dyskinesias occur in around one third of the patients [88]. DBS of the subthalamic nucleus (STN) or globus pallidus internus (GPi) are effective surgical treatments, but both STN- and GPi-DBS can also cause side effects, such as dyskinesias or neuropsychological side effects, for example [89]. Electrodes targeting the STN are shown in fig. 1.5A.

DBS-Target: Subthalamic Nucleus

The STN is a small structure located within the basal ganglia. Other components of the basal ganglia are the striatum, the GPi, the globus pallidus externus (GPe) and the substantia nigra pars compacta (SNpc) and pars reticulata (SNpr)) [90]. The basal ganglia are connected to cortex and thalamus. This basal ganglia-thalamocortical circuit is involved in movement control [91], cognitive functions [92], reward processing and motivation [93]. In regard to movement control, three main pathways are considered important: The indirect, direct and hyperdirect pathway (see 1.5B).

The activation of the **direct pathway** is thought to promote movement. The direct pathway begins with the motor cortex sending excitatory signals to the striatum, which in turn inhibits GPi and SNr. As a result, the thalamus becomes more active/less inhibited and sends excitatory signals back to the motor cortex. As a consequence, motor cortical activity increases, facilitating movement [90].

Activating the **indirect pathway** is assumed to suppress movement. The indirect pathway is initiated by the striatum receiving excitatory inputs from the motor cortex. As a consequence, the striatum inhibits the GPe, resulting in the STN becoming less inhibited/more active. The STN then excites the GPi and SNr. Subsequently, both GPi and SNr increase their inhibition on the thalamus, which in turn results in less excitatory input to motor cortex, leading to movement inhibition [90].

The **hyperdirect pathway** is assumed to provide fast inhibition of movements. In this pathway, the motor cortex sends excitatory signals to the STN, resulting in the STN exciting both GPi and SNr. Consequently, the thalamus is more inhibited/less active, leading again to reduced activity in the motor cortex [94].
The STN is involved in movement control via the indirect and hyperdirect pathway. In PD, the STN is assumed to be overactive, leading to bradykinesia [95].

Pathophysiology

PD is a neurodegenerative disease characterized by the loss of dopaminergic neurons in the SNpc, which is speculated to result from the accumulation of alpha-synuclein in Lewy bodies [96]. Different models exist which explain how dopamine depletion leads to Parkinsonian symptoms [97]. The classical rate model suggests that dopamine depletion induces changes of firing rates within the basal ganglia, with decreased activity in the direct and increased activity in the indirect pathway. This imbalance is thought to result in an 'overinhibition' of the thalamus, which in turn reduces motor cortex activation, leading to bradykinesia. The model has dominated the field for many decades, with numerous observations supporting its validity. For instance, the model's prediction that "silencing" the STN would help restore the balance between the direct and indirect pathway, was supported by studies showing that inactivating the STN results in symptom reduction [98, 99]. However, not all experimental findings fit within this framework. One of its major limitations is that it does not adequately explain rigidity or tremor [97].

Beyond changes in firing rate, alterations in firing patterns, e.g. enhanced oscillatory activity at tremor and beta frequencies, have been observed in the basal ganglia ("Oscillatory model") [100]. Beta oscillations are thought to originate within the indirect pathway, specifically involving the reciprocal connection between the STN and GPe [101, 102]. Under normal conditions, dopamine is thought to decouple activity between STN and GPe. In the dopamine-depleted state this connection may become stronger, introducing increased beta activity [97]. Throughout the motor system, beta activity has been suggested as a promoter of the motor status quo [103]. Consequently, excessive beta activity in Parkinson's disease may result in increased postural maintenance, hindering the initiation of new movements and leading to bradykinesia. However, the causal relationship between beta oscillations and bradykinesia remains uncertain. While STN stimulation at beta frequencies has been demonstrated to slow movement in humans [104–106], studies in animals have reported that symptoms can arise before the emergence of beta peaks [107, 108]. It should also be noted that in the past the rate and the oscillatory model have often been regarded as separate entities, but there is evidence that both models describe the same phenomenon on different scales [109].

1.2.2 Essential Tremor

Essential tremor is considered the most common neurological movement disorder worldwide, affecting around 0.32 to 1.32 % of the global population [110]. The incidence follows a bimodal distribution, peaking in the second and sixth decade of life [111]. Essential tremor is defined as an isolated tremor syndrome characterized by bilateral upper-limb action tremor (4-12 Hz) persisting for at least three years, with or without tremor in other body parts, and no other neurological signs. Essential tremor plus refers to essential tremor with additional signs like mild ataxia or dystonic postures [112]. Although identifying major risk genes has been difficult, essential tremor almost certainly has a genetic component [113]. Environmental factors also play a role in its etiology [114]. Essential tremor is not curable, but therapies can alleviate symptoms. Propranolol and primidone are the primary pharmacological treatments for essential tremor, reducing tremor severity by approximately 50 % in about half of patients [9, 115]. However, due to side effects or insufficient efficacy, a large number of patients eventually stops these medications. [9, 116]. In severe and medical-refractory cases, surgical interventions such as DBS targeting the ventral intermediate nucleus of the thalamus (VIM) are effective. However, VIM-DBS (see 1.5A) can also cause adverse side effects, such as gait ataxia, dysarthria or muscle contractions. Another problem can be the loss of benefit over time [9, 115].

DBS-Target: Ventral Intermediate Nucleus of the Thalamus

The VIM is located in the ventral part of the thalamus (motor thalamus), which is connected to major motor regions of the brain. It receives inputs from both cerebellum and basal ganglia and connects reciprocally to motor cortex (see 1.5C) [117].

The **cerebellum** is located between cerebrum and brainstem and is an important motor region in the brain [118]. It controls and coordinates voluntary movements, is involved in timing of movement and grip force [119] and important for balance and locomotion [120].

The **motor cortex** is part of the frontal lobe, involving primary motor, premotor and supplementary motor cortex. It generates electrical signals that project via spinal neurons to muscles, contributing to the planning, control, and execution of movements [121].

Historically, the **motor thalamus** was viewed as a passive relay station for motor signals from the periphery to the cortex [122]. However, recent studies emphasize its role as an active modulator of motor information [123]. Based on its cytoarchitecture, the motor thalamus is further divided into cerebellar and basal ganglia input zones. The VIM is located in the cerebellar receiving zone [117] and receives predominantly

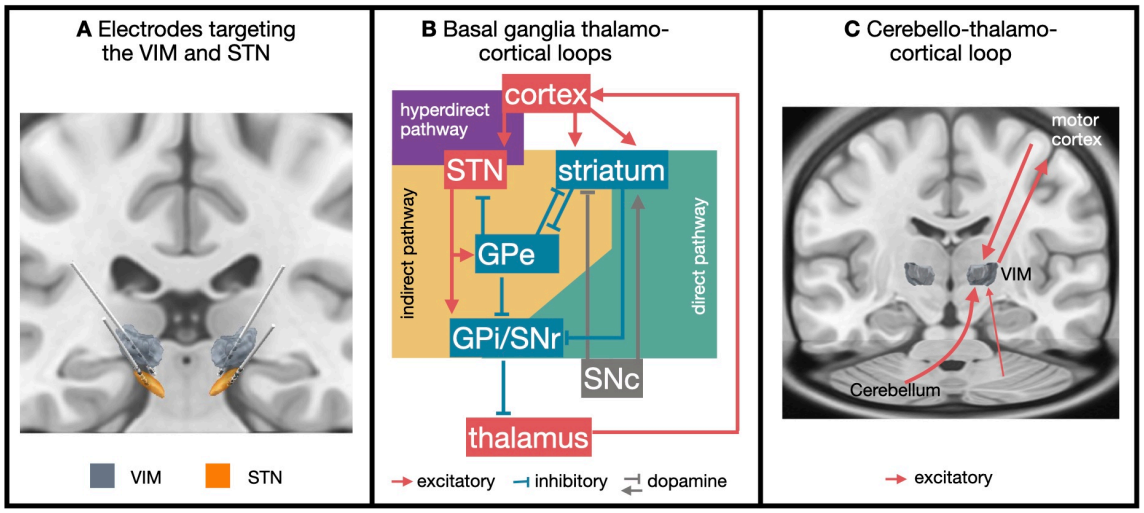

Figure 1.5: **Basal ganglia and cerebello-thalamo-cortical loops. A** Electrodes targeting the VIM and the STN. Electrodes were localized with LeadDBS [129]. **B** Scheme of basal ganglia thalamo-cortical loops: Direct, indirect and hyperdirect pathway. Figure adapted from [109]. CC BY 4.0. **C** Cerebello-thalamo-cortical circuit.

inputs from the contralateral cerebellum and to a minor extent from the ipsilateral cerebellum via the dentatorubrothalamic pathway [124, 125]. In the VIM, different firing patterns have been shown to be related to different motor states. For instance, during both passive and active movements of a limb, movement-related cells have been shown to fire [126], emphasizing the VIM's involvement in motor control. Additionally, neurons in the VIM exhibit tremor-related bursting activity during tremor episodes ("tremor cells") [127, 128]. The bursting patterns in these tremor cells have been found to be coherent with tremor activity [128]. The VIM serves as an effective neurosurgical target for tremor suppression and alongside reducing tremor, DBS seems to inhibit tremor firing within the VIM [127].

Pathophysiology

Electromyography (EMG) and accelerometry studies support a central, rather than a peripheral, origin of tremor. Specifically, a network involving the cerebellum, motor thalamus, cortex, and inferior olive is thought to be involved in essential tremor, supported by fMRI and electrophysiological studies [130–132]. However, the origin of pathological rhythmic activity remains poorly understood. For instance, it is not yet clear, whether essential tremor is a neurodegerative disease [9]. While some studies report indications for neurodegernation such as morphological changes or Purkinje cell loss in the cerebellum [133, 134], these findings have not been consistently replicated [135]. An additional observation that may or may not be related to neurodegeneration is a reduction in cerebellar gamma-aminobutyric acid (GABA)-

ergic tone in patients with essential tremor. Reduced GABAergic inhibition may lead to overactivity of cerebellar neurons resulting in abnormal oscillatory activity [136–138]. Moreover, pruning deficits of climbing fibers to Purkinje cell synapses have been reported in postmortem cerebella of patients with ET recently [139,140]. In a mouse model, such deficits have been shown to induce ET-like symptoms, and increased cerebellar oscillations have been linked to tremor severity in patients with essential tremor [139,141]. These findings point towards the cerebellum as primary source of tremor oscillations, which then propagate to efferent structures like the VIM [53]. However, other findings suggest that multiple nodes within the cerebello-thalamo-cortical circuit are capable of generating activity at tremor frequency, with tremor arising through dynamic interactions between these regions [116,117]. The oscillatory network hypothesis is supported by observations that neurons in the thalamus, inferior olive, and cerebellum possess distinct intrinsic electrical properties that enable independent oscillatory activity [130,142,143]. Moreover, the disruption of tremor by focal strokes at various sites within the circuit suggests that the network is initially involved in tremor generation [144].

1.2.3 Deep Brain Stimulation

A DBS-system consists of electrodes implanted in disorder-specific brain targets, an internal pulse generator, and connecting extension cables. The implantation of electrodes for DBS often already results in a short-term symptom relief after surgery, which is known as "stun-effect" [145,146]. To achieve therapeutic effects in the long-term, high-frequency stimulation ($>$100 Hz) is typically delivered via the internal pulse generator. While the exact mechanisms of action underlying DBS remain unclear, it has been observed that DBS affects both local and circuit activity.

On microscale, DBS modulates neural firing and interferes with neural plasticity. Each DBS pulse presumably activates presynaptic terminals in the target area, leading to neuronal responses depending on whether the synaptic input is inhibitory or excitatory [109]. In the VIM, high-frequency DBS initially increases firing, likely due to the predominant excitatory inputs that the VIM receives. This initial increase is followed by an attenuation in firing, probably caused by synaptic depression [127]. In the STN, where GPe-inhibitory inputs slightly dominate excitatory inputs, DBS results in sustained firing inhibition [147,148]. The local suppression of neuronal firing in both STN and VIM is associated with clinical symptom relief.

On mesoscale, DBS suppresses pathological oscillatory synchronization, such as STN beta activity in Parkinson's disease [149]. Another notable phenomenon observed in both the STN and GPi, but not in the VIM, is that DBS induces an evoked response within these structures [150,151]. The discovery of this DBS local evoked potentials or evoked resonant neuronal activity is relatively new and current research

is beginning to shed more light on its implications. **Article VI** reviews DBS local evoked potentials. These potentials are characterized by two positive-going peaks occurring within the 7 ms interstimulus interval during 130 Hz stimulation. This activity remains detectable for a short duration after stimulation cessation (see fig. 1.6A). It is speculated that DBS local evoked potentials are mediated by the inhibitory interaction with the GPe, as both STN and GPi, but not VIM, receive input from the GPe. DBS local evoked potentials can be observed under anesthesia and show their highest amplitude in regions with pronounced beta activity, suggesting their potential as biomarkers for precisely localizing stimulation targets.

At macroscale, STN-, GPi- and VIM-DBS have been shown to influence neural activity in cortical areas distant from the stimulation site, inducing evoked responses at different latencies [152,153]. Fig. 1.6B shows the cortical evoked response resulting from stimulation of the right STN in patients with PD. The responses are assumed to be a result of ortho- and antidromic activation of different pathways. Antidromic activation of the hyperdirect pathway by STN-DBS has particularly drawn attention, as it has been speculated to be related to the therapeutic effects in Parkinson's disease [152].

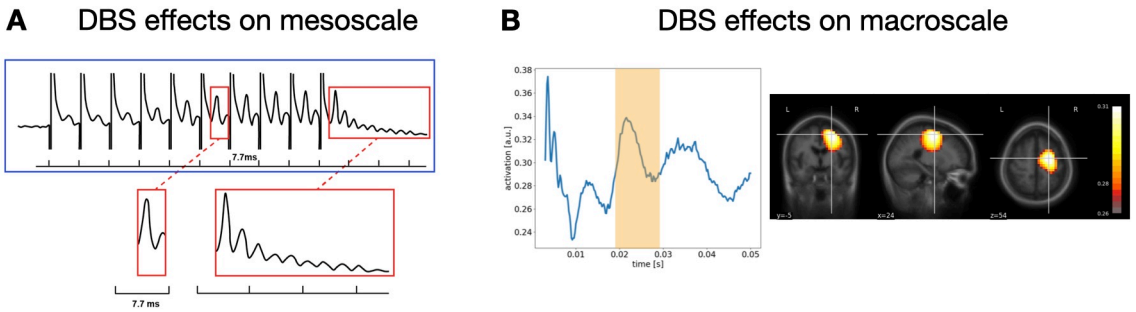

Figure 1.6: **DBS evoked potentials. A** STN-DBS elicits local evoked potentials within the STN. The evoked potential is characterized by a positive and two negative peaks in the interstimulus interval during 130 Hz stimulation. Figure is taken from **Paper VI** [154]. CC BY-NC-ND 4.0. **B** DBS of the right STN elicits evoked potentials in the cortex. The response occurring 19-29 s after the stimulation pulse is most pronounced in the right pre-motor cortex. The figure shows and average of 28 subjects that received low-frequency stimulation in the right STN (own-data).

1.3 Oscillations and Behavior

1.3.1 Electrophysiological Signals as Biomarkers

DBS is an effective therapy for movement disorders, but clinical outcomes vary between individuals, and stimulation-induced side effects may limit therapeutic suc-

cess [10]. Over the past years, considerable efforts have been made to identify markers reflecting symptoms with the aim of optimizing DBS treatment. Approaches to improve DBS involve adjustment of stimulation in response to signals associated with specific symptoms (adaptive or closed-loop DBS) [155, 156] or automated programming of stimulation parameters informed by electrophysiological markers [157, 158]. Neuronal oscillations, among other electrophysiological signals, have shown potential as biomarkers due to their correlation with disease states. However, oscillations occur under physiological conditions and before integrating these signals into clinical practice, it is crucial to distinguish pathologically altered oscillations from those reflecting normal brain function.

In non-invasive recordings, this issue can be addressed by comparing patient cohorts to healthy controls. For non-invasive recordings it becomes more challenging to unravel physiological and pathological activity, as invasive recordings cannot be performed in healthy individuals. There are different approaches to solve this problem. One possibility to link intracranial signals to pathology is to compare untreated (medication/stimulation OFF) with treated (medication/stimulation ON) states. Another approach is to compare activity across different disorders that use a common stereotactic target. Additionally, the relationship between symptom severity and neuronal oscillations can be investigated, or activity during specific motor symptoms, such as tremor or freezing of gait can be compared with episodes in which these symptoms are absent.

Moreover, it is important to note that oscillatory activity is not inherently pathological. For instance, beta oscillations occur in the healthy brain at rest and they undergo modulations during movement. However, in PD beta activity is pathologically altered and it is considered as a biomarker, reflecting the akinetic motor state. This characteristic makes beta oscillations a promising feedback variable for adaptive DBS [159, 160]. The following sections will provide an overview of how oscillations relate to behavior and disease.

1.3.2 Resting State

The human brain is constantly active, even during sleep or rest. The resting state refers to a condition in which a person is not focused on a specific task. Functional magnetic resonance imaging (fMRI)-studies, tracking slow fluctuations (<0.1 Hz) of the blood oxygenation level dependent (BOLD) signal [161], have shown that distinct networks form during rest that are consistent across individuals and studies, resembling those activated during sensory, motor, and cognitive tasks [162]. MEG and EEG studies have revealed corresponding networks, when appropriate frequency ranges are selected [163, 164]. The advantage of MEG compared to fMRI is that it captures fast dynamics that are not measurable by fMRI. Hence, MEG is able

to simultaneously investigate networks at different frequencies. Studies combining LFPs and MEG, for example, demonstrated that subcortical–cortex coupling shows frequency-specific coupling to different cortical regions during rest [165].

1.3.3 Movement

Voluntary Movement

Across various species, movement is linked to modulations of neuronal oscillations. At rest, the motor system is synchronized in the beta frequency range. This activity is suppressed just before and during movement [166]. Gamma activity, on the other hand, increases during movement. After movement termination, beta activity returns to its pre-movement level and temporary increases above this level (beta-rebound) [166]. The time-course of movement-related modulations of oscillatory activity in motor cortex and STN are displayed in fig 1.7A.

Beta oscillations are believed to stabilize the current motor state ("status quo") by suppressing distractions and alternative actions [103, 167]. Based on these findings, beta activity is often described as 'antikinetic', as it is thought to maintain the current behavioral state, with reductions in beta activity occurring when a change in the behavioral state is desired. The post-movement beta rebound may reflect an active inhibition of the motor network after movement together with the processing of sensory feedback [168].

Gamma oscillations scale with movement parameters like velocity and effort [169, 170] and might be involved in proprioceptive feedback processing to actively control movement [171]. In contrast to beta oscillations, gamma activity is often described as "prokinetic," meaning that it facilitates movement initiation and execution.

Movement-related modulations of oscillatory activity are usually stronger in the hemisphere contralateral than ipsilateral to movement. Such modulations of oscillatory activity have been found across the motor system in both cortical and subcortical structures and for inter-regional coupling [172–175]. Moreover, they occur in both the healthy state and in movement disorders and disturbances in these patterns may be related to pathology in movement disorders [176].

Tremor

Tremor is an involuntary, rhythmic movement of a body part [112], which can be physiological or pathological. Physiological tremor is of low amplitude, occurs in healthy individuals and can be enhanced by factors like drugs, fatigue, or anxiety. Pathological tremor has a higher amplitude and interferes with daily activities. It is a symptom of many movement disorders such as Parkinson's disease or essential tremor.

Tremor can have different origins, including mechanical oscillations of the limbs, reflex-induced oscillatory activity, central oscillators or an imbalance of feedforward and feedback systems. Tremor in essential tremor and Parkinson's disease is assumed to have a central origin, based on the observation that the frequency of tremor remains unaffected under mass loading [111]. The central source of tremor could be a single oscillator, or a system of interconnected oscillators [111].

Essential tremor is associated with pathological alteration within the cerebello-thalamo-cortical circuit [177]. Parkinsonian rest tremor is associated with two brain circuits: the basal ganglia and also the cerebello-thalamo-cortical circuit [178, 179]. The dimmer-switch model suggests, that the basal ganglia trigger resting tremor in PD, while the cerebello-thalamo-cortical circuit modulates its amplitude [177, 180].

Tremor-related oscillatory brain activity is assumed to be projected to muscles via motor pathways and peripheral nerves, resulting in observable tremor [181]. Fig. 1.7B shows the time resolved EMG, VIM and motor cortex power spectral densities in a patient with ET who experienced tremor. After tremor onset (0 s) power in the tremor frequency range (∼5 Hz) increases in the VIM and motor cortex contralateral to the tremulous limb.

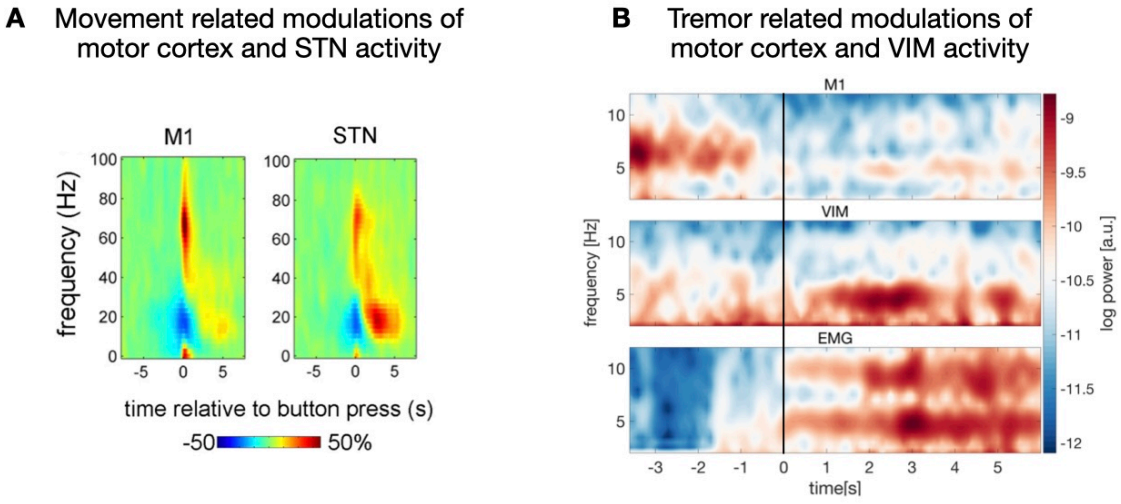

Figure 1.7: **Movement related modulations of oscillatory activity. A** Oscillatory activity in motor cortex (M1) and STN is modulated during simultaneous button pressing with index, middle and ring finger. Beta activity decreases shortly before and during movement, while gamma activity increases. Beta activity rebounds after movement cessation. Figure taken from [174]. CC BY-NC-SA 3.0. **B** After the onset of tremor (0 s) an increase of activity around tremor frequency can be observed in both VIM and M1 contralateral to tremor (own data).

1.3.4 Oscillations in Parkinson's Disease

Many spectral features are associated with specific symptoms in Parkinson's disease. Beta activity is the most frequently analyzed feature due to its strong link to motor symptoms such as bradykinesia and rigidity [10]. In the dopamine-depleted state of Parkinson's disease, exaggerated beta oscillations in the basal ganglia, especially in the STN, are correlated with bradykinesia [182,183]. Movement, DBS and L-Dopa reduce beta activity, and the beta reduction by both DBS and L-Dopa correlates with clinical improvements [183–186]. Beta activity in the STN also appears as a biomarker for guiding electrode implantation, as stimulating the dorsal region of the STN, where beta power is most pronounced, is associated with a stronger alleviation of symptoms.

Beyond bradykinesia and rigidity, resting tremor is associated with oscillations at tremor frequency, along with alterations gamma and high-frequency oscillations [187–189]. Further, tremor episodes have been linked to reductions in beta activity [190]. Moreover, excessive gamma activity (60-90 Hz) is linked to L-Dopa- and DBS-induced dyskinesias [191].

Oscillatory Coupling

Oscillatory coupling between the STN and cortex in the beta range has been extensively studied. The STN primarily couples with motor and premotor regions at beta frequencies during rest [165,192]. In contrast to STN power, which seems strongly correlated to PD symptoms, the relationship between STN-cortex coherence and motor impairment is less clear, as inconsistent results have been observed [192–194]. Furthermore, conflicting results have been observed following L-Dopa administration, with reports of both an increase and a decrease in STN-motor cortex coherence [165,192].

It has been proposed that this ambiguity might stem from STN-cortex coherence rather reflecting hyperdirect pathway activity rather than indirect pathway activity, which is more closely linked to PD pathophysiology (see 1.2.1). In context of these two pathways, there is also evidence for a sub-division of the beta band into a low-beta (13–21 Hz) and high-beta (21–35 Hz) band [169]. STN-cortex coupling in these bands appears to localize in different cortical regions, with high-beta coherence peaking more medially in the motor cortex and low-beta coherence peaking more laterally [193]. Furthermore, both beta sub-bands seem to play distinct roles in motor function and pathology [186,193,195]. Particularly, low-beta activity correlates with Parkinsonian symptoms [186] and may originate within the indirect pathway [193]. In contrast, high-beta oscillations in the STN are thought to be mediated by the hyperdirect pathway, and may be involved in physiological motor signaling [193,194].

1.3.5 Oscillations in Essential Tremor

Oscillatory activity in essential tremor has been less extensively studied than in Parkinson's disease. In essential tremor, oscillations related to tremor are the most frequently studied feature, as tremor is the primary symptom of ET. The spectral analysis of thalamic activity has revealed peaks at tremor frequency in the presence of tremor, that are absent when patients do not experience tremor [196]. Further, muscle activity from the tremulous limb has been found coherent with tremor-related thalamic activity [143]. Moreover, a negative correlation between beta power in the VIM and tremor amplitude has been reported [197].

Apart from tremor, VIM activity has also been studied when patients with ET were resting or performing a voluntary movement. For instance, one study reported beta peaks, primarily in the low-beta range, in the VIM power spectrum at rest [198]. During movement, beta activity has been shown to be suppressed, while gamma activity increases, with the onset of this gamma increase correlating with reaction time [170]. Both activity in the tremor frequency range and beta-band activity have been proposed as potential biomarkers for adapting DBS [196].

Oscillatory Coupling

VIM-cortex coupling, especially whole-brain coupling, has rarely been investigated. When investigated, the focus was again mainly on tremor. There are a few studies, that have combined recordings from the VIM with EEG recordings, but the sample sizes in these studies were relatively small. Another limitation is their focus on EEG activity from the motor cortex rather than examining whole-brain activity. For instance, one study reported coupling between the VIM and ipsilateral motor cortex at tremor frequency during tremor in two patients [199]. In line with these findings, a second study reported VIM-motor cortex coupling at tremor frequency in one essential tremor patient that experienced tremor during the experiment [200]. The same study reported beta band (8-27 Hz) coupling between VIM and ipsilateral sensorimotor cortex at rest [200].
A few other studies exist, that have investigated VIM-cortex coupling during voluntary movement, such as self-paced or externally triggered movement. These studies have found that VIM-motor cortex coupling in the beta range decreases during movement [200–202].

However, some studies exist that have examined whole-brain network activity in essential tremor. They did not investigate coupling between VIM and cortex, but focused on corticomuscular coherence, the coupling between muscle activity and MEG/EEG signals, during tremor.
Mixed findings have been made regarding coupling between muscle and motor cortex

during tremor: Some studies found increased coupling between muscle activity from the tremulous limb and motor cortex during tremor [178], while other studies made negative findings [203]. Further investigation revealed that cortical involvement might be intermittent [204], which might explain the ambiguous results regarding corticomuscular coherence in ET. In addition to activity in the motor cortex, activity in the cerebellum has been shown to be coherent with muscle activity during tremor [178]. In the same study both cerebellum and motor cortex coupled as well at tremor frequency in the presence of tremor [178].

2 Aims

This thesis investigated oscillatory coupling between the cortex and two subcortical nuclei: the VIM in essential tremor and the STN in Parkinson's disease.

In PD, oscillatory activity in the STN and coupling between STN and cortex has been extensively studied [165, 192, 193]. These studies have established the role of oscillations, particularly beta oscillations, in PD pathophysiology [169]. However, open questions remain, such as whether these oscillations provide insights into the therapeutic benefit of DBS.
In contrast, the oscillatory coupling between the VIM and cortex in essential tremor is not well understood, and its behavioral and clinical relevance needs to be established. A better understanding of VIM-cortex coupling could enhance clinical applications and improve therapeutic approaches. Key questions that remain unanswered include which cortical areas couple to the VIM at rest, whether the spatial organization of VIM-cortex coherence differs across frequency bands, and how VIM-cortex synchronization changes with tremor and voluntary movement.

The specific aims of the present thesis were as follows:

Study 1: Determine whether the symptom reduction following DBS can be predicted based on oscillatory activity and explore whether STN power or STN-cortex coherence serves as a stronger predictor of DBS outcome.

Study 2: Identify the cortical regions involved in resting-state coupling with the VIM and assess whether coupling in different frequency ranges exhibits distinct spatial topographies.

Study 3: Explore whether the VIM synchronizes with cortical and cerebellar activity at tremor frequency during tremor episodes in order to clarify the involvement of the cerebello-thalamo-cortical circuit in the pathophysiology of tremor.

Study 4: Assess whether VIM-cortex coherence is modulated during voluntary movement and identify the cortical regions involved in these modulations.

3 Methods

3.1 Recording Setup

The studies presented in this dissertation were based on simultaneous MEG and LFP recordings and had the same experimental setup. All patients who participated received surgery for DBS. Recordings happened the day after electrode implantation and the day before the simulator was implanted. This allowed for the recording of LFPs from the subcortical target in combination with MEG. For the LFP recordings, the deep brain electrodes were externalized and connected to amplifiers integrated into the MEG system via non-magnetic extension leads. The electrodes were implanted bilaterally, allowing for LFP recordings from both hemispheres. Dependent on the electrode type, signals were acquired from either four or eight contacts per electrode. The DBS electrodes were referenced against a surface electrode positioned on the left mastoid and then re-referenced offline using a bipolar referencing scheme to minimize volume conduction (see fig. 3.1). MEG signals were captured using a 306-channel MEG system by MEGIN (see fig. 1.2A). Additionally, muscle activity from the extensor and flexor muscles was recorded using surface EMG, and movement data was collected via accelerometers attached to the fingers.

3.2 Paradigm

Both PD and ET patients were recorded during rest (Study 1, Study 2). The PD patients were not recorded as part of this thesis, but were recorded in previous studies [165, 205]. After the resting state recordings, essential tremor patients were asked to perform multiple tasks, which were analyzed in Study 3 and Study 4 (for description see respective study).

3.3 Analysis of LFP and MEG Data

The data were processed with the Fieldtrip Toolbox [206], MNE-Python [207] and custom-written MATLAB and Python scripts. For local activity, the power spectral densities were calculated as described in 1.1.2 Box 3. The fitting oscillations and one over f (FOOOF) toolbox was used to decompose the spectrum into a periodic and aperiodic component [71], as illustrated in fig. 3.2A. To ensure good model fits, the results were visually inspected and the model parameters were adjusted if

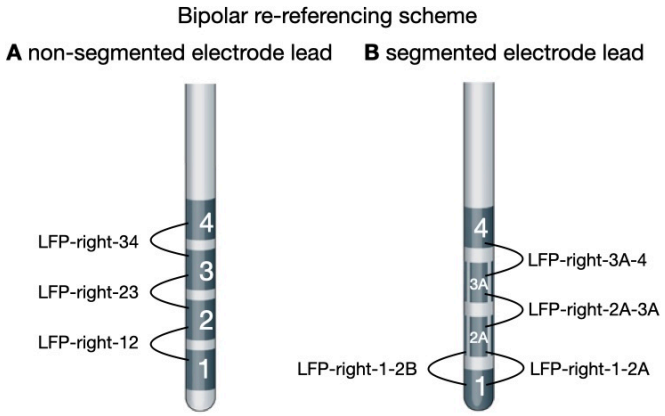

Figure 3.1: **Bipolar re-referencing scheme.** **A** For non-segmented leads, the signal from one ring contact is subtracted from the adjacent ring contact to create bipolar channels. For instance, subtracting the signal at level 1 from that at level 2 yields the bipolar channel '12'. **B** Segmented leads are typically composed of two ring contacts at top and bottom and two segmented contacts in between. Each segment on level 2 is referenced with each segment at level 3, resulting in channels such as '2A-3A', '2B-3B', '2C-3C'. Each segment at level 2/3 is referenced with the ring contact at level 1/4, resulting in bipolar channels such as '1-2A', '1-2B' or '3A-4'. Figure adapted from [160]. Reprinted with permission from Springer Nature.

necessary. Subsequently, the aperiodic component was substracted from the periodic component and only the latter was kept for further analysis. To quantify coupling between subcortical and cortical brain regions, coherence was calculated as described in Box 4. The MEG data was analyzed on source-level. For this, beamforming was applied on the data either in the time-domain using a linearly constrained minimum variance (LCMV [46]) beamformer or in the frequency domain using a dynamic imaging of coherent sources (DICS [47]) beamformer. Other methods, such as the machine-learning techniques (Study 1) and Granger causality (Study 2), specific to only one study can be found in the method section of the respective publication.

3.4 Statistical Analysis

For statistical analysis, cluster-based permutation tests were performed. The basic principles will be roughly explained in the following section. One challenge when performing statistical analysis on MEG data is the multiple comparisons problem which arises due to the large number of sensor/source, time and frequency pairs. Conducting a large number of statistical tests increases the family-wise error rate (FWER), which is the probability of falsely rejecting the null hypothesis or identifying a significant effect when none exists. A non-parametric cluster-based permutation

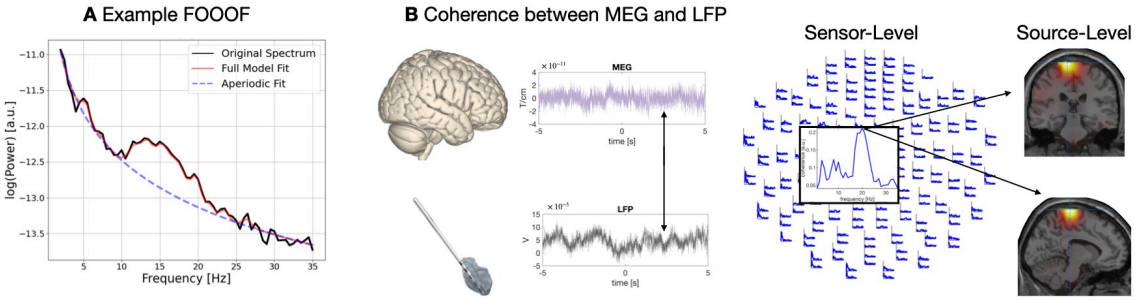

Figure 3.2: **Power and Coherence Analysis. A** Example of fitting oscillations and one over f (FOOOF) output. The FOOOF algorithm parameterizes the original spectrum into an aperiodic component (blue dashed line) and a full model fit (red line). **B** Coherence between MEG and LFP signal was calculated on sensor level and transferred to source space by beamforming.

test provides a solution for the multiple comparisons problem by controlling the FWER at a given critical alpha level. Cluster-based permutation tests can be applied to within-subject designs (e.g. testing the same participants under different conditions) and between-subject designs (e.g. comparing different cohorts under the same condition). The procedure works as follows: First, a test statistic (t-value) is calculated for each data point to identify potential significant effects. Then clusters are formed by grouping temporally and spatially adjacent data points that exceed a predetermined threshold and a summary statistic is calculated for each cluster. To obtain a p-value for a cluster, the data labels are randomly permuted, for example over the experimental condition. The result of this step is called a random partition and a test statistic is calculated on each random partition. The procedure is repeated many times (e.g. 1000 permutations) to construct a histogram of the test statistic (null distribution). For each random partition, only the cluster with the highest summed test statistic is kept. The null distribution is thus a description of the largest effects that might occur by chance. The p-value is calculated as the proportion of random partitions that resulted in a larger test statistic than the original one. If the p-value is smaller than the critical alpha-value, it can be concluded that the experimental conditions are significantly different [208].

4 Study 1: Neuronal Oscillations Predict Deep Brain Stimulation Outcome in Parkinson's Disease

4.1 Introduction

Current DBS systems face several limitations, including manual, time-consuming programming and the absence of automatic parameter adjustments. To improve therapy, it is essential to accelerate and automate the process of identifying optimal stimulation sites and parameters. A promising approach is to incorporate electrophysiological signals as feedback [209], as these signals have been linked to disease state and symptom severity (see 1.3.4).

For instance, oscillatory activity changes with fluctuations in symptom severity, a relation that can be exploited for the development of closed-loop DBS systems [210]. Moreover, oscillations have been shown to be informative about optimal stimulation site and can hence guide contact selection and lead placement [211, 212].

To automate and accelerate DBS programming, machine learning offers a powerful solution. Electrophysiological data, recorded by MEG or DBS macroelectrodes, are often complex and high-dimensional, making it challenging for traditional analysis methods to extract meaningful patterns [213]. Machine learning is particularly valuable in this context, as it can process large datasets, identify subtle patterns that might otherwise be missed, and make predictions based on these patterns. Moreover, machine learning models can adapt to new, unseen data, with the ability to generalize across patients and conditions. In context of DBS, machine-learning techniques can accelerate the identification of biomarkers, or the optimization of stimulation parameters. Further, machine learning techniques can operate in real-time which is useful for closed-loop DBS applications [214].

An important step toward more personalized DBS therapy would be the ability to predict stimulation efficacy based on short recordings after surgery. But why would electrophysiological data be predictive of DBS outcome? Beta oscillatory activity in the STN is correlated with bradykinesia and DBS suppresses this activity [184]. Further, a positive correlation between DBS outcome and both the length of the

oscillatory region in the dorsolateral STN and STN beta power had already been demonstrated [215]. Moreover, STN-cortex coherence may provide insights into which cortical regions are modulated by stimulation and could therefore serve as a predictor of DBS response (see 1.2.3). These observations suggest that neuronal oscillations might be useful biomarkers for predicting DBS efficacy. However, estimating stimulation outcomes based on network-level data involving multiple brain regions and frequency bands has not been done thus far.
Study 1 (**Article I**) aimed at predicting the reduction of motor impairment achieved by STN DBS based on local STN activity and STN-cortex coupling in patients with Parkinson's disease.

4.2 Methods

Simultaneous LFP-MEG recordings were acquired from 36 patients with Parkinson's disease as part of previous studies [165, 216, 217]. All patients were recorded at rest one day after electrode implantation in the medication-off state. In addition, motor symptoms were evaluated for each patient before surgery and again 3 to 6 months after electrode implantation. Motor symptom severity was quantified by the Unified Parkinson's Disease Rating Scale (UPDRS) III sum score.

For the machine learning analysis, features were extracted from the LFP-MEG data, including local STN power and STN-cortex coherence across eight frequency bands: delta/theta, alpha, low-beta, high-beta, low-gamma, high-gamma, slow high frequency oscillations (sHFO), fast high frequency oscillations (fHFO). STN-cortex coherence was localized using a beamformer and each source was mapped to one of 30 cortical parcels representing different brain regions (see fig. 4.1A).

The features were then used to predict stimulation outcome, which was defined as the symptom reduction achieved by DBS. The symptom reduction was quantified by the difference in UPDRS III scores before surgery and after DBS implantation with stimulation on. Only the features from the electrode contact that was used for stimulation when the post-surgery UPDRS III sum scores were assessed were included in the analysis.

Extreme gradient boosting was used to predict stimulation outcome, and predictions were generated by applying a leave-one-out approach where each subject was in the test set once and in the training set all other times (see fig. 4.1B). To assess model performance, the root mean square and Pearson correlation were calculated between the predicted and the actual data. Additionally, a null model was created that predicted DBS outcomes by averaging the results of the training set, serving as a baseline.

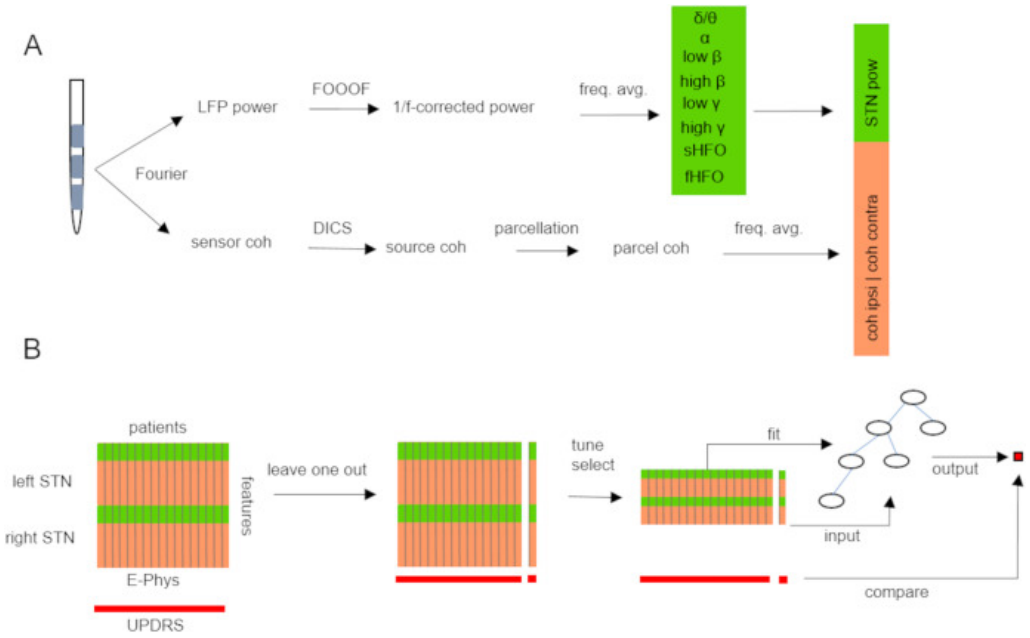

Figure 4.1: **Analysis Pipeline.** **A** Extraction of features. The power spectral densities and STN-cortex coherence were calculated for the selected LFP contacts. STN power spectra were 1/f corrected and activity within one frequency band was averaged. For coherence, a beamformer was applied to localize connectivity to the STN in source space. Each source was mapped to one of the 30 cortical parcels and coherence was averaged frequency- and parcel-wise. **B** Leave-One-Out Regression. Feature vectors from the left and right hemispheres were vertically concatenated to generate a subject-level feature vector. The subject features were combined horizontally for the feature matrix. In each iteration of the leave-one-out framework, one subject was held out as the test set, while the remaining data served as the training set. The training set was further split into three folds for cross-validated hyperparameter tuning and feature selection. The test set features were then fed into the regression model to predict reductions in the UPDRS III sum score. Taken from **Article I**. CC BY 4.0.

4.3 Results

4.3.1 Features

STN power contained peaks in the alpha, low-beta, high-beta band and in the sHFO range. Coherence between STN and cortex in the alpha band mapped mainly to temporal regions ipsilateral to the STN and in the beta band the STN coupled primarily to motor cortex.

4.3.2 Model Performance

The predictive model's performance was first evaluated separately for power and connectivity features as a function of number of features. The STN-cortex connectivity features performed better than the STN power features. A single connectivity feature was sufficient to outperform the null model, whereas at least four power features were needed. Based on these findings, a model was trained on five connectivity and five power features. A fixed feature set was taken for each subject and the taken features were the ones identified as most important features for predicting DBS outcome. For power, the most informative feature was high-beta activity and the connectivity model took particularly fHFOs and low-gamma oscillations into account (for details see **Article I** *2.2.6. Feature importance analysis* and *3.3. Feature importance*). The best performing connectivity model performed better than the best performing power model. Figure 4.2 shows the correlations between actual and predicted scores for the power and the connectivity model and the combination of both. A correlation of $r = 0.84$ between actual and predicted scores was achieved with the best performing connectivity (see fig. 4.2B), whereas a correlation of $r = 0.52$ was achieved with the best performing power model (see fig. 4.2A). Moreover, adding power features to the connectivity features did not improve the prediction of stimulation outcomes ($r = 0.84$, see fig. 4.2C).

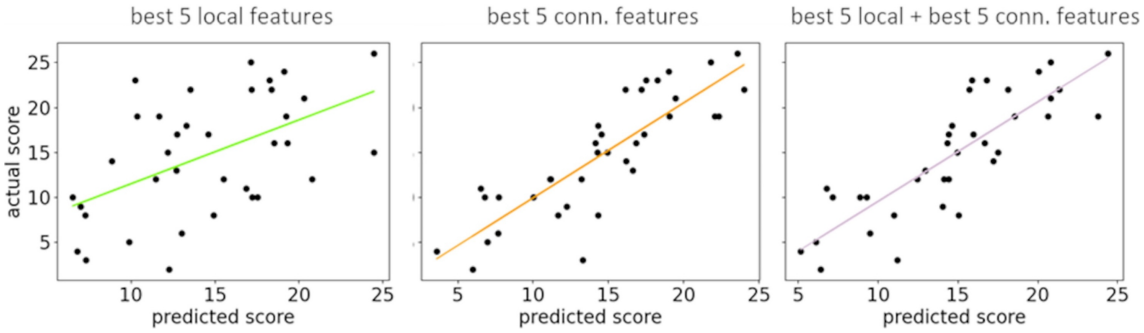

Figure 4.2: **Power and connectivity models.** The scatter plots illustrate the correlation between actual and predicted DBS outcomes when the five best power features (green), the five best connectivity features (orange) were taken and when the five best power and connectivity features were combined (purple). Taken from **Article I**. CC BY 4.0.

4.4 Discussion

Study 1 found that DBS outcomes can be predicted from STN power and STN-cortex coherence in Parkinson's disease patients, with STN-cortex coherence being a particularly strong predictor of DBS benefit.

There are several reasons why predicting the efficacy of DBS based on neuronal oscillations might be feasible. One reason is the close relationship between altered oscillatory activity and Parkinsonian symptoms. For instance, increased beta activity has been shown to correlate with bradykinesia [182,183], and there may even be a causal link between beta oscillations and motor symptoms (see 1.2.1). Moreover, DBS has been demonstrated to reduce these excessive beta oscillations [183]. If oscillations are indeed causal to symptoms and DBS effectively suppresses them, the strength of oscillatory activity at the stimulation site could serve as a potential indicator of DBS treatment efficacy.

Another possible explanation is that the efficacy of DBS may rely on its ability to reach and modulate distant cortical regions (see 1.2.3). In this context, STN-cortex coherence could reflect how strong a region of the STN is coupled to a cortical area. The present findings suggest that network effects of DBS may play a more critical role in its clinical efficacy, as connectivity models were found to be better predictors of DBS outcomes than STN power.

Furthermore, Study 1 may provide the electrophysiological counterpart to prior research linking DBS outcomes to anatomical connectivity [218,219]. These studies assessed the spatial reach of stimulation, often using methods like the volume of tissue activated, to determine which brain regions are affected by DBS [218]. Similarly, the functional connectivity used for predictions in the present study could reflect the strength of coupling between the stimulation site and the cortex.

A surprising finding of the study was that high-beta power emerged as the most informative feature of local activity, since low-beta oscillations are typically linked to symptom severity in Parkinson's disease [186]. However, this aligns with other studies suggesting that high-beta power better predicts motor improvement after therapies like DBS, while low-beta primarily reflects symptom severity [195,220,221]. The importance of high-beta activity for predicting DBS outcomes may relate to the hyperdirect pathway: high-beta activity in the STN is thought be mediated through the hyperdirect pathway [194], and DBS efficacy might involve antidromic activation of this pathway [152]. Thus, strong high-beta activity could indicate how effectively DBS activates the hyperdirect pathway. Notably, high-beta coherence was less important for prediction, which matches previous findings that showed no

correlation between STN-cortex coherence and symptom reduction following L-Dopa treatment (see 1.3.4).

4.5 Conclusion

Overall, the study confirms that neuronal oscillations provide valuable information about DBS outcomes. This relation could be exploited in the future for automated DBS programming, helping to accelerate the identification of the optimal stimulation contact or inform decisions about the most effective stimulation site.

5 Study 2: Mapping Subcortico-Cortical Coupling - A Comparison of Thalamic and Subthalamic Oscillations

5.1 Introduction

At rest, brain activity across different regions interacts, forming structured patterns observable in fMRI, MEG, or EEG recordings [163,164]. Moreover, frequency-specific subcortico-cortical oscillatory networks have been described for several nuclei targeted by DBS [193,222–224]. A well-studied example of subcortico-cortical coupling is resting state STN-cortex coherence. The STN primarily couples with temporal regions and the brainstem in the alpha band, while in the beta band, it predominantly couples with motor and premotor cortices [165]. These frequency-dependent interactions suggest a structured organization of subcortico-cortical coupling, which may be relevant for understanding DBS mechanisms.

While Study1 utilized the spectral and spatial features of coupling between cortex and STN to predict DBS outcomes in Parkinson's disease, it remains unclear whether the VIM exhibits frequency-specific coupling to the cortex, as comprehensive whole-brain descriptions of VIM-cortex coherence are lacking. However, there is some initial evidence that the VIM also engages in frequency-specific coupling with the cortex. For instance, combining EEG with LFP recordings from the VIM demonstrated beta-band coherence between the VIM and motor cortex at rest, which decreased during movement [201]. Study 2 (**Article II**) builds on this knowledge and aimed at characterizing VIM-cortex oscillatory coupling at rest in patients with essential tremor.

Furthermore, accumulating evidence suggests that subcortico-cortical coupling could be part of larger brain circuits that interconnect multiple brain regions, as similar frequency-dependent oscillatory networks have been observed across different subcortical nuclei [225]. To explore this further, Study 2 aimed to compare VIM-cortex coupling with STN-cortex coherence, seeking to identify both differences and similarities in oscillatory coupling.

5.2 Methods

19 patients with essential tremor undergoing surgery participated in the study and an equal number of patients with Parkinson's disease was included. MEG, LFP and EMG signals were recorded simultaneously, while patients were at rest. The patients were instructed to sit still with eyes open during the measurement. The recording length varied from 5-10 min for the ET group and from 5-30 min for the PD cohort. The PD patients were not recorded as part of this thesis, but were recorded in previous studies [165, 205].

For the PD patients, two measurements were conducted. One while on dopaminergic medication and one after medication withdrawal. The primary analysis of this study focused on the medication OFF state, while a control analysis was performed using signals recorded in the medication ON state.

At first, the power spectral densities were calculated for VIM and STN activity. The signal was decomposed into a periodic and aperiodic component and the aperiodic component was substracted from the original spectrum.
For further analysis, one contact was selected per hemisphere, chosen based on proximity to the suggested therapeutic "sweet spot" for VIM-DBS [226] and STN-DBS [211] (see fig 5.1A-B). Four hemispheres were excluded due to uncertain electrode position.

Whole brain maps of coherence were generated for the selected contacts in the theta (3-7 Hz), alpha (7-13 Hz), low-beta (13-21 Hz), and high-beta (21-35 Hz) frequency bands. To identify differences in VIM and STN spectral power and coherence, a cluster-based permutation test was performed, using hemisphere as the unit of observation rather than patient.

5.3 Results

5.3.1 Local Oscillations

Analysis of spectral power revealed that both the VIM and the STN exhibited activity in the alpha and low-beta frequency ranges (see fig. 5.1C). Spectral peaks in the high-beta range occurred particularly in the STN. Power in the high-beta range (19-33 Hz) was significantly higher than in the VIM.

5.3.2 Subcortico-Cortical Coupling

Interestingly, localizing brain regions coherent with VIM and STN activity demonstrated that the spatial patterns of VIM-cortex and STN-cortex coherence were very similar. Theta coherence localized to temporal cortex and hippocampus (fig 5.2A/B).

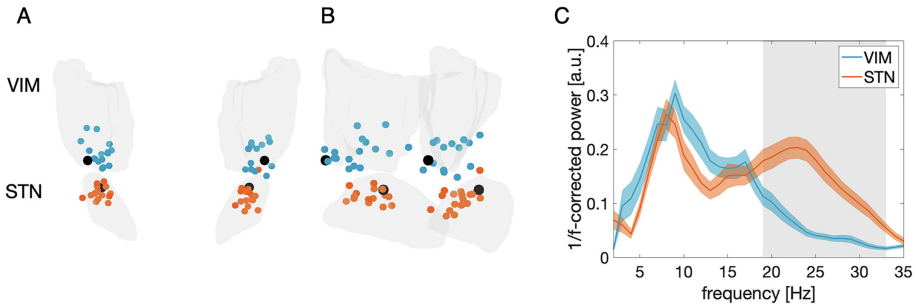

Figure 5.1: **Oscillatory activity in the ventral intermediate nucleus of the thalamus (VIM) and subthalamic nucleus (STN).** Reconstructed local field potentials recording sites shown in **A** frontal and **B** lateral view. Stimulation "sweet spots" are displayed in black. **C** Group- and hemisphere-averages of power spectral densities for VIM (blue) and STN (orange), following subtraction of the aperiodic component. Shaded regions indicate the standard error of the mean and gray shading represents significant differences between both nuclei. Taken from **Article II**. CC BY 4.0.

In the alpha band, VIM/STN coupled primarily to temporal cortex and brainstem (fig. 5.2C/D). In the low-beta band coherence was strongest to brainstem/cerebellum and motor cortex (fig. 5.2E/F), while in the high-beta band coherence localized to motor areas (fig. 5.2G/H).

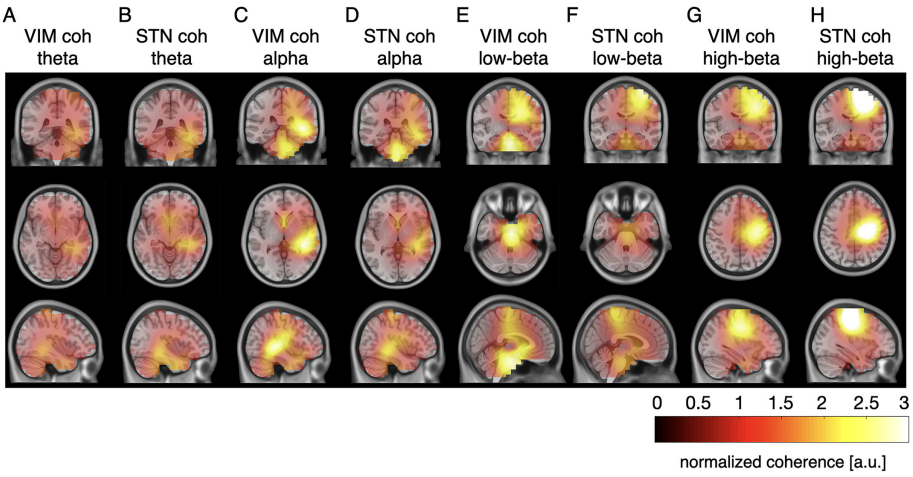

Figure 5.2: **Coupling between ventral intermediate nucleus of the thalamus (VIM)/subthalamic nucleus (STN) and cortex.** Group-averaged source-localized VIM-cortex coherence (**A**, **C**, **E**, **G**) and STN-cortex coherence (**B**, **D**, **F**, **H**). The right hemisphere corresponds to the ipsilateral side relative to the subcortical recording location. coh: coherence. **Article II**. CC BY 4.0.

5.3.3 Differences between VIM- and STN-Cortex Coupling

Despite the qualitative similarities, quantitative differences were observed. Low-beta coherence to the brainstem/cerebellum was stronger for the VIM (fig. 5.3A), while high-beta coherence to motor cortex was stronger for the STN (fig. 5.3B). Under dopaminergic medication, high-beta coupling between STN and motor cortex remained stronger than VIM-motor cortex coherence (see **Article II** Supplementary Fig. S2).

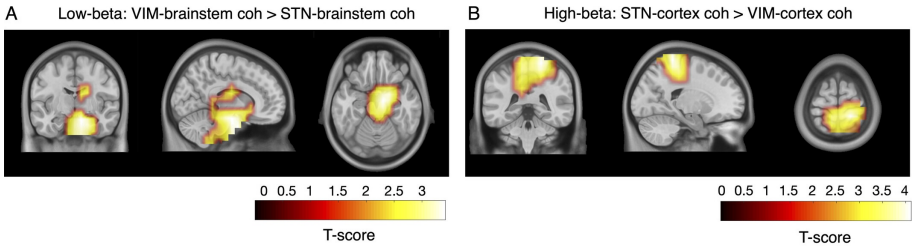

Figure 5.3: **Differences between cortical coupling to ventral intermediate nucleus of the thalamus (VIM) and subthalamic nucleus (STN).** **A** VIM–brainstem low-beta coherence > STN–brainstem low-beta coherence. **B** STN–cortex high-beta coherence > VIM–cortex high-beta coherence. Nonsignificant changes are masked. **Article II**. CC BY 4.0.

5.4 Discussion

Study 2 demonstrated in a whole-brain analysis that VIM-cortex coupling is spectrally and spatially organized. The cortical regions that were involved in coupling align with the VIM's anatomical connections to the motor cortex and the cerebellum [117].

One major discovery of Study 2 was that the topographies of VIM- and STN-cortex coupling were very similar. Previous studies have mapped oscillatory coupling between the cortex and other midbrain structures, such as GPi, nucleus basalis of Meynert, pedunculopontine nucleus in different diseases, including Parkinson's disease, obsessive-compulsive disorder, dystonia and Lewy body dementia [193, 222–224]. Interestingly, these studies found analogous resting state brain networks to the ones identified here, regardless of the specific subcortical structure or disease. This suggests that frequency-specific resting state subcortical-cortical coupling might reflect physiological large scale synchrony rather than disease specific networks.

Another key finding of Study 2 was that high-beta activity appeared as a distinct spectral feature of the STN, with both high-beta power and coherence higher in the STN compared to the VIM. While this could be related to PD, given the established

link between beta oscillations and PD pathophysiology, Study 2 found some indications for high-beta activity being STN- rather than PD-specific. When correlating high-beta coherence with disease severity, no correlation was found (**Article II** Supplementary Fig. S3). Furthermore, L-Dopa did not eliminate the difference in high-beta STN-cortex coherence and VIM-cortex coherence. Both findings suggest that high-beta activity may reflect a physiological rather than a pathological signal. This observation supports the notion that high-beta activity is linked to physiological motor signaling, whereas low-beta activity is more strongly associated with motor impairment (see also 4.4 for discussion) [183, 193, 194]. Moreover, Study 2 found evidence for high-beta activity being mediated through the hyperdirect pathway, as motor cortex activity led ("Granger-cause") STN activity in the high-beta band (for a detailed description of Granger causality analysis, see **Article II** *2.5 Directionality Analysis* and *3.4 Directionality Analysis*).

5.5 Conclusion

Study 2 revealed distinct spatial topographies of VIM-cortex coupling in different frequency bands. The similarity between VIM-cortex coupling and STN-cortex coupling suggests that some aspects of subcortical-cortex coupling might reflect universal features of oscillatory brain networks. Moreover, the study revealed that high-beta activity might be a spectral feature of the STN, possibly mediated by the hyperdirect pathway.

6 Study 3: Oscillatory Coupling between Thalamus, Cerebellum and Motor Cortex in Essential Tremor

6.1 Introduction

After presenting VIM-cortex coherence at rest in the previous study, Study 3 (**Article III**) explored how VIM-cortex coherence changes when patients experience tremor. The aim was to get an insight into the pathological mechanisms underlying tremor, with a particular focus on rhythmic brain activity at the tremor frequency.

As discussed in 1.2.2, essential tremor is thought to originate centrally rather than peripherally [111]. Consistent with this hypothesis, electrophysiological studies have demonstrated that various brain regions exhibit activity coherent with tremulous activity from the affected limb. For example, recordings from the VIM have revealed narrow-band oscillations at the tremor frequency when tremor is present [196, 227]. Additionally, studies combining MEG/EEG with EMG have shown coherence between tremor-related activity in the motor cortex and cerebellum [132, 178].

These findings suggest that synchronized oscillatory activity within the cerebello-thalamo-cortical circuit may play a key role in the pathophysiology of essential tremor. However, direct evidence for this hypothesis remains limited. To address this, the present study combined recordings from the VIM and cortex, allowing for the simultaneous investigation of both subcortical and cortical regions. Through this approach, Study 3 aimed to resolve the role of the cerebello-thalamo-cortical circuit in tremor.

6.2 Methods

This study included 19 patients with essential tremor. LFPs from the VIM were recorded simultaneously with MEG. Additionally, EMG electrodes were placed on both forearms to capture muscle activity. Measurements were conducted during a motor task designed to provoke postural tremor. In this postural task (HOLD), pa-

tients rested their elbows on a table and lifted both forearms with fingers spread and palms facing inward. The task lasted 7 min. The hold epochs (20 s) were interleaved with rest epochs (20 s) to minimize fatigue.

The EMG signals were visually inspected to identify epochs with tremor. This procedure was done for each body side separately. Figure 6.1A depicts an example trace of EMG activity in a patient that experienced tremor. Tremulous activity is visible as 5 Hz rhythmic activity. In this patient tremor started immediately after the arm was lifted. Tremor-free epochs were also determined. These were taken from the rest blocks in between the posture.

Although patients with essential tremor usually present with bilateral action tremor, due to the post-operative stun effect, tremor was only present in 10 patients in either one or both arms. One patient's hemisphere was excluded due to uncertainty regarding electrode placement. The data was analyzed per body side/hemisphere rather than per subject and 16 body sides were included in the final analysis.

VIM power spectra were calculated for all LFP contacts, and the contact exhibiting the strongest tremor-related peak contralateral to the tremulous limb was selected for further analysis. All power spectra were 1/f-corrected, and the aperiodic component was removed.

MEG signals were source-localized using beamforming. Coherence was calculated between the source-locaized activity and the selected LFP channel/the EMG channel recording muscle activity (corticomuscular coherence). Whole-brain coherence maps were constructed at the individual tremor frequency ±0.5 Hz. Both VIM-cortex coherence and corticomuscular coherence maps during tremor were contrasted with the respective maps when no tremor was present. Cortical regions showing the strongest differences were selected as regions of interest for correlation with tremor amplitude. Coupling strength at tremor frequency and coupling strength in the beta band (13-35 Hz) were correlated with tremor amplitude.

6.3 Results

6.3.1 Muscle and Thalamic Activity

In order to confirm the presence/absence of tremor, power spectra calculated from the EMG channels were inspected for peaks in the 4-8 Hz range. For the epochs labeled as tremor, clear peaks at tremor frequency were visible, which were absent in the tremor-free intervals (see fig. 6.1A). For each patient and each body side the individual peak tremor frequency was extracted (see **Article III** Table 2). The

average tremor frequency was 5.1 Hz ± 0.5 Hz. The averaged power spectral densities of the selected EMG channels are depicted in fig. 6.1B.
In the VIM, spectral peaks at tremor frequency emerged as well in the presence of tremor, which were absent during rest. Figure 6.1C shows the power spectra averaged over all VIMs contralateral to the tremulous body side. The spectra were shifted along the x-axis to align with individual tremor frequency.

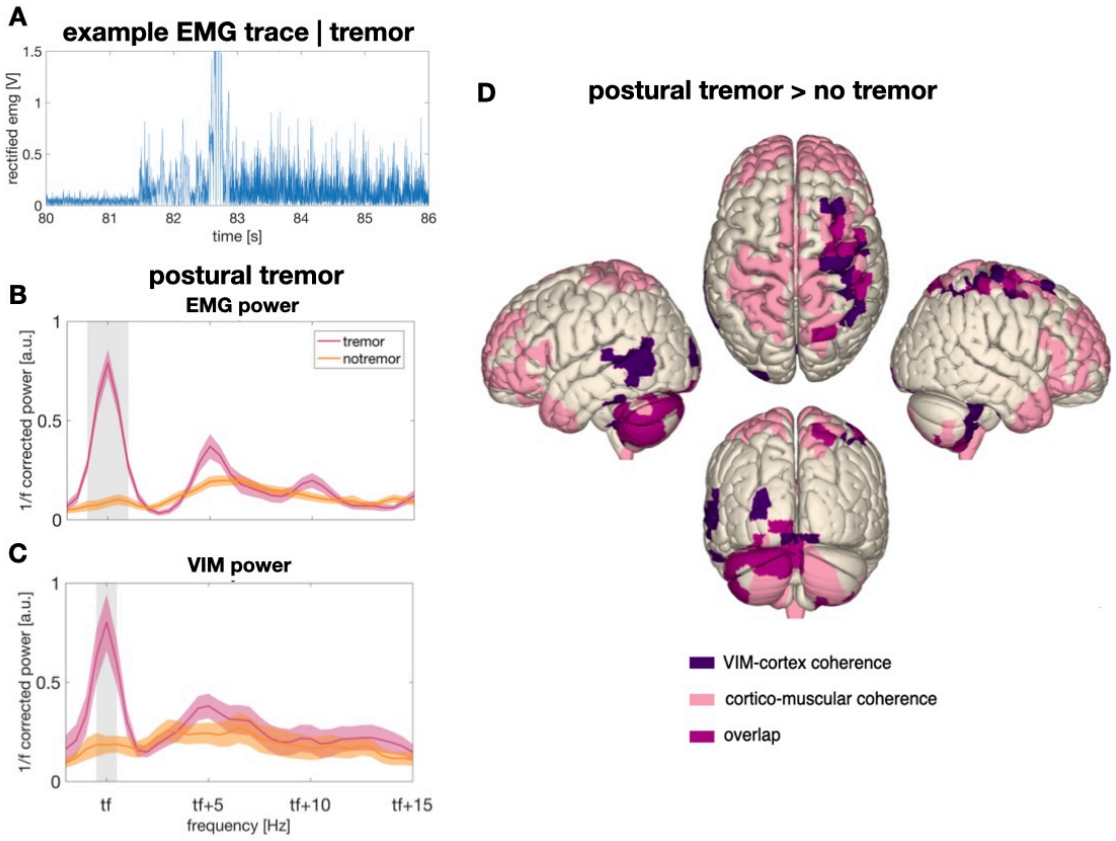

Figure 6.1: **Muscle/thalamic activity and coupling with cortex. A** Example trace of muscle activity recorded from a tremulous limb in one subject. Tremor started immediately after the arm was lifted. **B** 1/f corrected power spectral densities of muscle activity from the tremulous limb, **C** 1/f corrected power spectral densities of the VIM contralateral to tremor. **D** Thalamo-cortex coherence at individual tremor frequency increased during tremor. The surface plots indicate where in the brain significant increases where observed (purple). Corticomuscular coherence increased as well and the brain regions showing a significant effect are also illustrated (light pink). The overlap between thalamo-cortex coherence and corticomuscular coherence is displayed in pink. Only coherence with the VIM contralateral to tremor is displayed. Left hemisphere: ipsilateral to tremor; right hemisphere: contralateral to tremor. Reproduced from **Article III**. Rights are with author (Steina).

6.3.2 VIM-Cortex Coherence

Contrasting coupling at tremor with rest showed that VIM-cortex coherence at tremor frequency increased during tremor (see fig. 6.1D). This increase mapped to the primary motor cortex and the cerebellum ipsi- and contralateral to tremor. In addition, corticomuscular coherence increased as well. This increase was localized to the primary motor cortex, the cerebellum and the prefrontal gyrus. The spatial patterns of VIM-cortex and corticomuscular coherence overlapped, but were more wide-spread for the latter (see fig. 6.1D).

6.3.3 Coupling Strength and Tremor Amplitude

The cortical regions (motor cortex, cerebellum ipsi- and contralateral to tremor) showing the strongest differences were defined as regions of interest for correlation of coupling strength with tremor amplitude. For postural tremor, VIM-/EMG-motor cortex coupling strength at tremor frequency, but not VIM-/EMG-cerebellar coupling strength, correlated with tremor amplitude (see **Article III**, fig. 4/5). In the beta range VIM-motor cortex coupling strength was inversely correlated with tremor amplitude (see **Article III**, fig. 4).

6.4 Discussion

Study 3 demonstrated that oscillatory coupling between the VIM, cerebellum, and motor cortex increases during tremor. Moreover, it showed that this network is not only internally synchronized but couples with muscle activity as well. Hence, the findings provide further evidence for the involvement of the cerebello-thalamo-cortical circuit in the pathophysiology of essential tremor [117, 131–133, 178, 228].

A core achievement of the study was providing direct evidence for synchronization between the VIM and cerebellum. While this connection has long been hypothesized to be involved in tremor [177], it had not been demonstrated using simultaneous recordings from both the thalamus and cerebellum. One challenge in studying this relationship is that cerebellar activity is difficult to measure. In MEG, for example, there is an ongoing debate about whether cerebellar signals can be reliably detected [33]. In this study, tremor-synchronous activity was clearly localized to the cerebellum and from a methodological perspective these findings suggest that MEG is a valuable tool for studying cerebellar activity. However, further validation is necessary and could be done by comparing MEG recordings with recordings from DBS electrodes directly placed in the cerebellum, as recently implanted in patients with cerebral palsy in a clinical trial [229].

Apart from showing synchronization between cerebellum and thalamus, another contribution of this study was demonstrating that VIM and motor cortex synchronize during tremor. Previous studies have reported coherence at the tremor frequency between the VIM and EEG sensors positioned over the sensorimotor cortex, but only in a total of three subjects [199, 200]. Study 3 confirmed these findings and expanded upon them by explicitly showing motor cortex involvement in a brain-wide analysis. The correlation between VIM-/EMG-motor cortex coupling strength and tremor amplitude suggests that the connection between VIM and motor cortex may play a role in modulating tremor amplitude [230]. Clinically, this means that thalamo-cortical coupling could be used as a marker for tremor severity, and targeting this connection with neuromodulation techniques could help reduce tremors.

Another notable aspect of the study is the inverse relationship between VIM-motor cortex coherence in the beta band and tremor amplitude. This finding is particularly interesting, as typically voluntary movement is associated with a desynchronization of beta activity (see Study 4). However, previous studies have already shown a link between tremor and a reduction of beta activity. For example, in Parkinson's disease, tremor episodes have been associated with beta suppression [190], and in essential tremor, VIM beta power has been shown to negatively correlated with tremor power [197]. These results suggest that both tremor and voluntary movements share common underlying processes [181].

6.5 Conclusion

In summary, Study 3 confirmed the involvement of the cerbello-thalamo-cortical circuit in the pathophysiology underlying essential tremor.

7 Study 4: Modulations of Thalamo-Cortex Coupling during Voluntary Movement in Patients with Essential Tremor

7.1 Introduction

Study 4 (**Article IV**) explored the effects of voluntary movement on the VIM-cortex oscillatory networks determined in Study 2. As described in 1.2.2 the VIM is not only involved in tremor, but plays also a role for movement control, posture maintenance, and motor learning [231]. Along with this, movement related modulations of oscillatory activity have been observed in the VIM: Beta activity decreases during movement, while gamma activity increases [170]. As described in 1.3.3, these changes seem to be a characteristic feature of oscillatory activity across the whole motor system.

Movement-related modulations are not constrained to local activity but also affect inter-regional coherence. In the case of the VIM, studies have shown that beta coupling with the motor cortex decreases during self-paced or externally triggered hand movements [198,201,202]. However, the exact spatial distribution and temporal dynamics of these modulations are still not well understood. Study 4 aimed to explore the modulations of VIM-cortex coupling during an externally triggered button press task. More specifically, the study sought to identify the cortical regions involved in movement-related modulations.

As outlined in 1.3.3, beta activity is often considered as "antikinetic", based on findings in PD. Recording activity from the VIM in patients with essential tremor offers the unique opportunity to investigate if this relationship holds as well in patients who do not have akinesia. Hence, a second goal of the study was to assess whether there is a relationship between VIM-cortex coupling and how fast patients pressed a button after the presentation of a visual cue.

7.2 Methods

In Study 4, 10 patients with ET were asked to press a button with either the right or the left hand. The task was performed in 1-3 blocks, with each block lasting 8 min. Each block was evenly divided into left- and right-hand trials and began with a video showing which hand to use first. After half the trials, the hand was switched and the switch was indicated by a second video. At the beginning of each trial a black fixation cross was shown between 6-8 s, followed by a green cross signaling the Go cue to press the button. After pressing the button, the hand remained in motion as it returned to its starting position on the table.

One subject was excluded due to bad LFP signals throughout the recording and the hemisphere of a second subject was excluded due to unclear electrode position. Similar to study 2 and 3, the data was analyzed hemisphere-wise rather than subject-wise, with a total of 17 hemispheres going into final analysis. Dependent on the hand used for button pressing, one hemisphere was labeled as contralateral while the other was labeled as ipsilateral to movement.

Epochs were created from -4 s to 4 s relative to the button press (t = 0). Time-resolved power spectra were calculated for the VIM ipsilateral and contralateral to the moving hand. The LFP contact showing the strongest beta power suppression contralateral to movement was chosen for further analysis. VIM power during movement (-1.5 s to 2.0 s around button press) was compared against baseline (-3 s to -2 s before button press) activity. Time and frequency intervals showing significant differences were identified as intervals of interest for whole-brain coherence analysis.

VIM-cortex coherence was calculated on source-level for the identified time and frequency intervals. To assess movement-related changes, VIM-cortex coherence during the intervals of interest were contrasted with coherence during baseline by a cluster-based permutation test. Moreover, absolute coherence values around the time of the Go cue (-0.5 s to 0.5 s around Go cue) were calculated and correlated with reaction time (time of button press - time of Go cue).

7.3 Results

7.3.1 Thalamic Activity

Activity in the VIM was modulated before, during and after button pressing (fig. 7.1). Alpha and low-beta power in the VIM contralateral to movement decreased shortly before and during movement. Gamma activity increased during button pressing. After button pressing thalamic high-beta power increased. Similar patterns were visible in the VIM ipsilateral to the moving hand, but only the alpha-/beta-

suppression was significant compared to baseline. Based on these findings, the following time- and frequency-intervals were selected for coherence analysis: 8-20 Hz and -0.5 s to 0.5 s; 21-35 Hz and 0.5 s to 1.5 s; 65-85 Hz and -0.5 to 0.5 Hz.

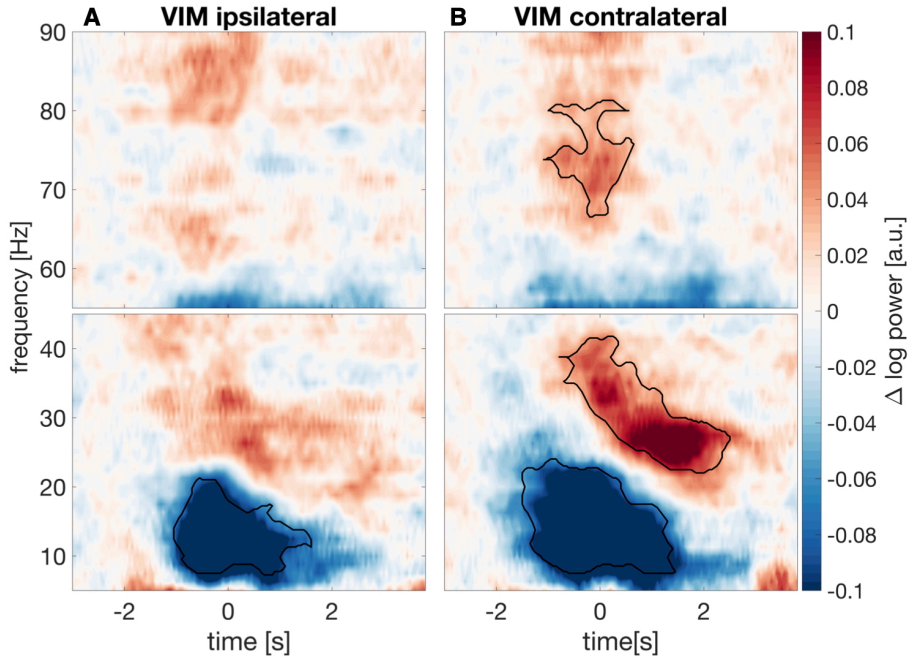

Figure 7.1: **Thalamic activity is modulated during voluntary movement** Modulations of activity in the VIM **A** ipsilateral and **B** contralateral to movement during button pressing. The black outlines mark significant changes ($p < 0.05$) compared to baseline (-3 s to -2 s before button press). Taken from **Article IV**.

7.3.2 Modulations of VIM-Cortex Coherence

A decrease in 8–20 Hz coherence was observed in the interval from -0.5 s to 0.5 s around the button press. This decrease occurred in coupling between cortex and both the VIM ipsi- and contralateral to movement. The strongest reductions in coherence were localized to the supplementary motor area and premotor cortex on both sides. Figure 7.2A indicates in which brain regions significant modulations occurred.

Additionally, an increase in high-beta coherence was observed following the button press (0.5 s to 1.5 s after button press). This increase was evident in the hemisphere contralateral to movement, with the strongest modulations occurring in similar regions as the coherence suppression, albeit more focally.

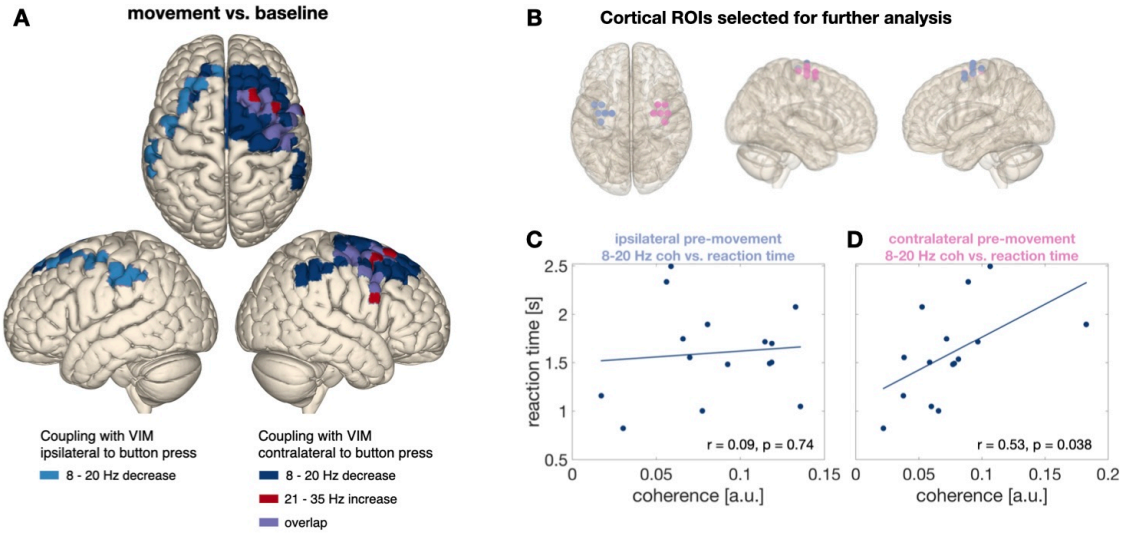

Figure 7.2: **Movement-related modulations of thamalamo-cortex coherence and correlation between thalamo-motor cortex coupling strength and reaction time. A** The surface plots illustrate significant effects observed when comparing VIM-cortex coherence during movement to baseline. Coupling between the cortex and VIM contralateral (dark blue) and ipsilateral (light blue) to movement increased in the 8–20 Hz range. Additionally, high-beta coherence (21–35 Hz) with the VIM contralateral to movement increased (red) after the button was pressed. The overlap between regions of coherence increase and decrease is marked in purple. Non-significant changes are masked. The left hemisphere corresponds to the ipsilateral side of movement, while the right hemisphere corresponds to the contralateral side. **B** Top and lateral views of grid points used as beamformer target locations for calculating coherence between the VIM and motor cortex to correlate reaction times with VIM-motor cortex coupling strength (8–20 Hz) around the Go cue in the hemisphere **C** ipsilateral and **D** contralateral to button press. Taken from **Article IV**.

7.3.3 Correlation with Reaction Time

Based on above results, a region of interest (ROI) was defined covering premotor and supplementary motor areas (see fig. 7.2B) in order to calculate VIM-motor cortex coupling strength in the two frequency interval 8-20 Hz and 21-35 Hz. Alpha/low-beta coherence (-0.5 s to 0.5 s around the Go cue) between the VIM and the motor cortex contralateral to the moving hand correlated with reaction time, meaning that higher 8-20 Hz coherence was associated with slower reactions (see fig. 7.2D). No significant correlation was observed for the hemisphere ipsilateral to movement (see fig. 7.2C) and no significant effect was observed for high-beta coupling.

7.4 Discussion

Study 4 demonstrated that voluntary movement is associated with modulations of thalamic oscillations and thalamo-cortical coupling in the hemisphere ipsi- and contralateral to movement. Thalamic power modulations were consistent with previous findings [170] and the movement related decrease of alpha-/low-beta coherence aligns with earlier studies as well [198, 201, 202]. Study 4, extends the knowledge by localizing the cortical regions involved to premotor and supplementary motor cortex. A novel finding of Study 4 was the increase in high-beta coherence following button press, which had not been described previously, and which might be analogous to the post-movement beta rebound (see 1.3.3).

Moreover, the findings indicate that low- and high-beta oscillations in the VIM are modulated differently during movement. This aligns with the commonly described subdivision of beta activity in the STN in Parkinson's disease. However, the origin of low- and high-beta activity in the VIM is less clear, since the VIM is not innervated by the indirect and the hyperdirect pathway like the STN (see Study 1 and Study 2 for further discussion). Despite the different origins, the sub-bands may serve similar roles in the VIM as in the STN. In this study, a positive correlation between low-beta VIM-cortex coupling and reaction time was observed, with stronger coupling in this band associated with slower button presses. This suggests that the concept of low-beta activity as "antikinetic" extends to thalamic oscillations in essential tremor, even in the absence of akinesia in this patient group. This finding underscores that low-beta oscillations are generally linked to movement slowing.
The origin and role of high-beta oscillations in the VIM requires further investigation, particularly as high-beta peaks were not prominent in the VIM during rest (see Study 2).

When comparing the findings of the present study with those of Study 3, which described tremor-related modulations, it appears that the brain regions involved in voluntary movement and tremor differ. Specifically, during tremor, the sensorimotor cortex proper was engaged rather than premotor or supplementary motor regions. This suggests that different thalamo-cortical connections may be active during tremor and voluntary movement. However, it is important to note that no direct statistical comparison was performed between these two tasks. As noted in Study 3, there were also some similarities between the two types of movement: in Study 3, stronger tremor was linked to weaker beta-band coupling between the VIM and motor cortex and in Study 4, beta activity was suppressed during voluntary movement. These findings suggest that beta suppression could be a common feature in both tremor and voluntary movement.

7.5 Conclusion

Study 4 demonstrated frequency-specific modulations of thalamo-cortical coupling during voluntary movement and highlighted that the notion of low-beta activity as antikinetic is also valid in the context of thalamo-cortical connectivity.

8 General Discussion

The present dissertation aimed at providing insights into oscillatory coupling between the cortex and two midbrain nuclei, the STN/VIM, in Parkinson's disease and essential tremor, respectively. By combining LFP recordings from the STN/VIM with MEG from cortical regions, subcortico-cortical coupling was characterized on network level and its role in both normal brain functions and the pathophysiology of PD and ET was assessed.

A major achievement of the thesis was the characterization of oscillatory coupling between the VIM and cortex in the human brain. While the VIM serves as an effective target for DBS, it's functional coupling to cortex had been largely unexplored. This work demonstrated that the VIM exhibits frequency-dependent coupling with the cortex at rest (Study 2) and that this coupling is modulated during both tremor (Study 3) and voluntary movement (Study 4). These findings highlight the VIM's involvement in tremor generation and motor control and align with the "modern perspective" on the VIM as an active modulator of output, while in the past it was seen merely as passive relay [117,231]. Hence, enhancing our knowledge about the VIM is crucial for understanding the mechanisms giving rise to both voluntary and involuntary movements.

The thesis not only expanded our knowledge about the VIM, it also contributed to research in essential tremor. Human brain functions are believed to require coordinated interactions between brain regions [181] and here the relevance of oscillatory coupling for both rest and movement in patients with ET was demonstrated. Additionally, the thesis provided novel insights into the pathological mechanisms that may underlie the disease (Study 3). It confirms the idea that pathologically synchronization across motor-related brain networks is involved in the generation of tremor [16,181]. Specifically, the thesis verified the involvement of pathologically synchronized oscillations across the cerebello-thalamo-cortical circuit in action tremor [230].

In regard to Parkinson's disease, this work confirmed previous results about STN-cortex coupling (Study 1 and Study 2). Particularly, high-beta activity emerged as a feature of the STN, which tallies with the idea that high-beta activity might be a characteristic signature of the STN [194]. Moreover, the thesis revealed that synchronization between STN and cortex is predictive of stimulation outcomes, supporting that DBS efficacy may be explained through network effects, with co-

herence indicating which cortical regions are modulated by DBS [232]. Study 1 further provided insights into how the knowledge of neuronal oscillations and their relationship to motor impairment or symptom severity can be applied in clinical practice. Currently, finding optimal stimulation settings remains a time-consuming trial-and-error process [233]. By leveraging the relationship between neuronal oscillations and disease-specific states, it may be possible to guide parameter selection or identify optimal stimulation sites, automating and accelerating the process with the goal of enhancing the efficacy of neuromodulation therapies.

In this context, the thesis identified specific markers that could serve as feedback variables. Study 1 demonstrated that STN-cortex coupling is a more informative predictor of DBS outcomes than STN power alone, highlighting coherence as a potential biomarker for treatment efficacy. Similarly, Study 3 revealed that VIM-motor cortex coupling strength at tremor frequency correlated with tremor amplitude, while beta coupling strength in the same connection was negatively correlated with tremor amplitude. These findings suggest that VIM-motor cortex coupling could serve as a marker reflecting tremor severity. Overall, these results underscore the clinical importance of oscillatory coupling between deep brain structures and the cortex.

While the exact relationship between structural and functional connectivity remains unknown [76], the thesis provides some evidence for a connection between structural and functional connectivity. The functional connectivity observed between the VIM and cortex (Study 2, 3 and 4) aligns with its structural connections to the cerebellum and motor cortex [234]. Furthermore, Study 1 suggests a potential link between structural and functional connectivity, as functional connectivity provided valuable information about stimulation outcomes, potentially due to its reflection of the fiber tracts modulated by stimulation. Additional support for this relationship comes from the observation that STN DBS-evoked cortical potentials (see 1.6) reach similar cortical regions to those involved in coupling to the STN.

Moreover, this thesis established some general ideas about oscillatory activity and oscillatory brain networks:
First, an interesting pattern emerges, when considering all studies collectively. While certain aspects of oscillatory coupling appear to be specific to a particular subcortical region or disease, other features seem to reflect universal properties of oscillatory brain networks. For instance, studies 1 and 3 demonstrated that the same cortical regions exhibit frequency-specific coupling with both the STN (in PD) and the VIM (in ET). Furthermore, when comparing these networks to oscillatory brain networks described for other midbrain nuclei, it becomes evident that they all share similar frequency-specific topographies [193, 222–224]. Additionally, movement appears to be accompanied by frequency-specific modulations of coherence that are

strikingly similar across subcortical nuclei and disorders. In Study 4, modulations of VIM-cortex coupling during voluntary movement were investigated in ET. Although these modulations were not directly compared to movement-related modulations of subcortico-cortex coherence in other patient groups, existing research indicates that the reduction in beta coherence during voluntary movement is not unique to ET or the VIM [174, 175]. Instead, it seems to be a general characteristic of the human brain. Similar observations apply to tremor-related coupling. The VIM couples with cortical regions and the cerebellum during tremor (Study 3), which aligns with previous studies in PD demonstrating that the STN couples as well with the cortex and the cerebellum during tremor [177, 180].
These findings provide evidence that functional connections may not be limited to a specific subcortical nucleus, but instead reflect synchrony within larger networks that comprise multiple brain regions. Additionally, these findings emphasize that understanding both the shared and distinct aspects of oscillatory brain networks is crucial for interpreting oscillations in the context of pathophysiology.

Second, this work revealed that several concepts of oscillatory activity, primarily described for the STN in PD, also apply to the VIM in PD, supporting the existence of "universal properties" of neuronal oscillatory activity. For instance, while the distinction between low- and high-beta oscillations is well established in the STN in PD, Studies 2–4 suggest that this sub-division, along with the distinct functional roles of different beta rhythms, also applies to the VIM in ET. In the STN, low- and high-beta activity is associated with the indirect and hyperdirect pathways, respectively. However, since the VIM is not innervated by these pathways, the origins of low- and high-beta activity in the VIM is less clear. Despite the potentially different mechanisms giving rise to these rhythms, VIM and STN beta oscillations appear to result in comparable behavioral outcomes. In PD, excessive low-beta activity correlates with bradykinesia. Study 4 found that higher low-beta VIM-cortex coherence was associated with longer reaction times in a cued button press task, suggesting that increased low-beta coherence may contribute to movement slowing, even in patients with ET who do not have akinesia. These findings reinforce the idea that certain characteristics of neuronal oscillations are universal across brain regions and disorders. They further emphasize the role of beta oscillations in motor control, showing that the concept of beta activity as antikinetic extends beyond Parkinson's disease. Generally, these observations also demonstrate that oscillations are not pathological per-se.

At the same time, while the observations made in the present work highlight shared oscillatory mechanisms across disorders, they also reveal that similar oscillatory dynamics can be linked to different behavioral states. For instance, both voluntary movement vs. tremor (involuntary movement) were associated with similar modula-

tions of oscillatory activity. Study 3 revealed that stronger tremor was associated with lower VIM-motor cortex coherence in the beta range and study 4 showed that VIM-motor coherence decreases with voluntary movement, suggesting that both types of movement may involve similar underlying mechanisms. Additionally, this highlights that beta reduction is not just a feature relating to voluntary movement, but relates also to involuntary movement, highlighting that it is crucial to account for the motor or disease state at the time of recording when interpreting oscillations.

8.1 Limitations

One limitation common to the studies presented is the relatively small sample sizes. In Study 1, the patient cohort was large for a MEG-LFP study (36 patients), but the sample size was not large for a machine learning study. To improve predictive accuracy and generalizability, larger cohorts and also patients from different centers should be included in the future.

Similarly, in Study 3, the sample size was small, as many patients did not exhibit tremor during the tremor-provoking task due to the post-operative stun effect. Nonetheless, when comparing the sample size in Study 3 to previous studies, it is still substantially larger [199, 200].

A broader concern involves the nature of oscillatory activity itself. Recent debates suggest that oscillations may not always be rhythmic [61] and that traditional analysis may not be able to capture certain aspects of the data, such as non-oscillatory aperiodic activity or waveform shapes [73]. For power, it was tried to account for that by utilizing the FOOOF algorithm which decomposes the power spectra into an aperiodic and a periodic component. However, there are also some methodological challenges of FOOOF that can introduce biased estimates [235].

8.2 Outlook

While it is well established that there is a correlative relationship between oscillations and both behavior and disease, the causal mechanisms remain poorly understood [236]. In the future, it is important to gain a deeper understanding of the causal link between oscillations, behavior and disease, to further advance our knowledge about the pathophysiological mechanisms underlying neurological diseases.
Beyond identifying the mechanisms that give rise to symptoms, it is equally important to understand how pathological activity spreads through brain circuits and where it originates. While Study 2 investigated Granger causality for resting state activity, Study 3 and 4 provided solely coherence measures, which do not allow for investigations of directionality. It is important that future studies investigate the

directionality of coupling also for tremor and voluntary movement. This knowledge could enable targeted interventions to suppress abnormal activity before it spreads, potentially enhancing treatment outcomes.
Especially in ET, there is still a need to advance therapies, such as new pharmacological treatments and DBS optimization [115,237]. Similar, patients with PD would benefit from improved and more personalized stimulation strategies.

Current efforts to enhance DBS are focused on the development of adaptive/closed-loop DBS systems that stimulate only when symptoms occur and adjust parameters based on e.g. electrophysiological feedback variables [160]. However, for the clinical use of adaptive/closed-loop DBS systems it is necessary to find reliable biomarkers [238]. In PD, beta activity and in ET, oscillations in the tremor range are considered potential biomarkers [196,210]. In the past, biomarkers have been mainly established through conventional analytic methods, such as spectral analysis of local brain activity. However, it has become evident that there are some limitations to these approaches as they fail to reflect some aspects of the data, such as bursts or waveform shape asymmetries. These aspects seem to contain valuable information about diseases as well, as they have been shown to relate to symptoms [238,239].

Moreover, while past efforts to identify biomarkers have primarily focused on activity within a single brain region, measures like coherence and phase-amplitude coupling may also serve as valuable biomarkers for adaptive/closed-loop DBS [202,238]. The present studies suggest that coherence can indeed act as a biomarker for adaptive DBS, as a direct relationship was observed between STN-cortex coherence and DBS efficacy, as well as between VIM-cortex coherence and tremor severity. Furthermore, Study 1 indicates that connectivity may, in some contexts, be more advantageous than local synchrony, as connectivity-based models outperformed power-based models for predicting DBS outcomes. This underscores the potential of network-based biomarkers to refine neuromodulation strategies.

In addition to optimizing DBS, future research might further explore the clinical utility of non-invasive stimulation techniques. Non-invasive techniques, such as transcranial alternating current stimulation have been shown to modulate oscillatory activity in both Parkinson's disease (PD) and essential tremor (ET), improving bradykinesia [240] and alleviating tremor [228,241]. They could hence complement existing therapeutic options without the need for brain surgery [240], but for movement disorders, they are not yet approved in clinical settings. To translate these techniques into clinical practice, a deeper understanding of which brain oscillations and cortical regions contribute to specific disorders is required.

However, this knowledge cannot be gained solely from controlled experiments in

research settings, it also requires studying brain activity in real-world conditions. A key step in this direction is the use of long-term recordings collected outside the traditional research setting including at home environments. Such data is essential for understanding how disease symptoms and brain activity change over time. Until recently, brain oscillations linked to neurological disorders could only be recorded during brief clinical visits, typically lasting just a few minutes or hours. Now, advances in technology allow for continuous brain activity recording [242], even after the DBS system has been implanted. This makes it possible to track how brain activity fluctuates in daily life, providing new insights into the relationship between symptoms and brain networks.

Apart from optimizing stimulation, it is important to gain deeper insights into the pathophysiology of ET. For this, the relationship between oscillatory activity and symptoms such as cognitive decline in patients with essential tremor plus could be explored in the future. In PD, cognitive impairment has been linked to alterations in oscillatory activity, particularly changes in beta synchronization within the cortico-striato-thalamo-cortical loop [243]. However, in ET, the role of oscillations in the VIM and VIM-cortex coupling in relation to cognitive deficits remains unexplored. Investigating this relationship could further advance our understanding of the underlying mechanisms of essential tremor.

8.3 Conclusion

In conclusion, this thesis provided novel insights into subcortico-cortical networks in the human brain. It identified some universal characteristics of oscillatory brain networks and established the role of oscillatory coupling for motor behavior. Moreover, the work made a significant contribution to deepening our understanding of the pathophysiology of essential tremor and Parkinson's disease. It also presented evidence for subcortical-cortex coupling as a potential clinical biomarker, which could inform future neuromodulatory therapies.

9 Scientific Publications

9.1 Article: Neuronal oscillations predict deep brain stimulation outcome in Parkinson's disease

Reproduced from

Jan Hirschmann*, Alexandra Steina,* Jan Vesper, Esther Florin,& Alfons Schnitzler
Neuronal oscillations predict deep brain stimulation outcome in Parkinson's disease
Brain Stimulation **15**, 792-802 (2022)

Digital Object Identifier (DOI): https://doi.org/10.1016/j.brs.2022.05.008
*These authors contributed equally to this work.

Statement of contribution

J.H. planned the research project. The data recordings took place as part of previous studies. My contribution to this work was to create a database of the previously recorded data. I did a part of the analysis (50%) and I was writing parts of the manuscript, together with J.H.

Copyright and license notice

Brain Stimulation 15 (2022) 792–802

Contents lists available at ScienceDirect

Brain Stimulation

journal homepage: http://www.journals.elsevier.com/brain-stimulation

Neuronal oscillations predict deep brain stimulation outcome in Parkinson's disease

Jan Hirschmann [a, 1, *], Alexandra Steina [a, 1], Jan Vesper [b], Esther Florin [a], Alfons Schnitzler [a, c]

[a] Institute of Clinical Neuroscience and Medical Psychology, Medical Faculty, Heinrich Heine University, 40225, Düsseldorf, Germany
[b] Functional Neurosurgery and Stereotaxy, Department of Neurosurgery, Medical Faculty, Heinrich Heine University, 40225, Düsseldorf, Germany
[c] Center for Movement Disorders and Neuromodulation, Department of Neurology, Medical Faculty, Heinrich Heine University, 40225, Düsseldorf, Germany

ARTICLE INFO

Article history:
Received 21 January 2022
Received in revised form
6 May 2022
Accepted 7 May 2022
Available online 11 May 2022

Keywords:
Parkinson's disease
Deep brain stimulation
Neuronal oscillations
Subthalamic nucleus
Machine learning

ABSTRACT

Background: Neuronal oscillations are linked to symptoms of Parkinson's disease. This relation can be exploited for optimizing deep brain stimulation (DBS), e.g. by informing a device or human about the optimal location, time and intensity of stimulation. Whether oscillations predict individual DBS outcome is not clear so far.
Objective: To predict motor symptom improvement from subthalamic power and subthalamo-cortical coherence.
Methods: We applied machine learning techniques to simultaneously recorded magnetoencephalography and local field potential data from 36 patients with Parkinson's disease. Gradient-boosted tree learning was applied in combination with feature importance analysis to generate and understand out-of-sample predictions.
Results: A few features sufficed for making accurate predictions. A model operating on five coherence features, for example, achieved correlations of $r > 0.8$ between actual and predicted outcomes. Coherence comprised more information in less features than subthalamic power, although in general their information content was comparable. Both signals predicted akinesia/rigidity reduction best. The most important local feature was subthalamic high-beta power (20–35 Hz). The most important connectivity features were subthalamo-parietal coherence in the very high frequency band (>200 Hz) and subthalamo-parietal coherence in low-gamma band (36–60 Hz). Successful prediction was not due to the model inferring distance to target or symptom severity from neuronal oscillations.
Conclusion: This study demonstrates for the first time that neuronal oscillations are predictive of DBS outcome. Coherence between subthalamic and parietal oscillations are particularly informative. These results highlight the clinical relevance of inter-areal synchrony in basal ganglia-cortex loops and might facilitate further improvements of DBS in the future.

1. Introduction

Parkinson's disease is a common neurodegenerative disease, affecting approximately 6.1 M people worldwide [1]. Besides pharmacological agents such as levodopa, deep brain stimulation (DBS) is used for symptomatic treatment of Parkinson's disease. A common target structure for DBS is the subthalamic nucleus (STN) which is interconnected with the pallidum, the thalamus and several cortical areas via basal-ganglia cortex loops [2]. In patients with Parkinson's disease, activity in these loops is characterized by strong neuronal oscillations, synchronized across the connected structures [3].

Neuronal oscillations are closely related to Parkinsonian symptoms. STN beta oscillations (13–35 Hz), in particular, have been shown to reflect the motor state [4]. They are reduced by voluntary movement, pharmacological therapy and DBS [5–10]. High-gamma oscillations (60–90 Hz), in contrast, are a marker of dyskinesia, typically arising as a side-effect of dopaminergic therapy [11]. Tremor is associated with narrow-band oscillations at individual

* Corresponding author. Institute of Clinical Neuroscience and Medical Psychology, Heinrich Heine University, Universitätsstr. 1, 40225, Düsseldorf, Germany.
E-mail address: Jan.Hirschmann@med.uni-duesseldorf.de (J. Hirschmann).
[1] These authors contributed equally to this work.

https://doi.org/10.1016/j.brs.2022.05.008

Abbreviations

DBS	deep brain stimulation
FDR	false discovery rate
fHFO	fast high frequency oscillations (300–400 Hz)
FOOOF	fitting oscillations and one over f
LFP	local field potential
MEG	magnetoencephalography
RMSE	root mean squared error
sHFO	slow high frequency oscillations (200–300 Hz)
STN	subthalamic nucleus
UPDRS	Unified Parkinson's disease Rating Scale

tremor frequency, observable throughout a distributed subcortico-cortical tremor network [12,13]. Given their intricate relationship with Parkinsonian symptoms, recent studies have explored the utility of neuronal oscillations for optimizing DBS.

Most of these studies have focused on the dynamics of electrophysiological signals and used oscillations for adapting DBS to spontaneous changes of symptom severity, such as on-off-fluctuations [14] or tremor [15,16]. Other studies have assessed the utility of quasi-stationary oscillatory activity for optimizing electrode placement, complementary to imaging studies on “sweet spots” in DBS [17,18]. Zaidel et al. demonstrated a positive linear correlation between DBS outcome and both the length of the oscillatory region in the dorsolateral STN and STN beta power [19].

Here, we adopted a similar, though more holistic approach for exploring the relationship between DBS outcome and neuronal oscillations. We analyzed simultaneous magnetoencephalography (MEG) and local field potential (LFP) recordings from Parkinson's disease patients with externalized leads to assess both STN oscillations and their synchrony with cortical activity. By applying machine learning techniques, we demonstrate that it is possible to predict DBS outcome for unseen patients based on their patterns of neuronal synchrony, considering many frequency bands and brain areas simultaneously.

2. Materials and methods

The aim of this study was to predict motor symptom reduction achieved by DBS based on band-limited STN power and STN-cortex coherence. For this purpose, we trained and evaluated a machine learning model operating on features extracted from MEG-LFP datasets, contributed by two previous studies performed at the University Hospital Düsseldorf [20,21]. Both studies recruited patients with Parkinson's disease selected for DBS of the STN according to standard clinical criteria.

2.1. Patient and measurement details

36 Parkinson's disease patients implanted with deep brain electrodes for STN DBS the day before the measurement took part with written informed consent, according to the Declaration of Helsinki. Patient details are given in Table S1 of the Supplementary Material. The experimental protocols were approved by the Ethics Committee of the Medical Faculty of Heinrich Heine University Düsseldorf (no. 3209 and 5608).

The experimental procedures have been described elsewhere [20,21]. Briefly, MEG signals were recorded by a 306-channel MEG system (Elekta Neuromag) with a sampling rate of 2 kHz (study 1) or 2.4 kHz (study 2). LFPs were recorded simultaneously using externalized leads and a mastoid reference. LFP signals were arranged into a bipolar montage offline. The cables used for externalization contained very little ferromagnetic material and did not cause major MEG artifacts. Forearm electromyograms as well as vertical and horizontal electrooculograms were recorded in addition. Patients were at rest in an upright position, with eyes open. The measurements took place after overnight withdrawal from dopaminergic medication (Med OFF). In a subset of patients, we performed additional recordings about 1 h after intake of levodopa (Med ON). Here, we analyzed the Med OFF data only.

The Unified Parkinson's Disease Rating Scale (UPDRS) part III of the Movement Disorders Society [22] was obtained by an experienced movement disorder specialist following optimization of DBS parameters. In most cases, scoring took place between 3 and 6 months after the LFP-MEG measurements (Table S1, Supplementary Material).

2.2. Data analysis

The general analysis pipeline is depicted in Fig. 1. It contained one sub-pipeline for feature extraction (Fig. 1A) and one for prediction (Fig. 1B).

2.2.1. Contact selection

First, we selected one electrode contact pair for each hemisphere by picking the contact used for therapeutic DBS at the time of UPDRS assessment and the closest neighboring contact in the direction of the midpoint between the most ventral and the most dorsal contact. This choice was adapted in case therapeutic DBS was bipolar or in case the initial choice included bad LFP channels, i.e. channels with strong noise/weak signal. In the former case, we selected the bipolar pair used for therapeutic DBS, and in the latter case, we took the closest neighbor of the bad channel in the direction of the electrode center. In case a group of segments was used for DBS in patients implanted with segmented leads, we first re-referenced the signal of each active segment from the original mastoid reference to the closest neighbor, computed features separately and averaged over segments. Lead localization, performed with LEAD DBS [23], confirmed correct placement for all electrodes under study (Fig. 2A).

2.2.2. Data preprocessing

The data were preprocessed with the Fieldtrip toolbox [24]. LFP and MEG data underwent visual screening. Bad channels and epochs containing artifacts were discarded. The data were segmented into 2s windows (frequency resolution: 0.5 Hz) with 50% overlap.

2.2.3. STN power

We applied a Hanning taper and computed power for each integer frequency between 1 and 398 Hz using Welch's method. Line noise and its harmonics were eliminated by replacing values ± 2 Hz from the harmonics by surrogate values obtained by linear interpolation. The aperiodic (1/f) component was removed from the LFP power spectra using the *fitting oscillations and one over f* (FOOOF) algorithm [25]. This step was necessary to ensure that the predictive models operated on neuronal oscillations proper. Note that coherence, unlike power, is a normalized quantity not requiring this correction. When applying FOOOF, we adapted its parameters iteratively until a good fit was achieved, confirmed visually for every case. Since a good description of the entire spectrum was usually not achievable with a single model, we performed separate fits for the frequency ranges below 90 Hz and above 200 Hz (frequencies between 90 and 200 Hz were not analyzed here). The periodic minus the aperiodic component was retained and power was averaged within eight frequency bands of interest: delta/theta (3–7 Hz), alpha (8–12 Hz), low-beta

J. Hirschmann, A. Steina, J. Vesper et al. Brain Stimulation 15 (2022) 792–802

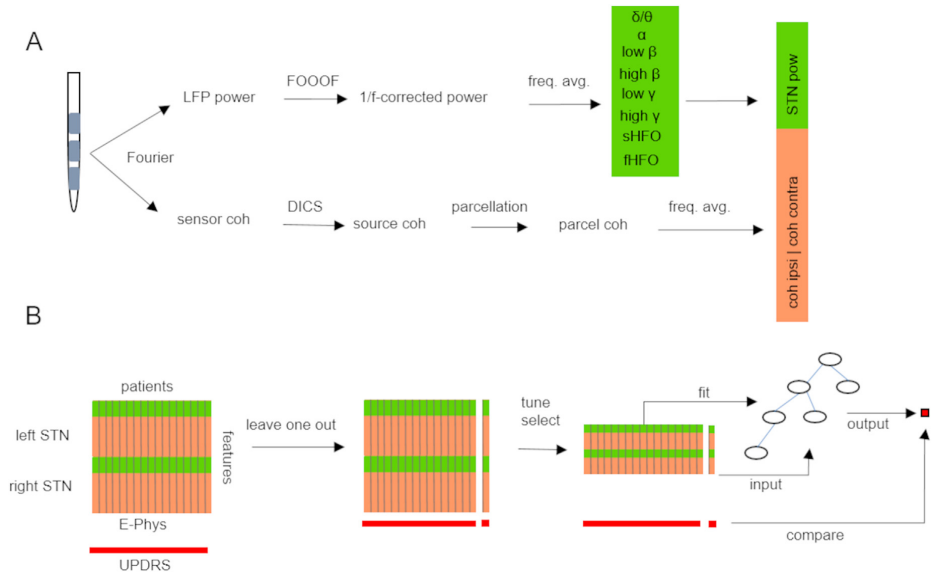

Fig. 1. Analysis pipeline. (**A**) Feature extraction. Following contact selection, STN power and STN-cortex coherence were computed from the Fourier spectrum. STN power underwent 1/f-correction and was averaged within frequency bands. STN-cortex coherence was source-localized using beamforming. Each source was assigned to one of 30 cortical parcels and source coherence was averaged within parcels and frequency bands. Band-limited STN power and STN-cortex coherence formed the hemisphere feature vector. (**B**) Leave-one-out regression. Left and right hemisphere feature vectors were stacked vertically to form the subject feature vector. The subject feature vectors were stacked horizontally to form the feature matrix. In each iteration through the leave-one-out cycle, one subject was set aside (test set). The remaining train set was divided into 3 folds for cross-validated hyper-parameter tuning and feature selection. The test features served as input to the regression model, which predicted UPDRS III sum score reduction.

(13–20 Hz), high-beta (21–35 Hz), low gamma (36–60 Hz), high-gamma (60–90 Hz), slow high-frequency oscillations (sHFO; 200–300 Hz) and fast high-frequency oscillations (fHFO; 300–400 Hz).

2.2.4. STN-cortex coherence

Coherence was estimated and localized once per frequency band rather than once per frequency. Using the multitaper method [26], we computed coherence at the band center frequency and applied appropriate spectral smoothing to include the entire band. For bands covering line noise harmonics, we computed estimates for sub-bands, excluding the harmonics, and averaged them. Coherence was source-localized using Dynamic Imaging of Coherent Sources [27]. We made use of realistic, single-shell head models based on the individual, T1-weighted MR image. The beamformer grid contained 567 locations spread out evenly across the cortical and cerebellar surface. It was aligned to Montreal Neurological Institute (MNI) space, allowing for grid parcellation into 30 supersets of regions defined in the Automatic Anatomic Labeling (AAL) atlas [28]. Details on these regions are provided in Table S2 of the Supplementary Material.

Following feature extraction, features were arranged into a feature matrix of size $N_{\text{patients}} \times N_{\text{features}}$ (Fig. 1). In this matrix, each subject was represented by one column comprising both STN power and STN-cortex coherence with ipsilateral and contralateral cortical parcels for both left and right STN. Two alternative designs were also tested, but found to have inferior performance (Fig. S2 of the Supplementary Material): one with hemispheres rather than subjects as unit of observation, and one in which hemispheres were ordered according their laterality with respect to the more affected body side.

2.2.5. Machine learning model

For predicting motor improvement, we employed extreme gradient boosting, as implemented in the XGBoost package for Python [29]. In this framework, the target score is predicted by a sequence of decision trees assembled tree-by-tree during training. Each new tree is trained on the error made by the group assembled so far, resulting in a stepwise refinement of the prediction. XGBoost has gained popularity by winning numerous machine learning competitions and is a commonly used tool in machine learning. It appears to be particularly well suited for electrophysiological datasets [30], which are typically small, structured and noisy. In a recent study by Merk et al. [31], XGBoost outperformed linear regression and artificial neural networks in the prediction of grip force based on STN and cortical oscillations.

2.2.6. Feature importance analysis

Feature importance analysis seeks to describe how much an individual feature or a subgroup of features contributed to a prediction made by a machine learning model. Here, we quantified feature importance using the Python implementation of SHapely Additive exPlanations (SHAP) [32]. SHAP values are estimates of Shapley values, a concept from cooperative game theory for a fair distribution of a payout among players. Besides having a range of desirable mathematical properties, SHAP values have an intuitive interpretation: they sum to the difference between the current and the average model output. While the concept is applicable to any machine learning model, specialized versions such as TreeSHAP have been developed, optimized for tree ensemble-based models such as XGBoost [33].

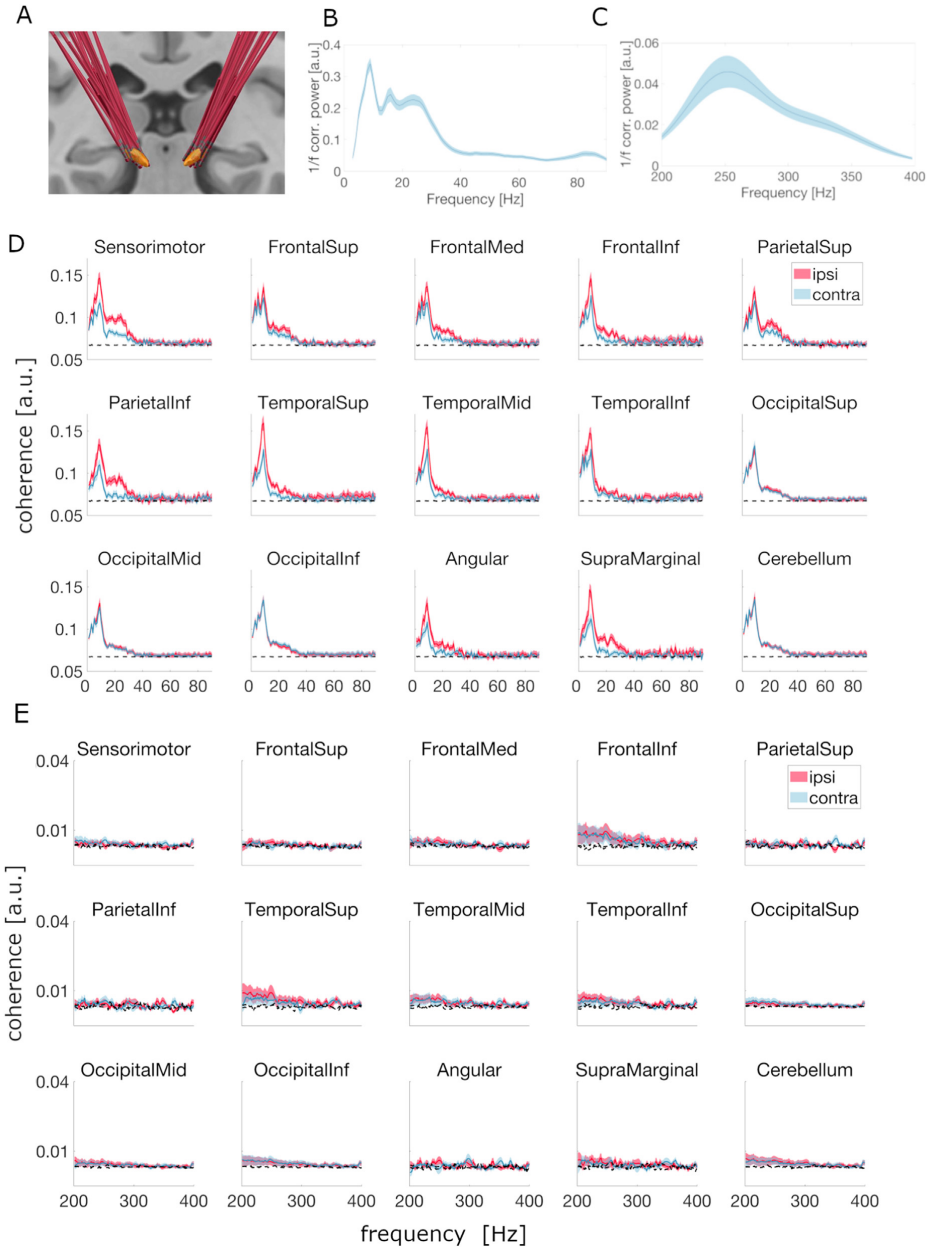

Fig. 2. Spectral characteristics of features. (**A**) Reconstruction of electrode locations. The subthalamic nucleus is depicted in yellow. (**B**) STN power, averaged over hemispheres, below 90 Hz. (**C**) as (**B**) for the high frequency range. (**D**) Group-mean STN-cortex coherence by cortical parcel. The solid lines represent the mean. Shadings represent the standard error of the mean. The labels "ipsi" and "contra" refer to the subthalamic nucleus. (E) as (D) for the high frequency range (multitaper method, ±5 Hz spectral smoothing). The dotted black lines indicate the level of ipsi- and contralateral coherence after shuffling data segments in time. (For interpretation of the references to color in this figure legend, the reader is referred to the Web version of this article.)

2.2.7. Predicting DBS outcome

DBS outcome was quantified by the difference in UPDRS III sum score Med OFF/Stim OFF - Med OFF/Stim ON, unless specified otherwise. Predictions were computed sequentially for each subject in a leave-one-out fashion, i.e. each subject served as the test set once and was part of the train set in all other iterations. In each iteration through the leave-one-out loop, features were standardized using mean and variance of the train set. Next, we selected the most important *k* features according to the mean absolute SHAP values computed on the train set. The train set was then sub-divided into three folds for cross-validated hyper-parameter tuning with the Hyperopt package [34]. The optimization procedure and the chosen parameters are detailed in the Supplementary Material.

Model performance was quantified by the root mean squared error (RMSE) and Pearson's correlation coefficient between the actual and the predicted DBS outcome. We further applied a null model agnostic of electrophysiology for establishing a performance baseline. The null model generated predictions of DBS outcome by averaging the outcomes of the train set.

2.3. Statistics

Significance of correlation was assessed using the *pearsonr* function of the *scipy.stats* package (two-sided test; statistic: β; significance level: 0.05). When computing the correlation coefficient repeatedly, we applied false discovery rate (FDR) correction using the Benjamini-Hochberg procedure.

3. Results

3.1. Features

The spectral and spatial characteristics of the features are illustrated in Figs. 2 and 3, respectively. STN power spectra contained peaks in the alpha, low-beta and high-beta band. Individual patients showed an additional high-gamma peak (Fig. 2B). The HFO spectrum was dominated by sHFO peaks, as described previously for the medication OFF state (Fig. 2C) [35,36]. The coherence spectra contained strong alpha peaks, which were ubiquitous but most pronounced in temporal areas ipsilateral to the STN (Fig. 2D). Medial sensorimotor and adjacent areas ipsilateral to the STN additionally showed strong beta peaks, as reported by previous studies (Fig. 3) [20,37]. The coherence spectra did not contain any consistent HFO peaks (Fig. 2E), but some subjects had more coherence in this range than others (Fig. S1 of the Supplementary Material). Finally, many coherence spectra had several narrow peaks in the delta/theta range, presumably reflecting tremor, occurring at slightly different frequencies in individual patients [12,13].

3.2. Model performance

We evaluated the performance of predictive models operating either on STN-cortex coherence (connectivity models) or STN power (local models) as a function of the number of features. In order to test whether the model predicted DBS benefit or symptom severity better, we predicted both the difference between the DBS OFF and the DBS ON score (benefit) and the DBS OFF score (symptom severity) separately. Note that all UPDRSIII scores were collected several months after surgery (Table S1).

When predicting DBS benefit, both connectivity and local models outperformed the null model, which estimated DBS outcome by averaging the outcomes of the train set (Fig. 4A; $RMSE_{Null}$: 6.74). Connectivity-based models outperformed the null model even with a single feature and generally performed better than local models (avg. $RMSE_{conn}$: 5.1, avg. r_{conn}: 0.64). Local models required at least four features to achieve better performance than the null model and a significant correlation between predicted and actual DBS outcomes (Fig. 4B; avg, $RMSE_{local}$: 6.0, avg. r_{local}: 0.42).

The OFF score was not predicted as accurately as DBS benefit. Connectivity models could not perform this task at all (Fig. 4C and D; $RMSE_{null\_off}$: 11.09; avg. $RMSE_{conn}$: 13.42, avg. r_{conn}: −0.10). Local models operating on 3–6 STN power features, however, achieved a significant correlation between actual and predicted DBS OFF scores (Fig. 4D; $RMSE_{null\_off}$: 11.09; $RMSE_{local\_5}$: 9.04, r_{local_5}: 0.55).

3.3. Feature importance

This analysis aimed at revealing the most important features for successfully predicting clinical benefit. To assess feature importance, we summed absolute SHAP values over all models contributing to the previous analysis (Fig. 4) and within categories of interest such as frequency band (Fig. 5A and B), brain region (Fig. 5C) and hemisphere with respect to the STN (Fig. 5D). For local models, STN high-beta power was the most important feature, followed by alpha and sHFO power (Fig. 5A). Strong high-beta power indicated a good DBS outcome. Strong beta-band coherence, in

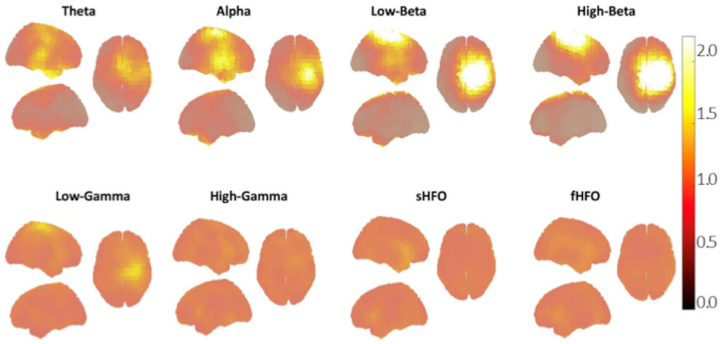

Fig. 3. Source-localized STN-cortex coherence. Coherence was normalized by the spatial mean prior to averaging over hemispheres. Whole-brain images were flipped such that the hemisphere ipsilateral the STN ended up on the right side. Normalized coherence is color-coded. Theta: 3–7 Hz; alpha: 8–12 Hz; low-beta: 13–20 Hz; high-beta: 21–35 Hz; low gamma: 36–60 Hz; high-gamma: 60–90 Hz; sHFO: 200–300 Hz; fHFO; 300–400 Hz. (For interpretation of the references to color in this figure legend, the reader is referred to the Web version of this article.)

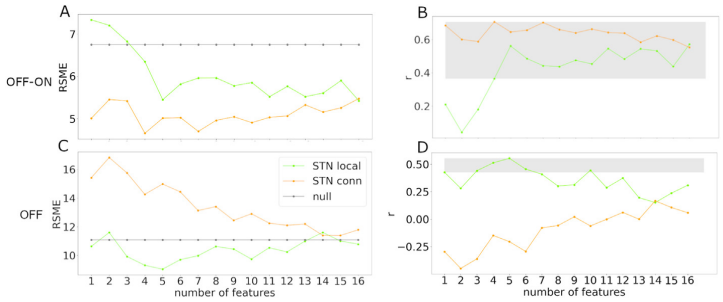

Fig. 4. Model performance vs. number of features. (**A**) Root mean squared error as a function of number of features for the prediction of DBS OFF-ON score. (**B**) Pearson's correlation coefficient quantifying the correlation between predicted and actual DBS outcome for the prediction of DBS OFF-ON score. Significant correlations are highlighted by gray shading ($p < 0.05$, FDR corrected). (**C**) as (**A**) for DBS OFF score. (**D**) as (**B**) for DBS OFF score. STN local: model operating on STN power features; STN conn: model operating on STN-cortex coherence features.

contrast, was not indicative of a good outcome (Fig. 5B). Connectivity models relied mostly on fHFO, low-gamma and theta oscillations. Connectivity with parietal areas was particularly important (Fig. 5C). As expected, coherence between STN and ipsilateral cortex was more important than coherence between STN and contralateral cortex (Fig. 5D).

3.4. Combining local and connectivity features

We investigated the potential merit of combining local and connectivity features when predicting DBS benefit. To simplify interpretation, we used a fixed feature set rather than running a data-driven selection for each individual subject as above. We chose the five local and the five connectivity features with the highest overall SHAP sum (as five was the lowest number for which both the local and the connectivity models reached good performance in the previous analysis). The selected features are listed in Fig. 6B. As depicted in Fig. 6A, the best-5 connectivity model ($RMSE_{conn} = 3.54$, $r_{conn} = 0.84$, $p_{conn} = 1e\text{-}14$) outperformed the best-5 local model ($RMSE_{local} = 5.77$, $r_{local} = 0.52$, $p_{local} = 0.001$). Adding local features to the connectivity features did not improve the connectivity model further ($RMSE_{comb} = 3.61$, $r_{comb} = 0.84$, $p_{comb} = 1.69e\text{-}10$).

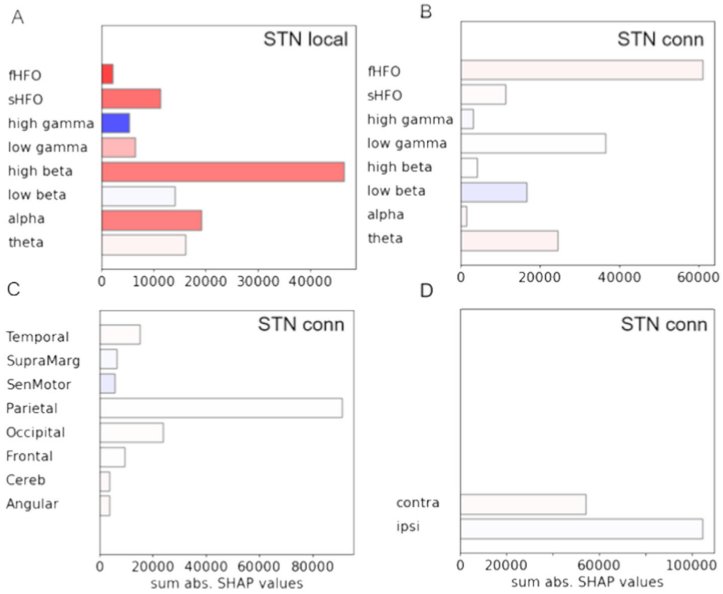

Fig. 5. Feature importance. Bars represent absolute SHAP values summed over all models and within the corresponding category. (**A,B**) frequency band. (**C**) brain region. (**D**) hemisphere. High bars indicate that features of the corresponding category had a strong impact on the prediction. Colors represent the mean correlation between SHAP values and feature values within each category. Dark red colors indicate that high feature values consistently drove the prediction toward higher values. Dark blue colors indicate that high feature values consistently drove the prediction towards lower values. (For interpretation of the references to color in this figure legend, the reader is referred to the Web version of this article.)

J. Hirschmann, A. Steina, J. Vesper et al. Brain Stimulation 15 (2022) 792–802

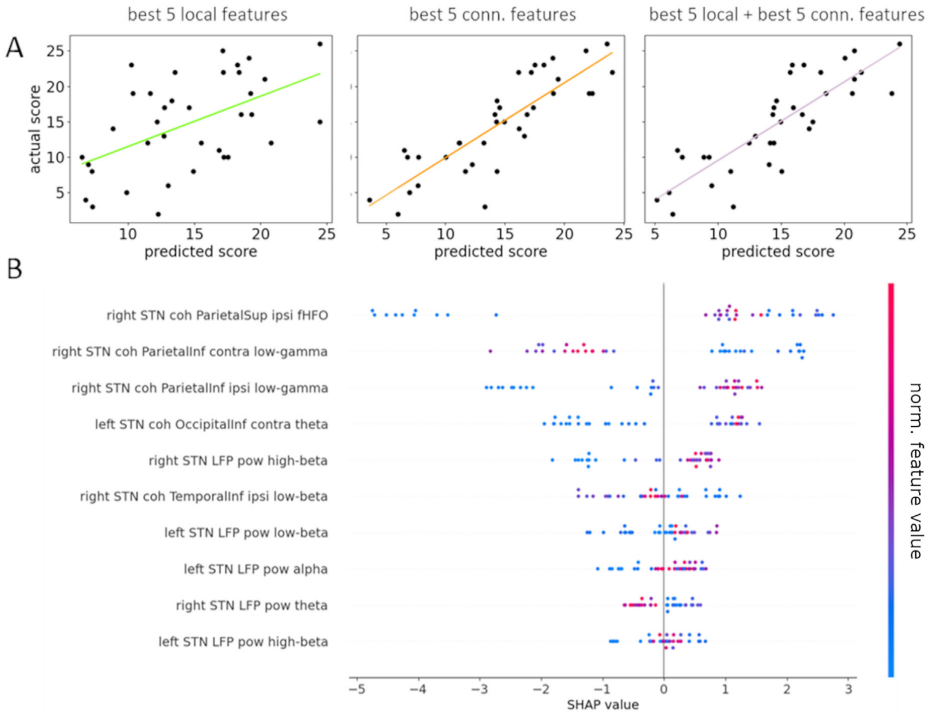

Fig. 6. Comparing local and connectivity models. (**A**) Scatter plots showing the correlation between actual and predicted DBS outcome using the five best local features (green), the five best connectivity features (orange) and the five best local and connectivity features combined (purple). (**B**) SHAP values for each feature of the combined model. Each dot represents one subject. High values on the x-axis indicate a strong influence on the prediction in either the negative (SHAP<0) or the positive direction (SHAP>0) relative to the mean. Normalized feature values are color-coded. (For interpretation of the references to color in this figure legend, the reader is referred to the Web version of this article.)

Fig. 6B illustrates feature importance and the relation between feature values and feature importance for the combined model. Connectivity features generally had a stronger impact on the prediction than local features. The strongest influence was attributed to fHFO coherence between the right STN and ipsilateral inferior parietal cortex. Low values strongly drove the prediction towards worse predicted outcomes. Indeed, when relating this feature to DBS outcome directly, we observed an approximately logarithmic relationship, i.e. outcomes dropped steeply with decreasing coherence (log(coherence)-outcome correlation: $r = 0.40$, $p = 0.02$). Feature importance analysis further revealed that strong coupling between the right STN and ipsilateral parietal cortex and a weak coupling between the right STN and contralateral parietal cortex in the low-gamma band drove the prediction toward a good DBS outcome. So did strong coupling between the left STN and contralateral, inferior occipital cortex in the theta band and weak coupling between right STN and temporal cortex in the low-beta band.

3.5. Feature correlations

Whereas the automatically selected set of most important local features contained frequency bands with clear peaks and an established role in Parkinson's disease pathophysiology, such as the beta and the HFO band, the set of most important connectivity features did not. To better understand the nature of these features, we investigated their correlation with all other features (Fig. 7A). Both fHFO and low-gamma coherence with parietal cortex were strongly correlated with a large set of other features, in particular >35 Hz connectivity with the entire hemisphere. Replacing each of the best five connectivity features by their closest correlate, however, decreased performance substantially (Fig. 7B; $RMSE_{best} = 3.61$, $r_{best} = 0.84$, $p_{best} = 1.69e\text{-}10$; $RMSE_{corr} = 6.47$, $r_{corr} = 0.29$, $p_{corr} = 0.09$), demonstrating that the selected features are not arbitrary representatives of a highly correlated feature group. Destroying true phase relationships by shuffling the LFP signals in time abolished the ability to predict clinical benefit from STN-cortex coherence, demonstrating that connectivity models relied on phase information (Fig. S3 of the Supplementary Material).

3.6. Control analyses

Given the critical role of lead placement for DBS benefit, we asked whether the most informative features might reflect distance to target. None of the best 10 features were significantly correlated with the distance of the LFP channel to a published "sweet spot" for STN DBS [38], and distance could not predict clinical benefit on its own (see Supplementary Material). Similar observations were made for a set of potential confounders, including *recording duration*, *electrode type (segmented vs. non-segmented)*, *days passed since recording* and *signal-to-noise ratio*. We conclude that the success of the electrophysiological models cannot be explained by correlation with these variables.

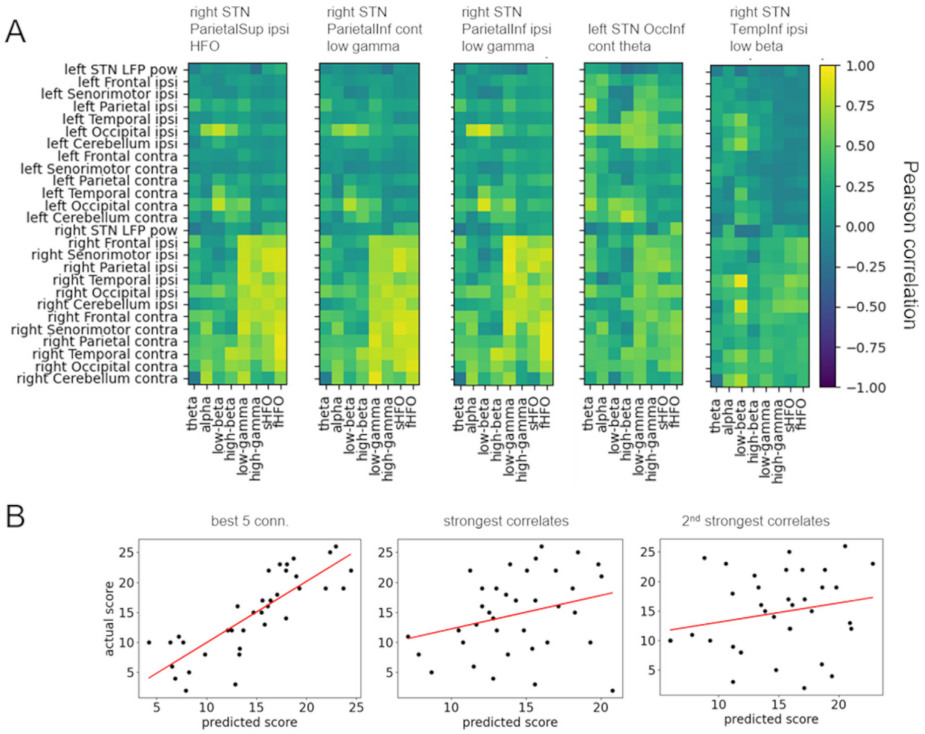

Fig. 7. Correlations and replaceability of the five best connectivity features. (**A**) Pearson correlation between the five most important connectivity features and all other features. Correlations were averaged within lobes (frontal, parietal, temporal, occipital) for the sake of readability. (**B**) Prediction performance for the five best connectivity features, their strongest correlates and their second strongest correlates.

3.7. Predicting improvement of particular symptoms

In the previous analyses, we quantified DBS outcome by the reduction of the UDPRS III sum score, representing overall motor symptom severity. To see whether local and connectivity features relate to particular and possibly different symptoms, we computed predictions for each individual UPDRS III item (Fig. 8A and C) and for the akinesia-rigidity, the tremor and the axial subset sum score (Fig. 8B and D) using the best-5 local and the best-5 connectivity model described above. The local and the connectivity model had a very similar RMSE profile. Both predicted the DBS-induced improvement of akinesia/rigidity best.

4. Discussion

We have demonstrated that is possible to predict DBS outcome from STN power and STN-cortex coherence in Parkinson's disease patients. Our results indicate that STN-cortex coherence, in particular, is a good predictor of clinical benefit.

4.1. Relation to previous studies

Few studies have made out-of-sample predictions of DBS outcome based on electrophysiological data. We know of only three studies, all of which investigated signals from within or nearby the STN, recorded during surgery [39–41]. Here, we applied a network approach, incorporating both subthalamic oscillations and their synchrony with oscillatory activity in various cortical areas. In this respect, our approach can be considered an electrophysiological pendant of discriminative tractography. This is a technique for predicting DBS outcome from structural connectivity with the volume of tissue activated (VTA), an estimate of the spatial extent of neuromodulation around the active contact. This approach and related methods have facilitated accurate predictions of DBS

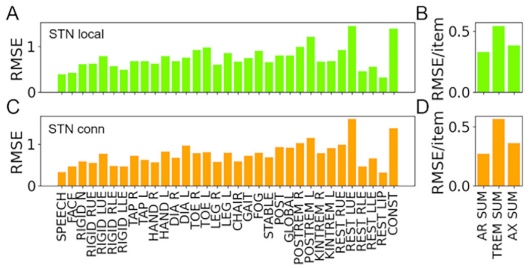

Fig. 8. Single item prediction. (**A**) Single item prediction for the local model. (**B**) Subset sum score predictions for the local model. (**C**) As (**A**) for connectivity model. (**D**) As (**B**) for connectivity model.

outcome in many disorders, including Parkinson's disease [42], obsessive-compulsive disorder [43,44], Tourette's Syndrome [45], and Essential Tremor [46]. Although structural and functional connectivity do not necessarily contain redundant information about DBS outcome [42], structural connectivity forms the basis of functional connectivity, suggesting that both might predict the efficacy of DBS in individual patients. In this study, we show that this is indeed the case. Predicted DBS outcomes, derived from a few functional connectivity features only, were highly correlated with the actual outcomes. The null model, which predicted DBS outcome based on the average outcome in the training set, performed worse, i.e. knowing the individual electrophysiology helps improving realistic expectations of DBS outcome.

4.2. The link between DBS outcome and oscillations

Predicting clinical benefit form neuronal oscillations might work for several reasons. First, exaggerated synchronization itself has been suggested to cause Parkinsonism [47]. If oscillations were the causal process, an estimate of how strong the process is around the stimulation contact might allow for predicting the DBS effect in the individual patient.

Alternatively, successful prediction might be explained by a consistent relationship between oscillations and contact location, which is known to be a crucial factor for DBS. Indeed, beta and HFO oscillations have a characteristic spatial distribution in the STN area [48,49]. Here, we found, however, that the distance of an LFP channel to a published sweet spot for STN DBS had little predictive power and did not correlate with the most informative oscillatory features [38]. This is likely a characteristic of our sample, which includes only the contacts with optimal clinical efficacy, which, in our case, differed little with respect to placement. Presumably, location would become a crucial piece of information if one were to include other contacts further off target, e.g. the contacts not selected for DBS. We could not investigate this here because we lacked a good characterization of the clinical effect for non-selected contacts.

It is possible that the prediction relied in part on information about the ability of DBS to modulate remote cortical areas, which may be key to the clinical effect of DBS [50]. This would explain why connectivity models performed better than local models and why they could predict DBS benefit but not symptom severity. Whether stimulation can reach a relevant anatomical connection might be relevant for the clinical effect of DBS, but is not relevant for the patient's motor state off stimulation.

STN-cortex coherence carries information on functional connectivity by definition. In addition, it has recently been demonstrated to correlate with the density of reconstructed fiber tracts connecting STN and cortical areas, i.e. it also contains information on anatomical connectivity [51]. Interestingly, the same study demonstrated that STN beta oscillations might arise as a consequence of cortical input, implying that even local oscillations can relate to STN-cortex connectivity.

4.3. Feature importance

In this paper, we applied feature analysis to identify particularly informative features. This analysis yielded STN high-beta power as the most import local feature, in line with a recent classification study in the primate model of PD [52]. The finding further aligns with a recent study reporting that high-beta oscillatory activity distinguishes the STN from neighboring structures [51]. STN-cortex beta coherence, in contrast, was less relevant for prediction. This observations tallies with studies on dopamine effects, which found no relation between the degree of symptom reduction achieved by levodopa and the degree of beta coherence reduction [8,53].

While beta coherence with motor cortex did not emerge as a very important feature, coherence in other frequency bands was strongly predictive of DBS outcome, even more so than STN high-beta power. Coherence between the STN and parietal cortex at high frequencies (low-gamma and fHFO) allowed for accurate estimates of DBS efficacy. This is somewhat surprising, given that these frequency bands did not contain coherence peaks. Despite this lack of structure and a strong correlation with high-frequency coupling (>35 Hz) to other cortical areas, these features appear to be particularly relevant for DBS outcome, as they were not replaceable without harming performance and lost their predictive potential through shuffling.

The importance of parietal features points towards a clinical relevance of parieto-STN connectivity. Yet, in light of the strong correlation between features, this hypothesis requires confirmation by independent studies. A number of PET studies have reported that STN DBS leads to metabolic changes in parietal areas, evidencing that DBS modulates parietal cortex [54,55]. Further, PD patients differ from healthy controls in their resting-state BOLD signal correlation between STN and parietal cortex, suggesting pathological relevance of this connection [56]. And lastly, both STN and parietal cortex were proposed to be part of brain network for response inhibition [57,58]. This network is believed to be lateralized to the right hemisphere [59,60], which might relate to the fact that all of the important parietal connectivity features identified here were right STN features, suggesting that left and right STN might not have the same relation to clinical improvement. The fact that good predictions required data from both hemispheres further supports this hypothesis.

4.4. STN power vs. STN-cortex coherence

One research question of this study was whether STN power and STN-cortex coherence carry different information about DBS outcome. Our results do not support this hypothesis. Although local models did achieve reasonable predictions, adding local features did not improve the best-performing connectivity models, indicating that the information carried by STN power was already contained in STN-cortex coherence – even though the frequency bands were different. Similarly, when predicting single UPDRS items both local and connectivity models showed a very similar performance profile, i.e. the accurately predicted symptom reductions and the non-accurately predicted symptom reductions were the same for both feature types. In conclusion, STN-cortex coherence seems to condense more information in a lower number of features, but power and coherence do not seem to be independent sources of information.

The same analysis revealed that both STN power and STN-cortex coherence predicted the reduction of akinesia/rigidity best. This might be due to the known link between akinesia and (beta) oscillations [61], and could additionally reflect common properties of the group under study. A certain level of akinesia and rigidity reduction was common to all patients, whereas only a subset of patients showed marked tremor and/or axial symptoms. Because learning occurred across subjects, oscillation-outcome relationships shared among patients were learned the best.

4.5. Limitations

While an analysis of feature importance can reveal new insights, it should be interpreted with caution. Identifying causal relationships is generally not possible with this approach [62]. Any feature related to DBS outcome might be so via correlation with other

features or unobserved variables, i.e. a feature important to the model is not necessarily important to the brain. This aspect is particularly relevant with regard to a possible pathophysiological role of high-frequency coupling, which requires further investigation.

Finally, a sample size of 36 patients is large for a MEG-LFP study (as far as we know, this is the largest sample so far) but it is not at all large for a machine learning study. Future studies should aim at including more data, potentially by fostering data sharing.

5. Conclusions and outlook

It is possible to predict DBS outcome based on subthalamic oscillations and their synchrony with cortical oscillations. Future studies may investigate whether this link between electrophysiology and clinical improvement can be leveraged to improve lead placement and/or contact selection.

CRediT authorship contribution statement

Jan Hirschmann: Investigation, Formal analysis, Writing – original draft. **Alexandra Steina:** Investigation, Formal analysis, Writing – review & editing. **Jan Vesper:** Conceptualization, Writing – review & editing, Resources. **Esther Florin:** Conceptualization, Investigation, Writing – review & editing. **Alfons Schnitzler:** Conceptualization, Writing – review & editing, Funding acquisition.

Declaration of interests

The authors declare that they have no known competing financial interests or personal relationships that could have appeared to influence the work reported in this paper.

Acknowledgements

This work was funded by Brunhilde Moll Stiftung. We are sincerely thankful to all patients who participated in this study and to Matthias Sure and Salome Peralta-Reyes for help with electrode localization. We thank Markus Butz for helpful feedback on the manuscript. Finally, this study would not have been possible without a large team supporting data acquisition and patient care.

Appendix A. Supplementary data

Supplementary data to this article can be found online at https://doi.org/10.1016/j.brs.2022.05.008.

References

[1] Ray Dorsey E, Elbaz A, Nichols E, Abbasi N, Abd-Allah F, Abdelalim A, et al. Global, regional, and national burden of Parkinson's disease, 1990–2016: a systematic analysis for the Global Burden of Disease Study 2016. Lancet Neurol 2018;17(11):939–53. https://doi.org/10.1016/S1474-4422(18)30295-3.

[2] Alexander GE, DeLong MR, Strick PL. Parallel organization of functionally segregated circuits linking basal ganglia and cortex. Annu Rev Neurosci 1986;9(1):357–81. https://doi.org/10.1146/annurev.ne.09.030186.002041.

[3] Halje P, Brys I, Mariman JJ, da Cunha C, Fuentes R, Petersson P. Oscillations in cortico-basal ganglia circuits: implications for Parkinson's disease and other neurologic and psychiatric conditions. J Neurophysiol 2019;122(1):203–31. https://doi.org/10.1152/JN.00590.2018.

[4] Brown P, Oliviero A, Mazzone P, Insola A, Tonali P, Di Lazzaro V. Dopamine dependency of oscillations between subthalamic nucleus and pallidum in Parkinson's disease. J Neurosci 2001;21(3):1033–8. http://www.ncbi.nlm.nih.gov/pubmed/11157088. [Accessed 31 August 2016].

[5] Levy R, Ashby P, Hutchison WD, Lang AE, Lozano AM, Dostrovsky JO. Dependence of subthalamic nucleus oscillations on movement and dopamine in Parkinson's disease. Brain 2002;125(6):1196–209. https://doi.org/10.1093/BRAIN/AWF128.

[6] Giannicola G, Marceglia S, Rossi L, Mrakic-Sposta S, Rampini P, Tamma F, et al. The effects of levodopa and ongoing deep brain stimulation on subthalamic beta oscillations in Parkinson's disease. Exp Neurol 2010;226(1):120–7. https://doi.org/10.1016/j.expneurol.2010.08.011.

[7] Eusebio A, Thevathasan W, Doyle Gaynor L, Pogosyan A, Bye E, Foltynie T, et al. Deep brain stimulation can suppress pathological synchronisation in parkinsonian patients. J Neurol Neurosurg Psychiatry 2011;82(5):569–73. https://doi.org/10.1136/jnnp.2010.217489.

[8] Oswal A, Beudel M, Zrinzo L, Limousin P, Hariz M, Foltynie T, et al. Deep brain stimulation modulates synchrony within spatially and spectrally distinct resting state networks in Parkinson's disease. Brain 2016;139(Pt 5):1482–96. https://doi.org/10.1093/brain/aww048.

[9] Zhang Y, Chen Y, Bressler SL, Ding AM. Response preparation and inhibition: the role of the cortical sensorimotor beta rhythm. Brain 2008. https://doi.org/10.1016/j.neuroscience.2008.06.061.

[10] Litvak V, Eusebio A, Jha A, Oostenveld R, Barnes G, Foltynie T, et al. Movement-related changes in local and long-range synchronization in Parkinson's disease revealed by simultaneous magnetoencephalography and intracranial recordings. J Neurosci 2012;32(31):10541–53. https://doi.org/10.1523/JNEUROSCI.0767-12.2012.

[11] Swann NC, de Hemptinne C, Miocinovic S, Qasim S, Wang S, Ziman N, et al. Gamma oscillations in the hyperkinetic state detected with chronic human brain recordings in Parkinson's disease. J Neurosci 2016;36(24):6445–58. https://doi.org/10.1523/JNEUROSCI.1128-16.2016.

[12] Timmermann L, Gross J, Dirks M, Volkmann J, Freund HJ, Schnitzler A. The cerebral oscillatory network of parkinsonian resting tremor. Brain 2003;126(1):199–212. https://doi.org/10.1093/brain/awg022.

[13] Hirschmann J, Hartmann CJ, Butz M, Hoogenboom N, Özkurt T, Elben S, et al. A direct relationship between oscillatory subthalamic nucleus-cortex coupling and rest tremor in Parkinson's disease. Brain 2013;136(12):3659–70. https://doi.org/10.1093/brain/awt271.

[14] Gilron R, Little S, Perrone R, Wilt R, Hemptinne C de, Yaroshinsky M, et al. Long-term wireless streaming of neural recordings for circuit discovery and adaptive stimulation in individuals with Parkinson's disease. Nat Biotechnol 2021. https://doi.org/10.1038/s41587-021-00897-5. Published online.

[15] He S, Baig F, Mostofi A, Pogosayan A, Debarros J, Green AL, et al. Closed-loop deep brain stimulation for essential tremor based on thalamic local field potentials. Mov Disord 2021;36(4):863–73. https://doi.org/10.1002/MDS.28513.

[16] Opri E, Cernera S, Molina R, Eisinger RS, Cagle JN, Almeida L, et al. Chronic embedded cortico-thalamic closed-loop deep brain stimulation for the treatment of essential tremor. Sci Transl Med 2020;12(572):eaay7680. https://doi.org/10.1126/scitranslmed.aay7680.

[17] Dembek TA, Roediger J, Horn A, Reker P, Oehrn C, Dafsari HS, et al. Probabilistic sweet spots predict motor outcome for deep brain stimulation in Parkinson disease. Ann Neurol 2019;86(4):527–38. https://doi.org/10.1002/ana.25567.

[18] Boutet A, Germann J, Gwun D, Loh A, Elias GJB, Neudorfer C, et al. Sign-specific stimulation 'hot' and 'cold' spots in Parkinson's disease validated with machine learning. Brain Commun 2021. https://doi.org/10.1093/braincomms/fcab027. Published online.

[19] Zaidel A, Spivak A, Grieb B, Bergman H, Israel Z. Subthalamic span of oscillations predicts deep brain stimulation efficacy for patients with Parkinson's disease. Brain 2010;133(7):2007–21. https://doi.org/10.1093/brain/awq144.

[20] Hirschmann J, Özkurt TE, Butz M, Elben S, Hartmann CJ, Vesper J, et al. Distinct oscillatory STN-cortical loops revealed by simultaneous MEG and local field potential recordings in patients with Parkinson's disease. Neuroimage 2011;55(3):1159–68. https://doi.org/10.1016/j.neuroimage.2010.11.063.

[21] Sharma A, Vidaurre D, Vesper J, Schnitzler A, Florin E. Differential dopaminergic modulation of spontaneous cortico–subthalamic activity in Parkinson's disease. Elife 2021;10. https://doi.org/10.7554/eLife.66057.

[22] Goetz CG, Tilley BC, Shaftman SR, Stebbins GT, Fahn S, Martinez-Martin P, et al. Movement Disorder Society-sponsored revision of the Unified Parkinson's Disease Rating Scale (MDS-UPDRS): scale presentation and clinimetric testing results. Mov Disord 2008;23(15):2129–70. https://doi.org/10.1002/mds.22340.

[23] Horn A, Li N, Dembek TA, Kappel A, Boulay C, Ewert S, et al. Lead-DBS v2: towards a comprehensive pipeline for deep brain stimulation imaging. Neuroimage 2019. https://doi.org/10.1016/j.neuroimage.2018.08.068. Published online.

[24] Oostenveld R, Fries P, Maris E, Schoffelen J-M. FieldTrip: open source software for advanced analysis of MEG, EEG, and invasive electrophysiological data. Comput Intell Neurosci 2011;2011:1–9. https://doi.org/10.1155/2011/156869.

[25] Donoghue T, Haller M, Peterson EJ, Varma P, Sebastian P, Gao R, et al. Parameterizing neural power spectra into periodic and aperiodic components. Nat Neurosci 2020;23(12):1655–65. https://doi.org/10.1038/s41593-020-00744-x.

[26] Thomson D. Spectrum estimation and harmonic analysis. Proc IEEE 1982;70(9):1055–96. https://doi.org/10.1109/PROC.1982.12433.

[27] Gross J, Kujala J, Hämäläinen M, Timmermann L, Schnitzler A, Salmelin R. Dynamic imaging of coherent sources: studying neural interactions in the

human brain. Proc Natl Acad Sci Unit States Am 2001;98(2):694–9. https://doi.org/10.1073/PNAS.98.2.694.
[28] Tzourio-Mazoyer N, Landeau B, Papathanassiou D, Crivello F, Etard O, Delcroix N, et al. Automated anatomical labeling of activations in SPM using a macroscopic anatomical parcellation of the MNI MRI single-subject brain. Neuroimage 2002;15(1). https://doi.org/10.1006/nimg.2001.0978.
[29] Chen T, Guestrin C. XGBoost: a scalable tree boosting system. In: Proceedings of the ACM SIGKDD international conference on knowledge discovery and data mining; 2016. https://doi.org/10.1145/2939672.2939785.
[30] Wu J, Zhou T, Li T. Detecting epileptic seizures in EEG signals with complementary ensemble empirical mode decomposition and extreme gradient boosting. Entropy 2020;22(2). https://doi.org/10.3390/E22020140.
[31] Merk T, Peterson V, Lipski W, Blankertz B, Turner RS, Li N, et al. Electrocorticography is superior to subthalamic local field potentials for movement decoding in Parkinson's disease. bioRxiv 2021. https://doi.org/10.1101/2021.04.24.441207. Published online May 1, 2021:2021.04.24.441207.
[32] Lundberg SM, Lee SI. A unified approach to interpreting model predictions. In: Advances in neural information processing systems; 2017.
[33] Lundberg SM, Erion GG, Lee S-I. Consistent individualized feature attribution for tree ensembles. Published online, https://arxiv.org/abs/1802.03888v3. [Accessed 18 August 2021].
[34] Bergstra J, Yamins D, Cox DD. Making a science of model search: hyperparameter optimization in hundreds of dimensions for vision architectures. In: 30th international conference on machine learning, ICML 2013; 2013.
[35] Özkurt TE, Butz M, Homburger M, Elben S, Vesper J, Wojtecki L, et al. High frequency oscillations in the subthalamic nucleus: a neurophysiological marker of the motor state in Parkinson's disease. Exp Neurol 2011;229(2):324–31. https://doi.org/10.1016/j.expneurol.2011.02.015.
[36] López-Azcárate J, Tainta M, Rodríguez-Oroz MC, Valencia M, González R, Guridi J, et al. Coupling between beta and high-frequency activity in the human subthalamic nucleus may be a pathophysiological mechanism in Parkinson's disease. J Neurosci 2010;30(19):6667–77. https://doi.org/10.1523/JNEUROSCI.5459-09.2010.
[37] Litvak V, Jha A, Eusebio A, Oostenveld R, Foltynie T, Limousin P, et al. Resting oscillatory cortico-subthalamic connectivity in patients with Parkinson's disease. Brain 2011;134(Pt 2):359–74. https://doi.org/10.1093/brain/awq332.
[38] Caire F, Ranoux D, Guehl D, Burbaud P, Cuny E. A systematic review of studies on anatomical position of electrode contacts used for chronic subthalamic stimulation in Parkinson's disease. Acta Neurochir 2013;155(9):1647–54. https://doi.org/10.1007/S00701-013-1782-1.
[39] Park KH, Sun S, Lim YH, Park HR, Lee JM, Park K, et al. Clinical outcome prediction from analysis of microelectrode recordings using deep learning in subthalamic deep brain stimulation for Parkinson's disease. PLoS One 2021. https://doi.org/10.1371/journal.pone.0244133. Published online.
[40] Kostoglou K, Michmizos KP, Stathis P, Sakas D, Nikita KS, Mitsis GD. Classification and prediction of clinical improvement in deep brain stimulation from intraoperative microelectrode recordings. IEEE Trans Biomed Eng 2017;64(5). https://doi.org/10.1109/TBME.2016.2591827.
[41] Shah A, Nguyen TAK, Peterman K, Khawaldeh S, Debove I, Shah SA, et al. Combining multimodal biomarkers to guide deep brain stimulation programming in Parkinson disease. Neuromodulation Technol Neural Interface 2022. https://doi.org/10.1016/J.NEUROM.2022.01.017. Published online.
[42] Horn A, Reich M, Vorwerk J, Li N, Wenzel G, Fang Q, et al. Connectivity predicts deep brain stimulation outcome in Parkinson disease. Ann Neurol 2017;82(1):67–78. https://doi.org/10.1002/ana.24974.
[43] Li N, Baldermann JC, Kibleur A, Treu S, Akram H, Elias GJ, et al. A unified connectomic target for deep brain stimulation in obsessive-compulsive disorder. Nat Commun 2020. https://doi.org/10.1038/s41467-020-16734-3. Published online.
[44] Baldermann JC, Melzer C, Zapf A, Kohl S, Timmermann L, Tittgemeyer M, et al. Connectivity profile predictive of effective deep brain stimulation in obsessive-compulsive disorder. Biol Psychiatr 2019. https://doi.org/10.1016/j.biopsych.2018.12.019. Published online.
[45] Johnson KA, Duffley G, Anderson DN, Ostrem JL, Welter M-L, Baldermann JC, et al. Structural connectivity predicts clinical outcomes of deep brain stimulation for Tourette syndrome. Brain 2020. https://doi.org/10.1093/brain/awaa188. Published online.
[46] Al-Fatly B, Ewert S, Kübler D, Kroneberg D, Horn A, Kühn AA. Connectivity profile of thalamic deep brain stimulation to effectively treat essential tremor. Brain 2019. https://doi.org/10.1093/brain/awz236. Published online.
[47] Little S, Brown P. The functional role of beta oscillations in Parkinson's disease. Park Relat Disord 2014;20(Suppl. 1):S44–8. https://doi.org/10.1016/S1353-8020(13)70013-0.
[48] Trottenberg T, Kupsch A, Schneider GH, Brown P, Kühn AA. Frequency-dependent distribution of local field potential activity within the subthalamic nucleus in Parkinson's disease. Exp Neurol 2007;205(1):287–91. https://doi.org/10.1016/J.EXPNEUROL.2007.01.028.
[49] Wang J, Hirschmann J, Elben S, Hartmann CJ, Vesper J, Wojtecki L, et al. High-frequency oscillations in Parkinson's disease: spatial distribution and clinical relevance. Mov Disord 2014;29(10):1265–72. https://doi.org/10.1002/mds.25962.
[50] Gradinaru V, Mogri M, Thompson KR, Henderson JM, Deisseroth K. Optical deconstruction of parkinsonian neural circuitry. Science 2009;(5925):324.
[51] Oswal A, Cao C, Yeh C-H, Neumann W-J, Gratwicke J, Akram H, et al. Neural signatures of hyperdirect pathway activity in Parkinson's disease. Nat Commun 2021;12(1):1–14. https://doi.org/10.1038/s41467-021-25366-0.
[52] Bore JC, Campbell BA, Cho H, Gopalakrishnan R, Machado AG, Baker KB. Prediction of mild parkinsonism revealed by neural oscillatory changes and machine learning. J Neurophysiol 2020. https://doi.org/10.1152/jn.00534.2020. Published online.
[53] Hirschmann J, Özkurt TE, Butz M, Homburger M, Elben S, Hartmann CJ, et al. Differential modulation of STN-cortical and cortico-muscular coherence by movement and levodopa in Parkinson's disease. Neuroimage 2013;68:203–13. https://doi.org/10.1016/j.neuroimage.2012.11.036.
[54] Trošt M, Su S, Su P, Yen R-F, Tseng H-M, Barnes A, et al. Network modulation by the subthalamic nucleus in the treatment of Parkinson's disease. Neuroimage 2006;31(1):301–7. https://doi.org/10.1016/J.NEUROIMAGE.2005.12.024.
[55] Hilker R, Voges J, Weisenbach S, Kalbe E, Burghaus L, Ghaemi M, et al. Subthalamic nucleus stimulation restores glucose metabolism in associative and limbic cortices and in cerebellum: evidence from a FDG-PET study in advanced Parkinson's disease. J Cerebr Blood Flow Metabol 2004;24(1):7–16. https://doi.org/10.1097/01.WCB.0000092831.44769.09.
[56] Mathys C, Caspers J, Langner R, Südmeyer M, Grefkes C, Reetz K, et al. Functional connectivity differences of the subthalamic nucleus related to Parkinson's disease. Hum Brain Mapp 2016;37(3):1235–53. https://doi.org/10.1002/HBM.23099.
[57] Osada T, Ohta S, Ogawa A, Tanaka M, Suda A, Kamagata K, et al. An essential role of the intraparietal sulcus in response inhibition predicted by parcellation-based network. J Neurosci 2019;39(13):2509–21. https://doi.org/10.1523/JNEUROSCI.2244-18.2019.
[58] Chen W, de Hemptinne C, Miller AM, Leibbrand M, Little SJ, Lim DA, et al. Prefrontal-subthalamic hyperdirect pathway modulates movement inhibition in humans. Neuron 2020;106(4):579–88. https://doi.org/10.1016/J.NEURON.2020.02.012. e3.
[59] Garavan H, Ross TJ, Stein EA. Right hemispheric dominance of inhibitory control: an event-related functional MRI study. Proc Natl Acad Sci Unit States Am 1999;96(14):8301–6. https://doi.org/10.1073/pnas.96.14.8301.
[60] Aron AR, Poldrack RA. Cortical and subcortical contributions to Stop signal response inhibition: role of the subthalamic nucleus. J Neurosci 2006;26(9):2424–33. https://doi.org/10.1523/JNEUROSCI.4682-05.2006.
[61] Neumann WJ, Kühn AA. Subthalamic beta power—unified Parkinson's disease rating scale III correlations require akinetic symptoms. Mov Disord 2017. https://doi.org/10.1002/mds.26858. Published online.
[62] Glaser JI, Benjamin AS, Farhoodi R, Kording KP. The roles of supervised machine learning in systems neuroscience. Prog Neurobiol 2019. https://doi.org/10.1016/j.pneurobio.2019.01.008. Published online.

Synchrony between subthalamic and cortical oscillations predicts deep brain stimulation outcome in Parkinson's disease

Supplementary Material

Tab. S1: Patient details. Note the difference in contact naming convention: most ventral Medtronic: 0; most ventral Boston Scientific and Abbott: 1.

ID	study	age [y]	sex	disease duration [y]	electrode type	UPDRS III Med Off/ Stim Off	UPDRS III Med Off/ Stim On	time btw. MEG and UPDRS [m]	data length [min]	active left	sel. chan left	active in biool ar	active right	sel. chan right	active in bipolar
S01	1	76	w	22	Medtronic/ non-seg	49	30	2	9.63	2	12	y	1	12	y
S02	1	70	m	11	Medtronic /non-seg	23	15	3	9.88	1	12	y	1	12	y
S03	1	64	w	19	Medtronic/ non-seg	34	21	5	9.42	12	12	y	12	12	y
S04	1	62	w	15	Medtronic /non-seg	46	37	3	9.84	23	23	y	23	23	y
S05	1	54	m	10	Medtronic/ non-seg	25	13	4	8.75	2	12	y	3	23	y
S06	1	48	m	10	Medtronic/ non-seg	51	29	3	9.93	2	12	y	23	23	y
S07	1	66	m	8	Medtronic/ non-seg	34	22	7	10	2	12	y	2	23	y
S08	1	60	m	6	Medtronic/ non-seg	33	12	4	10.00	1	12	y	0	01	y
S09	1	69	m	2	Medtronic/ non-seg	38	19	11	9.75	1	12	y	1	12	y
S10	1	53	m	11	StJude/non-seg	22	10	6	9.98	2	12	y	2	12	y
S11	1	61	w	10	Medtronic/ non-seg	44	28	5	9.87	1	12	y	1	12	y
S12	1	54	m	12	StJude/non-seg	37	22	6	10.00	1	12	y	1	12	y
S13	1	52	m	7	Boston Sc./non-seg	50	34	14	5.00	4	34	y	4	34	y
S14	1	53	m	6	Boston Sc./non-seg	35	12	5	4.65	3	23	y	3	23	y
S15	1	45	m	5	Medtronic/ non-seg	57	40	45	1.18	2	02	y	2	12	y
S16	1	45	w	9	Medtronic/ non-seg	30	16	3	3.09	0	01	y	0	02	y
S17	1	62	w	3	Medtronic /non-seg	38	15	3	5.17	1	02	n	1	02	n
S18	1	75	w	14	Medtronic/ non-seg	58	36	2	3.83	1	12	y	13	12	y
S19	1	52	m	4	Medtronic/ non-seg	40	18	5	4.52	1	12	y	1	12	y

S20	1	55	m	11	Boston Sc./non-seg	52	47	24	10.70	2	12	y	5	56	y
S21	2	69	m	12	Abbott/seg	42	18	4	23.98	2ABC	2A-3A,2B-3B,2C-3C	y	2B	2B-3B	y
S22	2	56	m	6	Abbott/seg	23	17	4	29.60	2AB	2A-3A,2B-3B	y	2B	2B-3B	y
S23	2	65	m	13	Abbott/seg	34	26	4	26.68	1	2A-3A,2B-3B,2C-3C	n	2ABC	2A-3A,2B-3B,2C-3C	y
S24	2	62	w	19	Abbott/seg	34	8	3	14.83	2ABC	3B-4,3C-4	n	2ABC	2A-3A,2B-3B,2C-3C	y
S25	2	70	m	5	Abbott/seg	53	34	4	27.37	2ABC	2C-3C	y	2ABC	2A-3A,2C-3C	y
S26	2	56	m	7	Abbott/seg	30	26	14	24.58	2B	3A-4	n	2C	1-2C	y
S27	2	60	w	6	Abbott/seg	48	34	4	29.83	3ABC	2B-3B,2C-3C	y	3ABC	3A-4,3B-4	y
S28	2	47	m	6	Abbott/seg	39	29	3	29.10	2AC	2A-3A,2C-3C	y	2ABC	2A-3A,2B-3B,2C-3C	y
S29	2	59	m	15	Abbott/seg	50	31	4	29.10	2ABC	2C-3C	y	2ABC	2B-3B,2C-3C	y
S30	2	41	m	7	Abbott/seg	55	30	3	21.58	2ABC	2A-3A,2B-3B,2C-3C	y	2ABC	2A-3A,2B-3B,2C-3C	y
S31	2	59	w	9	Abbott/seg	42	31	3	9.12	2C	2C-3C	y	2C	2A-3A	n
S32	2	72	w	3	Abbott/seg	28	18	6	28.97	3ABC	2A-3A,2C-3B	y	2ABC	2A-3A,2B-3B,2C-3C	y
S33	2	68	m	10	Abbott/seg	40	30	3	29.33	2ABC	2A-3A,2B-3B,2C-3C	y	2ABC	2A-3A,2B-3B,2C-3C	y
S34	2	54	m	3	Abbott/seg	13	11	14	28.17	1	1-2A,1-2B,1-2	y	2AC	2A-3A,2C-3C	y
S35	2	59	m	10	Abbott/seg	48	45	2	17.33	2C	2C-3C	y	3B	2B-3B	y
S36	2	56	w	5	Abbott/seg	34	16	15	27.83	3ABC	2B-3B,2C-3C	y	2B	2B-3B	y
μ		59.1		9.1		39.1	24.4	6.9	15.3						
σ		8.7		4.7		10.9	10.1	8.0	9.7						

Tab. S2: *Details on cortical areas.* The table lists parcel labels along with the x, y and z coordinates of the grid point cloud centroids.

area	x	y	z
SensorimotorR	38.28	-14.42	54.59
FrontalSupR	17.78	33.48	41.75
FrontalMedR	36.35	38.63	20.92
FrontalInfR	52.30	31.11	1.94
ParietalSupR	23.00	-60.67	64.84
ParietalInfR	52.73	-47.50	47.29
TemporalSupR	63.47	-13.85	3.22

TemporalMidR	59.85	-23.91	-11.06
TemporalInfR	58.30	-35.63	-24.14
OccipitalSupR	19.94	-94.60	24.55
OccipitalMidR	39.38	-85.00	17.80
OccipitalInfR	29.33	-95.00	-9.09
AngularR	47.81	-65.00	39.75
SupraMarginalR	61.83	-32.50	34.73
CerebellumR	33.90	-61.22	-46.50
SensorimotorL	-39.35	-12.95	54.26
FrontalSupL	-14.80	44.73	30.35
FrontalMedL	-32.91	40.96	24.72
FrontalInfL	-50.60	29.52	3.11
ParietalSupL	-17.14	-61.76	64.62
ParietalInfL	-49.08	-51.11	46.36
TemporalSupL	-59.66	-8.18	-1.40
TemporalMidL	-61.87	-31.36	-5.78
TemporalInfL	-59.29	-28.33	-25.71
OccipitalSupL	-8.64	-97.80	21.46
OccipitalMidL	-33.41	-91.75	10.92
OccipitalInfL	-24.92	-91.83	-10.07
AngularL	-48.73	-66.00	36.52
SupraMarginalL	-61.99	-33.33	30.51
CerebellumL	-31.65	-61.54	-46.86

Parameter tuning

Our tuning procedure was inspired by this blog post: https://www.analyticsvidhya.com/blog/2016/03/complete-guide-parameter-tuning-xgboost-with-codes-python. We started with an initial choice that differed slightly from the default settings to account for the small sample size and the associated risk of overfitting (*learning_rate* = 0.05 , *min_child_weight* = 2, *subsample* = 0.8, *colsample_bytree* = 0.8). Following an initial tuning of the number of trees, the parameters *subsample* and *colsample_bytree*, followed by *min_child_weight*, were tuned in nested cross-validation using the Hyperopt toolbox (Bergstra et al., 2013). We tuned these parameters specifically because they had the strongest effect on the model output in our study. After tuning, we lowered the leaning rate and re-estimated the best number of trees for the refined settings. This was the final parameter selection.

Tab. S3: *XGBoost parameters.* Parameters in italic were tuned in 3-fold cross-validation, nested in the leave-one-out loop. For these parameters, the table provides the minimum, the median and maximum value used in any of the models. The remaining parameters were the same for all models.

parameter name	**value**
base_score	0.5
booster	gbtree
colsample_bylevel	1
colsample_bynode	1
colsample_bytree	0.50; 0.70; 0.99
gamma	0

learning_rate	0.05
max_delta_step	0
max_depth	4
min_child_weight	1.00; 2.00; 12.00
missing	None
n_estimators	204; 363; 1874
objective	reg:squarederror
reg_alpha	0
reg_lambda	0
scale_pos_weight	1
subsample	0.5; 0.73; 0.99

High-frequency coherence

Fig. S1 depicts STN-cortex coherence in the HFO range for every hemsiphere.

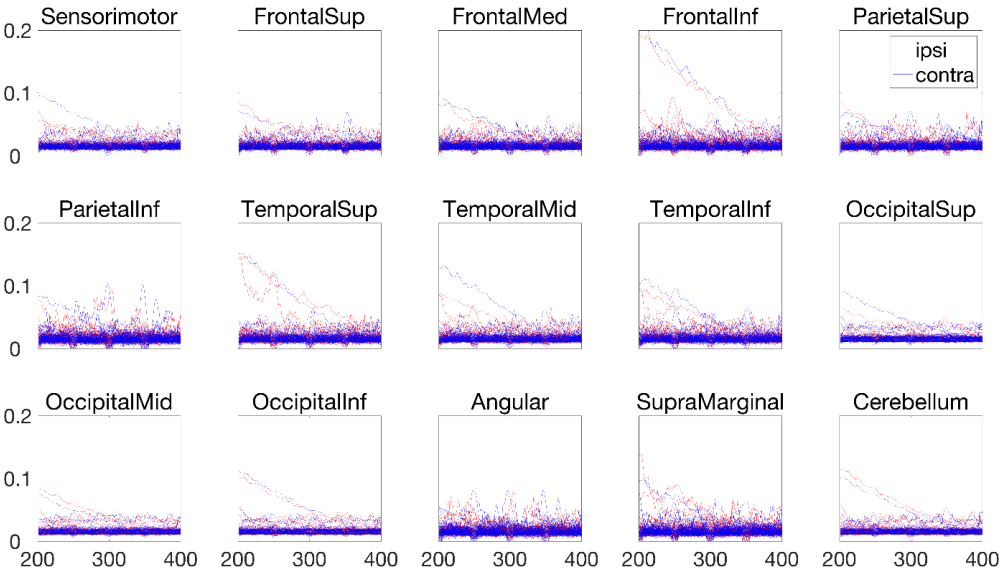

***Fig. S1** : High-frequency STN-cortex coherence.* Spectra were computed using the multitaper method with ±5Hz spectral smoothing. Occasional artifact at line noise harmonics were removed and replaced by interpolated values.

Alternative designs

For the analysis presented in the main paper, patient feature vectors were constructed by stacking the left hemisphere feature vector onto the right hemisphere feature vector (compare main paper Fig. 1). Here, we tested an alternative organization of features, reflecting the body-side asymmetry characteristic of PD. We stacked the features of the hemisphere contralateral to the more affected body side onto the features of the hemisphere ipsilateral to the more affected body side, and re-ran the performance analysis described in the main paper (compare main paper Fig. 4). Prediction with

the connectivity model was still possible, but the model required more features than in the original analysis (Fig. S2A). Local models could not predict DBS benefit with this design.

We further tried predicting the DBS-induced reduction of the UPDRSIII hemibody sum score using only the features of the contralateral hemisphere. Prediction was not successful with this setting (Fig. S2B), suggesting that information from both hemispheres is needed for estimating DBS benefit.

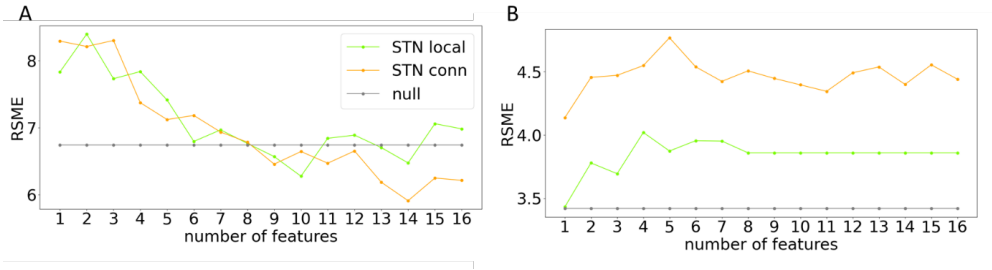

***Fig. S2** : Root mean squared error vs. number of features for alternative designs.* **A)** Predicting UPDRSIIII sum score improvement from features organized with respect to the symptom-dominant body side. **B)** Predicting UPDRSIIII hemibody score improvement from electrophysiological features of the contralateral hemisphere.

Control Analyses

Given the critical role of lead placement for DBS efficacy, we asked if the oscillatory features used here might reflect contact distance to target. First, we extracted the auxiliary features "distance between bipolar LFP channel and sweet spot left" and "distance between bipolar LFP channel and sweet spot right". The sweet spot was chosen according to (Caire et al., Acta Neurochir (Wien) 2013; 155: 1647– 1654; MNI coordinates: x = ±12.6, y = −13.4, z = −5.9 mm). This was done by computing the Euclidian distance between the sweet spot for both contacts of each bipolar contact pair. The distance between a bipolar channel and the sweet spot was defined as the smaller one of the two distances. An alternative definition of distance based on the midpoint of the line connecting both contacts of a pair was also tested and yielded similar results.

Neither of the five best connectivity features nor of the five best local features correlated significantly with distance to the sweet spot following FDR correction (lowest corrected p = 0.16). Distance alone was not sufficient to predict DBS outcome in our sample ($RMSE_{dist}$= 9.25, r_{dist}= -0.17, p_{dist}=0.33). When the distance features were added to the best-5 local model, performance increased slightly (ΔRMSE = 0.66) and the distance features ranked 5th and 6th of 7 with respect to SHAP value. When the distance features were added to the best-5 connectivity model, performance did not change (ΔRMSE = -0.02) and the distance features ranked 6th and 7th of 7 with respect to SHAP value. In summary, these results suggest that oscillations convey information on DBS outcome above and beyond distance to target.

In another set of control analyses, we assessed several potential confounders that might be trivially correlated with DBS benefit and/or neuronal oscillations and might underlie the predictions reported here. These included *recording duration*, *electrode type (segmented vs. non-segmented)* and *days passed since recording*, all of which differed markedly across the two studies contributing data. None of these variables allowed for predicting DBS outcome on their own ($RMSE_{dur}$=9.83, $RMSE_{type}$= 6.81, $RMSE_{days}$=8.77, $RMSE_{Null}$=6.74; r_{dur}= -0.26, r_{type}= -0.04, r_{days}= 0.08; p_{dur}= 0.12, p_{type}= 0.83, p_{days}=0.63). When added to the best-5 connectivity model or the best-5 local model, the performance of these models hardly changed ($\Delta RMSE_{local}$ = 0.60, $\Delta RMSE_{conn}$ = -0.07). When ranked by SHAP value, the

potential confounders ranked 8th (last), 7th and 6th for the connectivity model and 8th, 7th and 5th for the local model. We conclude that the success of the electrophysiological models cannot be explained by correlations with either recording duration, electrode type or time since recording.

We further investigated whether a contact's signal-to-noise ratio (SNR) might affect prediction. To estimate SNR, we assessed the STN power spectra. We integrated power over the periodic and the aperiodic components estimated by the FOOOF algorithm and divided these integrals, i.e. we computed the ratio between total peak power and total 1/f-background. In case of segmented leads, we averaged SNR over segments. SNR did not allow for predicting DBS outcome on its own ($RMSE_{SNR}$= 11.56, r_{SNR}=-0.45, p_{SNR}= 0.006). When added to the best-5 connectivity model or the best-5 local model, the performance of these models decreased slightly ($\Delta RMSE_{local}$ = -0.32 , $\Delta RMSE_{conn}$ = -0.23).

Shuffling

To test the importance of true phase relationships to our connectivity models, we repeated our analyses with shuffled, surrogate data. LFP data segments were randomly reassigned to MEG data segments from the same recording, but a different point in time. This approach destroys true phase relationships between STN and cortex while maintaining other properties such as the noise floor. Following shuffling, connectivity features were re-computed and DBS benefit was predicted as before. The procedure was repeated 50 times, to obtain a surrogate distribution of RMSE values. As depicted in Fig. S3, the original RMSE achieved by the best-5 connectivity model was lower than any value of the surrogate distribution, suggesting that phase relationships are indeed relevant.

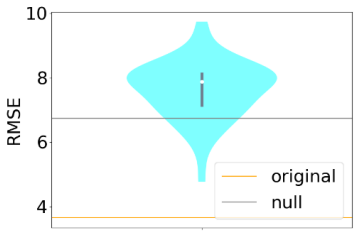

***Fig. S3**: Shuffling abolished the ability to predict DBS outcome from STN-cortex coherence. Blue: Full surrogate distribution of the root mean squared error (RMSE) obtained by shuffling data segments in time. The white dot represents the median, the gray bar the 2nd-3rd quartile range. The RMSE associated with the original best-5 connectivity features is shown as an orange line, the RMSE achieved by the null model as a gray line.*

9.2 Article II: Mapping Subcortico-Cortical Coupling—A Comparison of Thalamic and Subthalamic Oscillations

Reproduced from

Alexandra Steina, Sarah Sure, Markus Butz, Jan Vesper, Alfons Schnitzler, & Jan Hirschmann

Mapping Subcortico-Cortical Coupling—A Comparison of Thalamic and Subthalamic Oscillations

Movement Disorders **39**, 684-693 (2024)

Digital Object Identifier (DOI): https://doi.org/10.1002/mds.29730

Statement of contribution

S.S. and J.H. planned the research project (Paper II, III and IV). Data collection started before the start of my PhD. I recorded more patients throughout my doctorate with J.H., M.B. I planned the analysis, pre-processed and processed the data. I prepared the figures for the manuscript. All authors discussed the results. I wrote the manuscript. J.H., S.S., M.B., J.V., A.Sc. edited the manuscript.

Copyright and license notice

RESEARCH ARTICLE

Mapping Subcortico-Cortical Coupling—A Comparison of Thalamic and Subthalamic Oscillations

Alexandra Steina, MSc,[1] Sarah Sure, MD,[1] Markus Butz, PhD,[1] Jan Vesper, MD,[2] Alfons Schnitzler, MD,[1] and Jan Hirschmann, PhD[1*]

[1]*Institute of Clinical Neuroscience and Medical Psychology, Medical Faculty, Heinrich Heine University, Düsseldorf, Germany*
[2]*Department of Functional Neurosurgery and Stereotaxy, Neurosurgical Clinic, Medical Faculty, Heinrich Heine University, Düsseldorf, Germany*

ABSTRACT: Background: The ventral intermediate nucleus of the thalamus (VIM) is an effective target for deep brain stimulation in tremor patients. Despite its therapeutic importance, its oscillatory coupling to cortical areas has rarely been investigated in humans.
Objectives: The objective of this study was to identify the cortical areas coupled to the VIM in patients with essential tremor.
Methods: We combined resting-state magnetoencephalography with local field potential recordings from the VIM of 19 essential tremor patients. Whole-brain maps of VIM–cortex coherence in several frequency bands were constructed using beamforming and compared with corresponding maps of subthalamic nucleus (STN) coherence based on data from 19 patients with Parkinson's disease. In addition, we computed spectral Granger causality.
Results: The topographies of VIM–cortex and STN–cortex coherence were very similar overall but differed quantitatively. Both nuclei were coupled to the ipsilateral sensorimotor cortex in the high-beta band; to the sensorimotor cortex, brainstem, and cerebellum in the low-beta band; and to the temporal cortex, brainstem, and cerebellum in the alpha band. High-beta coherence to sensorimotor cortex was stronger for the STN ($P = 0.014$), whereas low-beta coherence to the brainstem was stronger for the VIM ($P = 0.017$). Although the STN was driven by cortical activity in the high-beta band, the VIM led the sensorimotor cortex in the alpha band.
Conclusions: Thalamo-cortical coupling is spatially and spectrally organized. The overall similar topographies of VIM–cortex and STN–cortex coherence suggest that functional connections are not necessarily unique to one subcortical structure but might reflect larger frequency-specific networks involving VIM and STN to a different degree. © 2024 The Authors. *Movement Disorders* published by Wiley Periodicals LLC on behalf of International Parkinson and Movement Disorder Society.

Key Words: essential tremor; ventral intermediate nucleus; local field potentials; magnetoencephalography; subthalamic nucleus

Essential tremor (ET) is the most common movement disorder with a global prevalence of 0.32% across all ages.[1] ET patients suffer primarily from isolated upper limb intention tremor and postural tremor.[2-4] The underlying pathophysiology is only partially understood, but abnormalities in the cerebello-thalamo-cortical circuit seem to play a key role in the generation of tremor.[4-7] Deep brain stimulation (DBS) of the ventral intermediate nucleus of the thalamus (VIM) is a standard therapy to treat severe ET. Recent studies have demonstrated that the optimal stimulation site for tremor suppression is the inferior border of the VIM in proximity to the dentatorubrothalamic tract (DRTT).[8-11]

*Correspondence to: Dr. Jan Hirschmann, Institute of Clinical Neuroscience and Medical Psychology, Medical Faculty, Heinrich Heine University, Moorenstraße 5, 40225 Düsseldorf, Germany; E-mail: jan.hirschmann@med.uni-duesseldorf.de

Funding agency: This project was funded by Brunhilde Moll Stiftung.

Relevant conflicts of interest/financial disclosures: Nothing to report.

Received: 27 June 2023; **Revised:** 29 November 2023; **Accepted:** 8 January 2024

Published online 21 February 2024 in Wiley Online Library (wileyonlinelibrary.com). DOI: 10.1002/mds.29730

Besides the clinical benefit, DBS can also facilitate insights into basic neurophysiology. The implantation of electrodes for DBS provides the unique opportunity to record local field potentials (LFPs) from the DBS target structure. LFP recordings from the VIM of tremor patients revealed prominent oscillatory activity at tremor frequency that increases in amplitude in the presence of tremor.[12] These oscillations can be used to detect tremor episodes and might be a potential feedback signal for closed-loop DBS.[13] Tremor oscillations in the VIM are coherent with accelerometer signals and electromyographic recordings from the tremulous hand at tremor and double tremor frequency,[7,14] and this connectivity is organized in distinct spatial clusters within the VIM.[15]

Oscillatory coupling between deep brain structures and cortical areas is commonly interpreted as communication in spatio-temporally organized networks.[16-18] Frequency-specific networks at rest have been described for several DBS targets, such as the subthalamic nucleus (STN)[17,19-22] and the globus pallidus internus (GPi),[23,24] for example. The STN forms an alpha-band (8–12 Hz) network with brainstem and temporal regions. At beta frequencies (13–30 Hz), the STN couples to motor and premotor cortex, with cortex driving STN activity.[17,19,22,24] The GPi couples to cerebellar sources in the alpha band and to sensorimotor areas in the beta frequency band.[23] A map of oscillatory coupling between the VIM and cortex has not been presented yet.

Here, we set out to close this knowledge gap. To localize cortical areas functionally coupled to the VIM, we performed simultaneous magnetoencephalography (MEG)–LFP recordings in 19 ET patients at rest. We compared the identified networks with STN–cortical networks, based on the data of 19 Parkinson's disease (PD) patients. Furthermore, we assessed spectral Granger causality between cortical and subcortical areas to estimate the directionality of coupling.

Materials and Methods

Patient and Measurement Details

A total of 19 patients undergoing DBS surgery participated in this study. All patients had been implanted with deep brain macroelectrodes of different types (see Table S1 of the Supplementary Material) for VIM DBS the day before measurement. The pulse generator was not implanted at this stage, and electrodes were externalized so that they could be used for LFP recordings. All measurements took place with prior written informed consent according to the Declaration of Helsinki, and the study was approved by the Ethics Committee of the Medical Faculty of Heinrich Heine University Düsseldorf (ET, "2018-217-Zweitvotum"; PD, nos. 3209 and 5608). In addition to the ET group, we included data from PD patients implanted with electrodes for STN stimulation (see Table S2 for patient details) collected in other studies.[19-21] PD patients were recorded with the same experimental setup as ET patients, after overnight withdrawal from dopaminergic medications for at least 12 hours.[19-21]

MEG signals were recorded by a 306-channel MEG system (Vectorview, MEGIN) with sampling rates of 2 kHz (ET) and 2.4 kHz (PD), respectively. LFP signals were recorded simultaneously using the externalized leads and a mastoid reference. LFP signals were rearranged into a bipolar montage offline by subtracting the signals of adjacent contacts. In addition, we recorded electromyograms (EMG) from both forearms, accelerometer signals from both index fingers, and horizontal and vertical electrooculograms. Patients were instructed to sit still in an upright position with eyes open for 5 to 10 minutes.

Data Analysis

Contact Selection

We localized the DBS electrodes using LeadDBS using preoperative magnetic resonance imaging (MRI) and postoperative computed tomography scans.[25] For VIM-DBS, recent studies have shown that the best tremor suppression can be achieved when stimulating at the ventral border of the VIM in the proximity of DRTT fibers.[8-11] For STN-DBS, the best overall motor improvement was achieved when stimulating the dorsolateral part of the STN.[26,27] We selected one bipolar contact pair for each hemisphere and each patient such that they were as close as possible to reported DBS "sweet spots" (VIM: $X = \pm 15$ mm, $Y = -18.5$ mm, $Z = -2.5$ mm[11]; STN: $X = 12.42/-12.58$ mm, $Y = -12.58/-13.53$ mm, $Z = -5.38$ mm[27]) while ensuring that at least one of the contacts was inside the target structure. We excluded four electrodes in each patient group based on the reconstructed position due to presumably suboptimal placement.

Data Preprocessing

The data were processed with the Fieldtrip toolbox[28] and self-written MATLAB (The MathWorks, Inc., Natick, MA, USA) scripts. MEG and LFP data were visually inspected for artifacts. EMG channels were scanned for tremor, and epochs with tremor were discarded. Bad channels and epochs with other artifacts such as sensor jumps were discarded. The remaining data length was 377 seconds (mean) ± 184 seconds (standard deviation) for the ET group and 409 seconds (mean) ± 80 seconds (standard deviation) for the PD group. For spectral analysis, data were high-pass filtered at 1 Hz, downsampled to 500 Hz, and segmented into 2-second trials with 50% overlap.

Local Oscillatory Activity

Power spectra (2–35 Hz) for VIM and STN were computed using a Hanning taper. Physiological power spectra are thought to be composed of two distinct components: an aperiodic component (1/f) and a periodic component, represented by distinct peaks in a spectrum.[29,30] To make spectra comparable between patients, the aperiodic component was modeled using the fitting oscillations and one over f algorithm and then subtracted from the power spectrum.[31] The aperiodic and periodic components were visually inspected, and the model order was adapted, if necessary, to ensure a good model fit.[32]

VIM/STN–Cortex Coupling

We localized brain areas coherent with VIM/STN activity in four different frequency bands: theta (3–7 Hz), alpha (7–13 Hz), low beta (13–21 Hz), and high beta (21–35 Hz). Rather than computing coherence for each integer frequency, we applied bandwidth-wide spectral smoothing to capture an entire band in one estimate using the multitaper method.[33] Coherence was localized by applying dynamic imaging of coherent sources[34] to the LFP-MEG cross-spectral densities. For this purpose, we created single-shell head models based on the individual T1-weighted MRI scan (Siemens Mangetom Tim Trio, 3-T MRI scanner). The three-dimensional beamformer grid had a spacing of 1 cm and was aligned to Montreal Neurological Institute (MNI) space. Beamforming yielded volumetric images of coherence for each contact pair and each frequency band. In addition, we mapped the imaginary part of coherency to exclude spurious coherence caused by volume conduction.[35]

All source images of coherence with the left VIM/STN were mirrored across the mid-sagittal plane to allow comparisons between the contra- and ipsilateral hemispheres. Coherence images were normalized by dividing by the mean over all voxels. For segmented leads, we averaged coherence and power across segments for reasons of comparability with a nonsegmented lead.

Directionality Analysis

We performed directionality analysis for VIM/STN and two cortical regions of interest ipsilateral to the DBS target: brainstem (X = ± 10 mm, Y = −10 mm, Z = −20 mm) and medial sensorimotor cortex (X = ± 20 mm, Y = −40 mm, Z = 70 mm). These regions were selected because coherence with these regions differed between the VIM and STN. For each region of interest (ROI) and its nine closest neighboring grid points, we first extracted time-domain source activity using a linearly constrained minimum variance beamformer.[36] Next, we computed directional connectivity with VIM/STN for each grid point and averaged it over neighboring grid points to improve the signal-to-noise ratio. Downsampling and filtering were not applied in this analysis. Directionality of subcortico–cortical coupling was quantified by a nonparametric variant of spectral Granger causality,[37,38] as implemented in the Fieldtrip function *ft_connectivity_granger*.

Granger causality estimates are influenced by several factors, including volume conduction. To reduce the influence of trivial factors, Granger causality estimates of the original data were compared with those of time-reversed data.[39] If a signal A Granger causes another signal B, Granger causality from A to B should be higher for the original data than for the time-reversed data, resulting in a positive difference between original and time-reversed data. Granger causality from B to A, in contrast, should be lower for the original than for the time-reversed case, resulting in a negative difference. Hence, the sign of the difference contains information about the direction, and the across-subject consistency of the difference is an indicator of significance.[39]

Statistical Analysis

Differences between the VIM and STN in power and coherence were assessed with a nonparametric, cluster-based permutation test (statistic: largest sum of cluster t values, 2000 permutations), as implemented in Fieldtrip.[40] As in many previous works on LFP-MEG coherence,[17,19,24] the unit of observation was hemispheres, not patients ($N_{ET} = 34$, $N_{PD} = 34$).

Differences in directed connectivity were assessed with a repeated measures analysis of variance in SPSS (IBM Corp.) with the following factors: direction (midbrain > cortex, cortex > midbrain), frequency band (alpha, low beta, high beta), and cortical area (sensorimotor cortex, brainstem).

Results

Local Oscillatory Activity

Figure 1A,B depicts the subcortical recording locations and group average; 1/*f*-corrected spectral power for the VIM and the STN is displayed in Figure 1C. Alpha and low-beta peaks were found in both structures. Spectral peaks in the high-beta range, however, occurred in the STN only. Power in this frequency band was significantly higher in the STN compared with the VIM (cluster-based permutation test, $t_{clustersum} = 49.51$, $P = 0.001$, frequency range: 19–33 Hz).

Subcortico–Cortical Coupling

Qualitatively, the topographies of VIM–cortex and STN–cortex coherence were similar (Fig. 2).

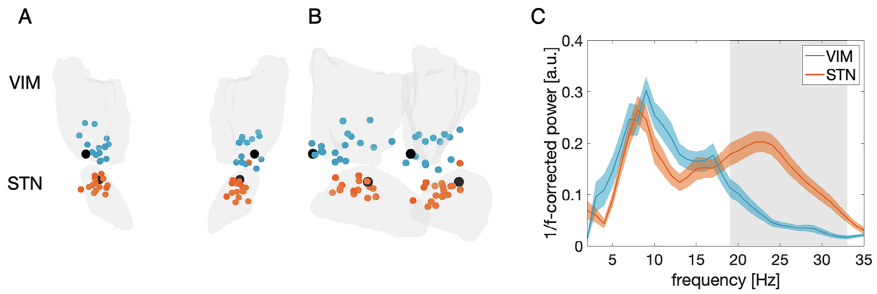

FIG. 1. Local oscillations in ventral intermediate nucleus of the thalamus (VIM) and subthalamic nucleus (STN). Frontal (A) and a lateral view (B) on reconstructed local field potential recording sites. Sweet spots in black. (C) Group- and hemisphere-average power spectral densities for VIM (blue) and STN (orange) after subtraction of the aperiodic component. Shaded areas represent the standard error of the mean. The gray shading indicates significant differences between the VIM and STN. [Color figure can be viewed at wileyonlinelibrary.com]

Spatial patterns of coherence were frequency specific and clearly lateralized to the ipsilateral hemisphere with respect to the subcortical recoding site. In the theta band, temporal cortex and hippocampus coupled strongest to the VIM and STN (Fig. 2A,B). Coupling in the alpha band likewise involved the temporal cortex and the brainstem (Fig. 2C,D). In the low-beta band, VIM and STN activity were coupled to the brainstem and the cerebellum, but also to motor areas (Fig. 2E,F). In the high-beta band, both structures displayed strongest coherence with the medial sensorimotor cortex (Fig. 2G,H). This coupling did not correlate with disease severity in PD patients (Fig. S3). The spatial patterns persisted when considering the imaginary part of coherency, an alternative coupling measure insensitive to volume conduction (Fig. S1).

Differences between VIM–Cortex and STN–Cortex Coupling

Notwithstanding their qualitative similarity, we observed quantitative differences between VIM– and STN–cortex coherence (Fig. 3). Coupling to the brainstem was stronger for the VIM than for the STN in the low-beta band (cluster-based permutation test: $t_{clustersum} = 311.82$, $P = 0.017$; Fig. 3A), whereas medial sensorimotor areas were more coherent with the STN than with the VIM in the high-beta band ($t_{clustersum} = 367.03$, $P = 0.014$; Fig. 3B). The difference in the high-beta band remained when PD patients were *on* medication ($t_{clustersum} = 275.03$, $P = 0.038$; Fig. S2).

Based on these results, we selected the cluster centroids of the low-beta brainstem cluster (MNI coordinates: X = 10 mm, Y = −10 mm, Z = 20 mm; Fig. 4C)

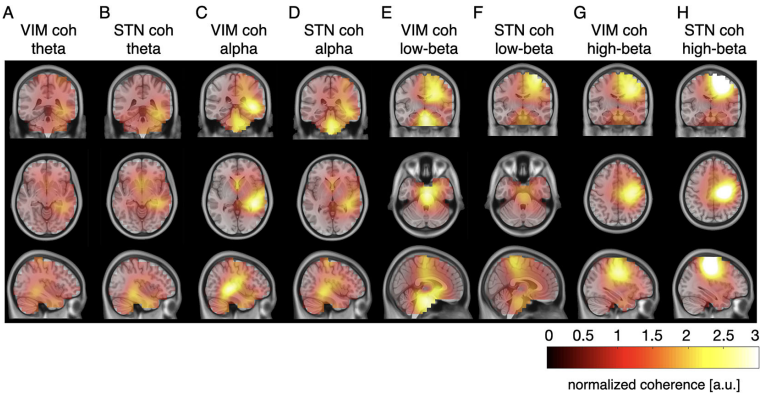

FIG. 2. Qualitative similarity between ventral intermediate nucleus of the thalamus (VIM) and subthalamic nucleus (STN)–cortex coherence. Group-average source images of normalized VIM–cortex (A, C, E, G) and STN–cortex (B, D, F, H) coherence for different frequency bands. The right side corresponds to the ipsilateral side with respect to the subcortical recording site. coh, coherence. [Color figure can be viewed at wileyonlinelibrary.com]

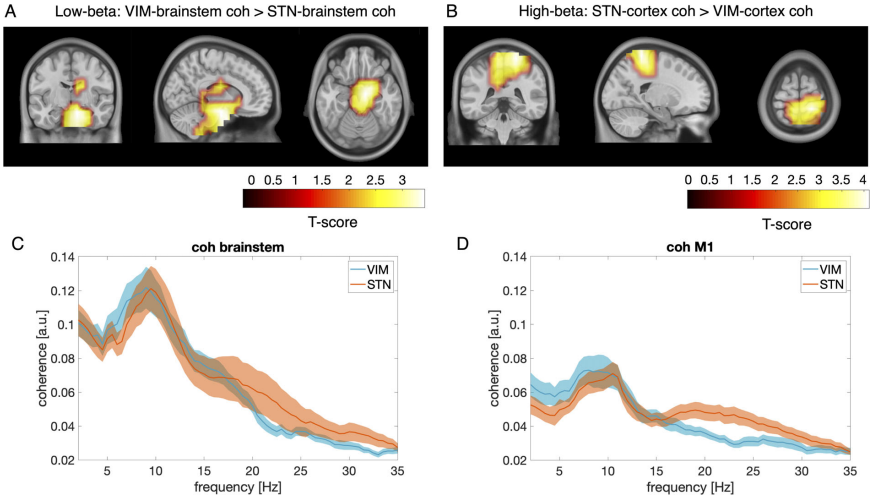

FIG. 3. Quantitative differences between ventral intermediate nucleus of the thalamus (VIM) and subthalamic nucleus (STN)–cortex coherence. (A) VIM–brainstem low-beta coherence > STN–brainstem low-beta coherence. (B) STN–cortex high-beta coherence > VIM–cortex high-beta coherence. Nonsignificant changes are masked. (C) Coherence with brainstem averaged over patients and hemispheres for the VIM (blue) and the STN (orange). (D) as (C) for sensorimotor cortex. Shaded areas represent the standard error of the mean. coh, coherence. [Color figure can be viewed at wileyonlinelibrary.com]

and of the high-beta sensorimotor cluster (MNI coordinates: X = 20 mm, Y = −40 mm, Z = 70 mm; Fig. 4D) as cortical ROIs for subsequent analyses.

Please note that results noted previously relate to spatially normalized coherence. The difference in low-beta coherence with the brainstem appeared to be accentuated by normalization (see Fig. 3C for non-normalized coherence). When testing for whole-brain differences without normalization, the cluster in the low-beta band was still detectable, but the *P*-value was above the significance threshold ($t_{clustersum} = 139.35$, $P = 0.13$). The difference in the high-beta band remained significant ($t_{clustersum} = 668.61$, $P = 0.025$). Hence, the low-beta effect is best understood as a difference in how coherence is distributed across brain areas rather than a difference in absolute coupling strength.

Directionality Analysis

We investigated the directionality of coupling between the VIM/STN and the cortical ROIs (Fig. 4) and found a three-way interaction between the cortical area, direction, and frequency band factors for the VIM ($F_{2,32} = 8.154$, $P = 0.001$) and a similar trend for the STN ($F_{2,32} = 83.214$, $P = 0.053$). We performed post hoc tests evaluating directional coupling for all factor combinations. The VIM showed significant directed coupling with sensorimotor cortex in the alpha band, with the VIM leading the sensorimotor cortex ($t = 2.4392$, $P = 0.0203$). The sensorimotor cortex drove STN activity in the alpha ($t = 2.5574$, $P = 0.0153$) and in the high-beta band ($t = 2.8103$, $P = 0.0083$). The brainstem drove STN activity in the alpha band ($t = 2.9917$, $P = 0.0052$), the low-beta band ($t = 2.4625$, $P = 0.0192$), and the high-beta band ($t = 2.5429$, $P = 0.0159$). The sign of the differences in Granger causality changed for the opposite direction in all cases, suggesting nonspurious directionality.

Discussion

Although beta coherence between the VIM and sensorimotor cortex has been described on the sensor level,[41,42] this is the first work presenting a whole-brain, frequency-resolved map of VIM–cortex resting-state coherence in ET patients and contrasting it with STN–cortex coherence in PD patients.

Local Oscillatory Activity in the VIM and STN

We found prominent alpha peaks in the VIM and STN at all recording locations. In the subcortical structures, the alpha rhythm is linked to cognition and emotion[43] and might be involved in motor functions.[44] The thalamus has been suggested to be a pacemaker for alpha oscillations,[45,46] a concept challenged by other studies favoring a cortical origin

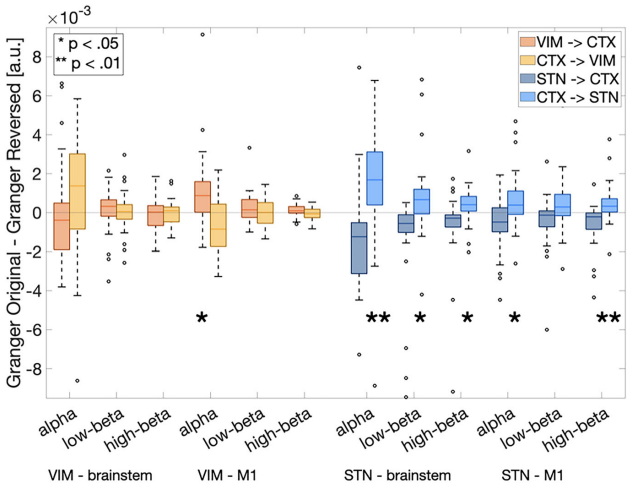

FIG. 4. Directionality of ventral intermediate nucleus of the thalamus (VIM)–cortex (CTX) and subthalamic nucleus (STN)–cortex (CTX) coupling. Boxplots represent differences in Granger causality between original data and time-reversed data. Differences significantly greater than zero indicate significant directionality. In the case of a cortical drive, values represented by the left box in a pair are negative, whereas values to the right are positive (and vice versa for subcortical drive). Asterisks indicate significant deviations from zero. [Color figure can be viewed at wileyonlinelibrary.com]

of alpha oscillations.[47-49] In our study, the significant directionality of VIM–sensorimotor cortex coupling at alpha frequencies, with the VIM leading cortical activity, supports the idea of a thalamic pacemaker. Notably, the dominant direction of alpha-band coupling with thesensorimotor cortex was opposite for the STN, with the cortex leading the STN, suggesting a local origin of the subcortical alpha drive. (A schematic illustration based on the present results is provided in Fig. 5.)

Beta oscillations in the STN, VIM, and cortex are linked to motor functions. They decrease in amplitude during voluntary movement[42,50] and tremor.[51] In PD patients, they are reduced by dopaminergic medication[52] and DBS.[53,54] The treatment-induced reductions of beta amplitude correlate with treatment-induced reductions of PD motor symptoms, akinesia, and rigidity in particular.[55,56] Based on previous reports,[17,57,58] we divided the beta band into low- and high-beta sub-bands, and we observed a clear separation of effects. Low-beta power was similar for the VIM and STN, and thus for ET and PD patients, despite being considered a potential marker of parkinsonism based on its responsiveness to levodopa.[57,59] High-beta power, in contrast, was strikingly different between the STN and VIM: only the STN exhibited strong high-beta activity, which was nearly absent in the VIM. This finding aligns with previous studies reporting weak high-beta oscillations in the VIM.[44] They further support the notion of high-beta oscillations being a unique spectral signature of the STN, possibly resulting from cortical input via the hyperdirect pathway[24] (see the Differences Between the VIM and STN Networks section).

VIM–Cortical Coupling

We found spectrally and spatially distinct patterns of oscillatory coupling between the VIM and cortex during

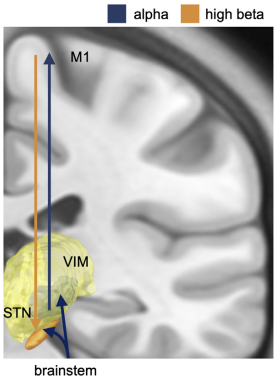

FIG. 5. Summary. Alpha oscillations (blue) were observed in the subthalamic nucleus (STN) and ventral intermediate nucleus of the thalamus (VIM). Oscillatory coupling in the alpha band appeared to have a bottom-up structure, with the thalamus driving the motor cortex. High-beta oscillations (yellow) were observed in the STN only, with the motor cortex driving the STN. [Color figure can be viewed at wileyonlinelibrary.com]

rest and identified two main networks: an alpha/low-beta network involving the temporal cortex, brainstem, and cerebellum and a high-beta network involving the medial sensorimotor cortex. This pattern of coupling is in agreement with the VIM's structural connections. The VIM is located in the ventrolateral thalamus.[60,61] It is reciprocally connected with the primary motor cortex,[62] likely explaining the mostly bidirectional coupling with motor areas observed here (with the exception of alpha oscillations). In addition, the VIM receives excitatory inputs from the dentate nucleus of the cerebellum via the DRTT.[63,64] Most but not all fibers of the DRTT decussate in the midbrain.[9,11,64] Given this pattern of structural connectivity, it is possible that the alpha/low-beta coherence described here is in part related to the DRTT input to the ventral thalamus. Rather than in the cerebellum proper, however, we found the strongest alpha/low-beta coherence in the midbrain and the brainstem. This might be related to the difficulty of capturing cerebellar activity with MEG as a result of the cerebellum's anatomy.[65]

Similarities between the VIM and STN Networks

We could reproduce results obtained in previous studies on STN–cortical coupling with a new patient cohort, reporting alpha-band coherence between the STN and temporal cortex and beta-band coherence between the STN and cortical motor areas.[17,19,22,24] One of the most remarkable findings of this study is that the topographies of VIM–cortex and STN–cortex coherence were very similar overall, suggesting that frequency-specific coupling to certain cortical "hubs" is a common phenomenon occurring in a larger number of midbrain nuclei.

Large-scale synchrony might explain the similarity of VIM–/STN–cortex coherence and analogous networks observed for other subcortical structures. In dystonia patients, the GPi couples to temporal regions in the theta frequency band, to cerebellar sources in the alpha frequency band, and to sensorimotor areas in the beta frequency band.[23] The pedunculopontine nucleus in PD patients forms networks with the brainstem and the cingulum in the alpha band and with motor areas in the beta band.[66] Subcortico-cortical coupling was also investigated for the nucleus basalis of Meynert (NBM) in patients suffering from PD dementia and Lewy body dementia.[67] The NBM was found to be coupled to temporal regions in the theta band and to sensorimotor areas in the beta band. All of these networks have substantial overlap, consistent with large-scale synchrony.

Differences between the VIM and STN Networks

Although the overall spatio-spectral structure was similar for VIM– and STN–cortex networks, we did observe quantitative differences. Deeper sources, such as brainstem and the dorsal edge of the cerebellum, were more coherent with the VIM than with the STN at low-beta frequencies, whereas the STN displayed greater coherence with motor areas in the high-beta band. These differences are likely attributed to the specific anatomical connections of VIM and STN, respectively. Unlike the STN, the VIM receives direct projections from the cerebellum, passing through the brainstem via the superior cerebellar peduncle and crossing hemispheres in the midbrain. Thus, one might expect stronger coupling to deep brain areas, the anatomical details of which might be insufficiently resolved by MEG. The STN, in contrast, receives cerebellar input only indirectly via a disynaptic pathway from the dentate nucleus to the striatum.[68]

Unlike alpha oscillations, which may arise subcortically,[45,46] beta oscillations are believed to be generated in the motor cortex.[69] The motor cortex has monosynaptic projections to both the STN and thalamus, but the symmetry of connections is different. Although the connections between the thalamus and motor cortical areas are reciprocal,[62] M1-STN coupling is asymmetric: the STN receives cortical afferents via the hyperdirect pathway, without sending direct projections back to the motor cortex.[70-72] This connectivity pattern was proposed to explain the findings of a recent study comparing STN and GPi power and oscillatory coupling in PD patients.[24] The study revealed stronger beta power for STN than GPi, along with stronger high-beta coherence with cortical motor areas, and showed that STN–motor cortex structural connectivity correlates with high-beta coherence specifically. Here, we demonstrate similar differences in power and coherence between the STN and VIM. In addition, we found a cortical drive specifically for STN–sensorimotor high-beta coupling, in accordance with earlier studies,[17,73] whereas no such cortical drive in the beta band was found for the thalamus (Fig. 5). In summary, these findings suggest that elevated high-beta coherence is an electrophysiological marker of the hyperdirect pathway.

Nucleus- Versus Disease-Specificity of Coupling

VIM and STN recordings were performed in two separate groups of patients, each suffering from a different disease (ET and PD), raising the question of whether the observed differences in coherence are attributable to the subcortical structure or to the disease. Given the pathological increase of beta oscillations in PD, a particular concern could be that the strong high-beta band coupling, which we assume to be STN specific, is really PD specific. Although we cannot rule out this possibility, we provide indications by relating coherence to disease severity and by investigating the effect of levodopa on coherence, thereby probing the importance of

parkinsonism for high-beta STN–cortex coupling. Neither did we find a correlation between symptom severity and high-beta coherence in PD patients, nor did levodopa intake abolish the difference between VIM– versus STN–cortex coherence in the high-beta band. These findings speak in favor of high-beta coherence being a characteristic of the STN, not the disease. Previous studies support this interpretation by demonstrating similar levels of STN–cortex beta coherence in PD and dystonia patients.[74] Strong high-beta coupling between the STN and motor cortex was also found in a patient with obsessive-compulsive disorder, evidence of its existence even in nonmotor disorders.[75]

This is not to say that the disease has no effects on oscillatory coupling in basal ganglia–cortex loops. Notwithstanding possible effects of the underlying pathology, we would definitely expect such effects when the groups experience different motor symptoms. Here, both groups were recorded at rest, and episodes with rest tremor (PD specific) were excluded.

Limitations

We found the spatial and spectral organization of VIM– and STN–cortex coherence to be rather similar. Although large-scale synchrony is a plausible explanation, we cannot rule out volume conduction as an alternative explanation. The "sweet spots" in the ventral thalamus and the dorsal STN are only approximately 10 mm apart. Although we were careful to exclude contact pairs reaching into the neighboring target, it is possible that a common subcortical source affected both VIM and STN measurements despite using a bipolar reference scheme. The spatial reach of LFP recordings is not exactly known, but computational and experimental studies have demonstrated that a DBS contact can pick up signals within a volume of several millimeters.[76] Some deep sources might even be strong enough to be registered by DBS electrodes and MEG.[77-80] The connectivity patterns presented here did not depend on this form of volume conduction, as confirmed by our analysis of the imaginary part of coherency.

Conclusions

Thalamocortical resting-state coherence is spatially and spectrally organized in frequency-specific networks involving medial sensorimotor cortex (beta band) as well as the temporal cortex, brainstem, and cerebellum (alpha band). These are roughly the same networks described for the STN and other midbrain nuclei, suggesting large-scale subcortico-cortical synchrony. The fact that similar patterns are found in different diseases supports a physiological rather than a pathological nature.

Acknowledgments: ASc and JH are supported by Brunhilde Moll Stiftung. ASc also acknowledges support by the Deutsche Forschungsgemeinschaft (German Research Foundation), Project 4247788381-TRR 295. Open Access funding enabled and organized by Projekt DEAL.

Data Availability Statement

Data will be made available in anonymized form upon reasonable request.

References

1. Song P, Zhang Y, Zha M, et al. The global prevalence of essential tremor, with emphasis on age and sex: a meta-analysis. J Global Heal 2021;11.
2. Deuschl G, Elble RJ. The pathophysiology of essential tremor. Neurology 2000;54(11 suppl 4):S14–S20.
3. Haubenberger D, Hallett M. Essential Tremor. N. Engl. J. Med. 2018;378(19):1802–1810. https://doi.org/10.1056/NEJMcp1707928
4. Welton T, Cardoso F, Carr JA, et al. Essential tremor (Primer). Nat Rev Dis Primers 2021;7(1):83. https://doi.org/10.1038/s41572-021-00314-w
5. Helmich RC, Toni I, Deuschl G, Bloem BR. The pathophysiology of essential tremor and Parkinson's tremor. Curr. Neurol. Neurosci. Rep. 2013;13(9):378. https://doi.org/10.1007/s11910-013-0378-8
6. Raethjen J, Deuschl G. The oscillating central network of essential tremor. Clin. Neurophysiol. 2012;123(1):61–64. https://doi.org/10.1016/j.clinph.2011.09.024
7. Schnitzler A, Münks C, Butz M, Timmermann L, Gross J. Synchronized brain network associated with essential tremor as revealed by magnetoencephalography. Mov. Disord. 2009;24(11):1629–1635. https://doi.org/10.1002/mds.22633
8. Al-Fatly B, Ewert S, Kübler D, et al. Connectivity profile of thalamic deep brain stimulation to effectively treat essential tremor. Brain 2019;142(10):3086–3098. https://doi.org/10.1093/brain/awz236
9. Coenen VA, Sajonz BE, Reinacher PC, et al. A detailed analysis of anatomical plausibility of crossed and uncrossed streamline rendition of the dentato-rubro-thalamic tract (DRT(T)) in a commercial stereotactic planning system. Acta Neurochir. 2021;163(10):2809–2824. https://doi.org/10.1007/s00701-021-04890-4
10. Middlebrooks EH, Okromelidze L, Wong JK, et al. Connectivity correlates to predict essential tremor deep brain stimulation outcome: evidence for a common treatment pathway. NeuroImage: Clinical 2021;32:102846. https://doi.org/10.1016/j.nicl.2021.102846
11. Tsuboi T, Wong JK, Eisinger RS, et al. Comparative connectivity correlates of dystonic and essential tremor deep brain stimulation. Brain 2021;144(6):1774–1786. https://doi.org/10.1093/brain/awab074
12. Hua SE, Lenz FA. Posture-related oscillations in human cerebellar thalamus in essential tremor are enabled by voluntary motor circuits. J. Neurophysiol. 2005;93(1):117–127. https://doi.org/10.1152/jn.00527.2004
13. Tan H, Debarros J, He S, et al. Decoding voluntary movements and postural tremor based on thalamic LFPs as a basis for closed-loop stimulation for essential tremor. Brain Stimul. 2019;12(4):858–867. https://doi.org/10.1016/j.brs.2019.02.011
14. Kane A, Hutchison WD, Hodaie M, Lozano AM, Dostrovsky JO. Enhanced synchronization of thalamic theta band local field potentials in patients with essential tremor. Exp. Neurol. 2009;217(1):171–176. https://doi.org/10.1016/j.expneurol.2009.02.005
15. Pedrosa DJ, Reck C, Florin E, et al. Essential tremor and tremor in Parkinson's disease are associated with distinct 'tremor clusters' in the ventral thalamus. Exp. Neurol. 2012;237(2):435–443. https://doi.org/10.1016/j.expneurol.2012.07.002
16. Laufs H, Krakow K, Sterzer P, et al. Electroencephalographic signatures of attentional and cognitive default modes in spontaneous brain activity fluctuations at rest. Proc. Natl. Acad. Sci. 2003;100(19):11053–11058. https://doi.org/10.1073/pnas.1831638100

17. Litvak V, Jha A, Eusebio A, et al. Resting oscillatory cortico-subthalamic connectivity in patients with Parkinson's disease. Brain 2011;134(2):359–374. https://doi.org/10.1093/brain/awq332
18. Schnitzler A, Gross J. Normal and pathological oscillatory communication in the brain. Nat. Rev. Neurosci. 2005;6(4):285–296. https://doi.org/10.1038/nrn1650
19. Hirschmann J, Özkurt TE, Butz M, et al. Distinct oscillatory STN-cortical loops revealed by simultaneous MEG and local field potential recordings in patients with Parkinson's disease. NeuroImage 2011;55(3):1159–1168. https://doi.org/10.1016/j.neuroimage.2010.11.063
20. Sharma A, Vidaurre D, Vesper J, Schnitzler A, Florin E. Differential dopaminergic modulation of spontaneous cortico–subthalamic activity in parkinson's disease. elife 2021;10:e66057. https://doi.org/10.7554/eLife.66057
21. Sure M, Vesper J, Schnitzler A, Florin E. Cortical network formation based on subthalamic beta bursts in Parkinson's disease. NeuroImage 2022;263:119619. https://doi.org/10.1016/j.neuroimage.2022.119619
22. van Wijk BCM, Neumann W-J, Kroneberg D, et al. Functional connectivity maps of theta/alpha and beta coherence within the subthalamic nucleus region. NeuroImage 2022;257:119320. https://doi.org/10.1016/j.neuroimage.2022.119320
23. Neumann W-J, Jha A, Bock A, et al. Cortico-pallidal oscillatory connectivity in patients with dystonia. Brain 2015;138(7):1894–1906. https://doi.org/10.1093/brain/awv109
24. Oswal A, Cao C, Yeh C-H, et al. Neural signatures of hyperdirect pathway activity in Parkinson's disease. Nat. Commun. 2021;12(1):5185. https://doi.org/10.1038/s41467-021-25366-0
25. Horn A, Li N, Dembek TA, et al. Lead-DBS v2: towards a comprehensive pipeline for deep brain stimulation imaging. NeuroImage 2019;184:293–316. https://doi.org/10.1016/j.neuroimage.2018.08.068
26. Dembek TA, Roediger J, Horn A, et al. Probabilistic sweet spots predict motor outcome for deep brain stimulation in Parkinson disease. Ann. Neurol. 2019;86(4):527–538.
27. Horn A, Neumann W-J, Degen K, Schneider G-H, Kühn AA. Toward an electrophysiological "sweet spot" for deep brain stimulation in the subthalamic nucleus: subcortical mapping of Beta band activity in Parkinson's disease. Hum. Brain Mapp. 2017;38(7):3377–3390. https://doi.org/10.1002/hbm.23594
28. Oostenveld R, Fries P, Maris E, Schoffelen J-M. FieldTrip: open source software for advanced analysis of MEG, EEG, and invasive electrophysiological data. Comput. Intell. Neurosci. 2011;2011:1–9.
29. Buzsáki G, Logothetis N, Singer W. Scaling brain size, keeping timing: evolutionary preservation of brain rhythms. Neuron 2013;80(3):751–764. https://doi.org/10.1016/j.neuron.2013.10.002
30. He BJ. Scale-free brain activity: past, present, and future. Trends Cogn. Sci. 2014;18(9):480–487. https://doi.org/10.1016/j.tics.2014.04.003
31. Donoghue T, Haller M, Peterson EJ, et al. Parameterizing neural power spectra into periodic and aperiodic components. Nat. Neurosci. 2020;23(12):1655–1665.
32. Krösche M, Kannenberg S, Butz M, et al. Slowing of frontal β oscillations in atypical parkinsonism. Mov. Disord. 2023;38(5):806–817. https://doi.org/10.1002/mds.29378
33. Thomson DJ. Spectrum estimation and harmonic analysis. Proc. IEEE 1982;70(9):1055–1096. https://doi.org/10.1109/PROC.1982.12433
34. Gross J, Kujala J, Hämäläinen M, et al. Dynamic imaging of coherent sources: studying neural interactions in the human brain. Proc. Natl. Acad. Sci. 2001;98(2):694–699.
35. Nolte G, Bai O, Wheaton L, et al. Identifying true brain interaction from EEG data using the imaginary part of coherency. Clin. Neurophysiol. 2004;115(10):2292–2307.
36. Van Veen BD, Van Drongelen W, Yuchtman M, Suzuki A. Localization of brain electrical activity via linearly constrained minimum variance spatial filtering. IEEE Trans. Biomed. Eng. 1997;44(9):867–880.
37. Brovelli A, Ding M, Ledberg A, et al. Beta oscillations in a large-scale sensorimotor cortical network: directional influences revealed by granger causality. Proc. Natl. Acad. Sci. 2004;101(26):9849–9854.
38. Dhamala M, Rangarajan G, Ding M. Analyzing information flow in brain networks with nonparametric granger causality. NeuroImage 2008;41(2):354–362.
39. Haufe S, Nikulin VV, Müller K-R, Nolte G. A critical assessment of connectivity measures for EEG data: a simulation study. NeuroImage 2013;64:120–133.
40. Maris E, Oostenveld R. Nonparametric statistical testing of EEG- and MEG-data. J. Neurosci. Methods 2007;164(1):177–190. https://doi.org/10.1016/j.jneumeth.2007.03.024
41. Marsden JF. Coherence between cerebellar thalamus, cortex and muscle in man: cerebellar thalamus interactions. Brain 2000;123(7):1459–1470. https://doi.org/10.1093/brain/123.7.1459
42. Paradiso G. Involvement of human thalamus in the preparation of self-paced movement. Brain 2004;127(12):2717–2731. https://doi.org/10.1093/brain/awh288
43. Yin Z, Zhu G, Zhao B, et al. Local field potentials in Parkinson's disease: a frequency-based review. Neurobiol. Dis. 2021;155:105372. https://doi.org/10.1016/j.nbd.2021.105372
44. Klostermann F, Nikulin VV, Kühn AA, et al. Task-related differential dynamics of EEG alpha- and beta-band synchronization in cortico-basal motor structures: EEG oscillations in motor structures. Eur. J. Neurosci. 2007;25(5):1604–1615. https://doi.org/10.1111/j.1460-9568.2007.05417.x
45. Goldman R, Stern J, Engel Jr. J, Cohen M. Simultaneous EEG and fMRI of the alpha rhythm. Neuroreport 2002;13(18):2487.
46. Hughes SW, Crunelli V. Thalamic mechanisms of EEG alpha rhythms and their pathological implications. Neuroscientist 2005;11(4):357–372. https://doi.org/10.1177/1073858405277450
47. Da Silva FL, Van Lierop T, Schrijer CF, Van Leeuwen WS. Organization of thalamic and cortical alpha rhythms: spectra and coherences. Electroencephalogr. Clin. Neurophysiol. 1973;35(6):627–639.
48. Da Silva FL, Vos JE, Mooibroek J, Van Rotterdam A. Relative contributions of intracortical and thalamo-cortical processes in the generation of alpha rhythms, revealed by partial coherence analysis. Electroencephalogr. Clin. Neurophysiol. 1980;50(5–6):449–456.
49. Halgren M, Ulbert I, Bastuji H, et al. The generation and propagation of the human alpha rhythm. Proc. Natl. Acad. Sci. 2019;116(47):23772–23782. https://doi.org/10.1073/pnas.1913092116
50. Kühn AA, Williams D, Kupsch A, et al. Event-related beta desynchronization in human subthalamic nucleus correlates with motor performance. Brain 2004;127(4):735–746. https://doi.org/10.1093/brain/awh106
51. Basha D, Dostrovsky JO, Lopez Rios AL, et al. Beta oscillatory neurons in the motor thalamus of movement disorder and pain patients. Exp. Neurol. 2014;261:782–790. https://doi.org/10.1016/j.expneurol.2014.08.024
52. Brown P, Oliviero A, Mazzone P, et al. Dopamine dependency of oscillations between subthalamic nucleus and pallidum in Parkinson's disease. J. Neurosci. 2001;21(3):1033–1038.
53. Abbasi O, Hirschmann J, Storzer L, et al. Unilateral deep brain stimulation suppresses alpha and beta oscillations in sensorimotor cortices. NeuroImage 2018;174:201–207. https://doi.org/10.1016/j.neuroimage.2018.03.026
54. Neumann W-J, Staub F, Horn A, et al. Deep brain recordings using an implanted pulse generator in P arkinson's disease. Neuromodulation 2016;19(1):20–24.
55. Kühn AA, Kupsch A, Schneider G-H, Brown P. Reduction in subthalamic 8–35 Hz oscillatory activity correlates with clinical improvement in Parkinson's disease. Eur. J. Neurosci. 2006;23(7):1956–1960.
56. Neumann W-J, Degen K, Schneider G-H, et al. Subthalamic synchronized oscillatory activity correlates with motor impairment in patients with Parkinson's disease. Mov. Disord. 2016;31(11):1748–1751.
57. Little S, Tan H, Anzak A, et al. Bilateral functional connectivity of the basal ganglia in patients with Parkinson's disease and its modulation by dopaminergic treatment. PLoS One 2013;8(12):e82762.

58. van Wijk BC, Beudel M, Jha A, et al. Subthalamic nucleus phase–amplitude coupling correlates with motor impairment in Parkinson's disease. Clin. Neurophysiol. 2016;127(4):2010–2019.
59. Priori A, Foffani G, Pesenti A, et al. Rhythm-specific pharmacological modulation of subthalamic activity in Parkinson's disease. Exp. Neurol. 2004;189(2):369–379. https://doi.org/10.1016/j.expneurol.2004.06.001
60. Ilinsky IA, Kultas-Ilinsky K. Motor thalamic circuits in primates with emphasis on the area targeted in treatment of movement disorders. Mov Disorders 2002;17(S3):S9–S14.
61. Macchi G, Jones EG. Toward an agreement on terminology of nuclear and subnuclear divisions of the motor thalamus. J. Neurosurg. 1997;86(1):77–92.
62. Bosch-Bouju C, Hyland BI, Parr-Brownlie LC. Motor thalamus integration of cortical, cerebellar and basal ganglia information: implications for normal and parkinsonian conditions. Front. Comput. Neurosci. 2013;7:163. https://doi.org/10.3389/fncom.2013.00163
63. Dum RP, Strick PL. An unfolded map of the cerebellar dentate nucleus and its projections to the cerebral cortex. J. Neurophysiol. 2003;89(1):634–639. https://doi.org/10.1152/jn.00626.2002
64. Gallay MN, Jeanmonod D, Liu J, Morel A. Human pallidothalamic and cerebellothalamic tracts: anatomical basis for functional stereotactic neurosurgery. Brain Struct. Funct. 2008;212(6):443–463. https://doi.org/10.1007/s00429-007-0170-0
65. Andersen LM, Jerbi K, Dalal SS. Can EEG and MEG detect signals from the human cerebellum? NeuroImage 2020;215:116817. https://doi.org/10.1016/j.neuroimage.2020.116817
66. Jha A, Litvak V, Taulu S, et al. Functional connectivity of the pedunculopontine nucleus and surrounding region in Parkinson's disease. Cereb. Cortex 2017;27(1):54–67. https://doi.org/10.1093/cercor/bhw340
67. Gratwicke J, Oswal A, Akram H, et al. Resting state activity and connectivity of the nucleus basalis of Meynert and globus pallidus in Lewy body dementia and Parkinson's disease dementia. NeuroImage 2020;221:117184. https://doi.org/10.1016/j.neuroimage.2020.117184
68. Hoshi E, Tremblay L, Féger J, Carras PL, Strick PL. The cerebellum communicates with the basal ganglia. Nat. Neurosci. 2005;8(11):1491–1493. https://doi.org/10.1038/nn1544
69. Sherman MA, Lee S, Law R, et al. Neural mechanisms of transient neocortical beta rhythms: converging evidence from humans, computational modeling, monkeys, and mice. Proc. Natl. Acad. Sci. 2016;113(33):E4885–E4894. https://doi.org/10.1073/pnas.1604135113
70. Coudé D, Parent A, Parent M. Single-axon tracing of the corticosubthalamic hyperdirect pathway in primates. Brain Struct. Funct. 2018;223(9):3959–3973. https://doi.org/10.1007/s00429-018-1726-x
71. Haynes WIA, Haber SN. The Organization of Prefrontal-Subthalamic Inputs in primates provides an anatomical substrate for both functional specificity and integration: implications for basal ganglia models and deep brain stimulation. J. Neurosci. 2013;33(11):4804–4814. https://doi.org/10.1523/JNEUROSCI.4674-12.2013
72. Nambu A, Takada M, Inase M, Tokuno H. Dual somatotopical representations in the primate subthalamic nucleus: evidence for ordered but reversed body-map transformations from the primary motor cortex and the supplementary motor area. J. Neurosci. 1996;16(8):2671–2683. https://doi.org/10.1523/JNEUROSCI.16-08-02671.1996
73. Oswal A, Beudel M, Zrinzo L, et al. Deep brain stimulation modulates synchrony within spatially and spectrally distinct resting state networks in Parkinson's disease. Brain 2016;139(5):1482–1496.
74. Cao C, Huang P, Wang T, et al. Cortico-subthalamic coherence in a patient with dystonia induced by chorea-acanthocytosis: a case report. Front. Hum. Neurosci. 2019;13:163. https://doi.org/10.3389/fnhum.2019.00163
75. Wojtecki L, Hirschmann J, Elben S, et al. Oscillatory coupling of the subthalamic nucleus in obsessive compulsive disorder. Brain 2017;140(9):e56. https://doi.org/10.1093/brain/awx164
76. Lempka SF, McIntyre CC. Theoretical analysis of the local field potential in deep brain stimulation applications. PLoS One 2013;8(3):e59839. https://doi.org/10.1371/journal.pone.0059839
77. Attal Y, Schwartz D. Assessment of subcortical source localization using deep brain activity imaging model with minimum norm operators: a MEG study. PLoS One 2013;8(3):e59856. https://doi.org/10.1371/journal.pone.0059856
78. Griffiths BJ, Martín-Buro MC, Staresina BP, Hanslmayr S. Disentangling neocortical alpha/beta and hippocampal theta/gamma oscillations in human episodic memory formation. NeuroImage 2021;242:118454. https://doi.org/10.1016/j.neuroimage.2021.118454
79. Joensen BH, Bush D, Vivekananda U, et al. Hippocampal theta activity during encoding promotes subsequent associative memory in humans. Cereb. Cortex 2023;33(13):8792–8802. https://doi.org/10.1093/cercor/bhad162
80. Spaak E, de Lange FP. Hippocampal and prefrontal theta-band mechanisms underpin implicit spatial context learning. J. Neurosci 2020;40(1):191–202. https://doi.org/10.1523/JNEUROSCI.1660-19.2019

Supporting Data

Additional Supporting Information may be found in the online version of this article at the publisher's web-site.

Mapping subcortico-cortical coupling – a comparison of thalamic and subthalamic oscillations

Supplementary Material

Alexandra Steina[1], Sarah Sure[1], Markus Butz[1],
Jan Vesper[2], Alfons Schnitzler[1], Jan Hirschmann[1]

Author affiliations:

[1] Institute of Clinical Neuroscience and Medical Psychology, Medical Faculty, Heinrich Heine University, 40225, Düsseldorf, Germany

[2] Department of Functional Neurosurgery and Stereotaxy, Neurosurgical Clinic, Medical Faculty, Heinrich Heine University, 40225, Düsseldorf, Germany

Tab. S1: ET patient details. The presence/absence of tremor is provided for the day of measurement. l = left upper extremity, r = right upper extremity, - = no tremor, n.a. = not assessed.

disease	**age [y]**	**sex**	**disease duration [y]**	**electrode type**	**data length (s)**	**action tremor**
ET01	65	m	19	Abbott Infinity	175	-
ET02	69	m	18	Abbott Infinity	92	l+r
ET03	71	m	20	Abbott Infinity	228	l+r
ET04	60	f	49	Abbott Infinity	258	-
ET05	62	m	50	Abbott Infinity	189	l
ET06	46	f	66	Boston Sc. Vercice standard	295	n.a.
ET07	65	m	30	Boston Sc. Vercice standard	626	l+r
ET08	58	m	5	Abbott Infinity	378	-
ET09	77	f	8	Boston Sc.Vercise Cartesia	398	l+r
ET10	74	m	20	Abbott Infinity	166	l+r
ET11	30	m	25	Abbott Infinity	318	-
ET12	44	m	40	Medtronic 3389	263	r
ET13	57	f	51	Abbott Infinity	384	-
ET14	76	m	n.a.	Medtronic SenSight	588	l
ET15	54	m	39	Abbott Infinity	598	l+r

ET16	62	f	56	Boston Sc.Vercise Cartesia	330	-
ET17	65	m	20	Boston Sc.Vercise Cartesia	705	l+r
ET18	71	m	20	Boston Sc.Vercise Cartesia	600	-
ET19	67	m	15	Abbott Infinity	574	l+r
μ $+/-\sigma$	62 +/- 12		31 +/- 18		377 +/- 184	

Tab. S2: PD patient details.

disease	**age [y]**	**sex**	**disease duration [y]**	**electrode type**	**data length (s)**	**UPDRS sum Med *off***	**UPDRS sum Med *on***	**PD subtype**
PD01	65	f	n.a.	Abbott Infinity	426	20	14	akinetic-rigid
PD02	56	m	6	Abbott Infinity	400	31	25	intermediate
PD03	45	m	3	Abbott Infinity	336	22	10	intermediate
PD04	47	m	6	Abbott Infinity	400	42	35	intermediate
PD05	62	f	2	Abbott Infinity	380	26	17	intermediate
PD06	52	m	7	Boston Sc. Vercise Standard	308	27	n.a.	tremor-dominant
PD07	59	f	9	Abbott Infinity	340	39	30	intermediate
PD08	69	m	6	Abbott Infinity	386	42	29	intermediate
PD09	54	m	7	Abbott Infinity	391	49	27	akinetic-rigid

PD10	72	f	3	Abbott Infinity	400	35	16	akinetic-rigid
PD11	69	m	12	Abbott Infinity	394	n.a.	38	intermediate
PD12	70	m	11	Medtronic 3389	300	39	31	akinetic-rigid
PD13	65	m	13	Abbott Infinity	400	64	23	intermediate
PD14	60	f	6	Abbott Infinity	400	23	13	intermediate
PD15	59	m	10	Abbott Infinity	352	41	28	akinetic-rigid
PD16	68	m	10	Abbott Infinity	559	27	11	intermediate
PD17	54	m	3	Abbott Infinity	600	53	14	intermediate
PD18	41	m	7	Abbott Infinity	516	27	8	tremor-dominant
PD19	59	m	15	Abbott Infinity	500	38	27	akinetic-rigid
$\mu +/- \sigma$	59 +/- 9		8 +/- 4		409 +/- 80	35.8 +/- 11.8	22 +/- 9.2	

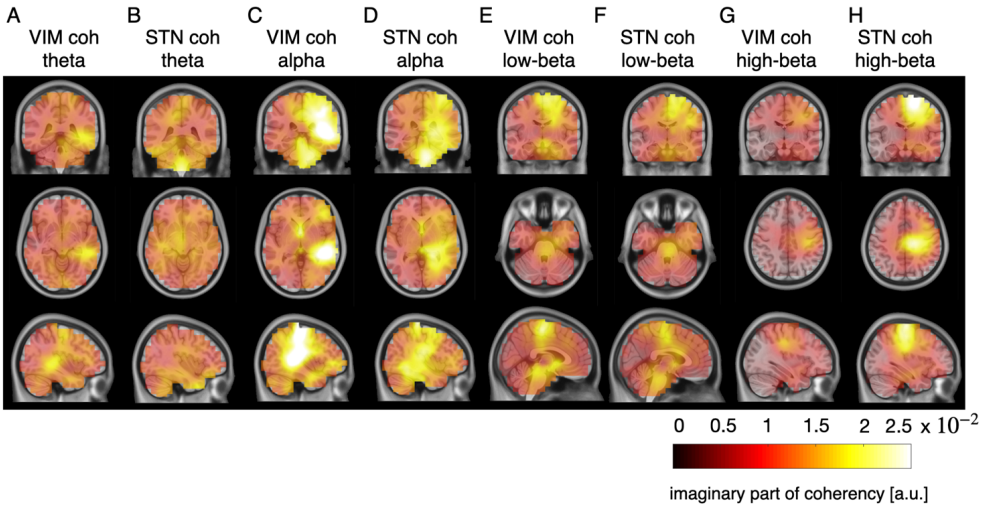

Fig. S1: **VIM- and STN imaginary part of coherency.** Group average source images of VIM- (A,C,E,G) and STN- (B,D,F,H) cortex imaginary part of coherency for different frequency bands (A/B, C/D, E/F, G/H). Sources on the right side correspond to the ipsilateral side (with respect to the subcortical recording site).

Differences between VIM- and STN-cortex coupling (medication *on*)

In addition to the measurements in the medication *off* state, the PD cohort underwent simultaneous MEG and LFP recordings in the medication *on* state. The measurements took place at least half an hour after the administration of the morning levodopa dose and after clinical improvement was seen as described in other studies[1,2]. We constructed whole-brain maps of STN-cortex coherence from the medication *on* data and tested if the quantitative differences in VIM- and STN-cortex coherence remained. The difference in the high-beta band remained when PD patients were in medication *on* (cluster-based-permutation-test: $t_{clustersum} = 275.03$, $p = 0.038$, Fig. S2), whereas the difference in the low-beta band did not remain.

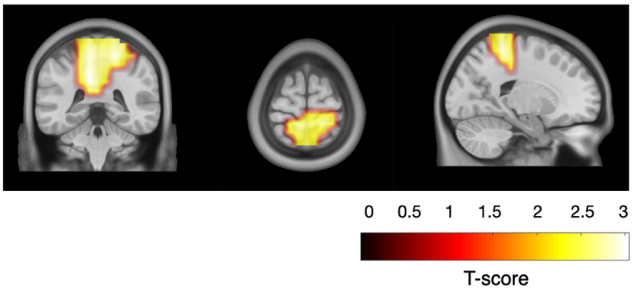

Fig. S2: **Quantitative differences between VIM- and STN-cortex coherence in the high-beta band (medication *on*).**

Coherence and symptom severity

We extracted time-domain source activity from the medial sensorimotor cortex (see Methods: Directionality analysis in main paper) for the PD cohort and calculated coherence with the STN. We correlated (Pearson's correlation coefficient) low- and high-beta STN-cortex coherence with the contralateral UPDRS hemibody sum score assessed on the day of the measurement. We found no correlation (Fig. S3) between symptom severity and low-/high-beta coherence in PD patients (low-beta: r = -0.003, p = 0.99, high-beta*:* r = -0.009, p = 0.96).

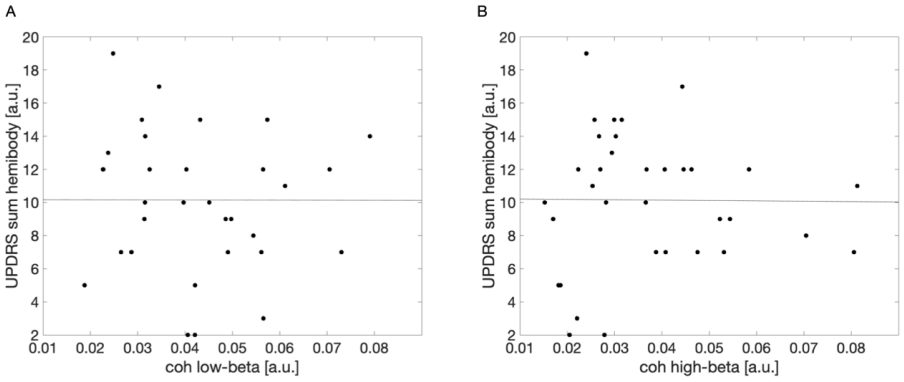

Fig. S3: **Correlation between symptom severity and resting-state coherence in PD patients.** UPDRS hemibody sum scores and contralateral low- (A) and high- (B) beta STN-M1 coherence.

References

1. Sharma, A., Vidaurre, D., Vesper, J., Schnitzler, A., & Florin, E. (2021). Differential dopaminergic modulation of spontaneous cortico–subthalamic activity in parkinson's disease. *Elife*, *10*, e66057.

2. Sure, M., Vesper, J., Schnitzler, A., & Florin, E. (2022). Cortical network formation based on subthalamic beta bursts in Parkinson's disease. *NeuroImage*, *263*, 119619. https://doi.org/10.1016/j.neuroimage.2022.119619

9.3 Article III: Oscillatory coupling between thalamus, cerebellum and motor cortex in essential tremor

Reproduced from

Alexandra Steina, Sarah Sure, Markus Butz, Jan Vesper, Alfons Schnitzler, & Jan Hirschmann
Oscillatory coupling between thalamus, cerebellum and motor cortex in essential tremor
Movement Disorders **40**, 896-905 (2025)

Digital Object Identifier (DOI): https://doi.org/10.1002/mds.30165

Statement of contribution

S.S. and J.H. planned the research project (Paper II, III and IV). Data collection started before the start of my PhD. I recorded more patients throughout my doctorate with J.H., M.B. I planned the analysis, preprocessed and processed the data. I prepared the figures for the manuscript. All authors discussed the results. I wrote the manuscript. J.H., S.S., M.B., J.V., A.Sc. edited the manuscript.

Copyright and license notice

RESEARCH ARTICLE

Oscillatory Coupling Between Thalamus, Cerebellum, and Motor Cortex in Essential Tremor

Alexandra Steina, MSc,[1] Sarah Sure, MD,[1] Markus Butz, PhD,[1] Jan Vesper, MD,[2] Alfons Schnitzler, MD,[1] and Jan Hirschmann, PhD[1*]

ABSTRACT: Background: Essential tremor is hypothesized to emerge from synchronized oscillatory activity within the cerebello-thalamo-cortical circuit. However, this hypothesis has not yet been tested using local field potentials directly recorded from the thalamus alongside signals from both the cortex and cerebellum, leaving a gap in the understanding of essential tremor.
Objectives: To clarify the importance of cerebello-thalamo-cortical oscillatory coupling for essential tremor.
Methods: We investigated oscillatory coupling between thalamic local field potentials and simultaneously recorded magnetoencephalography in 19 essential tremor patients with externalized deep brain stimulation electrodes. Brain activity was measured while patients repeatedly adopted a tremor-provoking posture and while pouring rice grains from one cup to another. In a whole-brain analysis of coherence between the ventral intermediate nucleus of the thalamus and cortex we contrasted epochs containing tremor and epochs lacking tremor.
Results: Both postural and kinetic tremor were associated with an increase of thalamic power and thalamo-cortex coherence at individual tremor frequency in the bilateral cerebellum and primary sensorimotor cortex contralateral to tremor. These areas also exhibited an increase in corticomuscular coherence in the presence of tremor. The coupling of motor cortex to both thalamus and muscle correlated with tremor amplitude during postural tremor.
Conclusions: These results demonstrate that essential tremor is indeed associated with increased oscillatory coupling at tremor frequency within a cerebello-thalamo-cortical network, with coupling strength directly reflecting tremor severity. © 2025 The Author(s). *Movement Disorders* published by Wiley Periodicals LLC on behalf of International Parkinson and Movement Disorder Society.

Key Words: ventral intermediate nucleus; functional connectivity; essential tremor; deep brain stimulation; magnetoencephalography

Upper limb action tremor is the main symptom of essential tremor, the most prevalent movement disorder worldwide.[1] Deep brain stimulation (DBS) of the ventral intermediate nucleus of the thalamus (VIM) is an effective therapy for severe essential tremor. The insertion of electrodes for DBS provides the unique opportunity to record signals directly from the VIM. Intraoperative studies have identified tremor-synchronous bursting cells in the VIM[2] and local field potential (LFP) recordings have uncovered oscillations at tremor and double tremor frequency, coherent with muscle activity in the tremulous arm.[3]

Apart from the VIM, other parts of the brain, such as cerebellum and motor cortex, have been implicated in the pathophysiology of essential tremor. Studies using functional magnetic resonance imaging (fMRI) have found tremor-related signal fluctuations in the cerebellum, the thalamus, and motor cortex.[4,5] Further, non-invasive electroencephalography (EEG) and magnetoencephalography (MEG) studies have revealed tremor-synchronous activity in the cerebellum and primary motor cortex.[6-9]

Based on these findings, it is assumed that essential tremor emerges through synchronized activity within

[1]Institute of Clinical Neuroscience and Medical Psychology, Medical Faculty, Heinrich Heine University, Düsseldorf, Germany; [2]Department of Functional Neurosurgery and Stereotaxy, Neurosurgical Clinic, Medical Faculty, Heinrich Heine University, Düsseldorf, Germany

*Correspondence to: Dr. Jan Hirschmann, Institute of Clinical Neuroscience and Medical Psychology, Medical Faculty, Heinrich Heine University Moorenstraße 5, 40225 Düsseldorf, Germany; E-mail: jan.hirschmann@med.uni-duesseldorf.de

Relevant conflicts of interest/financial disclosures: Nothing to report.

Funding agency: Brunhilde Moll Stiftung.

Received: 13 November 2024; **Revised:** 20 January 2025; **Accepted:** 13 February 2025

Published online 3 March 2025 in Wiley Online Library (wileyonlinelibrary.com). DOI: 10.1002/mds.30165

the cerebello-thalamo-cortical circuit, even though tremor-related synchronization of thalamic, cortical, and cerebellar oscillations has rarely been investigated to date. Two case studies describe coherence between the thalamus and motor cortex,[10,11] but a group-level, brain-wide analysis is lacking, as is evidence for tremor-related coupling between the thalamus and cerebellum.

Studying these network synchronization processes in humans is challenging. While fMRI has provided important evidence for the involvement of the cerebello-thalamo-cortical circuit in tremor,[4,5] it lacks the temporal resolution required to capture the fast dynamics of tremor. Conversely, MEG and EEG have sufficient temporal resolution but have limited sensitivity to deep sources, such as the thalamus.

Here, we overcome these difficulties by means of simultaneous recordings from externalized DBS electrodes, MEG, and muscle activity in patients with essential tremor. Using this methodology we provide, to the best of our knowledge, the first description of the network topology of thalamo-cortical coupling, for both postural and kinetic tremor. In addition, we demonstrate the behavioral relevance of thalamo-cortical coupling by relating it to tremor severity.

Methods

Patients and Recordings

A total of 19 patients with essential tremor undergoing surgery for DBS participated in the study, which was approved by the Ethics Committee of the Medical Faculty at Heinrich Heine University Düsseldorf (ET: '2018-217-Zweitvotum', '2021-1587-andere Forschung erstvotierend'). All patients provided written informed and fulfilled the Movement Disorder Society's diagnostic criteria for essential tremor.[12] Detailed patient information is provided in Table 1.

The recordings took place the day after implantation of DBS macroelectrodes, before the pulse generator was implanted. This allowed for the recording of LFPs from externalized leads, which were referenced to the mastoid and connected to amplifiers integrated into the MEG. We recorded from the bilateral electrodes targeting the VIM in combination with MEG, EMGs from both forearms (extensor digitorum communis and flexor digitorum communis), accelerometer signals from both index fingers, and electrooculograms. All signals were recorded by a 306-channel MEG system (Vectorview, MEGIN). The sampling rate was 2 kHz.

Paradigm

The experiment consisted of two motor tasks, which were performed following a 5–10 min resting state recording, analyzed previously.[13] In essential tremor, patients experience action tremor with a frequency of 4–8 Hz, which occurs when maintaining a posture against gravity (postural tremor) or during voluntary movement (kinetic tremor).[12] The tasks were designed to capture both kinds of tremor.

In the first motor task (HOLD; postural tremor), patients placed their elbows on a table in front of them and elevated both forearms with palms facing inward and fingers spread. This task was carried out for 7 min in total. To avoid fatigue, we alternated holding and resting every 20 s.

Throughout the second task (POUR; kinetic tremor) patients kept one plastic cup in each hand, one filled with rice grains and the other empty. A screen was positioned in front of the patients. They were instructed to start pouring the rice from one cup into the other, standing on the table, once the fixation cross turned green (Go cue), and to keep pouring until the cross turned red (Stop cue). Then, both cups were to be placed on the table until the next Go cue appeared. The Go and Stop cues were displayed for 10 s and 5 s, respectively. This task was performed in 2.5-min blocks and each patient completed 2–3 blocks. Due to fatigue, only 8 of 19 patients completed this task.

Data Preprocessing

Preprocessing and further analysis steps were performed with the FieldTrip toolbox,[14] MNE-Python,[15] and custom-written MATLAB scripts.

We scanned the raw data for bad MEG, LFP, and EMG channels and excluded these from further analyses. Next, we applied temporal signal space separation to the MEG data using MNE-Python's *mne.preprocessing.maxwell_filter* in order to reduce artefacts. We set *st_duration* to 10 s and *st_correlation* to 0.98.

The rest of the analysis was performed with the FieldTrip toolbox. The data were down-sampled to 200 Hz and only the 204 planar gradiometers were used for further analysis. LFPs were rearranged into a bipolar montage by subtracting the signals of adjacent contacts (see Fig. S1) and visually screened for artifacts. EMGs were high-pass filtered at 10 Hz and full-wave rectified.

Tremor

We inspected the continuous EMG and accelerometer signals to identify tremor and tremor-free epochs (Fig. 1A). To avoid any tremor-related activity, we labelled epochs as tremor-free only if we found no indication of tremor in either hand, which was mostly the case for the pauses in between movements. In three cases, tremor persisted in the pauses so that we had to extract tremor-free epochs from the resting-state recordings.[13]

The presence of tremor was evaluated separately for each body side. While this procedure accounts for the independence of left and right upper limb tremor,[16] it does not stratify the tremor state of the other body side,

TABLE 1 *Patient details*

Patient ID	Age (y)	Sex	Disease duration (y)	Electrode type
ET01	65	M	19	Abbott Infinity
ET02	69	M	18	Abbott Infinity
ET03	71	M	20	Abbott Infinity
ET04	60	F	49	Abbott Infinity
ET05	62	M	50	Abbott Infinity
ET06	65	M	30	Boston Sc. Vercice Standard
ET07	58	M	5	Abbott Infinity
ET08	77	F	8	Boston Sc. Vercice Cartesia
ET09	74	M	20	Abbott Infinity
ET10	30	M	25	Abbott Infinity
ET11	57	F	51	Abbott Infinity
ET12	76	M	NA	Abbott Infinity
ET13	54	M	39	Medtronic SenSight
ET14	62	F	56	Abbott Infinity
ET15	65	M	20	Boston Sc. Vercice Cartesia
ET16	71	M	20	Boston Sc. Vercice Cartesia
ET17	67	M	15	Abbott Infinity
ET18	82	F	62	Boston Sc. Vercice Cartesia
ET19	68	F	35	Boston Sc. Vercice Cartesia
$\mu \pm \sigma$	65 ± 11		31 ± 20	

Abbreviations: y, year; M, male; F, female; NA, not available; μ, mean; σ, standard deviation.

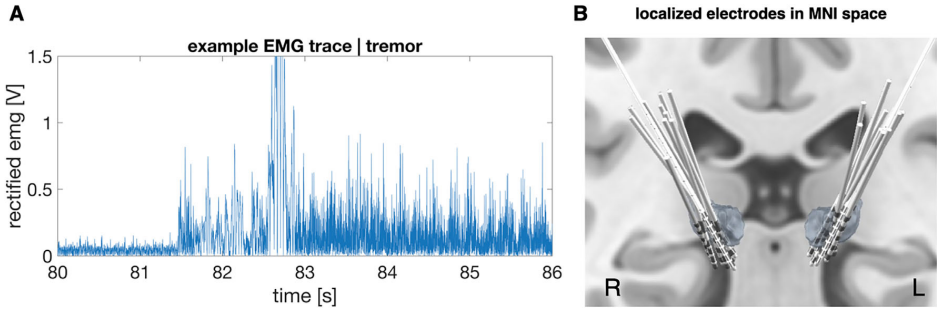

FIG. 1. Electromyography (EMG) signals and deep brain stimulation electrodes targeting the ventral intermediate nucleus of the thalamus. (A) 10 Hz High-pass filtered and rectified and EMG signal during change from rest to hold in one patient. Tremor started immediately after the arm had been lifted. (B) Electrodes targeting the ventral intermediate nucleus of the thalamus, localized with Lead-DBS. MNI, Montreal Neurological Institute. [Color figure can be viewed at wileyonlinelibrary.com]

which may or may not exhibit tremor at the same time. Because the tremor label pertained to one body side only, we limited all tremor analyses to the corresponding (contralateral) hemisphere.

To verify the presence/absence of tremor, we computed the EMG power spectra for each forearm between 1 and 35 Hz in 0.5 Hz steps. We averaged the spectra of flexor and extensor and identified individual tremor frequency for each body side (Table S1).

Power and Coherence Spectra

For the computation of spectra, we segmented the data into non-overlapping 2 s epochs, convolved

the epochs with a Hanning taper, and computed power and magnitude-squared coherence in the 1–35 Hz range using Welch's method (frequency resolution: 0.5 Hz).

Physiological power spectra are assumed to consist of a periodic component, visible as peaks in the spectrum, and an aperiodic (1/f) component. We used the fitting oscillations and 1/f (FOOOF) algorithm[17] to model both components of the EMG and LFP spectra (for details see Supporting Information 'Power spectra–FOOOF algorithm'). For further analysis, only the periodic component was considered.

Contact Localization and Contact Selection

DBS electrodes were localized with Lead-DBS[18] (Fig. 1B; see Supporting Information for details). We ensured that electrodes were on target and considered only contacts within the ventral thalamus according to the DISTAL atlas.[19] For each hemisphere, we selected the bipolar LFP channel with the highest power peak at individual tremor frequency. Depending on the individual lateralization of tremor, this procedure resulted in either one (one body side affected by tremor) or two selected channels per patient (both body sides affected by tremor). We excluded one patient due to uncertain electrode position.

Source Reconstruction

For each patient, a single-shell head model was generated based on their individual T1-weighted MRI scan (Siemens Mangetom Tim Trio, 3-T MRI scanner, München, Germany). Source reconstruction was performed for a grid with 567 points on the cortical surface, aligned to Montreal Neurological Institute (MNI) space, with a linear constrained minimum variance (LCMV) beamformer.[20] The regularization parameter λ was set to 5%. To account for the rank reduction resulting from temporal signal space separation, we truncated the covariance matrix such that it had the same rank as the Maxwell-filtered data. When computing condition contrasts (tremor vs. rest) we applied a common spatial filter to exclude confounds arising due to differences in spatial filters.

Source Coherence Images

We computed thalamocortical and corticomuscular coherence spectra (see 'Power and Coherence Spectra' for details). In addition, we averaged activity ±0.5 Hz around individual tremor frequency and computed one source image per hemisphere in this frequency range. Moreover, we constructed coherence maps in the beta range (13–35 Hz) for correlation with tremor severity. For epochs containing right-hand movement, we mirrored the source images across the midsagittal plane. In consequence, brain activity ipsilateral to movement appears in the left hemisphere, and brain activity contralateral to movement in the right hemisphere in all figures.

Tremor Amplitude

To quantify tremor amplitude, we extracted EMG spectral power at individual tremor frequency ±0.5 Hz from the 1/f-corrected power spectra and averaged power over flexor and extensor.

Statistical Analysis

As in previous studies,[13,21] the unit of observation was hemisphere rather than patient (postural tremor: $N_{\text{hemispheres}} = 16$, kinetic tremor: $N_{\text{hemispheres}} = 9$). The study had a within-hemisphere design, and we matched the amount of data across conditions for each hemisphere when computing condition contrasts (action tremor vs. rest). The statistical analysis was based on nonparametric, two-sample, cluster-based permutation tests with 1000 random permutations. The tests were two-tailed and the α-level was set to 0.05. Multiple comparison correction was implemented by relating all effects to the strongest effects observed in the permuted data.[22] Cortical areas showing differences served as regions of interest for further analyses, such as Pearson correlation between coherence and tremor amplitude.

When comparing spectra, we recentered them on individual tremor frequency (tf) and included the frequency range from tf – 2 Hz to tf + 15 Hz.

Results

Tremor

In the HOLD task, 7 of 19 patients experienced bilateral postural tremor and 3 patients experienced unilateral tremor. In the POUR task, 4 of 8 patients experienced bilateral kinetic tremor and 2 patients experienced unilateral tremor (Table S1). The average tremor frequency was 5.1 Hz ±0.9 Hz ($\mu \pm \sigma$) for postural tremor and 4.4 Hz ± 1.1 Hz for kinetic tremor.

Tremor-Related Thalamic Activity

When patients experienced tremor a clear spectral peak emerged at individual tremor frequency, which was absent during rest. This occurred in the EMG power spectrum (cluster-based permutation test: postural tremor: $t_{\text{clustersum}} = 27.6$, $P = 0.002$, Fig. 2A; kinetic tremor: $t = 19.7$, $P = 0.017$, Fig. 2B), the VIM power spectrum (postural tremor: $t = 13.0$, $P = 0.009$, Fig. 2C; kinetic tremor: $t = 14.2$, $P = 0.009$, Fig. 2D), and the VIM-EMG coherence spectrum (postural tremor: $t = 3.1$, $P = 0.15$, Fig. 2E; kinetic tremor: no cluster, Fig. 2F).

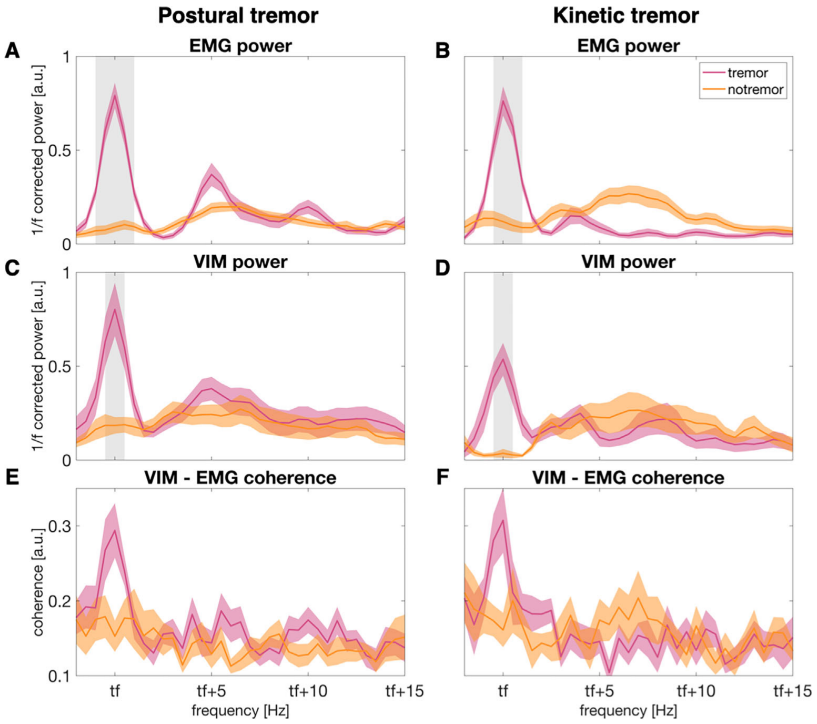

FIG. 2. Thalamic and muscle activity during postural and kinetic tremor and tremor-free epochs. Averaged electromyography (EMG) activity of the tremulous arm during postural (A) and kinetic (B) tremor and tremor-free epochs. 1/f-corrected ventral intermediate nucleus of the thalamus (VIM) power contralateral to the tremulous arm during postural (C) and kinetic (D) tremor. Coherence between the tremulous arm and the contralateral VIM during postural (E) and kinetic (F) tremor. Spectra were shifted along the frequency axis to align them on individual tremor frequency (tf). For postural tremor, the spectra were averaged over 16 hemispheres from 9 patients. For kinetic tremor, the spectra were averaged over 9 hemispheres from 5 patients. The shaded areas (pink and yellow) represent the standard error of the mean. The grey shading indicates significant differences between tremor and tremor-free epochs. [Color figure can be viewed at wileyonlinelibrary.com]

Coherence, Postural Tremor

Coupling at tremor frequency between the cortex and the VIM contralateral to the tremulous arm was stronger in the presence than in the absence of tremor. Figure 3 shows the brain regions where significant modulations ($P < 0.05$) occurred. The effect mapped to the sensorimotor cortex contralateral to tremor (cluster-based permutation test: $t_{clustersum} = 132.23$, $P = 0.002$; MNI-coordinates maximal t-value: $X = \pm 45.4$ mm, $Y = -30$ mm, $Z = 62.9$ mm), the ipsilateral cerebellum ($t = 68.19$, $P = 0.008$; $X = \pm 8.5$ mm, $Y = -90$ mm, $Z = -35$ mm), and the contralateral cerebellum ($t = 39.22$, $P = 0.021$; $X = \pm 25$ mm, $Y = -50$ mm, $Z = -60$ mm).

Corticomuscular coupling increased in similar regions: bilateral motor cortex ($t = 205.37$, $P = 0.004$; $X = \pm 23.7$ mm, $Y = -60$ mm, $Z = 70.2$ mm), bilateral cerebellum ($t = 172.83$, $P = 0.006$; $X = \pm 26.6$ mm, $Y = -90$ mm, $Z = -31.8$ mm), and bilateral prefrontal cortex ($t = 271.34$, $P = 0.002$; $X = \pm 40.7$ mm, $Y = 50$ mm, $Z = 21.7$ mm; Fig. 3A). The corresponding t-maps can be found in Figure S2A (VIM-cortex coherence) and Figure S3A (corticomuscular coherence).

VIM-cortex and corticomuscular coherence overlapped in several areas, such as the hand area of sensorimotor cortex contralateral to tremor, as well as in the cerebellum ipsilateral to tremor. Yet, the changes in corticomuscular coherence were more widespread, including additional frontal and parietal areas. The VIM-cortex and corticomuscular coherence spectra for the sensorimotor cortex contralateral to tremor, and the cerebellum ipsilateral and contralateral to tremor are displayed in Figure 4A,B.

Coherence, Kinetic Tremor

During kinetic tremor, similar changes occurred, but the effects were more circumscribed (Fig. 3B). Increases of coherence were observed in supplementary motor cortex contralateral to tremor ($t = 38.8$, $P = 0.012$; $X = \pm 39$ mm, $Y = -20$ mm, $Z = 66$ mm), the

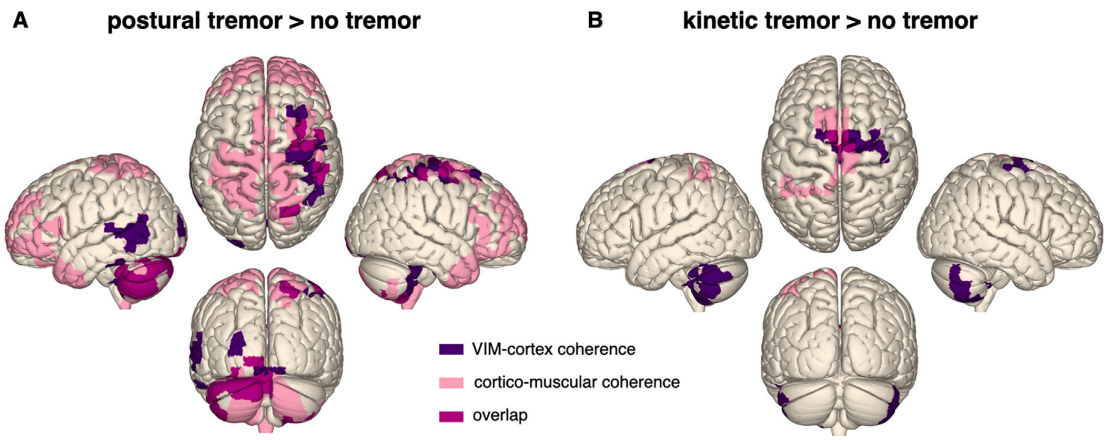

FIG. 3. Thalamo-cortical and corticomuscular coherence increased during postural and kinetic tremor. The surface plots illustrate the increase of ventral intermediate nucleus of the thalamus (VIM)-cortex (purple) and corticomuscular coherence (light pink) during postural (A) and kinetic (B) tremor at individual tremor frequency ±0.5 Hz. The overlap between VIM-cortex and corticomuscular coherence is displayed in pink. Only coherence to the VIM contralateral to movement is displayed. Left hemisphere: ipsilateral to tremor; right hemisphere: contralateral to tremor. [Color figure can be viewed at wileyonlinelibrary.com]

cerebellum ipsilateral ($t = 62.6$, $P = 0.002$; $X = \pm 50.6$ mm, $Y = -40$ mm, $Z = 41.8$ mm), and contralateral to tremor ($t = 37.84$, $P = 0.012$). Corticomuscular coherence increased in medial sensorimotor regions ($t = 73.3$, $P = 0.01$; $X = \pm 16.9$ mm, $Y = 10$ mm, $Z = 67.1$ mm). The corresponding t-maps are shown in Figure S2B (VIM-cortex coherence) and Figure S3B (corticomuscular coherence).

Relationship between VIM-Cortex Coherence and Tremor Amplitude–Postural Tremor

Tremor Frequency

The amplitude of tremor correlated with VIM-motor cortex coherence at tremor frequency ($r = 0.59$, $P = 0.017$, Fig. 4C(i)) during postural tremor. The relationship between tremor amplitude and VIM-cerebellar

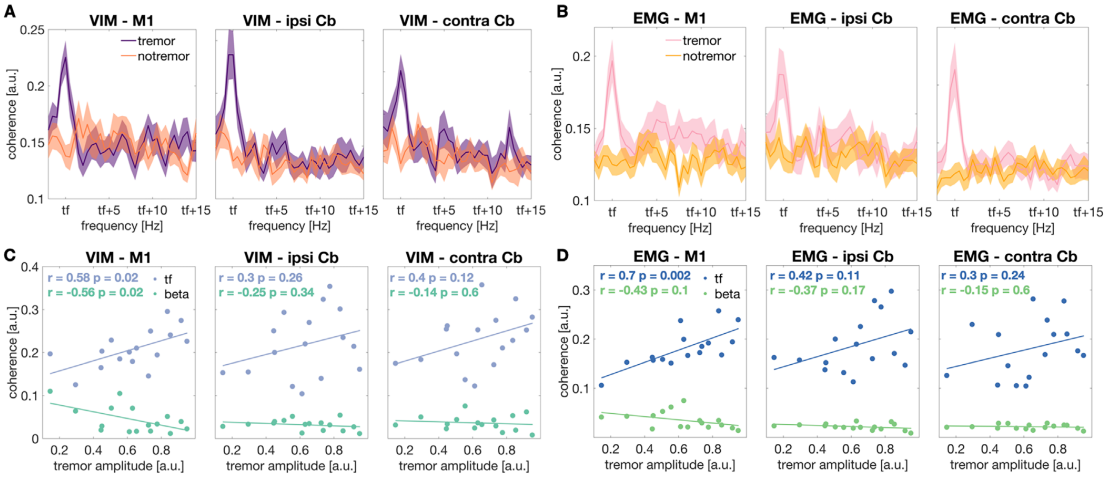

FIG. 4. Coherence spectra and correlation between postural tremor amplitude and coherence. Coherence between ventral intermediate nucleus of the thalamus (VIM) (A) electromyography (EMG) (B) and (i) motor cortex contralateral, (ii) cerebellum ipsilateral, and (iii) cerebellum contralateral to tremor, for postural tremor and tremor-free epochs. Spectra were averaged across patients. Shaded areas represent the standard error of the mean. Scatter plots illustrate the relationship between tremor amplitude and VIM-cortex (C) and EMG-cortex (D) coherence at tremor frequency and in the beta band (13–35 Hz) during postural tremor. Cb, cerebellum; M1, primary motor cortex; ipsi, ipsilateral to tremor; contra, contralateral to tremor; tf, individual tremor frequency. [Color figure can be viewed at wileyonlinelibrary.com]

coherence, however, was not significant (cerebellum ipsilateral to tremor: $r = 0.3$, $P = 0.26$, Fig. 4C(ii); cerebellum contralateral to tremor: $r = 0.4$, $P = 0.12$, Fig. 4C(iii)). Postural tremor amplitude also correlated with EMG-motor cortex coherence ($r = 0.72$, $P = 0.002$, Fig. 4D(i)). The correlation with EMG-cerebellar coherence was not significant (cerebellum ipsilateral to tremor: $r = 0.42$, $P = 0.1$, Fig. 4D(ii); cerebellum contralateral to tremor: $r = 0.3$, $P = 0.24$, Fig. 4D(iii)).

Beta Band

We found a negative correlation between tremor amplitude and VIM-motor cortex coherence in the beta band ($r = -0.56$, $P = 0.025$, Fig. 4C(i)). The relationship between tremor amplitude and VIM-cerebellar beta coherence, however, was not significant (cerebellum ipsilateral to tremor: $r = -0.25$, $P = 0.34$, Fig. 4C(ii); cerebellum contralateral to tremor: $r = -0.14$, $P = 0.6$, Fig. 4C(iii)). The correlation between tremor amplitude and EMG-cortex beta coherence was not significant (motor cortex: $r = -0.4$, $P = 0.1$, Fig. 4D(i); cerebellum ipsilateral to tremor: $r = -0.37$, $P = 0.17$, Fig. 4D(ii); cerebellum contralateral to tremor: $r = -0.15$, $P = 0.6$, Fig. 4D(iii)).

Discussion

In this study, we characterized VIM-cortex coupling during tremor in patients with essential tremor, using intracranial recordings from the VIM, in combination with MEG. During postural and kinetic tremor, VIM power and VIM-cortex coherence increased at individual tremor frequency. This effect was most prominent in the primary motor and primary somatosensory cortex ipsilateral to the VIM and the bilateral cerebellum. Corticomuscular coherence also increased during tremor and exhibited a similar spatial organization. Coupling strength of motor cortex to both VIM and muscle correlated with postural tremor amplitude.

Localization of Tremor-Related Activity

Using intracranial and MEG recordings, we demonstrated that neuronal oscillations in the ventral thalamus synchronize with motor cortical and cerebellar activity in the presence of tremor. Although this is a common narrative in the tremor literature, no study has, to the best of our knowledge, demonstrated this effect in a larger cohort of essential tremor patients.

Our findings add to a growing body of evidence for a central tremor network underlying essential tremor, gathered through a wide range of techniques, including clinical electrophysiology,[6,7] fMRI,[4,5] neuropathology,[23,24] neurostimulation,[25-28] and tractography.[29,30] Studies combining EMG and fMRI have localized tremor-associated brain activity by tracking BOLD signal modulations correlated with slow changes in tremor amplitude.[4,31,32] Similarly, MEG[7] and EEG[8] have been combined with EMG to investigate tremor at a smaller timescale. Across studies, the thalamus, the cerebellum, and primary motor cortex have emerged as major hubs of the essential tremor network. Complementary to these findings, neuromodulation has uncovered important functional aspects of the cerebello-thalamo-cortical circuit. It has been demonstrated, for example, that phase-locked VIM DBS[26] and non-invasive stimulation of the cerebellum[27] or motor cortex[25] can intensify or weaken tremor, depending on the phase difference between tremor and stimulation. These findings emphasize the importance of rhythmic neural activity synchronized across a distributed tremor network, similar to findings in Parkinson's disease.[33] A correlation between oscillatory coupling and essential tremor severity, however, has not been demonstrated to date. This is one important contribution of the current study, emphasizing the clinical relevance of thalamo-cortical coupling at tremor frequency.

Cerebellum

The cerebellum is thought to play a major role in the pathophysiology of essential tremor.[34,35] In line with this notion, we found that both VIM and muscle activity in the tremulous arm were coherent with the bilateral cerebellum during postural and kinetic tremor. In contrast, previous MEG/EEG studies have found tremor-associated neural activity to be limited to the cerebellar hemisphere ipsilateral to the tremulous arm.[6,7] This difference may stem from bilateral postural tremor in some of our patients, leading to bilateral cerebellar activation. Notwithstanding an effect of bilateral tremor in this scenario, bilateral cerebellar activation was also visible during unilateral kinetic tremor (POUR). An involvement of the bilateral cerebellum is plausible based on the structural connections of the VIM: it receives inputs from the contralateral cerebellum via decussating fibres and, to a minor extent, from the ipsilateral cerebellum via non-decussating fibers of the dentato-rubro-thalamic tract.[36] Moreover, studies combining EMG and fMRI reported bilateral cerebellar involvement during unilateral tremor in patients with essential tremor[32,37] and similar observations have been made for unilateral dystonic tremor.[38] However, only the cerebellum ipsilateral to movement was active during mimicked tremor in healthy individuals.[32,37] This indicates that the recruitment of both cerebellar hemispheres might be a pathological feature.

Primary Sensorimotor Cortex

It is well-established that the primary sensorimotor cortex plays an important role in many types of involuntary movement, such as Parkinsonian tremor[33] or focal dystonia.[39] The role of thalamo-sensorimotor cortex

coupling in essential tremor, however, is less clear. To date, simultaneous LFP-EEG recordings have been conducted in three patients across two studies, all showing tremor frequency peaks in the VIM–motor cortex coherence spectra.[10,11] For coupling between muscle and motor cortex, ambiguous results have been reported. Some studies found increased coupling during tremor,[6,7] while others found coupling in only a few patients,[40] and one study reported no coupling at all.[41] Trying to reconcile these findings, it has been speculated that the involvement of the sensorimotor cortex is intermittent.[42] In this study, we provide evidence for motor cortical involvement in essential tremor: VIM/EMG-motor cortex coupling increased during both postural and kinetic tremor.

During postural tremor, the strength of VIM−motor cortex and EMG-motor cortex coupling at tremor frequency, but not of VIM−cerebellar or EMG-cerebellar coupling correlated with tremor amplitude, underpinning the importance of the motor cortex. A prominent contribution by the motor cortex is supported by previous studies demonstrating that non-invasive stimulation of motor cortex reduces essential tremor amplitude.[43] Interestingly, similar observations have been made for re-emergent tremor in Parkinson's disease: transcranial magnetic stimulation of the primary motor cortex, but not the cerebellum, modulated tremor amplitude.[44,45] In addition, connectivity and network mapping studies have unveiled that VIM-DBS at sites more strongly connected to the primary sensorimotor cortex was associated with superior tremor improvement.[30,46] Notably, it has further been reported that sensorimotor cortex leads muscle activity during tremor,[47] suggesting that the increased synchronization with primary sensorimotor cortex might reflect an active involvement of motor cortex rather than field spread from primary somatosensory cortex.

Additionally, we found that coherence between the VIM and motor cortex in the beta band was inversely correlated with tremor amplitude. A negative association between beta activity and tremor has often been reported for resting tremor in Parkinson's disease.[33,48] In the case of essential tremor, previous studies have shown a similar negative correlation between beta activity and tremor within the VIM,[49] and our findings extend this relationship to thalamo-cortical coupling. Voluntary movements are likewise associated with a reduction of beta activity and, together, these results indicate that tremor and voluntary movements might have common underlying mechanisms.[50]

Postural Versus Kinetic Tremor

Action tremor can be divided into different types such as postural and kinetic tremor. These subtypes can co-occur in a single patient. It remains unclear whether the subtypes arise from distinct brain regions.[51] EMG-fMRI studies found activation of cerebellum, motor thalamus, and motor cortex in different kinds of action tremor, suggesting that the cerebello-thalamo-cortical circuit is involved in the generation of different types of tremor.[31,32] Our findings support this idea. However, the cortical distribution of coherence with thalamic activity was more widespread for postural tremor than for kinetic tremor. This may be due to postural tremor occurring simultaneously in both body sides in some patients, whereas kinetic tremor was unilateral.

Limitations

Due to the postoperative stun effect, uni- or bilateral tremor was present in 12 of 19 patients during the HOLD task, the POUR task, or both. While this sample size is small in absolute numbers, it is substantially larger compared to previous studies measuring thalamo-cortical coupling in humans ($N \leq 3$).[10,11]

Further, from a methodological perspective, it would be desirable to match the motor tasks perfectly (eg, HOLD with tremor versus HOLD without tremor or mimicked action tremor versus true action tremor). This was not possible in our cohort because the instruction to keep a static posture or to mimic action tremor inevitably elicits actual tremor.

Finally, we note that shaking extensions can cause artefactual tremor peaks in LFP power and coherence. The topography of MEG-LFP coherence observed here, however, is inconsistent with cable movement.

Conclusions

Recording thalamic and cortical activity simultaneously, we demonstrate that tremor episodes in patients are characterized by synchronized oscillations in the ventral intermediate nucleus of the thalamus, the cerebellum, and sensorimotor cortex, underpinning the role of the cerebello-thalamo-cortical circuit in the pathophysiology of essential tremor. ●

Author Roles: (1) Research Project: A. Conceptualization, B. Methodology, C. Visualization, D. Data Acquisition; E. Data Analysis; (2) Statistical Analysis: A. Design, B. Execution, C. Review and Critique; (3) Manuscript Preparation: A. Writing of the First Draft, B. Review and Critique; (4) Other: A. Resources, B. Project Administration, C. Supervision, D. Funding Acquisition.
A.S.: 1B, 1C, 1D, 1E, 3A.
S.S.: 1A, 1D, 3B.
M.B.: 1D, 3B.
J.V.: 3B, 4A.
A.Sc.: 1A, 3B, 4A, 4D.
J.H.: 1B, 1D, 3B, 4B, 4C.

Acknowledgment: Open Access funding enabled and organized by Projekt DEAL.

Financial Disclosures: A.Sc. and J.H. are funded by the Brunhilde Moll Stiftung. Additionally, A.Sc. acknowledges support from the

Deutsche Forschungsgemeinschaft (DFG, German Research Foundation) under Project ID 4247788381-TRR 295.

Full Financial Disclosures for the Previous 12 Months: A.Sc. has received consulting fees from Abbott, Zambon, and AbbVie and speaker's honoraria from BSH Medical Communication, Abbott, Kyowa Kirin, Novartis, AbbVie, Alexion, and GE Healthcare. A.S., S.S., M.B., J.V., and J.H. report no disclosures.

Data Availability Statement

Data can be made available in anonymized form upon reasonable request, contingent on patient consent.

References

1. Welton T, Cardoso F, Carr JA, Chan L-L, Deuschl G, Jankovic J, et al. Essential tremor. Nat Rev Dis Prim 2021;7(1):83. https://doi.org/10.1038/s41572-021-00314-w
2. Scherer M, Steiner LA, Kalia SK, Hodaie M, Kühn AA, Lozano AM, et al. Single-neuron bursts encode pathological oscillations in subcortical nuclei of patients with Parkinson's disease and essential tremor. Proc Natl Acad Sci U S A 2022;119(35): e2205881119. https://doi.org/10.1073/pnas.2205881119
3. Hua SE, Lenz FA. Posture-related oscillations in human cerebellar thalamus in essential tremor are enabled by voluntary motor circuits. J Neurophysiol 2005;93(1):117–127. https://doi.org/10.1152/jn.00527.2004
4. Buijink AWG, van der Stouwe AMM, Broersma M, et al. Motor network disruption in essential tremor: a functional and effective connectivity study. Brain 2015;138(10):2934–2947. https://doi.org/10.1093/brain/awv225
5. Younger EFP, Ellis EG, Parsons N, et al. Mapping essential tremor to a common brain network using functional connectivity analysis. Neurology 2023;101(15):e1483–e1494. https://doi.org/10.1212/WNL.0000000000207701
6. Muthuraman M, Raethjen J, Koirala N, et al. Cerebello-cortical network fingerprints differ between essential, Parkinson's and mimicked tremors. Brain 2018;141(6):1770–1781. https://doi.org/10.1093/brain/awy098
7. Schnitzler A, Münks C, Butz M, Timmermann L, Gross J. Synchronized brain network associated with essential tremor as revealed by magnetoencephalography. Mov Disord 2009;24(11):1629–1635. https://doi.org/10.1002/mds.22633
8. Muthuraman M, Heute U, Arning K, Anwar AR, Elble R, Deuschl G, Raethjen J. Oscillating central motor networks in pathological tremors and voluntary movements. What makes the difference? Neuroimage 2012;60(2):1331–1339. https://doi.org/10.1016/j.neuroimage.2012.01.088
9. Pan MK, Li YS, Wong SBC, et al. Cerebellar oscillations driven by synaptic pruning deficits of cerebellar climbing fibers contribute to tremor pathophysiology. Sci Transl Med 2020;12(526):eaay1769. https://doi.org/10.1126/scitranslmed.aay1769
10. Marsden JF, Ashby P, Limousin-Dowsey P, Rothwell JC, Brown P. Coherence between cerebellar thalamus, cortex and muscle in man: cerebellar thalamus interactions. Brain J Neurol 2000;123(Pt 7): 1459–1470. https://doi.org/10.1093/brain/123.7.1459
11. He F, Sarrigiannis PG, Billings SA, et al. Nonlinear interactions in the thalamocortical loop in essential tremor: A model-based frequency domain analysis. Neuroscience 2016;324:377–389. https://doi.org/10.1016/j.neuroscience.2016.03.028
12. Bhatia KP, Bain P, Bajaj N, et al. Consensus statement on the classification of tremors. From the task force on tremor of the International Parkinson and Movement Disorder Society. Mov Disord 2017;33(1):75–87. https://doi.org/10.1002/mds.27121
13. Steina A, Sure S, Butz M, Vesper J, Schnitzler A, Hirschmann J. Mapping subcortico-cortical coupling—A comparison of thalamic and subthalamic oscillations. Mov Disord 2024;39(4):684–693. https://doi.org/10.1002/mds.29730
14. Oostenveld R, Fries P, Maris E, Schoffelen JM. FieldTrip: open source software for advanced analysis of MEG, EEG, and invasive electrophysiological data. Comput Intell Neurosci 2011;2011:1–9.
15. Gramfort A. MEG and EEG data analysis with MNE-python. Front Neurosci 2013;7:2677. https://doi.org/10.3389/fnins.2013.002677
16. Raethjen J, Lindemann M, Schmaljohann H, Wenzelburger R, Pfister G, Deuschl G. Multiple oscillators are causing parkinsonian and essential tremor. Mov Disord 2000;15(1):84–94. https://doi.org/10.1002/1531-8257(200001)15:1<84::AID-MDS1014>3.0.CO;2-K
17. Donoghue T, Haller M, Peterson EJ, et al. Parameterizing neural power spectra into periodic and aperiodic components. Nat Neurosci 2020;23(12):1655–1665. https://doi.org/10.1038/s41593-020-00744-x
18. Horn A, Li N, Dembek TA, et al. Lead-DBS v2: towards a comprehensive pipeline for deep brain stimulation imaging. Neuroimage 2019; 184:293–316. https://doi.org/10.1016/j.neuroimage.2018.08.068
19. Ewert S, Plettig P, Li N, et al. Toward defining deep brain stimulation targets in MNI space: A subcortical atlas based on multimodal MRI, histology and structural connectivity. Neuroimage 2018;170: 271–282. https://doi.org/10.1016/j.neuroimage.2017.05.015
20. Van Veen BD, Drongelen W, Yuchtman M, Suzuki A. Localization of brain electrical activity via linearly constrained minimum variance spatial filtering. IEEE Trans Biomed Eng 1997;44(9):867–880.
21. Oswal A, Cao C, Yeh CH, et al. Neural signatures of hyperdirect pathway activity in Parkinson's disease. Nat Commun 2021;12(1): 5185. https://doi.org/10.1038/s41467-021-25366-0
22. Maris E, Oostenveld R. Nonparametric statistical testing of EEG- and MEG-data. J Neurosci Methods 2007;164(1):177–190. https://doi.org/10.1016/j.jneumeth.2007.03.024
23. Faust PL, McCreary M, Musacchio JB, Kuo SH, Vonsattel JPG, Louis ED. Pathologically based criteria to distinguish essential tremor from controls: analyses of the human cerebellum. Ann Clin Transl Neurol 2024;11:1514–1525. https://doi.org/10.1002/acn3.52068
24. Louis ED, Faust PL. Essential tremor pathology: neurodegeneration and reorganization of neuronal connections. Nat Rev Neurol 2020; 16(2):69–83. https://doi.org/10.1038/s41582-019-0302-1
25. Asamoah B, Khatoun A, Mc Laughlin M. tACS motor system effects can be caused by transcutaneous stimulation of peripheral nerves. Nat Commun 2019;10(1):266. https://doi.org/10.1038/s41467-018-08183-w
26. Cagnan H, Pedrosa D, Little S, et al. Stimulating at the right time: phase-specific deep brain stimulation. Brain 2016;140(1):132–145. https://doi.org/10.1093/brain/aww286
27. Schreglmann SR, Wang D, Peach RL, et al. Non-invasive suppression of essential tremor via phase-locked disruption of its temporal coherence. Nat Commun 2021;12(1):363. https://doi.org/10.1038/s41467-020-20581-7
28. Riis TS, Losser AJ, Kassavetis P, Moretti P, Kubanek J. Noninvasive modulation of essential tremor with focused ultrasonic waves. J Neural Eng 2024;21(1):016033. https://doi.org/10.1088/1741-2552/ad27ef
29. Neudorfer C, Kultas-Ilinsky K, Ilinsky I, et al. The role of the motor thalamus in deep brain stimulation for essential tremor. Neurotherapeutics 2024;21(3):e00313. https://doi.org/10.1016/j.neurot.2023.e00313
30. Tsuboi T, Wong JK, Eisinger RS, et al. Comparative connectivity correlates of dystonic and essential tremor deep brain stimulation. Brain 2021;144(6):1774–1786. https://doi.org/10.1093/brain/awab074
31. Neely KA, Kurani AS, Shukla P, et al. Functional brain activity relates to 0–3 and 3–8 Hz force oscillations in essential tremor. Cereb Cortex 2014;25(11):4191–4202. https://doi.org/10.1093/cercor/bhu142
32. Broersma M, Van Der Stouwe AMM, Buijink AWG, et al. Bilateral cerebellar activation in unilaterally challenged essential tremor. Neuroimage Clin 2016;11:1–9. https://doi.org/10.1016/j.nicl.2015.12.011
33. Hirschmann J, Hartmann CJ, Butz M, et al. A direct relationship between oscillatory subthalamic nucleus–cortex coupling and rest tremor in Parkinson's disease. Brain 2013;136(12):3659–3670. https://doi.org/10.1093/brain/awt271

34. Pan MK, Kuo SH. Essential tremor: clinical perspectives and pathophysiology. J Neurol Sci 2022;435:120198. https://doi.org/10.1016/j.jns.2022.120198

35. van den Berg KRE, Helmich RC. The role of the cerebellum in tremor-evidence from neuroimaging. Tremor Hyperkinetic Mov (N Y) 2021;11:49. https://doi.org/10.5334/tohm.660

36. Coenen VA, Sajonz BE, Reinacher PC, Kaller CP, Urbach H, Reisert M. A detailed analysis of anatomical plausibility of crossed and uncrossed streamline rendition of the dentato-rubro-thalamic tract (DRT(T)) in a commercial stereotactic planning system. Acta Neurochir 2021;163(10):2809–2824. https://doi.org/10.1007/s00701-021-04890-4

37. Boscolo Galazzo I, Magrinelli F, Pizzini FB, et al. Voxel-based morphometry and task functional magnetic resonance imaging in essential tremor: evidence for a disrupted brain network. Sci Rep 2020;10(1):15061. https://doi.org/10.1038/s41598-020-69514-w

38. Nieuwhof F, Toni I, Dirkx MF, et al. Cerebello-thalamic activity drives an abnormal motor network into dystonic tremor. Neuroimage Clin 2022;33:102919. https://doi.org/10.1016/j.nicl.2021.102919

39. Zoons E, Booij J, Nederveen AJ, Dijk JM, Tijssen MAJ. Structural, functional and molecular imaging of the brain in primary focal dystonia—A review. Neuroimage 2011;56(3):1011–1020. https://doi.org/10.1016/j.neuroimage.2011.02.045

40. Air EL, Ryapolova-Webb E, de Hemptinne C, et al. Acute effects of thalamic deep brain stimulation and thalamotomy on sensorimotor cortex local field potentials in essential tremor. Clin Neurophysiol 2012;123(11):2232–2238. https://doi.org/10.1016/j.clinph.2012.04.020

41. Halliday D, Conway B, Farmer S, Shahani U, Russell A, Rosenberg J. Coherence between low-frequency activation of the motor cortex and tremor in patients with essential tremor. Lancet 2000;355(9210):1149–1153. https://doi.org/10.1016/S0140-6736(00)02064-X

42. Sharifi S, Luft F, Verhagen R, Heida T, Speelman JD, Bour LJ, van Rootselaar A-F. Intermittent cortical involvement in the preservation of tremor in essential tremor. J Neurophysiol 2017;118(5):2628–2635. https://doi.org/10.1152/jn.00848.2016

43. Hellriegel H, Schulz EM, Siebner HR, Deuschl G, Raethjen JH. Continuous theta-burst stimulation of the primary motor cortex in essential tremor. Clin Neurophysiol 2012;123(5):1010–1015. https://doi.org/10.1016/j.clinph.2011.08.033

44. Helmich RC, Van den Berg KRE, Panyakaew P, et al. Cerebello-cortical control of tremor rhythm and amplitude in Parkinson's disease. Mov Disord 2021;36(7):1727–1729. https://doi.org/10.1002/mds.28603

45. Leodori G, Belvisi D, De Bartolo MI, et al. Re-emergent tremor in Parkinson's disease: the role of the motor cortex. Mov Disord 2020;35(6):1002–1011. https://doi.org/10.1002/mds.28022

46. Riskin-Jones HH, Kashanian A, Sparks H, Tsolaki E, Pouratian N. Increased structural connectivity of thalamic stimulation sites to motor cortex relates to tremor suppression. Neuroimage Clin 2021;30:102628. https://doi.org/10.1016/j.nicl.2021.102628

47. Govindan RB, Raethjen J, Arning K, Kopper F, Deuschl G. Time delay and partial coherence analyses to identify cortical connectivities. Biol Cybern 2006;94(4):262–275. https://doi.org/10.1007/s00422-005-0045-5

48. Asch N, Herschman Y, Maoz R, et al. Independently together: subthalamic theta and beta opposite roles in predicting Parkinson's tremor. Brain Commun 2020;2(2):fcaa074. https://doi.org/10.1093/braincomms/fcaa074

49. Basha D, Dostrovsky JO, Lopez Rios AL, Hodaie M, Lozano AM, Hutchison WD. Beta oscillatory neurons in the motor thalamus of movement disorder and pain patients. Exp Neurol 2014;261:782–790. https://doi.org/10.1016/j.expneurol.2014.08.024

50. Schnitzler A, Timmermann L, Gross J. Physiological and pathological oscillatory networks in the human motor system. J Physiol Paris 2006;99(1):3–7. https://doi.org/10.1016/j.jphysparis.2005.06.010

51. Fanning A, Kuo SH. Clinical heterogeneity of essential tremor: understanding neural substrates of action tremor subtypes. Cerebellum 2023;23(6):2497–2510. https://doi.org/10.1007/s12311-023-01551-3

Supporting Data

Additional Supporting Information may be found in the online version of this article at the publisher's web-site.

Oscillatory coupling between thalamus, cerebellum and motor cortex in essential tremor

Supplementary material

Alexandra Steina[1], Sarah Sure[1], Markus Butz[1],
Jan Vesper[2], Alfons Schnitzler[1], Jan Hirschmann[1]

Author affiliations:

1 Institute of Clinical Neuroscience and Medical Psychology, Medical Faculty, Heinrich Heine University, 40225, Düsseldorf, Germany

2 Department of Functional Neurosurgery and Stereotaxy, Neurosurgical Clinic, Medical Faculty, Heinrich Heine University, 40225, Düsseldorf, Germany

Supplementary Table 1 Task & tremor information.

Patient ID	Tasks performed	Postural tremor frequency L/R [Hz]	Kinetic tremor frequency L/R [Hz]	Postural tremor data length L/R [s]	Kinetic tremor data length L/R [s]
ET01	H, P	-	-	-	-
ET02	H	4.5 / 4.5	-	88 / 78	-
ET03	H	5 / 5.5	-	99 / 40	-
ET04	H	-	-	-	-
ET05	H	6 / -	-	153 / -	-
ET06	H	6.5 / 6.5	-	81 / 80	-
ET07	H	-	-	-	-
ET08	H	5 / 5.5	-	297 / 213	-
ET09	P	-	5 / 5.5	-	81 / 72
ET10	H	-	-	-	-
ET11	H, P	-	3 / 5	-	63 / 109
ET12[a]	H, P	5.5 / -	6.5 / -	236 / -	102 / -
ET13	H, P	-	-	-	-
ET14	H, P	-	4.5 / 3.5	-	130 / 146
ET15	H, P	5 / -	5 / 4.5	174 / -	128 / 109
ET16	H, P	-	-	-	-
ET17	H	3.5 / 3.5	3.5 / -	102 / 90	49 / -
ET18	H	5 / 4	-	69 / 65	-
ET19	H	5.5 / 5.5	-	87 / 137	-
$\mu \pm \sigma$		5.1±0.9	4.4 ± 1.1	122 ± 70	98.9 ± 32

H: Hold, B: Button press, P: Pour μ: mean, σ: standard deviation.
[a]Left VIM excluded due to uncertain electrode position.

Methods

Referencing scheme

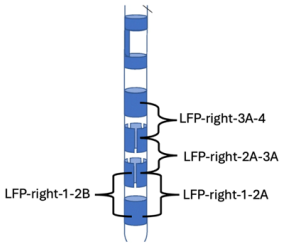

Supplementary Fig. 1: Bipolar montage used for re-referencing the contacts of a segmented lead. Each segment on level 2 was referenced to the corresponding segment on level 3, resulting in the bipolar channels 2A-3A, 2B-3C and 2C-3C. All segments were further referenced to the ring contact above (level 3) or below (level 2).

Lead localization

Lead localization was done in Lead-DBS v2.3, using pre-operative MRI and a post-operative CT scan. A linear co-registration of CT and MRI scans was performed with advanced normalization tools (ANTs).[1] The coregistration was visually inspected and adjusted if necessary. Subsequently, the pre-operative images were normalized from subject space to MNI space (ICBM 152 2009b Nonlinear Asymmetric),[2] with the ANTs-based diffeomorphic normalization SyN algorithms.[1] A brain shift correction was performed, using a coarse mask by Schönecker.[3] Lead trajectories were either automatically reconstructed with PACER[4] and manually refined or fully manually reconstructed if PACER failed.

Power spectra – FOOOF algorithm

We applied the fitting oscillations and one over f (FOOOF) algorithm to model the periodic and aperiodic component of the LFP and EMG spectra. The model was fitted to the spectrum in the 2-35 Hz range. The aperiodic component was fitted with either a fixed or a knee model. The peak width parameter was set to 1-3 Hz and the number of Gaussian fits was ranging from 8-12. All spectra were visually inspected and corrected if necessary to ensure good model fits.

Results

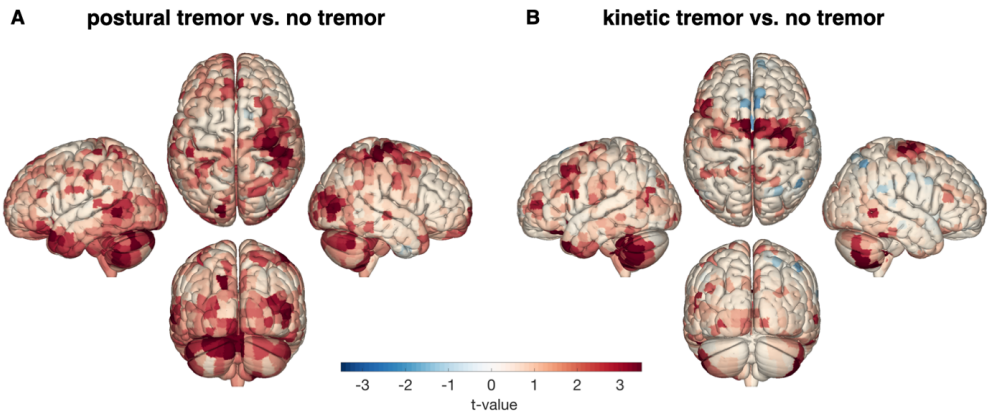

Supplementary Fig. 2: *t*-maps of tremor vs. no tremor for thalamocortical coherence. A Postural tremor vs. no tremor**. B** Kinetic tremor vs. no tremor. Cluster-based permutation test.

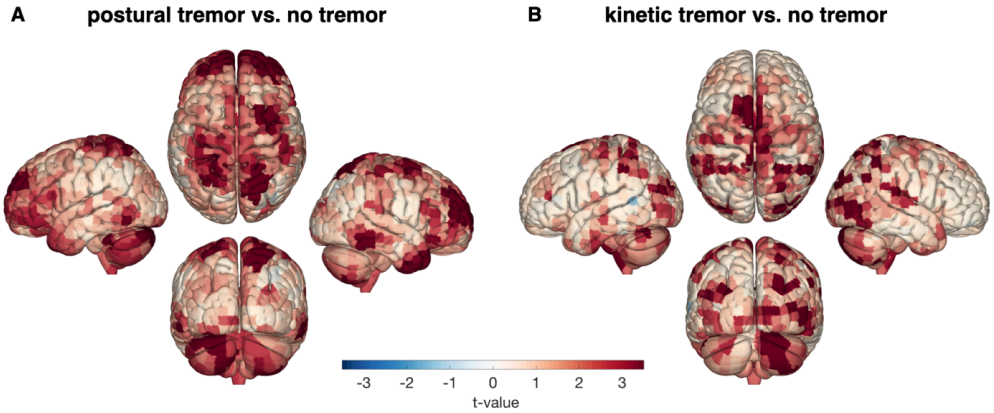

Supplementary Fig. 3: *t*-maps of tremor vs. no tremor corticomuscular coherence. A Postural tremor vs. no tremor. **B** Kinetic tremor vs. no tremor. Cluster-based permutation test.

References

1. Avants BB, Tustison NJ, Song G, Cook PA, Klein A, Gee JC. A reproducible evaluation of ANTs similarity metric performance in brain image registration. *NeuroImage*. 2011;54(3):2033-2044. doi:10.1016/j.neuroimage.2010.09.025

2. Fonov V, Evans AC, Botteron K, Almli CR, McKinstry RC, Collins DL. Unbiased average age-appropriate atlases for pediatric studies. *NeuroImage*. 2011;54(1):313-327. doi:10.1016/j.neuroimage.2010.07.033

3. Schönecker T, Kupsch A, Kühn AA, Schneider GH, Hoffmann KT. Automated Optimization of Subcortical Cerebral MR Imaging−Atlas Coregistration for Improved Postoperative Electrode Localization in Deep Brain Stimulation. *Am J Neuroradiol*. 2009;30(10):1914-1921. doi:10.3174/ajnr.A1741

4. Husch A, V. Petersen M, Gemmar P, Goncalves J, Hertel F. PaCER - A fully automated method for electrode trajectory and contact reconstruction in deep brain stimulation. *NeuroImage Clin*. 2018;17:80-89. doi:10.1016/j.nicl.2017.10.004

9.4 Article IV: Modulations of thalamo-cortical coupling during voluntary movement in patients with essential tremor

Reproduced from

Alexandra Steina, Sarah Sure, Markus Butz, Jan Vesper, Alfons Schnitzler, & Jan Hirschmann
Modulations of thalamo-cortical coupling during voluntary movement in patients with essential tremor
bioRxiv (2025)

Statement of contribution

S.S. and J.H. planned the research project (Paper II, III and IV). Data collection started before the start of my PhD. I recorded more patients throughout my doctorate with J.H., M.B. I planned the analysis, pre-processed and processed the data. I prepared the figures for the manuscript. All authors discussed the results. I wrote the manuscript. J.H., S.S., M.B., J.V., A.Sc. edited the manuscript.

Copyright and license notice

Modulations of thalamo-cortical coupling during voluntary movement in patients with essential tremor

Alexandra Steina[1], Sarah Sure[1], Markus Butz[1],
Jan Vesper[2], Alfons Schnitzler[1], Jan Hirschmann[1]

Abstract

The ventral intermediate nucleus of the thalamus (VIM) is the main thalamic hub for processing cerebellar inputs and the main deep brain stimulation target for the treatment of essential tremor (ET). As such, it presumably plays a critical role in motor control. So far, however, this structure has been rarely investigated in humans, and almost all of the existing studies focus on tremor. Here, we set out to study neural oscillations in the VIM and their coupling to cortical oscillations during voluntary movement.

We investigated thalamo-cortical coupling by means of simultaneous recordings of thalamic local field potentials and magnetoencephalography in 10 ET patients with externalized deep brain stimulation electrodes. Brain activity was measured while patients were pressing a button repeatedly in response to a visual cue. In a whole-brain analysis of coherence between VIM and cortex, we contrasted activity around a pre-movement baseline and button pressing.

Button pressing was associated with a bilateral decrease of thalamic power in the alpha (8–12 Hz) and beta (13–21 Hz) band and a contralateral power increase in the gamma (35–90 Hz) band. Moreover, changes in VIM-cortex coherence were observed. Alpha/low beta (8–20 Hz) coherence decreased before and during movement, and the effect localized to the supplementary motor area and premotor cortex. A rebound of high beta (21–35 Hz) coherence occurred in the same region, but was more focal than the suppression. Pre-movement levels of thalamo-cortex low-beta coherence correlated with reaction time.

Our results demonstrate that voluntary movement is associated with modulations of behaviourally relevant thalamic coupling, primarily to premotor areas. We observed a clear distinction between low- and high-beta frequencies and our results suggest that the concept of "antikinetic" beta oscillations, originating from research on Parkinson's disease, is transferable to ET.

Author affiliations:

1 Institute of Clinical Neuroscience and Medical Psychology, Medical Faculty, Heinrich Heine University, 40225 Düsseldorf, Germany

2 Department of Functional Neurosurgery and Stereotaxy, Neurosurgical Clinic, Medical Faculty, Heinrich Heine University, 40225 Düsseldorf, Germany

Correspondence to: Jan Hirschmann

Full address: Moorenstraße 5, 40225 Düsseldorf, Germany

E-Mail: Jan.Hirschmann@med.uni-duesseldorf.de

Running title: VIM-cortex coupling in essential tremor

Keywords: ventral intermediate nucleus; functional connectivity; essential tremor; motor system; coherence; deep brain stimulation; magnetoencephalography.

Introduction

The ventral intermediate nucleus of the motor thalamus (VIM) is believed to play a major role in the pathophysiology of essential tremor (ET).[1] Deep brain stimulation (DBS) of the VIM effectively suppresses tremor and oscillatory activity in the VIM has been demonstrated to be coherent with activity from the tremulous limb during tremor.[2]

Apart from its role in tremor, the motor thalamus is involved in controlling voluntary movements, maintaining postures, and motor learning.[3,4] Local field potential (LFP) recordings, for example, have revealed that oscillatory activity in the VIM is modulated during voluntary movements. During both self-paced and externally triggered movements, beta activity (13–30 Hz) decreases, while gamma activity (35–90 Hz) increases.[5–7] Such movement-related modulations of oscillatory activity are a ubiquitous phenomenon, occurring in several motor-related brain areas, such as motor cortex[8] or basal ganglia.[9] Beta activity is often interpreted as antikinetic,[10,11] i.e. anti-correlated with movement speed, while gamma activity is considered pro-kinetic.[12]

Expanding on these findings, studies combining LFP and cortical recordings have revealed that subcortical-cortical coupling follows similar dynamics. For example, in dystonia patients, low-beta (13–21 Hz) GPi-cortex coupling diminishes during cued movements, with coherence values correlating with reaction times,[11] in line with an antikinetic nature of beta oscillations. Similarly, in Parkinson's disease, movement onset is accompanied by suppression of beta coherence and an increase of gamma coherence between the STN and cortex,[13] with levodopa-induced bradykinesia improvements correlating with greater gamma coherence.[9] There is also initial evidence for modulations of thalamo-cortical coupling during voluntary movement,[6,7] but their topography, dynamics, and behavioural relevance remain elusive.

The aim of this study was to describe the network topology of thalamo-cortical coupling and its dynamic modulations before, during, and after voluntary movement. For this purpose, we performed LFP recordings from externalized VIM-DBS electrodes in combination with whole-head MEG during externally triggered button pressing in patients with ET. Moreover, we correlated coherence values with reaction times to demonstrate the behavioural relevance of thalamo-cortical coupling.

Materials and methods

Patients and recordings

10 patients diagnosed with essential tremor, undergoing surgery for DBS, participated in the study. Before the recording, patients provided written informed consent according to the Declaration of Helsinki and the study was approved by the Ethics Committee of the Medical Faculty at Heinrich Heine University Düsseldorf (ET: "2018-217-Zweitvotum"). The measurements happened the day after implantation of DBS electrodes and before the pulse generator was implanted, allowing for the recording of LFPs from the externalized leads. Patient details are provided in **Table 1**.

Electrophysiological measurements

We recorded MEG combined with intracranial LFPs from bilateral electrodes targeting the VIM. The LFPs were referenced to a mastoid reference. MEG signals were recorded by a 306-channel MEG system (Vectorview, MEGIN) with a sampling rate of 2 kHz. Moreover, we measured electromyograms (EMGs) from both forearms (extensor digitorum communis and flexor digitorum communis), accelerometer signals from both index fingers, and vertical and horizontal electrooculograms.

Paradigm

The experiment included one motor task, which followed a resting state recording[14] and two other motor tasks,[15] that were analysed in our previous works.

During the motor task, a button box was placed on a table in front of the patients. Upon the presentation of a visual cue, presented on a screen in front of them, patients pressed a button with either the left or the right index finger. Each trial started with a black fixation cross that was presented between 6-8 s, followed by a Go cue (green cross). Pressing the button started the next trial. The task was performed in blocks of 8 min and each patient completed 1-3 blocks. Each block was divided equally into a left-hand and a right-hand part, and started with a short video indicating which index finger to use first. The hand was switched after half of the trails had been recorded, with the hand switch indicated by a second video.

Data preprocessing

Data analysis was performed with the FieldTrip toolbox,[16] MNE-Python,[17] and custom written MATLAB (the MathWorks) scripts. Raw data were scanned for bad MEG and LFP channels and bad channels were excluded from further analyses. In order to reduce artefacts we applied temporal signal space separation to the MEG data using MNE-Python's *mne.preprocessing.maxwell_filter*, with *st_duration* set to 10 s and *st_correlation* to 0.98.

All following analysis steps were performed with the FieldTrip toolbox. For further analysis, we used only the 204 planar gradiometers and down-sampled the data to 200 Hz. We rearranged the LFPs into a bipolar montage by subtraction of signals from adjacent electrode contacts. EMGs were high-pass filtered at 10 Hz and full-wave rectified.

Epoching

The data were arranged in trials ranging from -4 to 4 s relative to button press (t = 0 s). Trials were visually inspected and bad trials were removed. Additional trials were discarded if the variance of any LFP channel exceeded 10^{-8} μV or if patients pressed the button more than once within the 8 s interval around the button press. One patient was excluded from further analysis because of bad LFP quality throughout the button pressing task. Information on the final number of trials can be found in **Supplementary Table 1**.

Source reconstruction

We generated a single-shell head model for each patient based on the individual T1-weighted MRI scan (Siemens Mangetom Tim Trio, 3-T MRI scanner, München, Germany) and reconstructed sources for a grid with 567 points. The grid points were distributed over the cortical surface, aligned to Montreal Neurological Institute (MNI) space. For source reconstruction, we used a linear constrained minimum variance (LCMV) beamformer,[18] with the regularization parameter λ set to 5%. Temporal signal space separation results in rank reduction, which can lead to erroneous beamformer output. To account for the rank reduction, we truncated the covariance matrix such that it had the same rank as the Maxwell-filtered data. To minimize confounds due to differences in spatial filters, we applied a common spatial filter to both condition contrasts (button press *vs*. baseline).

Time-resolved spectra

For the trial-based data, we calculated time-resolved power and thalamo-cortical coherence spectra with a sliding window of 800 ms which was moved in steps of 50 ms. At each time step, complex Fourier spectra were calculated from 5-45 Hz and 55-90 Hz using multi-

tapering with 2 Hz spectral smoothing, from which we derived power and coherence. The interval from 45-55 Hz was excluded due to 50 Hz line noise. For statistical analysis, we defined two intervals of interest: a baseline period from -3.0 to -2.0 s and a peri-movement interval from -1.5 to 2.5 s.

Contact localization and contact selection

Using a pre-operative MRI and a post-operative CT scan, we localized DBS electrodes with Lead-DBS.[19] The localized electrodes are displayed in **Fig. 1C**. We ensured that electrodes were on target and used only contacts within the ventral thalamus for further analysis. Moreover, we selected one bipolar LFP channel showing the strongest 8-20 Hz desynchronization contralateral to the button press. Because we alternated blocks of left- and right-hand button pressing, this procedure resulted in two selected channels per patient, i.e. one per hemisphere.

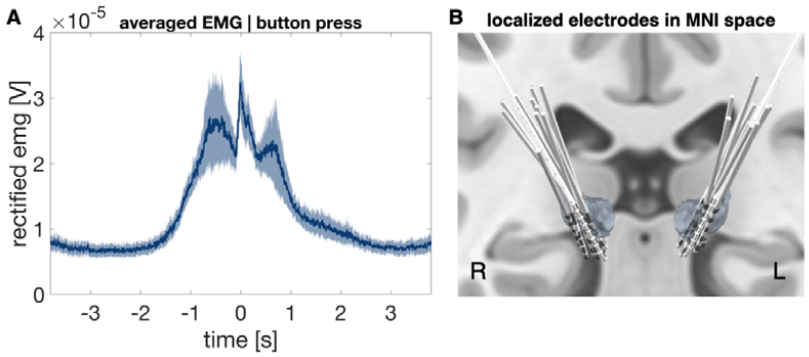

Figure 1: Electromyography signals and deep brain stimulation electrodes targeting the ventral intermediate nucleus of the thalamus (A) EMG timeseries averaged over all patients, aligned to button press (t = 0). The shaded blue area represents the standard error of mean. **(B)** Electrodes targeting the VIM localized with Lead-DBS.

Source images

We computed band-limited coupling between reconstructed sources and LFPs for three frequency ranges of interest: alpha/low-beta (8-20 Hz), high beta (21-35 Hz), and gamma (65-85 Hz). Alpha and low-beta were aggregated as they changed jointly in the button press task. We applied bandwidth-wide spectral smoothing to capture an entire band in one estimate, using multi-tapering.[20]

For epochs containing right hand movement, we mirrored the source images across the midsagittal plane. In consequence, brain activity ipsilateral to movement appears in the left hemisphere in all figures, and brain activity contralateral to movement in the right hemisphere.

Reaction time and pre-movement coherence

We tested if pre-movement coupling strength was predictive of reaction time. For this purpose, we calculated pre-movement coherence (-0.5 to 0.5 s relative to the Go cue) in the alpha/low-beta (8-20 Hz) and in the high beta (21-35 Hz) band and correlated it with reaction time. One patient's reaction time was not stored due to technical problems.

Statistical analysis

Rather than patient, the unit of observation of this study was hemisphere ($N_{hemispheres}$ = 17) in line with previous studies.[14,21,22] The statistical analysis had a within-hemisphere design (movement *vs*. baseline) and we used a nonparametric, two-sample, cluster-based-permutation tests with 1000 random permutations. The tests were two-tailed, with an α-level of 0.05. The results were corrected for multiple comparisons by relating all effects to the strongest effects observed in the permuted data (brain-wide or spectrum-wide).[23] Cortical areas showing differences served as regions of interest for further analyses, such as Pearson correlation with behavioural metrics or visualization of power/coherence dynamics.

Results

Button pressing

In the button pressing task, patients had to press a button every 6-8 s in response to a visual cue. Group average EMG activity, aligned to the button press, is displayed in **Fig. 1B**. On average, movement started between 2-1.5 s before the button was pressed, as patients had to first lift their hand from the table and reach towards the button box.

Movement-related power changes of thalamic oscillatory activity

Movement-related changes in VIM power ipsi- and contralateral to the button press are depicted in **Fig. 2**. VIM power in the 8–20 Hz range started to decrease below baseline levels ~ 1 s before the button press, and this decrease lasted until ~1.5 s after the button press. Besides this movement-related alpha/low-beta power suppression, which occurred bilaterally

(ipsilateral VIM: cluster-based-permutation-test, $t_{clustersum}$ = -1.61*10^3, p = 0.004; contralateral VIM: t = –2.5*10^3, p = 0.002), we observed movement-locked power increases with a pronounced hemispheric lateralization. In the VIM contralateral to movement, power in the 21-35 Hz range increased around 0-2 s relative to the button press (t = 1.7*10^3, p = 0.003), likely reflecting a combination of a low-gamma power increase around movement onset and a post-movement beta rebound. A further gamma power increase was observed at higher frequencies (65-85 Hz), around the time of button press (t = 746, p < 0.001).

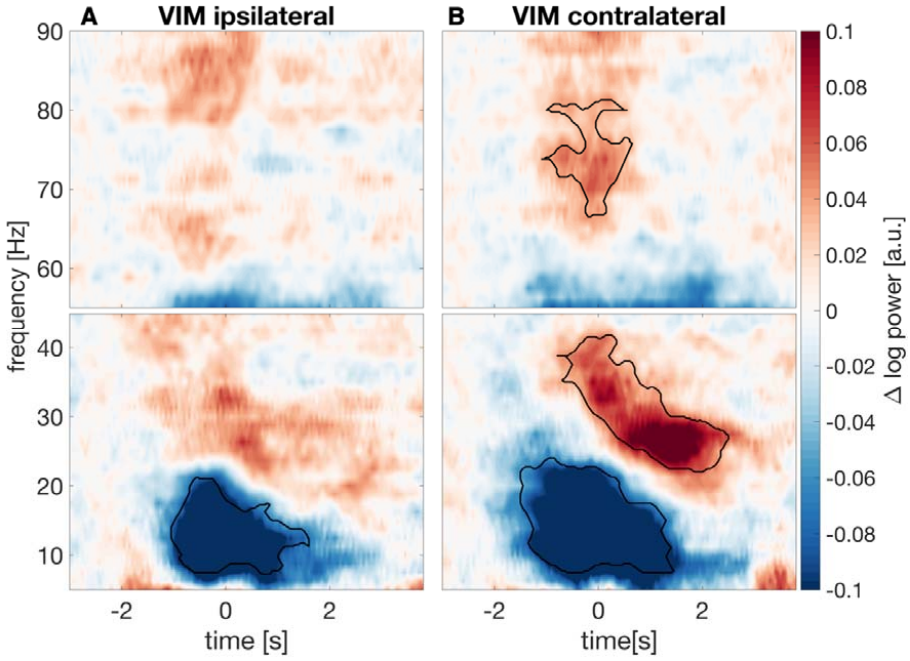

Figure 2: Thalamic power is modulated during button pressing. Baseline-corrected time frequency spectra of VIM power averaged over 17 hemispheres from nine patients in the hemisphere **(A)** ipsilateral and **(B)** contralateral to the button press (time point 0 s). Colours code absolute change in log10-transformed power compared to the mean baseline level (–3.0 – –2.0 s). Black contours mark significant changes (p < 0.05).

Movement related changes of VIM-cortex coherence

For the whole-brain VIM-cortex coherence analysis, we defined three time-frequency intervals of interest: -0.5-0.5 s/8-20 Hz, -0.5-0.5 s/ 65-85 Hz and 0.5-1.5 s/21-35 Hz. These intervals reflect the movement-related alpha/low-beta power suppression, the gamma power

increase locked to the button press and the high-beta power rebound, respectively, as observed for VIM power (**Fig. 2**). We assessed changes of VIM-cortex coherence in these intervals relative to baseline for the hemisphere contralateral to movement and for the hemisphere ipsilateral to movement.

Contralateral hemisphere

For the first time-frequency interval of interest (-0.5-0.5 s/8-20 Hz; movement-related alpha/low-beta suppression), we observed a decrease of VIM-cortex coherence in primary motor, premotor, and primary somatosensory cortex contralateral to movement (cluster-based-permutation test; $t_{clustersum} = -160$, $p = 0.002$; MNI-coordinates minimal t-value: X = +/–54.4 mm, Y = –40 mm, Z = 51.1 mm), which was strongest in superior frontal gyrus. For the second time-frequency interval of interest (0.5-1.5 s/21-35 Hz; high-beta rebound), we found an increase of coherence with precentral gyrus ($t = 46.2$, $p = 0.003$; X = +/–39.7 mm, Y = 0 mm, Z = 59.4 mm). This coherence rebound was mostly contained within the region presenting the movement-related suppression earlier in the trial (**Fig. 3**). Peri-movement VIM-cortex coherence changes in the gamma-band (-0.5-0.5 s/ 65-85 Hz) mapped to similar areas (**Supplementary Fig. 1**) but were not significant ($t = 15.4$, $p = 0.09$; X = 39.7 mm, Y = 0 mm, Z = 59.4 mm).

Ipsilateral hemisphere

For the VIM ipsilateral to movement, we observed a movement-related alpha/low-beta suppression, which mapped to the supramarginal gyrus ipsilateral to button press ($t = -38.8$, $p = 0.012$; X = –/+56.4 mm, Y = –30 mm, Z = 46.4 mm; **Fig. 3**), but no significant rebound.

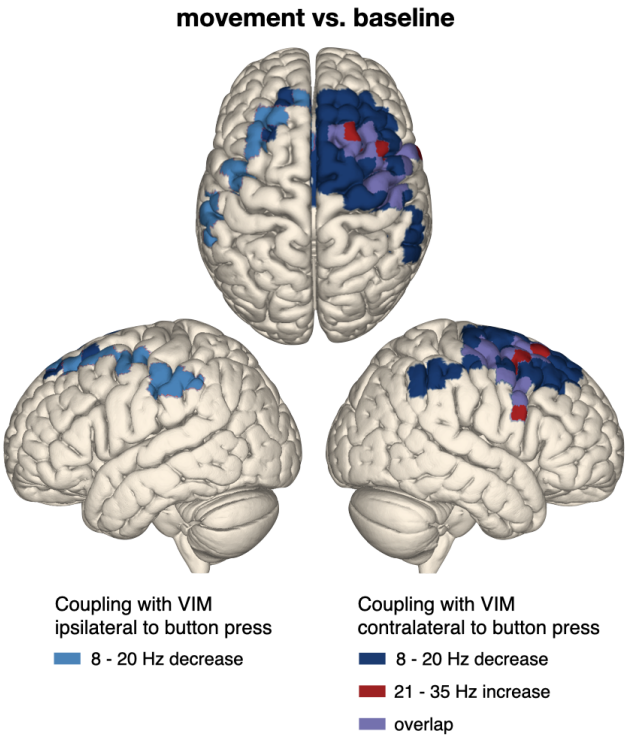

Figure 3: Thalamo-cortical coupling is modulated during button pressing. Coupling between cortex and VIM contralateral (dark blue) and ipsilateral (light blue) to button press decreased in the 8-20 Hz range during the button press, after which beta coherence rebounded in the 21-35 Hz range (red). The overlap between movement-related beta suppression and post-movement beta rebound is marked in purple. Non-significant changes are masked. Left hemisphere: ipsilateral to button press, right hemisphere: contralateral to button press. Note that the colours code significant effects rather than effect size.

Dynamics of thalamo-cortical coupling

To investigate the dynamics of thalamo-cortical coupling during button pressing, we computed a time-frequency spectrum of coherence between the VIM and the region with the strongest changes in the whole-brain analysis (bilateral motor and pre-motor cortex; see **Fig. 3**). Because the former analysis had already revealed significant deviations from baseline, we did not re-assess significance here.

The dynamics of coherence resembled those of VIM power (**Fig. 2**), with a peri-movement alpha/low-beta suppression in both the contra- and the ipsilateral hemisphere (with respect to movement). The post-movement beta rebound in the high-beta range was stronger in the hemisphere contralateral to movement (**Fig. 4**).

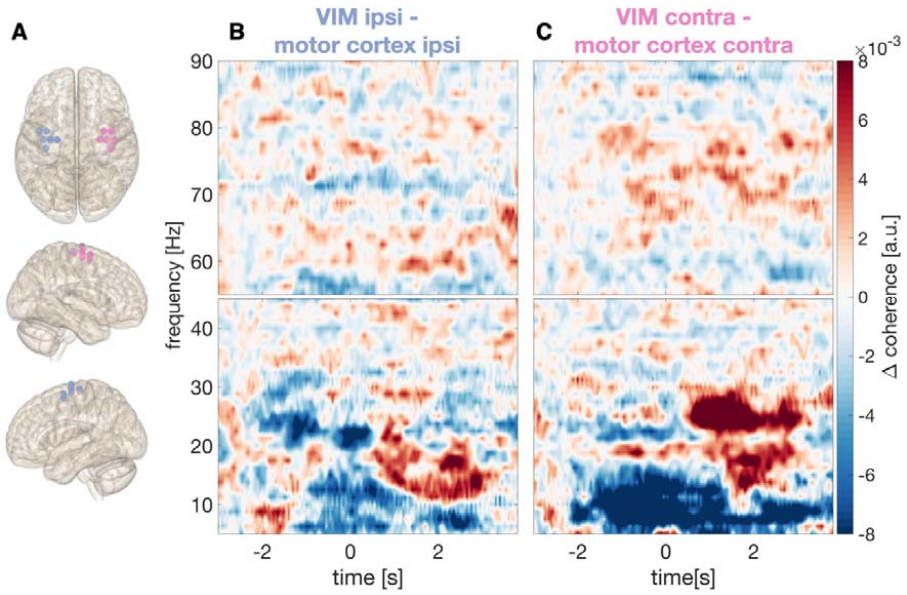

Figure 4: Time-resolved dynamics of thalamo-cortex coherence during button pressing. **(A)** Grid points (beamformer target locations) defining the regions of interest. Coherence was computed for each grid point and averaged within the region of interest. Left hemisphere: ipsilateral to button press, right hemisphere: contralateral to button press. (**B**-**C**) Baseline-corrected time frequency spectra of coherence between VIM and motor cortex **(B)** ipsilateral and **(C)** contralateral to button press (time point 0 s).

Dynamics of motor cortical power

We selected the same regions of interest as for coherence and computed time-resolved power spectra for the motor cortex ipsi- and contralateral to movement (**Fig. 5**). A strong power suppression ranging from 5–35 Hz was visible in both hemispheres (ipsilateral motor cortex: cluster-based-permutation-test, $t_{clustersum}$ = -7.9*10^3, $p < 0.001$; contralateral motor cortex: t = –1.1*10^4, $p < 0.001$). We did neither observe a strong beta rebound, nor a gamma increase in motor cortex. To examine whether beta power was rebounding in motor cortex, we aligned the time-resolved power spectra to the time point when the button was released

(**Supplementary Figure 2**). This analysis demonstrated a weak rebound in the alpha/beta range in the hemisphere contralateral to movement.

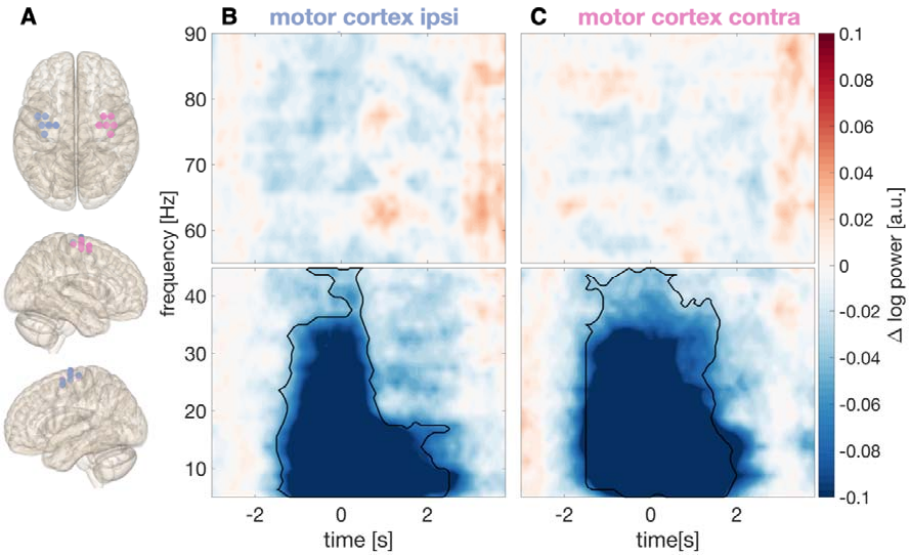

Figure 5: Time-resolved dynamics of cortical power during button pressing. (A) Grid points (beamformer target locations) defining the regions of interest. Left hemisphere: ipsilateral to button press, right hemisphere: contralateral to button press. (**B**-**C**) Baseline-corrected time frequency spectra of cortical power **(B)** ipsilateral and **(C)** contralateral to the button press (time point 0 s).

Pre-movement VIM-cortex coherence and reaction time

Based on studies of Parkinson's disease, beta band synchronisation has been labelled "antikinetic", i.e. inversely related to movement speed. Here, we tested the validity of this label in ET patients by correlating pre-movement levels of VIM-motor cortex beta coherence (8–20 Hz, 21–35 Hz; - 0.5–0.5 s around Go cue) to reaction time (time of button press - time of Go cue presentation).

Pre-movement levels of 8–20 Hz coupling between VIM and motor cortex contralateral to movement was positively correlated with reaction time (r = 0.53, p = 0.038; **Fig. 6B**). The correlation was not significant for the high-beta band (r = -0.06, p = 0.82). Coupling between VIM and motor cortex ipsilateral to button press was not significantly correlated with reaction

time, neither in the alpha/low-beta (8–20 Hz: r = 0.09, p = 0.74) nor in the high-beta band (**Fig. 6B;** 21–35 Hz: r = -0.45, p = 0.09).

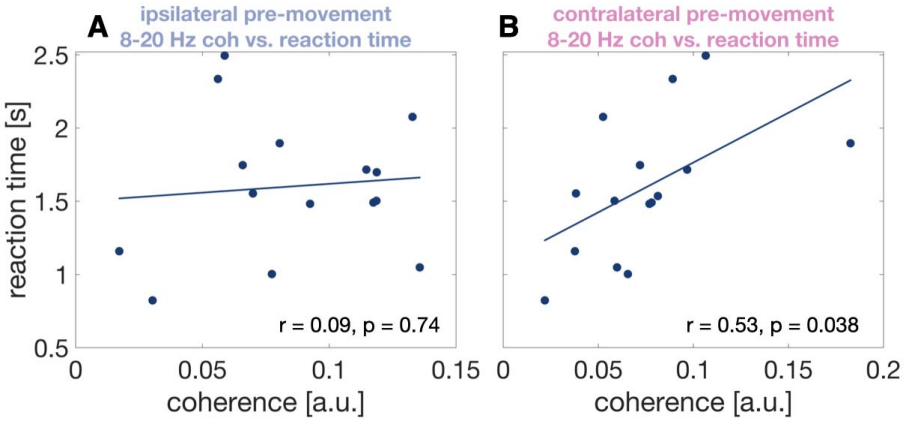

Figure 6: Correlation between coherence and reaction time. Scatterplot illustrating the relationship between pre-movement alpha/low-beta coherence and reaction time for coupling between ipsilateral VIM and ipsilateral motor cortex **(A)** and contralateral VIM and contralateral motor cortex **(B)**.

Discussion

In the present study, we revealed the brain areas and frequency bands involved in thalamo-cortical coupling during voluntary movements. We found that voluntary movement is associated with peri-movement modulation of beta band coherence, involving mostly supplementary motor area and premotor cortex. Pre-movement alpha/low-beta coherence between motor cortex and VIM contralateral to movement correlated with reaction time, suggesting that beta band synchronization is generally associated with slowness, even in the absence of akinesia.

Our study is one of few works relating thalamo-cortical coupling to voluntary movement. Most studies have investigated tremor, which has a different coupling profile, involving other frequency bands and other brain areas.[24–26] In fact, we have recently described tremor-related coherence profiles of half the patients analyzed in this work.[15] Strongest tremor-associated modulations of VIM-cortex coherence were observed in primary sensorimotor cortex rather than pre-motor areas, suggesting that different channels of thalamo-cortical communication might be active during tremor and voluntary movements. A further difference might be the modulation of VIM-cerebellar coupling, which was pronounced for tremor but non-significant for button pressing. However, voluntary movement and tremor seem to share some common frequency-specific modulations. Voluntary movement is linked to a suppression in the beta-band, for example, and tremor amplitude is also inversely related to beta-band VIM-motor cortex coupling.[15]

Overall, our results underscore how closely neuronal oscillations in the motor system are linked to the movement present at the time of recording – a link which should be kept in mind when attributing oscillatory patterns to any specific disease.

VIM power

Here, we reproduced previous findings on modulations of thalamic activity during voluntary movements.[5,7] Before and while the button was pressed, alpha (8-12 Hz) and low-beta (13-20 Hz) activity were desynchronized, while gamma activity was synchronized. Shortly after the button press, high-beta (21-35 Hz) oscillations increased to a higher level than baseline (rebound). This pattern has been replicated in numerous motor structures, such as motor cortex[27] or the STN,[9] and numerous cohorts, including patients with Parkinson's disease,[9]

dystonia,[11] and healthy controls.[8] Matching such a ubiquitous motive, we suggest that the spectral modulations of VIM activity observed here are of physiological rather than of pathophysiological nature.

The apparent divergence between the dynamics of low- and high-beta activity matches findings in Parkinson's disease indicating distinct roles of low- and high-beta activity.[28,29] Whether alpha oscillations change independently of low-beta oscillations or result from spectral leakage from the beta band is under debate.[30,31] Whereas Klostermann et al. suggested a distinction between alpha and beta (13-35 Hz) activity,[7] we found no evidence for independence between thalamic alpha and low-beta oscillations and treated both bands as a single entity.

Motor cortical power

Motor cortical power largely resembled VIM power, but, in contrast to the VIM, motor cortex did not reveal a strong beta rebound in this paradigm. However, a weak rebound was visible in the hemisphere contralateral to movement when the spectral modulations were related to the time when the button was released (**Supplementary Fig. 2**). This finding suggests a differential response of the thalamus and motor cortex to single elements of the motor sequence.

VIM-cortex coupling

VIM-cortex coupling followed a similar pattern as VIM power: alpha-/low-beta coherence decreased prior to and throughout the button press, and high-beta coherence increased after the button press. The decrease of alpha-/low-beta coherence has been reported before for externally paced[7,32] and self-paced movements.[6] We extend previous findings by localizing the coherence decrease to premotor cortex and the supplementary motor area. This localization is different from the spatial minimum of the cortical beta power suppression, which is typically observed in sensorimotor cortex proper, around the hand knob.[8]

Compared to baseline, high-beta coupling between cortex and the VIM contralateral to movement increased shortly after the button press. This effect was strongest in similar regions as the preceding 8–20 Hz decrease, but more focal. The coherence increase might be analogous to the post-movement rebound of beta power that is typically observed in

sensorimotor cortex.[8] This rebound is usually lateralized to the contralateral hemisphere,[8] while the beta power suppression has been reported to be bilaterally symmetric.[33,34] This pattern is in line with our results, as coherence decreased bilaterally during movement, whereas the post-movement coherence increase was lateralized to the contralateral hemisphere.

VIM-cortex coupling and reaction time

Pre-movement levels of 8-20 Hz VIM-motor cortex coherence in the contralateral hemisphere correlated positively with reaction time, i.e. higher coupling around Go cue onset were associated with slower responses. These findings tally with the proposed antikinetic nature of low-beta oscillations, derived mainly from studies on Parkinson's disease. These studies have established a relationship between elevated beta power in the STN and the severity of bradykinesia and rigidity.[35,36] Moreover, movements of healthy individuals have been demonstrated to be slower when low-beta activity happens to be elevated in the course of spontaneous fluctuations or is elevated artificially by transcranial alternating current stimulation.[37,38] Further, in patients with Parkinson's disease deep brain stimulation in the beta range has shown to slow movements.[39] The antikinetic nature of low-beta oscillations is not only reflected by local oscillatory power, but extends to coupling between different regions, as observed for GPi-cortex[11] and cortico-spinal coherence,[40] for example. Here, we demonstrate that the concept holds for VIM-cortex coupling, too.

Interestingly, other pre-movement features of thalamic activity have likewise been linked to reaction time. The amplitude of the contingent negative variation in between a pre- and a Go-cue was predictive of reaction time in a cued Go/NoGo task.[41] Moreover, increased levels of thalamic gamma activity have been revealed to result in faster task performance.[5] These observations align well with the modern view on the role of the thalamus in motor control. For a long time, the motor thalamus was believed to simply relay inputs from cerebellum to motor cortex. However, in the last decades, it became evident that information to cortex is not just passively relayed, but modified by the thalamus.[3] Our study further supports this notion.

Limitations

Intracranial recordings from the human thalamus are only possible in patients. Therefore, we cannot be sure whether the oscillatory dynamics described here indeed relate to normal motor

control. Yet, several of our findings match observations made in other patient populations and in healthy participants, who, at the cortical level, exhibit the same beta and gamma power dynamics at movement start and stop.[42]

Although the patient cohort consisted of individuals with ET, tremor was only present in 6 out of 17 analyzed body sides during button pressing most likely due to the stun effect (see **Supplementary Table 1**). Thus, we could not compute a meaningful statistical contrast between button pressing with intention tremor to button pressing without intention tremor, which would have been an interesting addition to our recent work on essential tremor .[15]

Conclusions

Our study demonstrates behaviourally relevant modulations of thalamo-cortical coupling during voluntary movement. Further it extends the notion of beta oscillations being "antikinetic" to thalamo-cortical coupling.

Data availability

Data can be made available in anonymized form upon reasonable request, conditional on patient consent.

Funding

ASc and JH are supported by Brunhilde Moll Stiftung. ASc also acknowledges support by the Deutsche Forschungsgemeinschaft (DFG, German Research Foundation) - Project ID 4247788381 - TRR 295.

Competing interests

The authors report no competing interests.

References

1. Neudorfer C, Kultas-Ilinsky K, Ilinsky I, et al. The role of the motor thalamus in deep brain stimulation for essential tremor. *Neurotherapeutics*. 2024;21(3):e00313. doi:10.1016/j.neurot.2023.e00313

2. Hua SE, Lenz FA. Posture-Related Oscillations in Human Cerebellar Thalamus in Essential Tremor Are Enabled by Voluntary Motor Circuits. *Journal of Neurophysiology*. 2005;93(1):117-127. doi:10.1152/jn.00527.2004

3. Sommer MA. The role of the thalamus in motor control. *Current Opinion in Neurobiology*. 2003;13(6):663-670. doi:10.1016/j.conb.2003.10.014

4. Bosch-Bouju C, Hyland BI, Parr-Brownlie LC. Motor thalamus integration of cortical, cerebellar and basal ganglia information: implications for normal and parkinsonian conditions. *Front Comput Neurosci*. 2013;7. doi:10.3389/fncom.2013.00163

5. Brücke C, Bock A, Huebl J, et al. Thalamic gamma oscillations correlate with reaction time in a Go/noGo task in patients with essential tremor. *NeuroImage*. 2013;75:36-45. doi:10.1016/j.neuroimage.2013.02.038

6. Paradiso G. Involvement of human thalamus in the preparation of self-paced movement. *Brain*. 2004;127(12):2717-2731. doi:10.1093/brain/awh288

7. Klostermann F, Nikulin VV, Kühn AA, et al. Task-related differential dynamics of EEG alpha- and beta-band synchronization in cortico-basal motor structures: EEG oscillations in motor structures. *European Journal of Neuroscience*. 2007;25(5):1604-1615. doi:10.1111/j.1460-9568.2007.05417.x

8. Jurkiewicz MT, Gaetz WC, Bostan AC, Cheyne D. Post-movement beta rebound is generated in motor cortex: Evidence from neuromagnetic recordings. *NeuroImage*. 2006;32(3):1281-1289. doi:10.1016/j.neuroimage.2006.06.005

9. Litvak V, Eusebio A, Jha A, et al. Movement-Related Changes in Local and Long-Range Synchronization in Parkinson's Disease Revealed by Simultaneous Magnetoencephalography and Intracranial Recordings. *J Neurosci*. 2012;32(31):10541-10553. doi:10.1523/JNEUROSCI.0767-12.2012

10. Engel AK, Fries P. Beta-band oscillations — signalling the status quo? *Current Opinion in Neurobiology*. 2010;20(2):156-165. doi:10.1016/j.conb.2010.02.015

11. van Wijk BCM, Neumann WJ, Schneider GH, Sander TH, Litvak V, Kühn AA. Low-beta cortico-pallidal coherence decreases during movement and correlates with overall reaction time. *NeuroImage*. 2017;159:1-8. doi:10.1016/j.neuroimage.2017.07.024

12. Brown P. Oscillatory nature of human basal ganglia activity: Relationship to the pathophysiology of Parkinson's disease. *Movement Disorders*. 2003;18(4):357-363. doi:10.1002/mds.10358

13. Alegre M, Rodríguez-Oroz MC, Valencia M, et al. Changes in subthalamic activity during movement observation in Parkinson's disease: Is the mirror system mirrored in the basal ganglia? *Clinical Neurophysiology*. 2010;121(3):414-425. doi:10.1016/j.clinph.2009.11.013

14. Steina A, Sure S, Butz M, Vesper J, Schnitzler A, Hirschmann J. Mapping Subcortico-Cortical Coupling—A Comparison of Thalamic and Subthalamic Oscillations. *Movement Disorders*. 2024;39(4):684-693. doi:10.1002/mds.29730

15. Steina A, Sure S, Butz M, Vesper J, Schnitzler A, Hirschmann J. Oscillatory coupling between thalamus, cerebellum and motor cortex in essential tremor. Published online November 11, 2024:2024.11.11.622917. doi:10.1101/2024.11.11.622917

16. Oostenveld R, Fries P, Maris E, Schoffelen JM. FieldTrip: open source software for advanced analysis of MEG, EEG, and invasive electrophysiological data. *Computational intelligence and neuroscience*. 2011;2011:1-9.

17. Gramfort A. MEG and EEG data analysis with MNE-Python. *Front Neurosci*. 2013;7. doi:10.3389/fnins.2013.00267

18. Van Veen BD, Van Drongelen W, Yuchtman M, Suzuki A. Localization of brain electrical activity via linearly constrained minimum variance spatial filtering. *IEEE Transactions on biomedical engineering*. 1997;44(9):867-880.

19. Horn A, Li N, Dembek TA, et al. Lead-DBS v2: Towards a comprehensive pipeline for deep brain stimulation imaging. *NeuroImage*. 2019;184:293-316. doi:10.1016/j.neuroimage.2018.08.068

20. Thomson DJ. Spectrum estimation and harmonic analysis. *Proceedings of the IEEE*. 1982;70(9):1055-1096. doi:10.1109/PROC.1982.12433

21. Oswal A, Cao C, Yeh CH, et al. Neural signatures of hyperdirect pathway activity in Parkinson's disease. *Nat Commun*. 2021;12(1):5185. doi:10.1038/s41467-021-25366-0

22. Hirschmann J, Özkurt TE, Butz M, et al. Distinct oscillatory STN-cortical loops revealed by simultaneous MEG and local field potential recordings in patients with Parkinson's disease. *NeuroImage*. 2011;55(3):1159-1168. doi:10.1016/j.neuroimage.2010.11.063

23. Maris E, Oostenveld R. Nonparametric statistical testing of EEG- and MEG-data. *Journal of Neuroscience Methods*. 2007;164(1):177-190. doi:10.1016/j.jneumeth.2007.03.024

24. Schnitzler A, Münks C, Butz M, Timmermann L, Gross J. Synchronized brain network associated with essential tremor as revealed by magnetoencephalography. *Mov Disord*. 2009;24(11):1629-1635. doi:10.1002/mds.22633

25. He F, Sarrigiannis PG, Billings SA, et al. Nonlinear interactions in the thalamocortical loop in essential tremor: A model-based frequency domain analysis. *Neuroscience*. 2016;324:377-389. doi:10.1016/j.neuroscience.2016.03.028

26. Marsden JF. Coherence between cerebellar thalamus, cortex and muscle in man: Cerebellar thalamus interactions. *Brain*. 2000;123(7):1459-1470. doi:10.1093/brain/123.7.1459

27. Salmelin R, Hámáaláinen M, Kajola M, Hari R. Functional Segregation of Movement-Related Rhythmic Activity in the Human Brain. *NeuroImage*. 1995;2(4):237-243. doi:10.1006/nimg.1995.1031

28. van Wijk BC, Beudel M, Jha A, et al. Subthalamic nucleus phase–amplitude coupling correlates with motor impairment in Parkinson's disease. *Clinical Neurophysiology*. 2016;127(4):2010-2019.

29. Cao C, Litvak V, Zhan S, et al. Low-beta versus high-beta band cortico-subcortical coherence in movement inhibition and expectation. *Neurobiology of Disease*. 2024;201:106689. doi:10.1016/j.nbd.2024.106689

30. Brown P, Williams D. Basal ganglia local field potential activity: Character and functional significance in the human. *Clinical Neurophysiology*. 2005;116(11):2510-2519.

doi:10.1016/j.clinph.2005.05.009

31. Khawaldeh S, Tinkhauser G, Shah SA, et al. Subthalamic nucleus activity dynamics and limb movement prediction in Parkinson's disease. *Brain*. 2020;143(2):582-596. doi:10.1093/brain/awz417

32. Opri E, Cernera S, Okun MS, Foote KD, Gunduz A. The Functional Role of Thalamocortical Coupling in the Human Motor Network. *J Neurosci*. 2019;39(41):8124-8134. doi:10.1523/JNEUROSCI.1153-19.2019

33. Pfurtscheller G, Berghold A. Patterns of cortical activation during planning of voluntary movement. *Electroencephalography and Clinical Neurophysiology*. 1989;72(3):250-258. doi:10.1016/0013-4694(89)90250-2

34. Winkler L, Butz M, Sharma A, et al. Beta Waves in Action: Context-Dependent Modulations of Subthalamo-Cortical Synchronization during Rapid Reversals of Movement Direction. *eLife*. 2024;13. doi:10.7554/eLife.101769.1

35. Kühn AA, Kupsch A, Schneider GH, Brown P. Reduction in subthalamic 8–35 Hz oscillatory activity correlates with clinical improvement in Parkinson's disease. *European Journal of Neuroscience*. 2006;23(7):1956-1960.

36. Neumann WJ, Degen K, Schneider GH, et al. Subthalamic synchronized oscillatory activity correlates with motor impairment in patients with Parkinson's disease. *Movement Disorders*. 2016;31(11):1748-1751.

37. Gilbertson T, Lalo E, Doyle L, Lazzaro VD, Cioni B, Brown P. Existing Motor State Is Favored at the Expense of New Movement during 13-35 Hz Oscillatory Synchrony in the Human Corticospinal System. *J Neurosci*. 2005;25(34):7771-7779. doi:10.1523/JNEUROSCI.1762-05.2005

38. Pogosyan A, Gaynor LD, Eusebio A, Brown P. Boosting Cortical Activity at Beta-Band Frequencies Slows Movement in Humans. *Current Biology*. 2009;19(19):1637-1641. doi:10.1016/j.cub.2009.07.074

39. Werner LM, Schnitzler A, Hirschmann J. Subthalamic nucleus deep brain stimulation in the beta frequency range boosts cortical beta oscillations and slows down movement. *J Neurosci*. Published online January 7, 2025. doi:10.1523/JNEUROSCI.1366-24.2024

40. van Wijk BCM, Daffertshofer A, Roach N, Praamstra P. A Role of Beta Oscillatory Synchrony in Biasing Response Competition? *Cerebral Cortex*. 2009;19(6):1294-1302. doi:10.1093/cercor/bhn174

41. Nikulin VV, Marzinzik F, Wahl M, et al. Anticipatory activity in the human thalamus is predictive of reaction times. *Neuroscience*. 2008;155(4):1275-1283. doi:10.1016/j.neuroscience.2008.07.005

42. Alegre M, Gurtubay IG, Labarga A, Iriarte J, Valencia M, Artieda J. Frontal and central oscillatory changes related to different aspects of the motor process: a study in go/no-go paradigms. *Exp Brain Res*. 2004;159(1):14-22. doi:10.1007/s00221-004-1928-8

Table 1 Patient details

Patient ID	age [y]	sex	disease duration [y]	electrode type
ET01	65	m	19	Abbott Infinity
ET02	71	m	20	Abbott Infinity
ET03	60	f	49	Abbott Infinity
ET04	62	m	50	Abbott Infinity
ET05	57	f	51	Abbott Infinity
ET06	76	m	n.a.	Abbott Infinity
ET07	54	m	39	Medtronic SenSight
ET08	62	f	56	Abbott Infinity
ET09	65	m	20	Boston Sc. Vercice Cartesia
ET10	71	m	20	Boston Sc. Vercice Cartesia
$\mu \pm \sigma$	65 ± 11		31 ± 20	

y: year, m: male, f: female, n.a.: not available, μ: mean, σ: standard deviation.

Modulations of thalamo-cortex coupling during voluntary movement in patients with essential tremor

Supplementary material

Alexandra Steina[1], Sarah Sure[1], Markus Butz[1],
Jan Vesper[2], Alfons Schnitzler[1], Jan Hirschmann[1]

Author affiliations:

1 Institute of Clinical Neuroscience and Medical Psychology, Medical Faculty, Heinrich Heine University, 40225, Düsseldorf, Germany

2 Department of Functional Neurosurgery and Stereotaxy, Neurosurgical Clinic, Medical Faculty, Heinrich Heine University, 40225, Düsseldorf, Germany

Supplementary Table 1 Task information

L: left, R: Right, n.p.: not present, -.: not available, y: yes.
[a]Data length, tremor.
[b]Amount of trials after cleaning.
[c]Right VIM excluded due to uncertain electrode position.
[d]Button press from ET09 was excluded from further analysis due to bad LFP data quality.

Patient ID	Button press L / R tremor	Button press L / R trials[b]
ET01	n.p.	53 / 45
ET02	y / y	83 / 85
ET03	n.p.	89 / 87
ET04	n.p. / n.p.	76 / 76
ET05	y / n.p.	44 / 37
ET06[c]	y / n.p.	54 / 54
ET07	n.p.	63 / 59
ET08	y / y	54 / 49
ET09[d]	y / y	-
ET10	n.p. / y	51 / 63

Movement related changes of VIM-cortex coherence

VIM-cortex coherence in the gamma range increased during movement. This increase was strongest in the pre-central gyrus, but the increase was not significant ($t_{clustersum}$ = 15.4, p = 0.09; X = 39.7 mm, Y = 0 mm, Z = 59.4 mm; **Supplementary Fig. 1**).

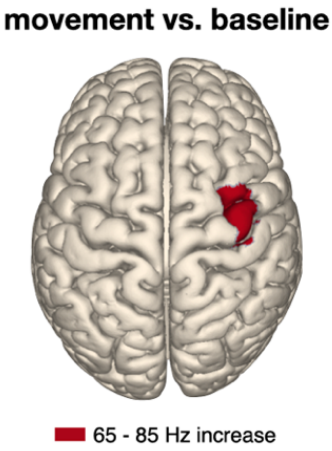

Supplementary Fig. 1: Change of thalamo-cortical coupling in the gamma range during button pressing. Coupling between cortex and the VIM contralateral to movement in the 65-85 Hz range increased during button pressing. Strongest changes are displayed ($t_{clustersum}$ = 15.4, p = 0.09; non-significant).

Dynamics of motor cortical power

We aligned time-resolved power in motor cortex to the time point when the button was released (t = 0) to investigate if beta power was rebounding in motor cortex. On a descriptive level, this analysis suggests a weak rebound in the alpha/beta range in the hemisphere contralateral to movement (**Supplementary Figure 2**). The weakness of the rebound might be due to the fact that the hand was still in motion after the button press, as patients returned their hand to the table in front of them. Note, however, the VIM and VIM-cortex coupling showed a marked rebound even in this situation.

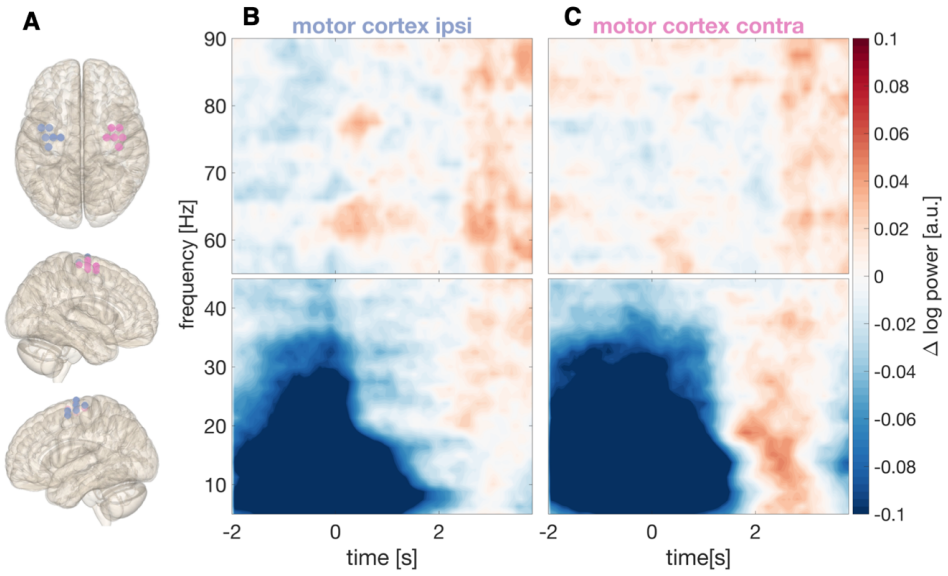

Supplementary Fig. 2: Time-resolved dynamics of cortical power during button pressing aligned to end of button press. (A) Grid points used for extracting cortical activity. Left hemisphere: ipsilateral to button press, right hemisphere: contralateral to button press. (**B-C**) Baseline-corrected (-3 to -2 s before onset of button press) time frequency spectra of cortical power **(B)** ipsilateral and **(C)** contralateral to the button press (time point 0 s marks the time when the button was released).

References

[1] LeMoyne, R., Mastroianni, T., Whiting, D. & Tomycz, N. Movement disorders: Parkinson's disease and essential tremor—a general perspective. In *Wearable and Wireless Systems for Healthcare II: Movement Disorder Evaluation and Deep Brain Stimulation Systems*, 17–24 (Springer, 2024).

[2] Louis, E. D. The roles of age and aging in essential tremor: an epidemiological perspective. *Neuroepidemiology* **52**, 111–118 (2019).

[3] Reeve, A., Simcox, E. & Turnbull, D. Ageing and parkinson's disease: why is advancing age the biggest risk factor? *Ageing research reviews* **14**, 19–30 (2014).

[4] Shorvon, S. Neurology worldwide: The epidemiology and burden of neurological disease. *Neurology: A Queen Square Textbook* 1–10 (2016).

[5] Bradley, C., Garrison, N., Washington, A. & Wood, B. Essential tremor: A focused literature review on its pathophysiology, neurophysiology, etiology, and management (2024).

[6] Bicknell, B., Liebert, A. & Herkes, G. Parkinson's disease and photobiomodulation: Potential for treatment. *Journal of Personalized Medicine* **14**, 112 (2024).

[7] Wong, J. K. *et al.* Deep brain stimulation in essential tremor: targets, technology, and a comprehensive review of clinical outcomes. *Expert review of neurotherapeutics* **20**, 319–331 (2020).

[8] Deuschl, G. *et al.* A randomized trial of deep-brain stimulation for parkinson's disease. *New England Journal of Medicine* **355**, 896–908 (2006).

[9] Soto, M. C. S. & Fasano, A. Essential tremor: new advances. *Clinical Parkinsonism & Related Disorders* **3**, 100031 (2020).

[10] van Wijk, B. C., de Bie, R. M. & Beudel, M. A systematic review of local field potential physiomarkers in parkinson's disease: from clinical correlations to adaptive deep brain stimulation algorithms. *Journal of neurology* **270**, 1162–1177 (2023).

[11] Buzsáki, G., Logothetis, N. & Singer, W. Scaling brain size, keeping timing: evolutionary preservation of brain rhythms. *Neuron* **80**, 751–764 (2013).

[12] Buzsaki, G. *Rhythms of the Brain* (Oxford university press, 2006).

[13] Nimmrich, V., Draguhn, A. & Axmacher, N. Neuronal network oscillations in neurodegenerative diseases. *Neuromolecular medicine* **17**, 270–284 (2015).

[14] Fries, P. A mechanism for cognitive dynamics: neuronal communication through neuronal coherence. *Trends in cognitive sciences* **9**, 474–480 (2005).

[15] Fries, P. Rhythms for cognition: communication through coherence. *Neuron* **88**, 220–235 (2015).

[16] Schnitzler, A. & Gross, J. Normal and pathological oscillatory communication in the brain. *Nature reviews neuroscience* **6**, 285–296 (2005).

[17] Sultana, O. F., Bandaru, M., Islam, M. A. & Reddy, P. H. Unraveling the complexity of human brain: Structure, function in healthy and disease states. *Ageing Research Reviews* **100**, 102414 (2024).

[18] Carrillo-Reid, L. & Yuste, R. Playing the piano with the cortex: role of neuronal ensembles and pattern completion in perception and behavior. *Current opinion in neurobiology* **64**, 89–95 (2020).

[19] Luo, L. Architectures of neuronal circuits. *Science* **373**, eabg7285 (2021).

[20] Von Bartheld, C. S., Bahney, J. & Herculano-Houzel, S. The search for true numbers of neurons and glial cells in the human brain: A review of 150 years of cell counting. *Journal of Comparative Neurology* **524**, 3865–3895 (2016).

[21] Hansen, P., Kringelbach, M. & Salmelin, R. *MEG: An introduction to methods* (Oxford university press, 2010).

[22] Thio, B. J. & Grill, W. M. Relative contributions of different neural sources to the eeg. *Neuroimage* **275**, 120179 (2023).

[23] Buzsáki, G., Anastassiou, C. A. & Koch, C. The origin of extracellular fields and currents—eeg, ecog, lfp and spikes. *Nature reviews neuroscience* **13**, 407–420 (2012).

[24] Kucewicz, M. T., Cimbalnik, J., Garcia-Salinas, J. S., Brazdil, M. & Worrell, G. A. High frequency oscillations in human memory and cognition: a neurophysiological substrate of engrams? *Brain* **147**, 2966–2982 (2024).

[25] Einevoll, G. T., Kayser, C., Logothetis, N. K. & Panzeri, S. Modelling and analysis of local field potentials for studying the function of cortical circuits. *Nature Reviews Neuroscience* **14**, 770–785 (2013).

[26] Næss, S. *et al.* Biophysically detailed forward modeling of the neural origin of eeg and meg signals. *NeuroImage* **225**, 117467 (2021).

[27] Hämäläinen, M., Hari, R., Ilmoniemi, R. J., Knuutila, J. & Lounasmaa, O. V. Magnetoencephalography—theory, instrumentation, and applications to noninvasive studies of the working human brain. *Reviews of modern Physics* **65**, 413 (1993).

[28] Baillet, S., Mosher, J. C. & Leahy, R. M. Electromagnetic brain mapping. *IEEE Signal processing magazine* **18**, 14–30 (2001).

[29] Shibasaki, H. Human brain mapping: hemodynamic response and electrophysiology. *Clinical Neurophysiology* **119**, 731–743 (2008).

[30] Neymotin, S. A. *et al.* Human neocortical neurosolver (hnn), a new software tool for interpreting the cellular and network origin of human meg/eeg data. *Elife* **9**, e51214 (2020).

[31] da Silva, F. L. Eeg and meg: relevance to neuroscience. *Neuron* **80**, 1112–1128 (2013).

[32] Pu, Y., Cheyne, D. O., Cornwell, B. R. & Johnson, B. W. Non-invasive investigation of human hippocampal rhythms using magnetoencephalography: a review. *Frontiers in neuroscience* **12**, 273 (2018).

[33] Andersen, L. M., Jerbi, K. & Dalal, S. S. Can eeg and meg detect signals from the human cerebellum? *NeuroImage* **215**, 116817 (2020).

[34] Roux, F., Wibral, M., Singer, W., Aru, J. & Uhlhaas, P. J. The phase of thalamic alpha activity modulates cortical gamma-band activity: evidence from resting-state meg recordings. *Journal of Neuroscience* **33**, 17827–17835 (2013).

[35] Parkkonen, L., Fujiki, N. & Mäkelä, J. P. Sources of auditory brainstem responses revisited: contribution by magnetoencephalography. *Human brain mapping* **30**, 1772–1782 (2009).

[36] Demosthenous, A. Advances in microelectronics for implantable medical devices. *Advances in Electronics* **2014**, 981295 (2014).

[37] Fagaly, R. Superconducting quantum interference device instruments and applications. *Review of scientific instruments* **77** (2006).

[38] Buckel, W. & Kleiner, R. *Superconductivity: fundamentals and applications* (John Wiley & Sons, 2008).

[39] Taulu, S., Simola, J. & Kajola, M. Applications of the signal space separation method. *IEEE transactions on signal processing* **53**, 3359–3372 (2005).

[40] Taulu, S. & Hari, R. Removal of magnetoencephalographic artifacts with temporal signal-space separation: Demonstration with single-trial auditory-evoked responses. *Human brain mapping* **30**, 1524–1534 (2009).

[41] Abbasi, O., Hirschmann, J., Schmitz, G., Schnitzler, A. & Butz, M. Rejecting deep brain stimulation artefacts from meg data using ica and mutual information. *Journal of neuroscience methods* **268**, 131–141 (2016).

[42] Nolte, G. The magnetic lead field theorem in the quasi-static approximation and its use for magnetoencephalography forward calculation in realistic volume conductors. *Physics in Medicine & Biology* **48**, 3637 (2003).

[43] Westner, B. U. *et al.* A unified view on beamformers for m/eeg source reconstruction. *NeuroImage* **246**, 118789 (2022).

[44] Hincapie, A.-S. *et al.* The impact of meg source reconstruction method on source-space connectivity estimation: A comparison between minimum-norm solution and beamforming. *Neuroimage* **156**, 29–42 (2017).

[45] Knösche, T. R. & Haueisen, J. *EEG/MEG Source Reconstruction* (Springer, 2022).

[46] Van Veen, B. D., Van Drongelen, W., Yuchtman, M. & Suzuki, A. Localization of brain electrical activity via linearly constrained minimum variance spatial filtering. *IEEE Transactions on biomedical engineering* **44**, 867–880 (1997).

[47] Gross, J. *et al.* Dynamic imaging of coherent sources: studying neural interactions in the human brain. *Proceedings of the National Academy of Sciences* **98**, 694–699 (2001).

[48] Marmor, O. *et al.* Local vs. volume conductance activity of field potentials in the human subthalamic nucleus. *Journal of neurophysiology* **117**, 2140–2151 (2017).

[49] Lindén, H. *et al.* Modeling the spatial reach of the lfp. *Neuron* **72**, 859–872 (2011).

[50] Tanaka, T. & Nakamura, K. C. Focal inputs are a potential origin of local field potential (lfp) in the brain regions without laminar structure. *PLoS One* **14**, e0226028 (2019).

[51] Brown, P. & Williams, D. Basal ganglia local field potential activity: character and functional significance in the human. *Clinical neurophysiology* **116**, 2510–2519 (2005).

[52] Kühn, A. A. *et al.* The relationship between local field potential and neuronal discharge in the subthalamic nucleus of patients with parkinson's disease. *Experimental neurology* **194**, 212–220 (2005).

[53] Scherer, M. *et al.* Single-neuron bursts encode pathological oscillations in subcortical nuclei of patients with parkinson's disease and essential tremor. *Proceedings of the National Academy of Sciences* **119**, e2205881119 (2022).

[54] Lobb, C. J. Abnormal bursting as a pathophysiological mechanism in parkinson's disease. *Basal ganglia* **3**, 187–195 (2014).

[55] Wennberg, R. A. & Lozano, A. M. Intracranial volume conduction of cortical spikes and sleep potentials recorded with deep brain stimulating electrodes. *Clinical Neurophysiology* **114**, 1403–1418 (2003).

[56] Cohen, M. *Analyzing neural time series data: theory and practice* (MIT press, 2014).

[57] Wang, J. *et al.* High-frequency oscillations in parkinson's disease: Spatial distribution and clinical relevance. *Movement disorders* **29**, 1265–1272 (2014).

[58] Salehi, N. *et al.* Theta frequency deep brain stimulation in the subthalamic nucleus improves working memory in parkinson's disease. *Brain* **147**, 1190–1196 (2024).

[59] Pogosyan, A., Gaynor, L. D., Eusebio, A. & Brown, P. Boosting cortical activity at beta-band frequencies slows movement in humans. *Current biology* **19**, 1637–1641 (2009).

[60] Guerra, A. *et al.* Driving motor cortex oscillations modulates bradykinesia in parkinson's disease. *Brain* **145**, 224–236 (2022).

[61] Jones, S. R. When brain rhythms aren't 'rhythmic': implication for their mechanisms and meaning. *Current opinion in neurobiology* **40**, 72–80 (2016).

[62] van Bree, S., Levenstein, D., Krause, M. R., Voytek, B. & Gao, R. Processes and measurements: a framework for understanding neural oscillations in field potentials. *Trends in Cognitive Sciences* (2025).

[63] Singmann, H., Kellen, D., Spieler, D. & Schumacher, E. New methods in cognitive psychology (2019).

[64] Llinás, R. R. The intrinsic electrophysiological properties of mammalian neurons: insights into central nervous system function. *Science* **242**, 1654–1664 (1988).

[65] Bean, B. P. Mechanisms of pacemaking in mammalian neurons. *The Journal of Physiology* (2024).

[66] Singer, W. Neuronal oscillations: unavoidable and useful? *European Journal of Neuroscience* **48**, 2389–2398 (2018).

[67] Jensen, O., Gips, B., Bergmann, T. O. & Bonnefond, M. Temporal coding organized by coupled alpha and gamma oscillations prioritize visual processing. *Trends in neurosciences* **37**, 357–369 (2014).

[68] Schaworonkow, N. & Voytek, B. Enhancing oscillations in intracranial electrophysiological recordings with data-driven spatial filters. *PLOS Computational Biology* **17**, e1009298 (2021).

[69] Cohen, M. X. Multivariate cross-frequency coupling via generalized eigendecomposition. *elife* **6**, e21792 (2017).

[70] Lowet, E., Roberts, M. J., Bonizzi, P., Karel, J. & De Weerd, P. Quantifying neural oscillatory synchronization: a comparison between spectral coherence and phase-locking value approaches. *PloS one* **11**, e0146443 (2016).

[71] Donoghue, T. *et al.* Parameterizing neural power spectra into periodic and aperiodic components. *Nature neuroscience* **23**, 1655–1665 (2020).

[72] Gao, R., Peterson, E. J. & Voytek, B. Inferring synaptic excitation/inhibition balance from field potentials. *Neuroimage* **158**, 70–78 (2017).

[73] Donoghue, T., Schaworonkow, N. & Voytek, B. Methodological considerations for studying neural oscillations. *European journal of neuroscience* **55**, 3502–3527 (2022).

[74] Cohen, M. X. A better way to define and describe morlet wavelets for time-frequency analysis. *NeuroImage* **199**, 81–86 (2019).

[75] Varela, F., Lachaux, J.-P., Rodriguez, E. & Martinerie, J. The brainweb: phase synchronization and large-scale integration. *Nature reviews neuroscience* **2**, 229–239 (2001).

[76] Stam, C. *et al.* The relation between structural and functional connectivity patterns in complex brain networks. *International Journal of Psychophysiology* **103**, 149–160 (2016).

[77] Palmigiano, A., Geisel, T., Wolf, F. & Battaglia, D. Flexible information routing by transient synchrony. *Nature neuroscience* **20**, 1014–1022 (2017).

[78] Schneider, M. *et al.* A mechanism for inter-areal coherence through communication based on connectivity and oscillatory power. *Neuron* **109**, 4050–4067 (2021).

[79] Vinck, M. *et al.* Principles of large-scale neural interactions. *Neuron* **111**, 987–1002 (2023).

[80] Jafari, Z., Kolb, B. E. & Mohajerani, M. H. Neural oscillations and brain stimulation in alzheimer's disease. *Progress in neurobiology* **194**, 101878 (2020).

[81] Riddle, J. & Frohlich, F. Targeting neural oscillations with transcranial alternating current stimulation. *Brain research* **1765**, 147491 (2021).

[82] Friston, K. J. Functional and effective connectivity: a review. *Brain connectivity* **1**, 13–36 (2011).

[83] Bastos, A. M. & Schoffelen, J.-M. A tutorial review of functional connectivity analysis methods and their interpretational pitfalls. *Frontiers in systems neuroscience* **9**, 175 (2016).

[84] McGregor, M. M. & Nelson, A. B. Circuit mechanisms of parkinson's disease. *Neuron* **101**, 1042–1056 (2019).

[85] Kalia, L. V. & Lang, A. E. Parkinson's disease. *The Lancet* **386**, 896–912 (2015).

[86] Moustafa, A. A. *et al.* Motor symptoms in parkinson's disease: A unified framework. *Neuroscience & Biobehavioral Reviews* **68**, 727–740 (2016).

[87] Poewe, W. Non-motor symptoms in parkinson's disease. *European journal of neurology* **15**, 14–20 (2008).

[88] Jankovic, J. & Tan, E. K. Parkinson's disease: etiopathogenesis and treatment. *Journal of Neurology, Neurosurgery & Psychiatry* **91**, 795–808 (2020).

[89] Vitek, J. L. Deep brain stimulation for parkinson's disease: a critical re-evaluation of stn versus gpi dbs. *Stereotactic and functional neurosurgery* **78**, 119–131 (2003).

[90] Haber, S. N. & Gdowski, M. J. The basal ganglia. *Scientific basis for the treatment of Parkinson's disease* 1–31 (2005).

[91] DeLong, M. & Wichmann, T. Update on models of basal ganglia function and dysfunction. *Parkinsonism & related disorders* **15**, S237–S240 (2009).

[92] Middleton, F. A. & Strick, P. L. Basal ganglia and cerebellar loops: motor and cognitive circuits. *Brain research reviews* **31**, 236–250 (2000).

[93] Ikemoto, S., Yang, C. & Tan, A. Basal ganglia circuit loops, dopamine and motivation: a review and enquiry. *Behavioural brain research* **290**, 17–31 (2015).

[94] Nambu, A., Tokuno, H. & Takada, M. Functional significance of the cortico–subthalamo–pallidal 'hyperdirect'pathway. *Neuroscience research* **43**, 111–117 (2002).

[95] Obeso, J. A., Rodríguez-Oroz, M. C., Rodríguez, M., Arbizu, J. & Giménez-Amaya, J. M. The basal ganglia and disorders of movement: pathophysiological mechanisms. *Physiology* **17**, 51–55 (2002).

[96] Kalia, L. V. *et al.* Clinical correlations with lewy body pathology in lrrk2-related parkinson disease. *JAMA neurology* **72**, 100–105 (2015).

[97] Nambu, A., Tachibana, Y. & Chiken, S. Cause of parkinsonian symptoms: firing rate, firing pattern or dynamic activity changes? *Basal ganglia* **5**, 1–6 (2015).

[98] Alvarez, L. *et al.* Bilateral subthalamotomy in parkinson's disease: initial and long-term response. *Brain* **128**, 570–583 (2005).

[99] Bergman, H., Wichmann, T. & DeLong, M. R. Reversal of experimental parkinsonism by lesions of the subthalamic nucleus. *Science* **249**, 1436–1438 (1990).

[100] Williams, D. Why so slow? models of parkinsonian bradykinesia. *Nature Reviews Neuroscience* **25**, 573–586 (2024).

[101] Tachibana, Y., Iwamuro, H., Kita, H., Takada, M. & Nambu, A. Subthalamo-pallidal interactions underlying parkinsonian neuronal oscillations in the primate basal ganglia. *European Journal of Neuroscience* **34**, 1470–1484 (2011).

[102] Mallet, N. *et al.* Parkinsonian beta oscillations in the external globus pallidus and their relationship with subthalamic nucleus activity. *Journal of neuroscience* **28**, 14245–14258 (2008).

[103] Engel, A. K. & Fries, P. Beta-band oscillations—signalling the status quo? *Current opinion in neurobiology* **20**, 156–165 (2010).

[104] Eusebio, A. *et al.* Effects of low-frequency stimulation of the subthalamic nucleus on movement in parkinson's disease. *Experimental neurology* **209**, 125–130 (2008).

[105] Chen, C. C. *et al.* Stimulation of the subthalamic region at 20 hz slows the development of grip force in parkinson's disease. *Experimental neurology* **231**, 91–96 (2011).

[106] Werner, L. M., Schnitzler, A. & Hirschmann, J. Subthalamic nucleus deep brain stimulation in the beta frequency range boosts cortical beta oscillations and slows down movement. *Journal of Neuroscience* (2025).

[107] Leblois, A. *et al.* Late emergence of synchronized oscillatory activity in the pallidum during progressive parkinsonism. *European Journal of Neuroscience* **26**, 1701–1713 (2007).

[108] Brazhnik, E. *et al.* Early decreases in cortical mid-gamma peaks coincide with the onset of motor deficits and precede exaggerated beta build-up in rat models for parkinson's disease. *Neurobiology of disease* **155**, 105393 (2021).

[109] Neumann, W.-J., Steiner, L. A. & Milosevic, L. Neurophysiological mechanisms of deep brain stimulation across spatiotemporal resolutions. *Brain* **146**, 4456–4468 (2023).

[110] Song, P. *et al.* The global prevalence of essential tremor, with emphasis on age and sex: a meta-analysis. *Journal of global health* **11** (2021).

[111] Deuschl, G. *et al.* The clinical and electrophysiological investigation of tremor. *Clinical Neurophysiology* **136**, 93–129 (2022).

[112] Bhatia, K. P. *et al.* Consensus statement on the classification of tremors. from the task force on tremor of the international parkinson and movement disorder society. *Movement disorders* **33**, 75–87 (2018).

[113] Sullivan, K. L., Hauser, R. A. & Zesiewicz, T. A. Essential tremor: epidemiology, diagnosis, and treatment. *The neurologist* **10**, 250–258 (2004).

[114] Pan, M.-K. & Kuo, S.-H. Essential tremor: clinical perspectives and pathophysiology. *Journal of the neurological sciences* **435**, 120198 (2022).

[115] Hopfner, F. & Deuschl, G. Managing essential tremor. *Neurotherapeutics* **17**, 1603–1621 (2020).

[116] Okelberry, T., Lyons, K. E. & Pahwa, R. Updates in essential tremor. *Parkinsonism & Related Disorders* 106086 (2024).

[117] Neudorfer, C. *et al.* The role of the motor thalamus in deep brain stimulation for essential tremor. *Neurotherapeutics* e00313 (2024).

[118] Arleo, A. *et al.* Consensus paper: cerebellum and ageing. *The Cerebellum* **23**, 802–832 (2024).

[119] Manto, M. *et al.* Consensus paper: roles of the cerebellum in motor control—the diversity of ideas on cerebellar involvement in movement. *The Cerebellum* **11**, 457–487 (2012).

[120] Morton, S. M. & Bastian, A. J. Cerebellar control of balance and locomotion. *The neuroscientist* **10**, 247–259 (2004).

[121] Yip, D. W., Awosika, A. O. & Lui, F. Physiology, motor cortical. In *StatPearls [Internet]* (StatPearls Publishing, 2024).

[122] Ward, L. M. The thalamus: gateway to the mind. *Wiley Interdisciplinary Reviews: Cognitive Science* **4**, 609–622 (2013).

[123] Sherman, S. M. Thalamus plays a central role in ongoing cortical functioning. *Nature neuroscience* **19**, 533–541 (2016).

[124] Middlebrooks, E. H. *et al.* Connectivity correlates to predict essential tremor deep brain stimulation outcome: evidence for a common treatment pathway. *NeuroImage: Clinical* **32**, 102846 (2021).

[125] Coenen, V. A. *et al.* A detailed analysis of anatomical plausibility of crossed and uncrossed streamline rendition of the dentato-rubro-thalamic tract (drt (t)) in a commercial stereotactic planning system. *Acta Neurochirurgica* **163**, 2809–2824 (2021).

[126] Lenz, F. *et al.* Single unit analysis of the human ventral thalamic nuclear group: activity correlated with movement. *Brain* **113**, 1795–1821 (1990).

[127] Milosevic, L. *et al.* Physiological mechanisms of thalamic ventral intermediate nucleus stimulation for tremor suppression. *Brain* **141**, 2142–2155 (2018).

[128] Lenz, F. *et al.* Single unit analysis of the human ventral thalamic nuclear group: correlation of thalamic" tremor cells" with the 3-6 hz component of parkinsonian tremor. *Journal of Neuroscience* **8**, 754–764 (1988).

[129] Neudorfer, C. *et al.* Lead-dbs v3. 0: Mapping deep brain stimulation effects to local anatomy and global networks. *Neuroimage* **268**, 119862 (2023).

[130] Raethjen, J. & Deuschl, G. The oscillating central network of essential tremor. *Clinical neurophysiology* **123**, 61–64 (2012).

[131] Buijink, A. W. *et al.* Motor network disruption in essential tremor: a functional and effective connectivity study. *Brain* **138**, 2934–2947 (2015).

[132] Schnitzler, A., Münks, C., Butz, M., Timmermann, L. & Gross, J. Synchronized brain network associated with essential tremor as revealed by magnetoencephalography. *Movement disorders: official journal of the Movement Disorder Society* **24**, 1629–1635 (2009).

[133] Faust, P. L. *et al.* Pathologically based criteria to distinguish essential tremor from controls: analyses of the human cerebellum. *Annals of Clinical and Translational Neurology* (2024).

[134] Louis, E. D. & Faust, P. L. Essential tremor pathology: neurodegeneration and reorganization of neuronal connections. *Nature Reviews Neurology* **16**, 69–83 (2020).

[135] Symanski, C. *et al.* Essential tremor is not associated with cerebellar purkinje cell loss. *Movement Disorders* **29**, 496–500 (2014).

[136] Paris-Robidas, S. *et al.* Defective dentate nucleus gaba receptors in essential tremor. *Brain* **135**, 105–116 (2012).

[137] Kuo, S.-H. & Louis, E. D. Is essential tremor a disorder primarily due to gaba dysfunction? *International review of neurobiology* **163**, 259 (2022).

[138] Nietz, A. *et al.* Selective loss of the gabaaα1 subunit from purkinje cells is sufficient to induce a tremor phenotype. *Journal of neurophysiology* **124**, 1183–1197 (2020).

[139] Pan, M.-K. *et al.* Cerebellar oscillations driven by synaptic pruning deficits of cerebellar climbing fibers contribute to tremor pathophysiology. *Science translational medicine* **12**, eaay1769 (2020).

[140] Lin, C.-Y. *et al.* Abnormal climbing fibre-purkinje cell synaptic connections in the essential tremor cerebellum. *Brain* **137**, 3149–3159 (2014).

[141] Wong, S.-B. *et al.* Cerebellar oscillations in familial and sporadic essential tremor. *The Cerebellum* **21**, 425–431 (2022).

[142] Llinás, R. R. Rebound excitation as the physiological basis for tremor: a biophysical study of the oscillatory properties of mammalian central neurones in vitro. In *Movement disorders: tremor*, 165–182 (Springer, 1984).

[143] Pedrosa, D. J. *et al.* Essential tremor and tremor in parkinson's disease are associated with distinct 'tremor clusters' in the ventral thalamus. *Experimental neurology* **237**, 435–443 (2012).

[144] Dupuis, M. J.-M., Evrard, F. L., Jacquerye, P. G., Picard, G. R. & Lermen, O. G. Disappearance of essential tremor after stroke. *Movement disorders* **25**, 2884–2887 (2010).

[145] Chen, C. C. *et al.* Intra-operative recordings of local field potentials can help localize the subthalamic nucleus in parkinson's disease surgery. *Experimental neurology* **198**, 214–221 (2006).

[146] Mann, J. M. *et al.* Brain penetration effects of microelectrodes and dbs leads in stn or gpi. *Journal of Neurology, Neurosurgery & Psychiatry* **80**, 794–798 (2009).

[147] Milosevic, L. *et al.* Neuronal inhibition and synaptic plasticity of basal ganglia neurons in parkinson's disease. *Brain* **141**, 177–190 (2018).

[148] Steiner, L. A. *et al.* Persistent synaptic inhibition of the subthalamic nucleus by high frequency stimulation. *Brain Stimulation* **15**, 1223–1232 (2022).

[149] Feldmann, L. K. *et al.* Subthalamic beta band suppression reflects effective neuromodulation in chronic recordings. *European Journal of Neurology* **28**, 2372–2377 (2021).

[150] Sinclair, N. C. *et al.* Subthalamic nucleus deep brain stimulation evokes resonant neural activity. *Annals of neurology* **83**, 1027–1031 (2018).

[151] Johnson, K. A. *et al.* Globus pallidus internus deep brain stimulation evokes resonant neural activity in parkinson's disease. *Brain Communications* **5**, fcad025 (2023).

[152] Miocinovic, S. *et al.* Cortical potentials evoked by subthalamic stimulation demonstrate a short latency hyperdirect pathway in humans. *Journal of Neuroscience* **38**, 9129–9141 (2018).

[153] Hartmann, C. *et al.* Distinct cortical responses evoked by electrical stimulation of the thalamic ventral intermediate nucleus and of the subthalamic nucleus. *NeuroImage: Clinical* **20**, 1246–1254 (2018).

[154] Noor, M. S., Steina, A. K. & McIntyre, C. C. Dissecting deep brain stimulation evoked neural activity in the basal ganglia. *Neurotherapeutics* **21**, e00356 (2024).

[155] Oliveira, A. M. *et al.* Machine learning for adaptive deep brain stimulation in parkinson's disease: closing the loop. *Journal of Neurology* **270**, 5313–5326 (2023).

[156] Meidahl, A. C. *et al.* Adaptive deep brain stimulation for movement disorders: the long road to clinical therapy. *Movement disorders* **32**, 810–819 (2017).

[157] Sarikhani, P. *et al.* Automated deep brain stimulation programming with safety constraints for tremor suppression in patients with parkinson's disease and essential tremor. *Journal of neural engineering* **19**, 046042 (2022).

[158] Peeters, J. *et al.* Towards biomarker-based optimization of deep brain stimulation in parkinson's disease patients. *Frontiers in Neuroscience* **16**, 1091781 (2023).

[159] Pardo-Valencia, J., Fernández-García, C., Alonso-Frech, F. & Foffani, G. Oscillatory vs. non-oscillatory subthalamic beta activity in parkinson's disease. *The Journal of Physiology* **602**, 373–395 (2024).

[160] Krauss, J. K. *et al.* Technology of deep brain stimulation: current status and future directions. *Nature Reviews Neurology* **17**, 75–87 (2021).

[161] Josephs, O. & Henson, R. N. Event-related functional magnetic resonance imaging: modelling, inference and optimization. *Philosophical transactions of the royal society of london. series b: biological sciences* **354**, 1215–1228 (1999).

[162] de Pasquale, F. & Marzetti, L. Temporal and spectral signatures of the default mode network. *Magnetoencephalography: From Signals to Dynamic Cortical Networks* 571–603 (2019).

[163] Brookes, M. J. *et al.* Investigating the electrophysiological basis of resting state networks using magnetoencephalography. *Proceedings of the National Academy of Sciences* **108**, 16783–16788 (2011).

[164] Pelzer, E. A., Sharma, A. & Florin, E. Data-driven meg analysis to extract fmri resting-state networks. *Human Brain Mapping* **45**, e26644 (2024).

[165] Hirschmann, J. *et al.* Distinct oscillatory stn-cortical loops revealed by simultaneous meg and local field potential recordings in patients with parkinson's disease. *Neuroimage* **55**, 1159–1168 (2011).

[166] Cheyne, D. O. Meg studies of sensorimotor rhythms: a review. *Experimental neurology* **245**, 27–39 (2013).

[167] Little, S. & Brown, P. The functional role of beta oscillations in parkinson's disease. *Parkinsonism & related disorders* **20**, S44–S48 (2014).

[168] Tan, H., Wade, C. & Brown, P. Post-movement beta activity in sensorimotor cortex indexes confidence in the estimations from internal models. *Journal of Neuroscience* **36**, 1516–1528 (2016).

[169] Lofredi, R. *et al.* Dopamine-dependent scaling of subthalamic gamma bursts with movement velocity in patients with parkinson's disease. *Elife* **7**, e31895 (2018).

[170] Brücke, C. *et al.* Thalamic gamma oscillations correlate with reaction time in a go/nogo task in patients with essential tremor. *Neuroimage* **75**, 36–45 (2013).

[171] Nowak, M., Zich, C. & Stagg, C. J. Motor cortical gamma oscillations: what have we learnt and where are we headed? *Current behavioral neuroscience reports* **5**, 136–142 (2018).

[172] Jurkiewicz, M. T., Gaetz, W. C., Bostan, A. C. & Cheyne, D. Post-movement beta rebound is generated in motor cortex: evidence from neuromagnetic recordings. *Neuroimage* **32**, 1281–1289 (2006).

[173] Winkler, L. *et al.* Beta waves in action: Context-dependent modulations of subthalamo-cortical synchronization during rapid reversals of movement direction. *bioRxiv* 2024–08 (2024).

[174] Litvak, V. *et al.* Movement-related changes in local and long-range synchronization in parkinson's disease revealed by simultaneous magnetoencephalography and intracranial recordings. *Journal of Neuroscience* **32**, 10541–10553 (2012).

[175] van Wijk, B. C. *et al.* Low-beta cortico-pallidal coherence decreases during movement and correlates with overall reaction time. *Neuroimage* **159**, 1–8 (2017).

[176] Boon, L. I. *et al.* A systematic review of meg-based studies in parkinson's disease: The motor system and beyond. *Human brain mapping* **40**, 2827–2848 (2019).

[177] Helmich, R. C., Toni, I., Deuschl, G. & Bloem, B. R. The pathophysiology of essential tremor and parkinson's tremor. *Current neurology and neuroscience reports* **13**, 1–10 (2013).

[178] Muthuraman, M. *et al.* Cerebello-cortical network fingerprints differ between essential, parkinson's and mimicked tremors. *Brain* **141**, 1770–1781 (2018).

[179] Hirschmann, J. *et al.* A direct relationship between oscillatory subthalamic nucleus–cortex coupling and rest tremor in parkinson's disease. *Brain* **136**, 3659–3670 (2013).

[180] Dirkx, M. F. *et al.* The cerebral network of parkinson's tremor: an effective connectivity fmri study. *Journal of Neuroscience* **36**, 5362–5372 (2016).

[181] Schnitzler, A., Timmermann, L. & Gross, J. Physiological and pathological oscillatory networks in the human motor system. *Journal of Physiology-Paris* **99**, 3–7 (2006).

[182] Neumann, W.-J. *et al.* Subthalamic synchronized oscillatory activity correlates with motor impairment in patients with parkinson's disease. *Movement Disorders* **31**, 1748–1751 (2016).

[183] Lofredi, R. & Kühn, A. A. Electrophysiological connectivity measures from deep brain stimulation (dbs)-targets in parkinson's disease and dystonia. In *Connectomic Deep Brain Stimulation*, 339–356 (Elsevier, 2022).

[184] Kühn, A. A., Kupsch, A., Schneider, G.-H. & Brown, P. Reduction in subthalamic 8–35 hz oscillatory activity correlates with clinical improvement in parkinson's disease. *European Journal of Neuroscience* **23**, 1956–1960 (2006).

[185] Kühn, A. A. *et al.* High-frequency stimulation of the subthalamic nucleus suppresses oscillatory β activity in patients with parkinson's disease in parallel with improvement in motor performance. *Journal of Neuroscience* **28**, 6165–6173 (2008).

[186] Mathiopoulou, V. *et al.* Modulation of subthalamic beta oscillations by movement, dopamine, and deep brain stimulation in parkinson's disease. *npj Parkinson's Disease* **10**, 77 (2024).

[187] Beudel, M. *et al.* Tremor reduction by deep brain stimulation is associated with gamma power suppression in parkinson's disease. *Neuromodulation: Technology at the Neural Interface* **18**, 349–354 (2015).

[188] Hirschmann, J. *et al.* Parkinsonian rest tremor is associated with modulations of subthalamic high-frequency oscillations. *Movement Disorders* **31**, 1551–1559 (2016).

[189] Reck, C. *et al.* Characterisation of tremor-associated local field potentials in the subthalamic nucleus in parkinson's disease. *European journal of neuroscience* **29**, 599–612 (2009).

[190] Qasim, S. E. *et al.* Electrocorticography reveals beta desynchronization in the basal ganglia-cortical loop during rest trehuamor in parkinson's disease. *Neurobiology of disease* **86**, 177–186 (2016).

[191] Olaru, M. *et al.* Motor network gamma oscillations in chronic home recordings predict dyskinesia in parkinson's disease. *Brain* **147**, 2038–2052 (2024).

[192] Litvak, V. *et al.* Resting oscillatory cortico-subthalamic connectivity in patients with parkinson's disease. *Brain* **134**, 359–374 (2011).

[193] Cao, C. *et al.* Low-beta versus high-beta band cortico-subcortical coherence in movement inhibition and expectation. *Neurobiology of Disease* 106689 (2024).

[194] Oswal, A. *et al.* Neural signatures of hyperdirect pathway activity in parkinson's disease. *Nature communications* **12**, 5185 (2021).

[195] Binns, T. S. *et al.* Shared pathway-specific network mechanisms of dopamine and deep brain stimulation for the treatment of parkinson's disease. *bioRxiv* 2024–04 (2024).

[196] Tan, H. *et al.* Decoding voluntary movements and postural tremor based on thalamic lfps as a basis for closed-loop stimulation for essential tremor. *Brain stimulation* **12**, 858–867 (2019).

[197] Basha, D. *et al.* Beta oscillatory neurons in the motor thalamus of movement disorder and pain patients. *Experimental neurology* **261**, 782–790 (2014).

[198] Klostermann, F. *et al.* Task-related differential dynamics of eeg alpha-and beta-band synchronization in cortico-basal motor structures. *European journal of Neuroscience* **25**, 1604–1615 (2007).

[199] He, F. *et al.* Nonlinear interactions in the thalamocortical loop in essential tremor: a model-based frequency domain analysis. *Neuroscience* **324**, 377–389 (2016).

[200] Marsden, J., Ashby, P., Limousin-Dowsey, P., Rothwell, J. & Brown, P. Coherence between cerebellar thalamus, cortex and muscle in man: cerebellar thalamus interactions. *Brain* **123**, 1459–1470 (2000).

[201] Paradiso, G. *et al.* Involvement of human thalamus in the preparation of self-paced movement. *Brain* **127**, 2717–2731 (2004).

[202] Opri, E., Cernera, S., Okun, M. S., Foote, K. D. & Gunduz, A. The functional role of thalamocortical coupling in the human motor network. *Journal of Neuroscience* **39**, 8124–8134 (2019).

[203] Halliday, D. *et al.* Coherence between low-frequency activation of the motor cortex and tremor in patients with essential tremor. *The Lancet* **355**, 1149–1153 (2000).

[204] Raethjen, J., Govindan, R. B., Kopper, F., Muthuraman, M. & Deuschl, G. Cortical involvement in the generation of essential tremor. *Journal of neurophysiology* **97**, 3219–3228 (2007).

[205] Sure, M., Mertiens, S., Vesper, J., Schnitzler, A. & Florin, E. Alterations of resting-state networks of parkinson‘s disease patients after subthalamic dbs surgery. *NeuroImage: Clinical* **37**, 103317 (2023).

[206] Oostenveld, R., Fries, P., Maris, E. & Schoffelen, J.-M. Fieldtrip: open source software for advanced analysis of meg, eeg, and invasive electrophysiological data. *Computational intelligence and neuroscience* **2011**, 156869 (2011).

[207] Gramfort, A. *et al.* Meg and eeg data analysis with mne-python. *Frontiers in Neuroinformatics* **7**, 267 (2013).

[208] Maris, E., Schoffelen, J.-M. & Fries, P. Nonparametric statistical testing of coherence differences. *Journal of neuroscience methods* **163**, 161–175 (2007).

[209] Cole, E. R., Miocinovic, S. & Miocinovic, S. Are we ready for automated deep brain stimulation programming? *OSF Preprint https://doiorg/1031219/osfio/8zh73* (2025).

[210] Bouthour, W. *et al.* Biomarkers for closed-loop deep brain stimulation in parkinson disease and beyond. *Nature Reviews Neurology* **15**, 343–352 (2019).

[211] Horn, A., Neumann, W.-J., Degen, K., Schneider, G.-H. & Kühn, A. A. Toward an electrophysiological "sweet spot" for deep brain stimulation in the subthalamic nucleus. *Human brain mapping* **38**, 3377–3390 (2017).

[212] Muller, M. *et al.* Online prediction of optimal deep brain stimulation contacts from local field potentials in chronically-implanted patients with parkinson's disease. *medRxiv* 2024–11 (2024).

[213] Vu, M.-A. T. *et al.* A shared vision for machine learning in neuroscience. *Journal of Neuroscience* **38**, 1601–1607 (2018).

[214] Peralta, M., Jannin, P. & Baxter, J. S. Machine learning in deep brain stimulation: A systematic review. *Artificial Intelligence in Medicine* **122**, 102198 (2021).

[215] Zaidel, A., Spivak, A., Grieb, B., Bergman, H. & Israel, Z. Subthalamic span of β oscillations predicts deep brain stimulation efficacy for patients with parkinson's disease. *Brain* **133**, 2007–2021 (2010).

[216] Sure, M., Vesper, J., Schnitzler, A. & Florin, E. Dopaminergic modulation of spectral and spatial characteristics of parkinsonian subthalamic nucleus beta bursts. *Frontiers in Neuroscience* **15**, 724334 (2021).

[217] Sharma, A., Vidaurre, D., Vesper, J., Schnitzler, A. & Florin, E. Differential dopaminergic modulation of spontaneous cortico–subthalamic activity in parkinson's disease. *Elife* **10**, e66057 (2021).

[218] Horn, A. *et al.* Connectivity predicts deep brain stimulation outcome in p arkinson disease. *Annals of neurology* **82**, 67–78 (2017).

[219] Al-Fatly, B. *et al.* Connectivity profile of thalamic deep brain stimulation to effectively treat essential tremor. *Brain* **142**, 3086–3098 (2019).

[220] Morelli, N. & Summers, R. L. Association of subthalamic beta frequency sub-bands to symptom severity in patients with parkinson's disease: A systematic review. *Parkinsonism & Related Disorders* **110**, 105364 (2023).

[221] Chen, P.-L. *et al.* Subthalamic high-beta oscillation informs the outcome of deep brain stimulation in patients with parkinson's disease. *Frontiers in Human Neuroscience* **16**, 958521 (2022).

[222] Jha, A. *et al.* Functional connectivity of the pedunculopontine nucleus and surrounding region in parkinson's disease. *Cerebral Cortex* **27**, 54–67 (2017).

[223] Oswal, A. *et al.* Cortical connectivity of the nucleus basalis of meynert in parkinson's disease and lewy body dementias. *Brain* **144**, 781–788 (2021).

[224] Neumann, W.-J. *et al.* Cortico-pallidal oscillatory connectivity in patients with dystonia. *Brain* **138**, 1894–1906 (2015).

[225] van Wijk, B. C. *et al.* Functional connectivity maps of theta/alpha and beta coherence within the subthalamic nucleus region. *Neuroimage* **257**, 119320 (2022).

[226] Tsuboi, T. *et al.* Comparative connectivity correlates of dystonic and essential tremor deep brain stimulation. *Brain* **144**, 1774–1786 (2021).

[227] Hua, S. E. & Lenz, F. A. Posture-related oscillations in human cerebellar thalamus in essential tremor are enabled by voluntary motor circuits. *Journal of neurophysiology* **93**, 117–127 (2005).

[228] Schreglmann, S. R. *et al.* Non-invasive suppression of essential tremor via phase-locked disruption of its temporal coherence. *Nature communications* **12**, 363 (2021).

[229] Cajigas, I., Morrison, M. A., San Luciano, M. & Starr, P. Cerebellar deep brain stimulation in cerebral palsy: promising early results and a look forward to a larger clinical trial. *World neurosurgery* **174**, 223 (2023).

[230] Pan, M.-K. Targeting the fundamentals for tremors: the frequency and amplitude coding in essential tremor. *Journal of Biomedical Science* **32**, 18 (2025).

[231] Sommer, M. A. The role of the thalamus in motor control. *Current opinion in neurobiology* **13**, 663–670 (2003).

[232] Asadi, A. *et al.* Electrophysiological approaches to informing therapeutic interventions with deep brain stimulation. *npj Parkinson's Disease* **11**, 20 (2025).

[233] Roediger, J. *et al.* Automated deep brain stimulation programming based on electrode location: a randomised, crossover trial using a data-driven algorithm. *The Lancet Digital Health* **5**, e59–e70 (2023).

[234] Bosch-Bouju, C., Hyland, B. I. & Parr-Brownlie, L. C. Motor thalamus integration of cortical, cerebellar and basal ganglia information: implications for normal and parkinsonian conditions. *Frontiers in computational neuroscience* **7**, 163 (2013).

[235] Gerster, M. *et al.* Separating neural oscillations from aperiodic 1/f activity: challenges and recommendations. *Neuroinformatics* **20**, 991–1012 (2022).

[236] Weiss, E., Kann, M. & Wang, Q. Neuromodulation of neural oscillations in health and disease. *Biology* **12**, 371 (2023).

[237] Louis, E. D. The pharmacotherapeutic landscape for essential tremor: quantifying the level of unmet need from a patient and epidemiologic perspective. *Clinical neuropharmacology* **45**, 99–104 (2022).

[238] Karekal, A., Miocinovic, S. & Swann, N. C. Novel approaches for quantifying beta synchrony in parkinson's disease. *Experimental Brain Research* **240**, 991–1004 (2022).

[239] Cole, S. R. & Voytek, B. Brain oscillations and the importance of waveform shape. *Trends in cognitive sciences* **21**, 137–149 (2017).

[240] Davidson, B. *et al.* Neuromodulation techniques–from non-invasive brain stimulation to deep brain stimulation. *Neurotherapeutics* **21**, e00330 (2024).

[241] Asamoah, B., Khatoun, A. & Mc Laughlin, M. tacs motor system effects can be caused by transcutaneous stimulation of peripheral nerves. *Nature communications* **10**, 266 (2019).

[242] Gilron, R. *et al.* Long-term wireless streaming of neural recordings for circuit discovery and adaptive stimulation in individuals with parkinson's disease. *Nature biotechnology* **39**, 1078–1085 (2021).

[243] Paulo, D. L. *et al.* Corticostriatal beta oscillation changes associated with cognitive function in parkinson's disease. *Brain* **146**, 3662–3675 (2023).

Danksagung

Ich möchte mich bei allen Menschen, die mir das Verfassen dieser Arbeit ermöglicht haben, bedanken.

Zunächst möchte ich Herrn Prof. Dr. Alfons Schnitzler meinen herzlichen Dank aussprechen, der mir die Möglichkeit gegeben hat, meine Doktorarbeit an seinem Institut zu verfassen. Besonders schätze ich seine hervorragende wissenschaftliche Betreuung.

In gleicher Weise danke ich Herrn Dr. Jan Hirschmann, für seine ausgezeichnete Betreuung und stetige Unterstützung. Vielen Dank, dass ich ein Teil deiner Arbeitsgruppe sein durfte und an vielen spannenden Forschungsprojekten arbeiten durfte. Danke für deine Inspiration und wissenschaftliche Begeisterung, die meine Arbeit in dieser Form ermöglicht hat.

Des Weiteren danke ich Herrn Prof. Dr. Thomas Heinzel, der die Rolle meines Mentors übernahm.

Vielen Dank an Markus Butz, der meine Begeisterung für die Neurowissenschaften geweckt hat, als er mir ermöglicht hat, eine Masterarbeit im Institut für Klinische Neurowissenschaften zu schreiben.

Außerdem bedanke ich mich beim Deutschen Akademischen Austauschdienst für die Förderung eines Forschungsaufenthalt in den USA, den ich in der Gruppe von Prof. Dr. Cameron McIntyre absolviert habe. Weiterer Dank gilt der gesamten Arbeitsgruppe von Prof. McIntyre, die mir spannende Einblicke in die Computer-gestützte Modellierung von tiefen Hirnstimulation gegeben hat.

Ebenso danke ich allen meinen Kollegen und dem gesamten Institut für klinische Neurowissenschaften und Medizinische Psychologie. Vor allem danke ich Marius. Ich hätte mir keinen besseren Office-Mate vorstellen können. Ich danke dir für die vielen tollen fachlichen und nicht-fachlichen Gespräche und dafür, dass wir in der gemeinsamen Zeit des Doktors Freunde geworden sind. Besonderer Dank geht auch an Lucy und Lucie, vor allem auch für zwei coole Konferenzen, die wir zusammen verbracht haben. Thank you Fayed for exchanging plants, soil, scientific and non-scientific nonsense. Moreover, a big thanks to Vai, Michelle, Fabrice, Thomas and Agnes for nice evenings outside of work.

Besonders danke ich außerdem Marius, Hannah, Lucy, Lucie, Florian und Jan, die

meine Arbeit Korrektur gelesen haben und mich mit hilfreichen Tipps motiviert haben.

Des Weiteren geht ein großes Dank an alle Patienten, die an den Studien teilgenommen haben, ohne die, diese Arbeit nicht möglich gewesen wäre.

Des weiteren danke ich all meinen Freunden, für die schöne Zeit jenseits der wissenschaftlichen Arbeit. Besonders freue ich mich auch über die Freundschaften, die ich während meines Forschungsaufenthalts in den USA geknüpft haben. Thanks Katya and Zhenya for letting me assemble your furniture.
Ich bedanke mich bei meinen Eltern, die mich während der gesamten Zeit bedingungslos unterstützt haben. Besonderer Dank geht an Florian, der mir immer mit Rat beiseite stand. Danke, dass du mir immer Mut gemacht hast, wenn ich Unterstützung brauchte und mich außerdem immer liebevoll mit dem leckersten Essen unterstützt hast.

Eidesstattliche Versicherung

Ich versichere an Eides Statt, dass die Dissertation von mir selbständig und ohne unzulässige fremde Hilfe unter Beachtung der „Grundsätze zur Sicherung guter wissenschaftlicher Praxis an der Heinrich-Heine-Universität Düsseldorf“ erstellt worden ist.

Düsseldorf, _____ _____